

# Advances

## in Clinical and Experimental Medicine

MONTHLY ISSN 1899-5276 (PRINT) ISSN 2451-2680 (ONLINE)

[www.advances.umed.wroc.pl](http://www.advances.umed.wroc.pl)

2019, Vol. 28, No. 8 (August)

Impact Factor (IF) – 1.227  
Ministry of Science and Higher Education – 40 pts.  
Index Copernicus (ICV) – 155.19 pts.



WROCLAW  
MEDICAL UNIVERSITY

Advances  
in Clinical and Experimental  
Medicine



# Advances in Clinical and Experimental Medicine

ISSN 1899-5276 (PRINT)

ISSN 2451-2680 (ONLINE)

www.advances.umed.wroc.pl

**MONTHLY 2019**  
**Vol. 28, No. 8**  
**(August)**

Advances in Clinical and Experimental Medicine is a peer-reviewed open access journal published by Wrocław Medical University. Its abbreviated title is Adv Clin Exp Med. Journal publishes original papers and reviews encompassing all aspects of medicine, including molecular biology, biochemistry, genetics, biotechnology, and other areas. It is published monthly, one volume per year.

---

## Editorial Office

ul. Marcinkowskiego 2–6  
50-368 Wrocław, Poland  
Tel.: +48 71 784 11 36  
E-mail: redakcja@umed.wroc.pl

## Publisher

Wrocław Medical University  
Wybrzeże L. Pasteura 1  
50-367 Wrocław, Poland

© Copyright by Wrocław Medical University,  
Wrocław 2019

Online edition is the original version of the journal

---

## Editor-in-Chief

Maciej Bagłaż

## Vice-Editor-in-Chief

Dorota Frydecka

---

## Editorial Board

Piotr Dziągłiel  
Marian Klinger  
Halina Milnerowicz  
Jerzy Mozrzyński

---

## Thematic Editors

Marzenna Bartoszewicz (microbiology)  
Marzena Dominiak (dentistry)  
Paweł Domośławski (surgery)  
Maria Ejma (neurology)  
Jacek Gajek (cardiology)  
Mariusz Kuształ  
(nephrology and transplantology)  
Rafał Matkowski (oncology)  
Ewa Milnerowicz-Nabzdzyk (gynecology)  
Katarzyna Neubauer (gastroenterology)  
Marcin Ruciński (basic sciences)  
Robert Śmigiel (pediatrics)  
Paweł Tabakow (experimental medicine)  
Anna Wiela-Hojeńska  
(pharmaceutical sciences)  
Dariusz Wołowicz (internal medicine)

---

## International Advisory Board

Reinhard Berner (Germany)  
Vladimir Bobek (Czech Republic)  
Marcin Czyż (UK)  
Buddhadeb Dawn (USA)  
Kishore Kumar Jella (USA)

---

## Secretary

Katarzyna Neubauer

---

Piotr Ponikowski  
Marek Sąsiadek  
Leszek Szenborn  
Jacek Szepietowski

---

## Statistical Editors

Dorota Diakowska  
Leszek Noga  
Lesław Rusiecki

## Technical Editorship

Joanna Gudarowska  
Paulina Kunicka  
Marek Misiak

## English Language Copy Editors

Eric Hilton  
Sherill Howard Pocięcha  
Jason Schock  
Marcin Tereszewski

---

Pavel Kopel (Czech Republic)  
Tomasz B. Owczarek (USA)  
Ivan Rychlík (Czech Republic)  
Anton Sculean (Switzerland)  
Andriy B. Zimenkovsky (Ukraine)

## Editorial Policy

Advances in Clinical and Experimental Medicine (Adv Clin Exp Med) is an independent multidisciplinary forum for exchange of scientific and clinical information, publishing original research and news encompassing all aspects of medicine, including molecular biology, biochemistry, genetics, biotechnology and other areas. During the review process, the Editorial Board conforms to the "Uniform Requirements for Manuscripts Submitted to Biomedical Journals: Writing and Editing for Biomedical Publication" approved by the International Committee of Medical Journal Editors ([www.ICMJE.org/](http://www.ICMJE.org/)). The journal publishes (in English only) original papers and reviews. Short works considered original, novel and significant are given priority. Experimental studies must include a statement that the experimental protocol and informed consent procedure were in compliance with the Helsinki Convention and were approved by an ethics committee.

For all subscription-related queries please contact our Editorial Office:  
[redakcja@umed.wroc.pl](mailto:redakcja@umed.wroc.pl)

For more information visit the journal's website:  
[www.advances.umed.wroc.pl](http://www.advances.umed.wroc.pl)

Pursuant to the ordinance No. 134/XV R/2017 of the Rector of Wrocław Medical University (as of December 28, 2017) from January 1, 2018 authors are required to pay a fee amounting to 700 euros for each manuscript accepted for publication in the journal Advances in Clinical and Experimental Medicine.

„Podniesienie poziomu naukowego i poziomu umiędzynarodowienia wydawanych czasopism naukowych oraz upowszechniania informacji o wynikach badań naukowych lub prac rozwojowych – zadanie finansowane w ramach umowy 784/p-DUN/2017 ze środków Ministra Nauki i Szkolnictwa Wyższego przeznaczonych na działalność upowszechniającą naukę”.



Indexed in: MEDLINE, Science Citation Index Expanded, Journal Citation Reports/Science Edition, Scopus, EMBASE/Excerpta Medica, Ulrich's™ International Periodicals Directory, Index Copernicus

Typographic design: Monika Kołęda, Piotr Gil  
DTP: Wydawnictwo UMW  
Cover: Monika Kołęda  
Printing and binding: EXDRUK

## Contents

### Original papers

- 1005 Zhenhuan Huang, Qi Lin, Jianwen Wang, Zejuan Zhan, Xuezhao Tu  
**Relationship between quantitative parameters of lumbar vertebral perfusion and bone mineral density (BMD) in postmenopausal women**
- 1013 Sevda Tanrikulu-Küçük, Canan Başaran-Küçükgergin, İbrahim Söğüt, Matem Tunçdemir, Semra Dođru-Abbasođlu, Muhammed Seyithanođlu, Hikmet Koçak, Yıldız Öner-İyidođan  
**Dietary curcumin and capsaicin: Relationship with hepatic oxidative stress and apoptosis in rats fed a high fat diet**
- 1021 Begumhan Turhan, Piraye Kervancioglu, Eda Didem Yalcin  
**The radiological evaluation of the nasal cavity, conchae and nasal septum volumes by stereological method: A retrospective cone-beam computed tomography study**
- 1027 Katarzyna Agnieszka Zabłocka-Słowińska, Katarzyna Skórska, Sylwia Płaczowska, Anna Prescha, Konrad Pawełczyk, Monika Kosacka, Irena Porebska, Halina Grajeta  
**The relationships between glycemic index and glycemic load of diets and nutritional status and antioxidant/oxidant status in the serum of patients with lung cancer**
- 1037 Maciej Sebastian, Maciej Sroczyński, Jerzy Rudnicki  
**Using laparoscopic ultrasound to delineate dangerous anatomy during difficult laparoscopic cholecystectomies**
- 1043 Youming Lei, Yunfei Shi, Jin Duan, Yinqiang Liu, Guoli Lv, Rou Shi, Fujun Zhang, Qingmei Yang, Wei Zhao  
**Identification of alternative splicing and lncRNA genes in pathogenesis of small cell lung cancer based on their RNA sequencing**
- 1051 Elżbieta Iskierka-Jążdżewska, Bartosz Puła, Agnieszka Szeremet, Marek Hus, Aleksandra Gołos, Jadwiga Hołodja, Weronika Piszczek, Paweł Steckiewicz, Małgorzata Wojciechowska, Jan Maciej Zaucha, Krzysztof Warzocha, Krzysztof Jamroziak  
**Ibrutinib discontinuation in patients with relapsed or refractory chronic lymphocytic leukemia treated in a compassionate use program: A report from the Polish Adult Leukemia Study Group (PALG)**
- 1059 Qingqing Tang, Hengyi Wang, Xingyu Wang, Maoyong Fang, Hong Zhang  
**Effect of PI3K/PKB signal pathway inhibitor wortmannin pretreatment on intestinal barrier function in severe acute pancreatitis rats**
- 1067 Adam Kamiński, Anna Bogacz, Małgorzata Górską-Paukszta, Agnieszka Seremak-Mrozikiewicz, Bogusław Czerny  
**Correlation of rs749292 and rs700518 polymorphisms in the aromatase gene (CYP19A1) with osteoporosis in postmenopausal Polish women**
- 1073 Grzegorz Mięksiak, Krzysztof Kołtowski, Piotr Menartowicz, Zygmunt Oleksik, Dariusz Kotulski, Tomasz Potaczek, Martin Repko, Milan Filipovič, Anna Danielewicz, Marek Fatyga, Michał Latański  
**The titanium-made growth-guidance technique for early-onset scoliosis at minimum 2-year follow-up: A prospective multicenter study**
- 1079 Maria Lelakowska, Paweł Tomasz Matusik, Piotr Stanisław Podolec, Maria Olszowska, Jadwiga Maria Nessler, Natalia Podolec, Tadeusz Przewłocki, Monika Komar  
**Transcatheter closure of atrial septal communication: Impact on quality of life in mid-term follow-up**
- 1087 Anna Dębińska, Hanna Danielewicz, Anna Drabik-Chamerska, Danuta Kalita, Andrzej Boznański  
**Genetic polymorphisms in pattern recognition receptors are associated with allergic diseases through gene–gene interactions**
- 1095 Justyna Rybka, Bogdan Małkowski, Monika Olejniczak, Ewa Chmielowska, Ewelina Sokołowska, Kazimierz Kuliczkowski, Tomasz Wróbel  
**Comparing radioactive tracers <sup>18</sup>F-FDG and <sup>18</sup>F-FLT in the staging of diffuse large B-cell lymphoma by PET/CT examination: A single-center prospective study**

- 1101 Xu Hong Lin, Hui Chao Wang, Yong Yu Li, Jun Ling Guo, Yu Xia Li, Guan Chang Cheng, Dan Dan Wei, Rui Lin Yang, Jun Jie Zhang, De Sheng Yang, Bin Wang, Xue Qun Ren  
**IgG plasma cells initiate changes in the protein C system in mouse ulcerative colitis through CD14<sup>+</sup>CD64<sup>+</sup> macrophage activation**

## Reviews

- 1111 Monika Augustynowicz, Agnieszka Bargenda-Lange, Krzysztof Kałwak, Danuta Zwolińska, Kinga Musiał  
**Markers of acute kidney injury in children undergoing hematopoietic stem cell transplantation**
- 1119 Magdalena Olszewska-Szopa, Tomasz Wróbel  
**Gastrointestinal non-Hodgkin lymphomas**
- 1125 Tymoteusz Skok, Paweł Tabakow, Krzysztof Chmielak  
**Methods of integrating the human nervous system with electronic circuits**
- 1137 Agata Kołodziejczyk, Tomasz Pawłowski  
**Negative body image in breast cancer patients**
- 1143 Klementyna Kępińska, Daria Maria Adamczak, Marta Kałużna-Oleksy  
**Advanced heart failure: A review**

# Relationship between quantitative parameters of lumbar vertebral perfusion and bone mineral density (BMD) in postmenopausal women

Zhenhuan Huang<sup>1,A–D,F</sup>, Qi Lin<sup>1,E,F</sup>, Jianwen Wang<sup>1,B</sup>, Zejuan Zhan<sup>1,C</sup>, Xuezhao Tu<sup>2,A,C</sup>

<sup>1</sup> Department of Radiology, First Hospital of Longyan of Fujian Medical University, China

<sup>2</sup> Department of Orthopedics, First Hospital of Longyan of Fujian Medical University, China

A – research concept and design; B – collection and/or assembly of data; C – data analysis and interpretation;

D – writing the article; E – critical revision of the article; F – final approval of the article

Advances in Clinical and Experimental Medicine, ISSN 1899–5276 (print), ISSN 2451–2680 (online)

*Adv Clin Exp Med.* 2019;28(8):1005–1011

## Address for correspondence

Xuezhao Tu

E-mail: xuezhao@sina.com

## Funding sources

None declared

## Conflict of interest

None declared

Received on December 26, 2017

Reviewed on January 4, 2018

Accepted on August 9, 2018

Published online on April 13, 2019

## Abstract

**Background.** Dynamic contrast-enhanced magnetic resonance imaging (DCE-MRI) is a noninvasive method to evaluate the microcirculation of bone marrow in local tissue, which will be a new tool for the diagnosis of osteoporosis.

**Objectives.** To investigate the relationship between quantitative perfusion parameters ( $K^{trans}$ ,  $K_{ep}$  and  $V_e$ ) and bone mineral density (BMD) in postmenopausal women.

**Material and methods.** The subjects were divided into 3 groups according to T value: normal bone mass group (T value  $\geq -1.0$ ); bone loss group ( $-2.5 < T < -1.0$ ); and osteoporosis group ( $T \leq -2.5$ ).  $K^{trans}$ ,  $K_{ep}$  and  $V_e$  of the lumbar spine were measured using quantitative DCE-MRI. The relationship between these parameters and age was analyzed.

**Results.** Bone mineral density of the lumbar spine and femoral neck gradually decreased with age. The values of  $K^{trans}$ ,  $K_{ep}$  and  $V_e$  significantly decreased with age. The values of  $K^{trans}$ ,  $K_{ep}$  and  $V_e$  of the lumbar vertebrae in the osteoporosis group were lower than those in the bone loss and normal bone mass group. Bone mineral density was positively correlated with the  $K^{trans}$  and  $V_e$  of the lumbar vertebrae.

**Conclusions.** The incidences of bone loss and osteoporosis increased with age. The measurement of BMD was conducive to early diagnosis of osteoporosis.  $K^{trans}$ ,  $K_{ep}$  and  $V_e$  values of the lumbar vertebra decreased with age, and have a positive correlation with lumbar BMD. The value of DCE-MRI may play a role in the diagnostic algorithm of osteoporosis.

**Key words:** osteoporosis, bone mineral density (BMD), quantitative dynamic contrast-enhanced magnetic resonance (DCE-MRI), quantitative parameters

## Cite as

Huang Z, Lin Q, Wang J, Zhan Z, Tu X. Relationship between quantitative parameters of lumbar vertebral perfusion and bone mineral density (BMD) in postmenopausal women.

*Adv Clin Exp Med.* 2019;28(8):1005–1011.

doi:10.17219/acem/94150

## DOI

10.17219/acem/94150

## Copyright

© 2019 by Wrocław Medical University

This is an article distributed under the terms of the Creative Commons Attribution Non-Commercial License (<http://creativecommons.org/licenses/by-nc-nd/4.0/>)

## Introduction

Osteoporosis is a systemic skeletal disease characterized by bone loss, microstructural degradation with a resulting increase in bone fragility and, as a consequence, susceptibility to fracture.<sup>1</sup> Primary osteoporosis (including in the postmenopausal and elderly women) is a physiological degeneration that inevitably occurs with the growth of age. Osteoporosis-induced pain, height shortening, humpback, fractures, and other complications seriously reduce the quality of life of patients. Patients are also under several economic burdens due to the pain. Therefore, osteoporosis has become a serious public health problem in the world.

It is widely known that bone biochemical markers are one of the methods for assessing bone metabolism in humans,<sup>2–5</sup> but their use has been limited to providing comprehensive information about the overall bone response, which does not reflect changes of the hip or other specific parts. Bone mineral density (BMD) is still a gold standard in the diagnosis of osteoporosis,<sup>6</sup> but the strength of bone is affected not only by BMD, but also by bone mass (bone mass is an important factor of the strength of bone). Therefore, the determination of BMD also has some limitations.<sup>7–10</sup>

Researchers have not yet reached a consensus on the pathogenesis of osteoporosis. The main hypotheses include decreasing sex hormones, excess fat and bone marrow perfusion.<sup>11,12</sup> In recent years, decreasing blood flow in bone marrow has also been considered as an important factor of osteoporosis. Dynamic contrast-enhanced magnetic resonance imaging (DCE-MRI) is a noninvasive method of evaluating the microcirculation of bone marrow in local tissue, which can be a new tool for the diagnosis of osteoporosis. Through the analysis of the quantitative parameters ( $K^{\text{trans}}$ ,  $K_{\text{ep}}$  and  $V_e$ ) of lumbar vertebrae bone marrow perfusion in 197 postmenopausal women, the changes of BMD of the lumbar spine with age were analyzed.

## Material and methods

### Study subjects

A total of 197 postmenopausal women with ages ranging from 47 to 86 years were examined from May 2014 to August 2016. The dual-energy X-ray absorptiometry (DXA) and DCE-MRI examinations in osteoporosis were performed in the First Hospital of Longyan of Fujian Medical University, China. Inclusion criteria were as follows: (1) no deformity of the lumbar spine or hip; (2) no tumors, metastases or other diseases which affect the metabolism of bone; (3) no history of surgery or radiotherapy and chemotherapy; (4) no drugs taken that affect bone metabolism or the excretion of urinary creatinine;

(5) no contraindications for MRI. This study was approved by the ethics committee of the First Hospital of Longyan of Fujian Medical University, China. All participants signed informed consent of the corresponding rights and obligations.

### DXA inspection

Bone mineral density of the anteroposterior lumbar spine and the femoral neck were measured with DXA (DPX-L, Lunar; GE Healthcare, Chicago, USA). The unit of measure was  $\text{g}/\text{cm}^2$ . Manual errors, which included postural swings and other technical problems, were eliminated by technical experts during the measurements. Standard periosteal type instrumentation was used before the measurement. The coefficient of variation of the instrument was less than 1%. The results of the DXA measurements were considered as the criteria for grouping. The subjects were divided into 3 groups according to T value: normal bone mass group (T value  $\geq -1.0$ ); bone loss group ( $-2.5 < T < -1.0$ ); and osteoporosis group ( $T \leq -2.5$ ). The division was based on the diagnostic criteria of postmenopausal osteoporosis established by the World Health Organization (WHO) in 1994.

### MRI examination

All subjects underwent conventional scanning and DCE-MRI examination on Signa HDi 1.5T superconducting MRI equipment (GE Healthcare, Chicago, USA). Conventional scans were used to observe the morphology and signal intensity of the lumbar vertebrae, including sagittal FSE-XL sequence T1WI (TR 450 ms, TE 14.4 ms, matrix  $320 \times 192$ ) and sagittal FRFSE-XL sequence T2WI (TR 2500 ms, TE 110 ms, matrix  $320 \times 224$ ). The scanning sequence had a layer thickness of 4 mm, an interlayer pitch of 0.5 mm and a FOV of 35 mm, which scanned 11 layers in total.

DCE-MRI was set as LAVA sequence (T1WI: TR 3.5 ms, TE 1.2 ms, FOV 35 mm), matrix  $256 \times 160$ , and slice thickness 5 mm. The conventional scan, which can show the dynamic central lumbar vertebral level for the enhancement was chosen. The layer (Gd-BOPTA) was injected intravenously at a dose of 0.1 mmol/kg and a rate of 5 mL/s. Analysis software from the workstation was used to draw the region of interest (ROI). The ROI included cancellous bone part of the whole vertebral body, more than 3 mm from the edge of the vertebral body, and avoiding bone island, posterior venous plexus and so on. The arterial input function (AIF) was calculated using the pharmacokinetic blood dual compartment model (Tofts model) to get the quantitative parameters. The quantitative parameters can reflect microvascular permeability, tissue perfusion and extravascular extracellular space directly. The volume constant ( $K^{\text{trans}}$ ) and the rate constant ( $K_{\text{ep}}$ ,  $K_{\text{ep}} = K^{\text{trans}}/V_e$ ) of the contrast agent from plasma to extravascular



extracellular space (EES) represent the transfer constant ( $K^{trans}$ ) and contrast agent from EES.  $V_e$  represents the volume of EES per unit volume of tissue in mL/100 mL.  $K^{trans}$  represents the comparative dose of blood into the EES per unit volume of tissue per unit time, that is, volume capillary permeability-surface area product in  $min^{-1}$ .  $K_{ep}$  represents the comparative dose of EES returned to the blood vessel per unit time (the exchange rate of the contrast agent between the plasma and the EES gap) in  $min^{-1}$ .

### Statistical analysis

The diversification of BMD in the lumbar spine and femoral neck as well as the changes of  $K^{trans}$ ,  $K_{ep}$  and  $V_e$  of the lumbar spine were analyzed in each age group using 2 samples to test. The diagnostic criterion of osteoporosis was  $T \leq 2.5$ , which was used to calculate the bone mass reduction and the detection rate of osteoporosis in all age groups. The relationship between age, T value, BMD, and  $K^{trans}$ ,  $K_{ep}$  and  $V_e$  of lumbar, was analyzed using analysis of variance (ANOVA) test in normal, bone loss and osteoporosis groups. To determine the relationship between  $K^{trans}$ ,  $K_{ep}$  and  $V_e$  of the lumbar and age and BMD of lumbar, linear correlation was analyzed. A value of  $p < 0.05$  represented a statistically significant difference. The data was analyzed using SPSS v. 16.0 software (SPSS Inc., Chicago, USA). Data was expressed as mean  $\pm$  standard deviation (SD) ( $X \pm s$ ).

## Results

### Comparison of bone mineral density between lumbar spine and femoral neck in all age groups

The decrease of bone mass of the lumbar spine and femoral neck, and the rate of detection of osteoporosis are shown in Table 1. Bone mineral density of the lumbar spine and femoral neck gradually decreased with age. It decreased rapidly over 50 years of age and declined again at or after 70 years of age. There was no significant difference in BMD between lumbar vertebrae and femoral neck at the same age ( $p > 0.05$ ).

Table 1. Bone mineral density (BMD) of lumbar vertebrae and femur neck and detection rate of osteoporosis in all age groups

Age group [years]	n	BMD of lumbar vertebrae [g/cm <sup>2</sup> ], X $\pm$ s	BMD of femoral neck [g/cm <sup>2</sup> ], X $\pm$ s	Lumbar vertebrae		Femur neck	
				bone loss, n [%]	osteoporosis, n [%]	bone loss, n [%]	osteoporosis, n [%]
40~	5	1.112 $\pm$ 0.093	1.065 $\pm$ 0.023	2 (40.0)	0 (0.0)	1 (20.0)	0 (0.0)
50~	66	0.841 $\pm$ 0.028*	0.845 $\pm$ 0.023*	22 (33.3)	18 (27.3)*	20 (30.3)	14 (21.2)*
60~	72	0.745 $\pm$ 0.021*	0.744 $\pm$ 0.020*	26 (36.1)	32 (44.4)*	30 (41.7)	26 (34.7)*
70~	44	0.646 $\pm$ 0.013*	0.643 $\pm$ 0.010*	6 (13.7)	33 (75.0)*	14 (31.8)	25 (56.8)*
80~	10	0.559 $\pm$ 0.003*	0.571 $\pm$ 0.002*	1 (10.0)	9 (90.0)*	2 (20.0)	8 (80.0)*

The values between different groups were compared using ANOVA test; \* $p < 0.05$  vs 40~ years age group.

### Comparison of the decline of bone mass and detection rate of osteoporosis in all age groups

$T \leq 2.5$  is the diagnostic criterion for osteoporosis. The incidence of osteoporosis increased significantly with age, together with decreasing bone mass. People over 50 years of age will be at significantly increased risk of osteoporosis, which will be more emergent at each additional 10 years of age. After the age of 70, the increase of the incidence was further intensified, which will be increased by 15% or more in the development of osteoporosis. Occurrences in the lumbar appeared earlier than in the femoral neck. Therefore, a site examination of the lumbar could help find osteoporosis earlier.

### Comparison of the $K^{trans}$ , $K_{ep}$ and $V_e$ of lumbar in all age groups

The parameters of  $K^{trans}$ ,  $K_{ep}$  and  $V_e$  of the lumbar spine were analyzed in each age group. The results showed that the values of  $K^{trans}$  and  $K_{ep}$  of the lumbar spine decreased gradually with age.  $V_e$  of the lumbar also showed a significant downward trend (Table 2).

### Relationship analysis between $K^{trans}$ , $K_{ep}$ , $V_e$ and age

Linear correlation analysis of  $K^{trans}$ ,  $K_{ep}$  and  $V_e$  of the lumbar spine and age was performed using linear correlation with age as an independent variable. There was a negative

Table 2. Hemodynamics parameters of lumbar vertebrae in all age groups (X  $\pm$  s)

Age groups [years]	n	$K^{trans}$ [min <sup>-1</sup> ]	$K_{ep}$ [min <sup>-1</sup> ]	$V_e$ [mL/100 mL]
40~	5	1.123 $\pm$ 0.192	3.118 $\pm$ 0.023	0.358 $\pm$ 0.021
50~	66	0.721 $\pm$ 0.077*	3.000 $\pm$ 0.100*	0.235 $\pm$ 0.006*
60~	72	0.514 $\pm$ 0.039*	2.727 $\pm$ 0.114*	0.184 $\pm$ 0.003*
70~	44	0.361 $\pm$ 0.017*	2.459 $\pm$ 0.112*	0.144 $\pm$ 0.001*
80~	10	0.213 $\pm$ 0.005*	2.096 $\pm$ 0.068*	0.100 $\pm$ 0.001*

The values between different groups were compared using ANOVA test; \* $p < 0.05$  vs 40~ years age group.

correlation between age and  $K^{trans}$  and  $V_e$  of the lumbar spine. The correlation coefficients ( $r$ ) were 0.907, 0.913 and 0.864, respectively ( $p < 0.05$ ). These results are shown in Fig. 1.

### Morphometric differences of dynamic enhancement curve of lumbar vertebrae in normal, bone loss and osteoporosis groups

Compared with bone loss and normal groups, the quantitative dynamic enhancement curve of lumbar spine was more stable, and the  $K^{trans}$  value was lower in osteoporosis group. Meanwhile, the quantitative dynamic enhancement curve of lumbar spine and the  $K^{trans}$  value were the highest in osteoporosis group. These results are shown in Fig. 2.

### Comparison of $K^{trans}$ , $K_{ep}$ and $V_e$ of lumbar in each group

According to the T value, 197 cases were divided into a normal group ( $n = 48$ ), bone loss group ( $n = 57$ ) and osteoporosis group ( $n = 92$ ). The BMD of lumbar vertebrae was  $1.025 \pm 0.009 \text{ g/cm}^2$ ,  $0.778 \pm 0.000 \text{ g/cm}^2$  and  $0.600 \pm 0.001 \text{ g/cm}^2$  in the above groups, respectively. Statistical significance was found in each group ( $p < 0.01$ ). In the osteoporosis group,  $K^{trans}$  value was  $0.326 \pm 0.005 \text{ min}^{-1}$ ,  $K_{ep}$  value was  $2.344 \pm 0.030 \text{ min}^{-1}$ ,

and  $V_e$  value was  $0.318 \pm 0.000 \text{ mL/100 mL}$ ,  $p < 0.01$ . In the bone loss group,  $K^{trans}$  value was  $0.563 \pm 0.006 \text{ min}^{-1}$ ,  $K_{ep}$  value was  $3.023 \pm 0.039 \text{ min}^{-1}$  and  $V_e$  value was  $0.185 \pm 0.000 \text{ mL/100 mL}$ ,  $p < 0.01$ , and those values were lower than in the normal group ( $K^{trans} 0.961 \pm 0.048 \text{ min}^{-1}$ ,  $K_{ep} 3.150 \pm 0.018 \text{ min}^{-1}$  and  $V_e 0.306 \pm 0.005 \text{ mL/100 mL}$ ,  $p < 0.01$ , respectively). The values of  $K^{trans}$ ,  $K_{ep}$  and  $V_e$  parameters in the osteoporosis group were lower than in the bone loss group ( $p < 0.01$ ). These results are shown in Table 3.

### Correlation analysis between $K^{trans}$ , $K_{ep}$ and $V_e$ , and bone mineral density of lumbar

The linear correlation analysis of the correlation between  $K^{trans}$ ,  $K_{ep}$  and  $V_e$  values of lumbar vertebrae and the BMD value of the lumbar spine was performed using a linear correlation method, with BMD value as an independent variable. There was a positive correlation between BMD and the  $K^{trans}$ ,  $K_{ep}$  and  $V_e$  values. Lumbar  $K^{trans}$ ,  $K_{ep}$  and  $V_e$  values decreased together with lower lumbar BMD. The correlation coefficients ( $R$ ) were 0.969, 0.818 and 0.944 ( $p < 0.05$ ), respectively. These results are shown in Fig. 3.

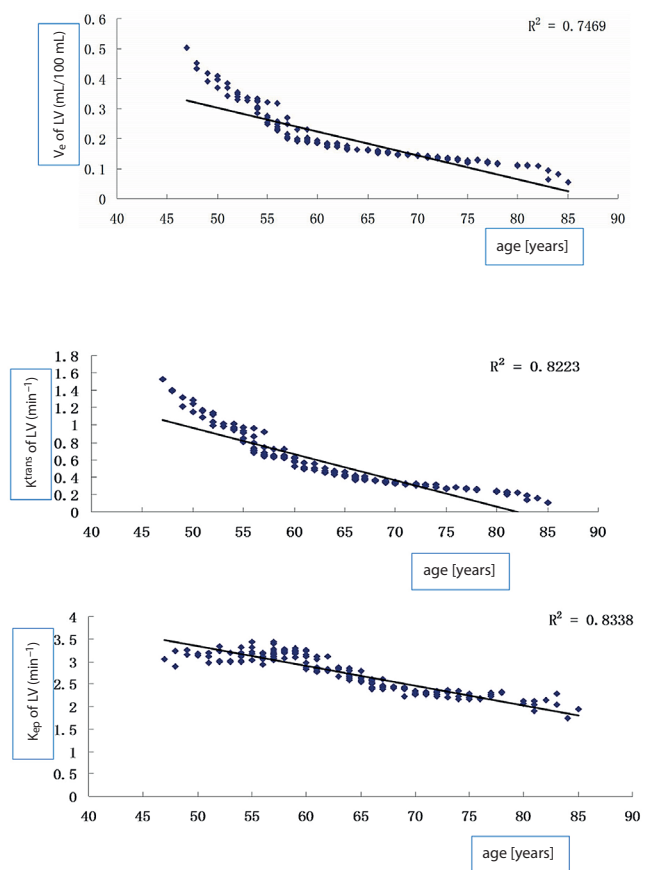


Fig. 1. Relationship analysis between  $K^{trans}$ ,  $K_{ep}$  and  $V_e$  values of lumbar vertebrae and age

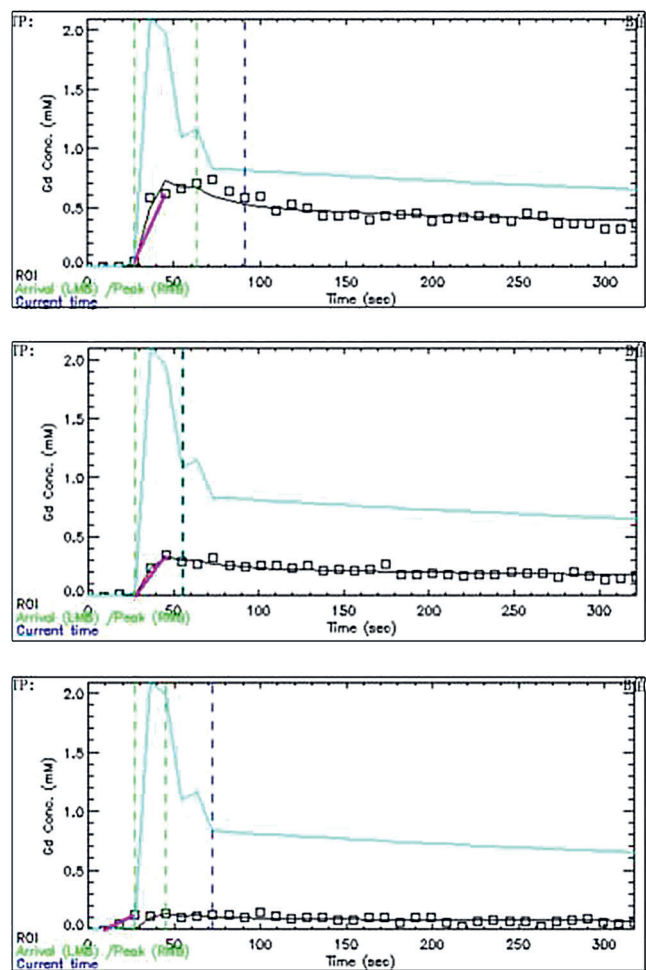
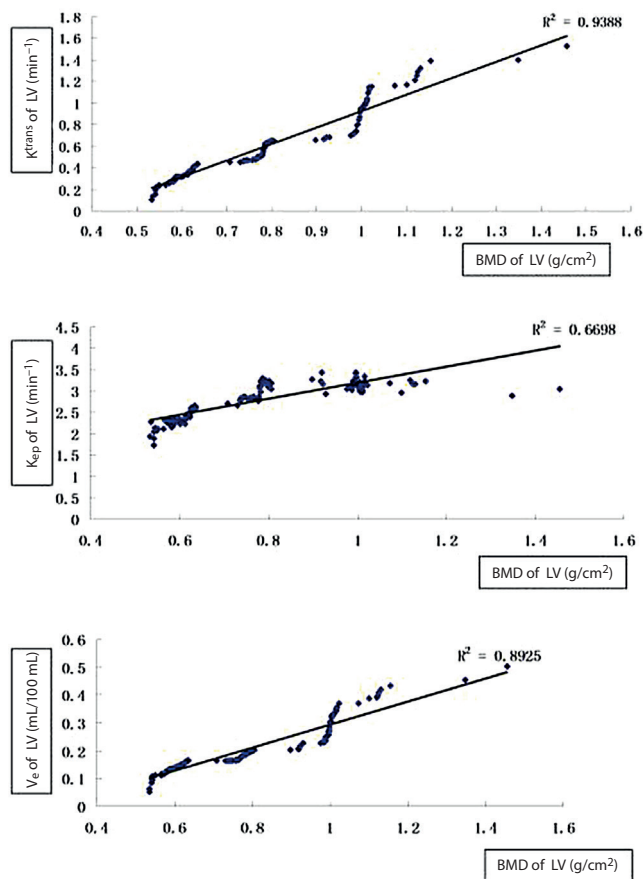


Fig. 2. Morphometric differences of dynamic enhancement curve of lumbar vertebrae with normal, bone loss and osteoporosis groups (A – normal group; B – bone loss group; C – osteoporosis group)

**Table 3.** Comparison of the hemodynamics parameters and bone mineral density (BMD) of lumbar vertebrae in all age groups (X ±s)

Groups	n	Age [years]	T	BMD [g/cm <sup>2</sup> ]	K <sup>trans</sup> [min <sup>-1</sup> ]	K <sub>ep</sub> [min <sup>-1</sup> ]	V <sub>e</sub> [mL/100 mL]
Normal	48	57.077 ±6.685	0.356 ±0.277	1.025 ±0.009	0.961 ±0.048	3.150 ±0.018	0.306 ±0.005
Bone loss	57	61.386 ±6.643*	-1.625 ±0.067*	0.778 ±0.000*	0.563 ±0.006*	3.023 ±0.039*	0.185 ±0.000*
Osteoporosis	92	68.207 ±7.983*†	-2.989 ±0.047*†	0.600 ±0.001*†	0.326 ±0.005*†	2.344 ±0.030*†	0.318 ±0.000*†

The values of different groups were compared using ANOVA test. \*p < 0.01 vs normal group; †p < 0.01 vs bone loss group.



**Fig. 3.** Correlation analysis between K<sup>trans</sup>, K<sub>ep</sub> and V<sub>e</sub> values, and bone mineral density (BMD) of the lumbar

## Discussion

By analyzing BMD of the lumbar spine and femoral neck in postmenopausal women, we found that BMD decreased significantly after the age of 50. This may be because estrogen plays an important role in regulating bone metabolism in women. Postmenopausal women have lower estrogen levels, which would accelerated the resorption of bone.<sup>13</sup> When people are over 70 years old, the reduction of BMD will be aggravated, which is related to the diversification of diet, decreased activity, and reduced vitamin D synthesis and conversion. All these reasons lead to accelerated bone loss. This study also found that the incidence of osteoporosis increased gradually with age. With each additional 10 years of age, osteoporosis increased by a more than 15% rate of development. Osteoporosis occurred in the lumbar earlier than the femoral neck. Therefore,

the site of the lumbar for BMD testing could help find osteoporosis earlier.

In recent years, some scholars hypothesized that decreased bone marrow perfusion leads to osteoporosis. Bone marrow includes red and yellow bone marrow types. Red bone marrow has a rich vascular network made up of adipose tissue (40%), water (40%) and protein (20%). Yellow bone marrow has little vascular network, with adipose tissue, water and protein accounting for 80%, 15% and 5%, respectively. The proportion of red and yellow bone marrow gradually shifts from primarily red until it inverts into primarily yellow gradually with age.<sup>14,15</sup> Because of the limited space for of bone marrow, excessive adipose tissue will oppress trabecular microvascular microcirculation. Therefore, age is a key factor of bone marrow perfusion level. In our study, K<sup>trans</sup>, K<sub>ep</sub> and V<sub>e</sub> values of the lumbar vertebrae of postmenopausal women gradually decreased with age. K<sup>trans</sup>, K<sub>ep</sub> and V<sub>e</sub> values of the lumbar spine in patients older than 50 years of age were significantly lower than in younger people. The normal menopausal age was below 50. Postmenopausal women suffer dual factors, menopause and aging, which induces significant reduction of bone marrow perfusion. Figure 1 also shows a negative correlation between K<sup>trans</sup>, K<sub>ep</sub> and V<sub>e</sub> values of the lumbar, and age in postmenopausal women.

Primary osteoporosis is common among postmenopausal women and the elderly. The pathological features are decreased bone marrow unit area within the capillaries and blood sinus number, increased number of adipocytes and the volume, and increased bone mineral deposition decrease.<sup>16,17</sup> Our results showed that there were positive correlations between K<sup>trans</sup>, K<sub>ep</sub> and V<sub>e</sub>, and BMD of the lumbar spine in postmenopausal women. The correlation coefficients were 0.969, 0.818 and 0.944, respectively. The decrease of K<sup>trans</sup>, K<sub>ep</sub> and V<sub>e</sub> values was associated with BMD. We also found that K<sup>trans</sup>, K<sub>ep</sub> and V<sub>e</sub> values of lumbar vertebrae in the osteoporosis group were lower than in the normal group. The decrease in the osteoporosis group was the most significant and the dynamic enhancement curve was the smoothest. Decreased K<sub>ep</sub> and K<sup>trans</sup> values suggest degradation of vascular function and decreased permeability of the vessel wall, while decreased V<sub>e</sub> value suggests that fat content increased and interstitial space decreased. These affect the supply of blood in bone tissue and are consistent with reports the literature.<sup>11,18–21</sup>

Interestingly, we also found that DCE-MRI can reflect the blood supply characteristics of local lumbar spine and hemodynamic changes. Through the intravenous

contrast agent Gd-DTPA and changes in the local tissue magnetic field, the time-signal intensity curve obtained with the contrast agent can produce semi-quantitative parameters such as slope, maximum contrast enhancement rate and enhanced peak value. The time-signal intensity curve can also be obtained by post-processing quantitative parameters such as volume transfer constant ( $K^{\text{trans}}$ ), extravascular extracellular volume fraction ( $V_e$ ) of the contrast agent permeating from the plasma to extravascular extracellular space (EES), and rate constants of return of the contrast agent from EES to plasma ( $K_{ep}$ ),  $K_{ep} = K^{\text{trans}}/V_e$ . Some studies<sup>22</sup> have found that in patients with osteoporosis, semi-quantitative MRI enhanced peak intensity decrease, and decreased BMD was significantly positively correlated. Ma et al.<sup>23</sup> reported that the quantitative parameters  $K^{\text{trans}}$  and  $V_e$  in the osteoporosis group were significantly lower than in the normal (control) group.

Another investigator found that there was a negative correlation between age, the bone marrow fat fraction (FF) value and quantitative parameters  $K^{\text{trans}}$  and  $K_{ep}$ , and semi-quantitative parameters (fortified peak) in the population without osteoporosis.<sup>24</sup> Zhu et al.<sup>25</sup> found that  $K^{\text{trans}}$  and BMD decreased significantly 2 weeks after ovariectomy in rats, while  $V_e$  decreased significantly 10 weeks after ovariectomy. There was a negative correlation between  $K_{ep}$ , FF value and BMD reduction. The relationship between  $K_{ep}$ , FF and BMD is not clear. Wáng et al.<sup>26</sup> reported that bilateral ovariectomy led to a rapid decrease in BMD, increased bone marrow FF and decreased blood flow perfusion. Decreased blood perfusion is one of the mechanisms of osteoporosis. Due to dysfunction of bone marrow microcirculation, vascular endothelial cells are closely connected and the late stage is caused by the accumulation of bone marrow fat and microvascular pressure. It is indicated that DCE-MRI plays a role in osteoporosis therapy targets or early assessment of efficacy.

The limitations of this study were as follows: (1) quantitative DCE-MRI is complex and time-consuming and may increase the errors of parameter evaluation; (2) the choice of different pharmacokinetic models and analysis software would lead to differences in measurement data<sup>11,27</sup>; (3) there is a lack of strict design of the pathology-image for a control study.

A cross-sectional study of postmenopausal women found that BMD decreased with age. Bone mineral density of the vertebrae can detect osteoporosis earlier. Similarly,  $K^{\text{trans}}$ ,  $K_{ep}$  and  $V_e$  values of the lumbar spine were negatively correlated with age. The decrease of  $K^{\text{trans}}$ ,  $K_{ep}$  and  $V_e$  values in the lumbar spine were associated with a decrease of BMD, and were positively correlated with BMD of the lumbar spine.  $K^{\text{trans}}$ ,  $K_{ep}$  and  $V_e$ , bone mass reduction and osteoporosis were reduced, suggesting that bone marrow cavity fat was increased and tissue space and microcirculation were reduced. These will be useful for early diagnosis of osteoporosis and provide a reference for treatment of this condition.

## Conclusions

The incidence of bone loss and osteoporosis increases with age. The measurement of BMD was conducive to early diagnosis of osteoporosis. The  $K^{\text{trans}}$ ,  $K_{ep}$  and  $V_e$  values of lumbar vertebrae decreased with age and have a positive correlation with lumbar BMD. This shows the potential value of DCE-MRI in the diagnostic algorithm of osteoporosis.

## References

- Langdahl B, Ferrari S, Dempster DW. Bone modeling and remodeling: Potential as therapeutic targets for the treatment of osteoporosis. *Ther Adv Musculoskelet Dis*. 2016;8(6):225–235.
- Lv H, Jiang F, Guan D, et al. Metabolomics and its application in the development of discovering biomarkers for osteoporosis research. *Int J Mol Sci*. 2016;17(12). Pii: E2018.
- Cauley JA. Osteoporosis: Fracture epidemiology update 2016. *Curr Opin Rheumatol*. 2017;29(2):150–156.
- Yoshiki F, Nishikawa A, Taketsuna M, Kajimoto K, Enomoto H. Efficacy and safety of teriparatide in bisphosphonate-pretreated and treatment-naïve patients with osteoporosis at high risk of fracture: Post hoc analysis of a prospective observational study. *J Orthop Sci*. 2017;22(2):330–338.
- Shehata AS, Amer MG, Abd El-Haleem MR, Karam RA. The ability of hesperidin compared to that of insulin for preventing osteoporosis induced by type I diabetes in young male albino rats: A histological and biochemical study. *Exp Toxicol Pathol*. 2017;69(4): 203–212.
- Bell KJ, Hayen A, Glasziou P, et al. Potential usefulness of BMD and bone turnover monitoring of zoledronic acid therapy among women with osteoporosis: Secondary analysis of randomized controlled trial data. *J Bone Miner Res*. 2016;31(9):1767–1773.
- Popp AW, Meer S, Krieg MA, Perrelet R, Hans D, Lippuner K. Bone mineral density (BMD) and vertebral trabecular bone score (TBS) for the identification of elderly women at high risk for fracture: The SEMOF cohort study. *Eur Spine J*. 2016;25(11):3432–3438.
- Miyauchi A. Relationship of pharmacokinetics, changes of bone turnover markers and BMD/fractures efficacy during treatment with anabolic agents: Teriparatide daily and once weekly subcutaneous injections [in Japanese]. *Clin Calcium*. 2016;26(11):1583–1595.
- Compston J. Bone quality: What is it and how is it measured? *Arq Bras Endocrinol Metabol*. 2006;50(4):579–585.
- Su Y, Leung J, Hans D, Aubry-Rozier B, Kwok T. Added clinical use of trabecular bone score to BMD for major osteoporotic fracture prediction in older Chinese people: The Mr. OS and Ms. OS cohort study in Hong Kong. *Osteoporos Int*. 2017;28(1):151–160.
- Ma HT, Griffith JF, Zhao X, Lv H, Yeung DK, Leung PC. Relationship between marrow perfusion and bone mineral density: A pharmacokinetic study of DCE-MRI. *Conf Proc IEEE Eng Med Biol Soc*. 2012;2012: 377–379.
- Griffith JF, Wang YX, Zhou H, et al. Reduced bone perfusion in osteoporosis: Likely causes in an ovariectomy rat model. *Radiology*. 2010; 254(3):739–746.
- Leslie WD, Majumdar SR, Morin SN, Hans D, Lix LM. Change in trabecular bone score (TBS) with antiresorptive therapy does not predict fracture in women: The Manitoba BMD Cohort. *J Bone Miner Res*. 2016;32(3):618–623.
- Basu S, Houseni M, Bural G, et al. Magnetic resonance imaging based bone marrow segmentation for quantitative calculation of pure red marrow metabolism using 2-deoxy-2-[F-18]fluoro-D-glucose-positron emission tomography: A novel application with significant implications for combined structure-function approach. *Mol Imaging Biol*. 2007;9(6):361–365.
- Sheu Y, Cauley JA. The role of bone marrow and visceral fat on bone metabolism. *Curr Osteoporos Rep*. 2011;9(2):67–75.
- Li GW, Tang GY, Liu Y, Tang RB, Peng YF, Li W. MR spectroscopy and micro-CT in evaluation of osteoporosis model in rabbits: Comparison with histopathology. *Eur Radiol*. 2012;22(4):923–929.

17. Griffith JF, Wang YX, Zhou H, et al. Reduced bone perfusion in osteoporosis: Likely causes in an ovariectomy rat model. *Radiology*. 2010;254(3):739–746.
18. Liu Y, Cao L, Hillengass J, et al. Quantitative assessment of microcirculation and diffusion in the bone marrow of osteoporotic rats using VCT, DCE-MRI, DW-MRI, and histology. *Acta Radiol*. 2013;54(2):205–213.
19. Ma HT, Lv H, Griffith JF, Yuan J, Leung PC. Bone marrow perfusion of proximal femur varied with BMD: A longitudinal study by DCE-MRI. *Conf Proc IEEE Eng Med Biol Soc*. 2013;2013:2607–2610.
20. Griffith JF, Yeung DK, Antonio GE, et al. Vertebral marrow fat content and diffusion and perfusion indexes in women with varying bone density: MR evaluation. *Radiology*. 2006;241(3):831–838.
21. Griffith JF, Yeung DK, Antonio GE, et al. Vertebral bone mineral density, marrow perfusion, and fat content in healthy men and men with osteoporosis: Dynamic contrast-enhanced MR imaging and MR spectroscopy. *Radiology*. 2005;236(3):945–951.
22. Biffar A, Schmidt GP, Sourbron S, et al. Quantitative analysis of vertebral bone marrow perfusion using dynamic contrast-enhanced MRI: Initial results in osteoporotic patients with acute vertebral fracture. *J Magn Reson Imaging*. 2011;33:676–683.
23. Ma HT, Lv H, Griffith JF, et al. Bone marrow perfusion of proximal femur varied with BMD: A longitudinal study by DCE-MRI. *Conf Proc IEEE Eng Med Biol Soc*. 2013;2013:2607–2610.
24. Breault SR, Heye T, Bashir MR, et al. Quantitative dynamic contrast-enhanced MRI of pelvic and lumbar bone marrow: Effect of age and marrow fat content on pharmacokinetic parameter values. *AJR Am J Roentgenol*. 2013;200(33):W297–303.
25. Zhu JQ, Zhang L, Tang GY, et al. Vertebral blood perfusion and its likely causes: A quantitative dynamic contrast-enhanced MR imaging study of a rat osteoporosis model. *Radiology*. 2017;282:369–380.
26. Wang YX, Griffith JF, Deng M, et al. Rapid increase in marrow fat content and decrease in marrow perfusion in lumbar vertebra following bilateral oophorectomy: An MR imaging-based prospective longitudinal study. *Korean J Radiol*. 2015;16(1):154–159.
27. Song Y, Cho G, Suh JY, et al. Dynamic contrast-enhanced MRI for monitoring antiangiogenic treatment: Determination of accurate and reliable perfusion parameters in a longitudinal study of a mouse xenograft model. *Korean J Radiol*. 2013;14(4):589–596.



# Dietary curcumin and capsaicin: Relationship with hepatic oxidative stress and apoptosis in rats fed a high fat diet

Sevda Tanrıkulu-Küçük<sup>1,A,D,F</sup>, Canan Başaran-Küçükgergin<sup>2,B,C</sup>, İbrahim Söğüt<sup>3,B</sup>, Matem Tunçdemir<sup>4,B</sup>, Semra Doğru-Abbasoğlu<sup>2,A,C</sup>, Muhammed Seyithanoğlu<sup>5,A,B</sup>, Hikmet Koçak<sup>1,C-E</sup>, Yıldız Öner-İyidoğan<sup>2,A,C,D</sup>

<sup>1</sup> Department of Biochemistry, Faculty of Medicine, Istanbul Bilim University, Turkey

<sup>2</sup> Department of Biochemistry, Istanbul Faculty of Medicine, Istanbul University, Turkey

<sup>3</sup> Vocational School of Health Services, Istanbul Bilim University, Turkey

<sup>4</sup> Department of Medical Biology, Cerrahpasa Medical Faculty, Istanbul University, Turkey

<sup>5</sup> Department of Biochemistry, Faculty of Medicine, Kahramanmaraş Sütçü İmam University, Turkey

A – research concept and design; B – collection and/or assembly of data; C – data analysis and interpretation;

D – writing the article; E – critical revision of the article; F – final approval of the article

Advances in Clinical and Experimental Medicine, ISSN 1899–5276 (print), ISSN 2451–2680 (online)

*Adv Clin Exp Med.* 2019;28(8):1013–1020

## Address for correspondence

Sevda Tanrıkulu-Küçük

E-mail: sevda.kucuk@istanbulbilim.edu.tr

## Funding sources

This work was supported by the Research Fund of Istanbul University, Turkey, project No. 55331 and BEK-2017-24926.

## Conflict of interest

None declared

Received on November 2, 2017

Reviewed on December 21, 2017

Accepted on August 9, 2018

Published online on April 15, 2019

## Cite as

Tanrıkulu-Küçük S, Başaran-Küçükgergin C, Söğüt İ, et al. Dietary curcumin and capsaicin: Relationship with hepatic oxidative stress and apoptosis in rats fed a high fat diet. *Adv Clin Exp Med.* 2019;28(8):1013–1020. doi:10.17219/acem/94145

## DOI

10.17219/acem/94145

## Copyright

© 2019 by Wrocław Medical University

This is an article distributed under the terms of the Creative Commons Attribution Non-Commercial License (<http://creativecommons.org/licenses/by-nc-nd/4.0/>)

## Abstract

**Background.** Apoptosis plays a major role in fatty liver disease. High-fat diets are related to the onset of fatty liver disease and hepatic oxidant–antioxidant imbalance. Curcumin and capsaicin are somewhat beneficial in reducing hepatic triglycerides; this is most likely because they are known to downregulate reactive oxygen species (ROS) and apoptosis.

**Objectives.** The aim of this study was to investigate the effects of curcumin and capsaicin on apoptosis through the oxidative effect in an animal model of fatty liver disease.

**Material and methods.** Male Sprague Dawley rats were fed a normal control diet, a high-fat diet (HFD; 60% of total calories from fat), a HFD+curcumin (1.5 g curcumin/kg HFD), a HFD+capsaicin (0.15 g capsaicin/kg HFD), or a HFD+curcumin+capsaicin (1.5 g curcumin and 0.15 g capsaicin/kg HFD). Liver lysate levels of BAX, Bcl-2 and caspase-3 were determined via immunoblotting. Caspase-3 activity was measured with a colorimetric caspase-3 measurement kit. Total antioxidant status (TAS) and total oxidant status (TOS) were assayed using commercial kits. The generation of hepatic ROS was measured with fluorimetry. Fragmentation of DNA was detected using the TUNEL method.

**Results.** High-fat diet caused increased expression of BAX and caspase-3, as well as increased TOS and caspase-3 activity, but decreased expression of Bcl-2. HFD+curcumin+capsaicin caused decreased BAX, caspase-3, TOS, and ROS levels as compared to HFD, but increased TAS and Bcl-2. A HFD +curcumin+capsaicin also decreased the number of TUNEL-positive cells.

**Conclusions.** These results suggest that supplementation with curcumin and capsaicin balances the hepatic oxidant-antioxidant status and may have a protective role in the apoptotic process in an HFD-induced fatty liver model.

**Key words:** apoptosis, curcumin, high-fat diet, fatty liver, capsaicin

## Introduction

Apoptosis is defined as programmed cell death. It has been reported that several liver diseases, as well as liver injury, induce apoptotic pathways in hepatocytes.<sup>1</sup> Non-alcoholic fatty liver disease (NAFLD) is associated with obesity and various metabolic disorders, such as steatosis-induced apoptosis.<sup>1</sup> Hepatocyte apoptosis plays a very important role in liver injury. In order to properly treat liver diseases, the molecular mechanisms and regulating factors of apoptosis must be fully understood. Hepatocyte apoptosis correlates with liver disease severity and can indicate the progression of hepatic fibrosis.<sup>1</sup>

It has been reported that lipid peroxidation products may induce steatosis-induced apoptosis through the activation of the c-Jun N-terminal kinase (JNK) and transcription factor activated protein 1 (AP-1) signaling pathways.<sup>2</sup> A high-fat diet (HFD) may cause an increase in hepatic lipid content, and also may induce excess generation of reactive oxygen species (ROS).<sup>3</sup> The accumulation of hepatic fat causes oxidative stress and necrosis, and activates caspase-independent cell death, all of which lead to fibrosis.<sup>4,5</sup> Among the apoptotic pathways, oxidative stress plays the most important role in NAFLD by facilitating ROS generation.<sup>6</sup>

Curcumin and capsaicin are 2 ingredients of spices commonly used to enhance the taste and flavor of food; in addition, they have been shown to induce several beneficial effects in the pathogenesis of fatty liver disease.<sup>4,7,8</sup> Curcumin (1,7-Bis (4-hydroxy-3-methoxyphenyl)-1,6-heptadiene-3,5-dione, turmeric yellow, diferuloylmethane) is a natural yellow polyphenol extracted from the rhizome of turmeric (*Curcuma longa* L.; *Zingiberaceae*). It has been reported to have many positive effects on health, as it has anti-inflammatory, anti-cancer and anti-hyperlipidemic properties.<sup>4</sup> Capsaicin (8-methyl-N-vanillyl-6-nonenamide) is a major and very pungent ingredient of red pepper (*Capsicum annuum* L.; *Solanaceae*) that has been shown to have some pharmacological uses in pain relief, weight reduction, anti-cancer properties, cardiovascular effects, and gastrointestinal effects.<sup>9</sup> A few studies have reported the antioxidant and anti-inflammatory potentials of these 2 spices.<sup>10,11</sup> Again, very limited reports have experimentally demonstrated the antiapoptotic effects of curcumin and/or capsaicin.<sup>12–15</sup> However, the potential protective role of curcumin and capsaicin on the fatty liver-induced apoptotic process is still unclear. We have recently reported the beneficial influences of dietary curcumin and capsaicin on the reduction of liver fat.<sup>8</sup> In the present investigation, we specifically focused on elucidating the additive and/or synergistic effect of curcumin and capsaicin in combination on antiapoptotic and anti-inflammatory status in an experimental fatty liver model. Therefore, the aim of our current study is to examine the effects of curcumin and capsaicin on oxidant–antioxidant status and the development of apoptosis in fatty liver disease in rats fed a HFD.

## Material and methods

### Animals and diets

The experimental procedure used in this study meets the guidelines of the Animal Care and Use Committee of the University of Istanbul, Turkey (No. 133/2013). Male Sprague Dawley rats (217 ±12 g; n = 40) were obtained from the Experimental Medical Research Institute of Istanbul University. The animals were housed 4 per cage at room temperature (24–25°C) and a 12-hour dark/light cycle with free access to food and water. The rats were randomly divided into 5 equal groups: Group 1 (control group) was fed a normal control diet (standard laboratory chow, 2.6 kcal/g; MBD, Istanbul, Turkey), Group 2 (HFD group) was fed a HFD (60% of total calories from sheep fat, 3.9 kcal/g; MBD), Group 3 (HFD+CUR) received a HFD supplemented with curcumin (Product No. 820354; Merck, Darmstadt, Germany; 1.5 g curcumin/kg HFD), Group 4 (HFD+CAP) was given a HFD supplemented with capsaicin (Product No. J62865; Alfa Aesar, Karlsruhe, Germany; 0.15 g capsaicin/kg HFD), and Group 5 (HFD+CUR+CAP) received a HFD supplemented with curcumin and capsaicin (1.5 g curcumin + 0.15 g capsaicin/kg HFD) for a total of 16 weeks. The curcumin dosage was calculated based on our previous studies<sup>7</sup> and on the study of Ejaz et al.<sup>16</sup> The capsaicin dose was calculated according to the study of Kang et al.<sup>17</sup> Body weight and food intake were recorded weekly, and the average daily food consumption for each rat was calculated.<sup>8</sup> The animals were weighed at the end of the experimental period. Then, they were anesthetized with sodium pentobarbital (50 mg/kg, i.p.), sacrificed by cardiac puncture and their blood was collected into dry tubes. Liver tissues were rapidly removed, weighed, washed in ice-cold saline, and frozen at –80°C until further analysis. For TUNEL staining, liver tissues were fixed in 10% neutral formalin and embedded in paraffin.

### Liver triglycerides and total cholesterol

Liver tissue homogenate (10% w/v) was prepared in ice-cold 0.15M KCl. Tissue lipid extracts were obtained according to the procedure of Folch et al.<sup>18</sup> Hepatic liver triglycerides (TG) and total cholesterol (TC) levels were measured in lipid extracts with commercial colorimetric assay kits ((triglycerides, GPO-POD Liquid kit and Cholesterol, CHOD-POD Liquid kit; BIOLABO, Maizy, France).

### Liver total antioxidant status, total oxidant status and oxidative stress index

Rat liver tissues were weighed and homogenized in ice-cold 0.15M KCl using an Ultra Turrax T18 basic homogenizer (IKA, Wilmington, USA). The homogenate was centrifuged at 600 × g for 10 min at 4°C, and the supernatant was used for the determination of liver total antioxidant status



(TAS) and total oxidant status (TOS) levels using commercial assay kits (Rel Assay Diagnostics, Gaziantep, Turkey). Tissue TAS and TOS levels are presented as  $\mu\text{mol/L}$ . Oxidative stress index (OSI) values were calculated using the following formula:  $\text{OSI} = (\text{TOS}/\text{TAS}) \times 100$ .<sup>19</sup>

## Determination of reactive oxygen species levels

Liver ROS generation was measured using a fluorimetric assay with dichlorofluorescein.<sup>20</sup> In this assay, 1mM 2',7'-dichlorodihydrofluorescein diacetate (DCFH<sub>2</sub>-DA, Product No. D 6883; Sigma-Aldrich, St. Louis, USA) diffuses passively into the cells, and the DCFH<sub>2</sub>-DA acetate groups are cleaved by intracellular esterases, yielding intracellular 2',7'-dichlorodihydrofluorescein (DCFH<sub>2</sub>). Reactive oxygen species oxidize DCFH<sub>2</sub> to form a fluorescent compound, 2',7'-dichlorofluorescein (DCF), which can be measured using a microplate fluorimeter (Fluoroskan Ascent FL; Thermo Fisher Scientific, Inc., Waltham, USA) with an excitation of 485 nm and an emission of 538 nm. Results are expressed as relative fluorescence units (RFU).

## Hepatic caspase-3 activity

Liver tissue samples were homogenized (1/10 w/v) in lysis buffer (250 mM HEPES, pH 7.4, 25 mM CHAPS, 25 mM DTT) and then centrifuged for 20 min at 3,000 rpm (+4°C). Supernatants were collected and centrifuged twice at 14,000 rpm for 15 min each.<sup>21</sup> A colorimetric caspase-3 measurement kit (Sigma-Aldrich) was used to determine caspase-3 activities in the supernatant. This kit is based on the hydrolyzation of acetyl-Asp-Glu-Val-Asp-nitroanilide by caspase-3, which generates p-nitroaniline (pNA). The absorbance of pNA was measured at 405 nm, and results are expressed as  $\mu\text{mol pNA}/\text{min}$ .

## TUNEL assay

The terminal deoxynucleotidyl transferase-mediated dUTP nick end-labeling (TUNEL) assay is a technique that detects DNA fragmentation by labeling the terminal end of nucleic acids. This assay has also been used to confirm apoptosis of liver tissues. Herein, the TUNEL assay was performed as previously described<sup>22</sup> with the ApopTag Peroxidase In Situ Apoptosis Detection Kit (S7101-KIT; Merck Millipore, Burlington, USA). Briefly, each liver tissue slide was deparaffinized, rehydrated and treated with proteinase K (20 mg/L) for 15 min at room temperature. The endogenous peroxidase was inhibited with 3% hydrogen peroxide for 5 min, and then the slide was incubated with the TUNEL reaction mixture (containing terminal deoxynucleotidyl transferase (TdT)) in a humidified chamber at 37°C for 1 h. Then, the 3,3'-diaminobenzidine (DAB) chromogen was applied, and methyl green was used for counterstaining. The TdT was omitted from the reaction mixture as a negative control.

## Apoptotic index

Marked apoptotic cells were counted under high-power fields ( $\times 40$ ) with a light microscope (Leica DM2500; Leica Camera AG, Wetzlar, Germany). Cell nuclei stained with methyl green were considered to be healthy, while those with brown nuclear staining were considered TUNEL-positive. All TUNEL-positive cells were counted in 15 randomly selected fields by a researcher who was blinded to the identity of the samples. The average number of cells per unit area for each set of specimens in each group was calculated and compared.

## Liver caspase-3, Bax, and Bcl-2 protein expression

To detect Bax, Bcl-2, and anti-active caspase-3, livers were homogenized (10% w/v) in a buffer containing 50 mM Tris-HCl (pH 7.4), 150  $\mu\text{M}$  NaCl, 2  $\mu\text{M}$  ethylenediaminetetraacetic acid (EDTA), 8.7% glycerol, 0.5% sodium deoxycholate, 1% Triton X-100, 0.1% sodium dodecyl sulfate (SDS), and protease inhibitor cocktail (P8340; Sigma-Aldrich). The samples were then centrifuged at 600  $\times$  g for 10 min (+4°C), and then the supernatants were collected and centrifuged at 10,000  $\times$  g for 20 min (+4°C).<sup>23</sup> The total protein content of the supernatant was determined with bicinchoninic acid (BCA) protein assay (Pierce, Rockford, USA).<sup>24</sup> Equal amounts of protein (80  $\mu\text{g}/\text{well}$ ) were loaded onto 8–10% SDS-polyacrylamide gels and blotted onto polyvinylidene (PVDF) membranes (Merck Millipore). Non-specific binding sites were blocked with 5% non-fat dry milk in phosphate-buffered saline-Tween 20 (PBS-T), and then the membranes were incubated for 16 h at +4°C with primary antibodies as follows: BAX (1:200; sc-493; Santa Cruz Biotechnology, Dallas, USA), Bcl-2 (1:200; sc-492; Santa Cruz Biotechnology) and anti-active caspase-3 (1:200; JM-3015-100; MBL Life, Woburn, USA). Then, the membranes were washed with PBS-T and incubated for 1 h at room temperature with secondary antibody (goat anti-rabbit immunoglobulin (IgG) conjugated with horseradish peroxidase (HRP); 1:5,000; sc-2004; Santa Cruz Biotechnology). Immunoreactivity of the protein bands was detected with enhanced chemiluminescent autoradiography (ECL kit; Amersham Pharmacia Biotech, Piscataway, USA). Protein bands were quantified via measurement of band density with ImageJ software (National Institutes of Health, Bethesda, USA); the same pixel scale was used for all blots. An internal standard (actin; sc-1616R; Santa Cruz Biotechnology) was used to normalize the values of Bax, Bcl-2 and anti-active caspase-3.<sup>24–26</sup>

## Statistical analysis

SPSS software v. 21.0 (IMB Corp., Armonk, USA) was used to statistically analyze all biochemical parameters. GraphPad InStat DTCG (GraphPad Software, San Diego,

USA) was used to analyze data collected from the TUNEL method. All variables are expressed as means  $\pm$  standard deviation (SD). A one-way analysis of variance (ANOVA) was used to compare all values, while a Levene test was used to assess the homogeneity of the variances. Tukey's test or Tamhane's T2 test were used in cases with overall significance. Apoptotic cell counts of each group were compared using a one-way ANOVA and Tukey-Kramer test. Pearson's correlation test was used to evaluate correlations between variables. Values of  $p < 0.05$  were considered significant.

## Results

The weekly food intake of each rat was recorded throughout the 16 weeks of the study. Supplementation of HFD with curcumin and capsaicin decreased daily food intake compared with the control group and the HFD group. However, with the exception of the HFD group, the energy intakes were not significantly different between groups (Table 1). Liver TG ( $5.47 \pm 1.45 \mu\text{mol/g}$  tissue vs  $14.2 \pm 3.09 \mu\text{mol/g}$  tissue) and TC ( $3.00 \pm 0.41 \mu\text{mol/g}$  tissue vs  $5.13 \pm 1.00 \mu\text{mol/g}$  tissue) levels were significantly higher in the HFD group than in the controls. In addition, the augmentation of liver fat appeared to decrease with the individual or combined treatments of curcumin and capsaicin (Table 1).

Hepatic TOS and OSI levels increased in the HFD group compared to the control group ( $p < 0.05$  and  $p < 0.01$ , respectively), but TOS and OSI levels were decreased with supplementation of curcumin and capsaicin (HFD+CUR+CAP) when compared to the HFD group ( $p < 0.01$  for both). In addition, the TAS levels of the HFD+CUR+CAP group

were significantly increased over those of the HFD group ( $p < 0.01$ ) (Table 2).

Liver ROS generation was not affected by HFD; however, supplementation with curcumin and/or capsaicin reduced ROS levels compared with the HFD group ( $p < 0.05$ ) (Fig. 1).

The expression of the hepatic proapoptotic proteins BAX and caspase-3 significantly increased in HFD-fed rats compared to those fed a control chow ( $p < 0.01$  for both). Supplementation of the HFD with either CUR or CAP led to decreases in BAX and caspase-3 expression; however, only BAX expression was significantly lower than that of the HFD-fed rats for both CUR and CAP ( $p < 0.05$ ). There was a significant decrease in both BAX and caspase-3 protein in rats fed a HFD+CUR+CAP diet ( $p < 0.01$ ) (Fig. 2).

Hepatic caspase-3 activities increased in HFD group ( $p < 0.01$ ); this activity was significantly suppressed in the HFD+CUR+CAP group ( $p < 0.05$ ) (Fig. 3).

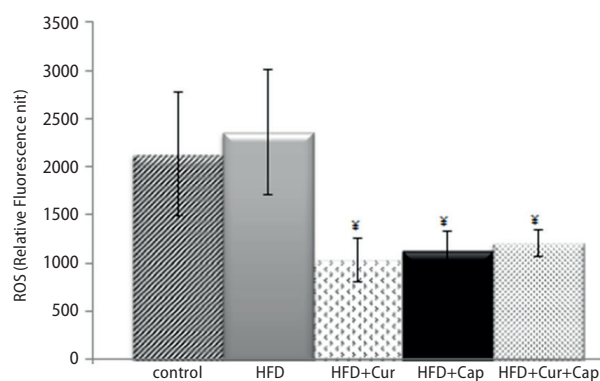


Fig. 1. Hepatic ROS levels in the experimental groups. Values are expressed as mean  $\pm$  standard deviation (SD).

‡  $p < 0.05$ , compared to the HFD group

Table 1. Daily food and energy intake, liver triglycerides (TG) and total cholesterol (TC) levels in control rats and rats fed a high-fat diet (HFD). Values are expressed as mean  $\pm$  standard deviation (SD)

Parameter	Control group (n = 8)	HFD group (n = 8)	HFD+CUR group (n = 8)	HFD+CAP group (n = 8)	HFD+CUR+CAP group (n = 8)
Daily food intake [g/rat]	21.1 $\pm$ 1.25	17.2 $\pm$ 2.10 <sup>a3</sup>	13.4 $\pm$ 1.30 <sup>a3,b3</sup>	14.5 $\pm$ 2.32 <sup>a3,b1</sup>	14.4 $\pm$ 1.82 <sup>a3,b2</sup>
Daily energy intake [kcal/rat]	54.8 $\pm$ 3.26	68.3 $\pm$ 8.34 <sup>a3</sup>	53.2 $\pm$ 5.17 <sup>b3</sup>	57.6 $\pm$ 9.23 <sup>b1</sup>	57.3 $\pm$ 7.22 <sup>b2</sup>
Liver TG [ $\mu\text{mol/g}$ tissue]	5.47 $\pm$ 1.45	14.2 $\pm$ 3.09 <sup>a3</sup>	6.38 $\pm$ 1.76 <sup>b3</sup>	4.54 $\pm$ 1.10 <sup>b3</sup>	6.09 $\pm$ 0.82 <sup>b3</sup>
Liver TC [ $\mu\text{mol/g}$ tissue]	3.00 $\pm$ 0.41	5.13 $\pm$ 1.00 <sup>a2</sup>	2.45 $\pm$ 0.27 <sup>b3</sup>	1.86 $\pm$ 0.51 <sup>b3</sup>	2.96 $\pm$ 0.44 <sup>b2</sup>

<sup>a1</sup> $p \leq 0.05$ , <sup>a2</sup> $p \leq 0.01$ , <sup>a3</sup> $p \leq 0.001$ ; compared to the control group.

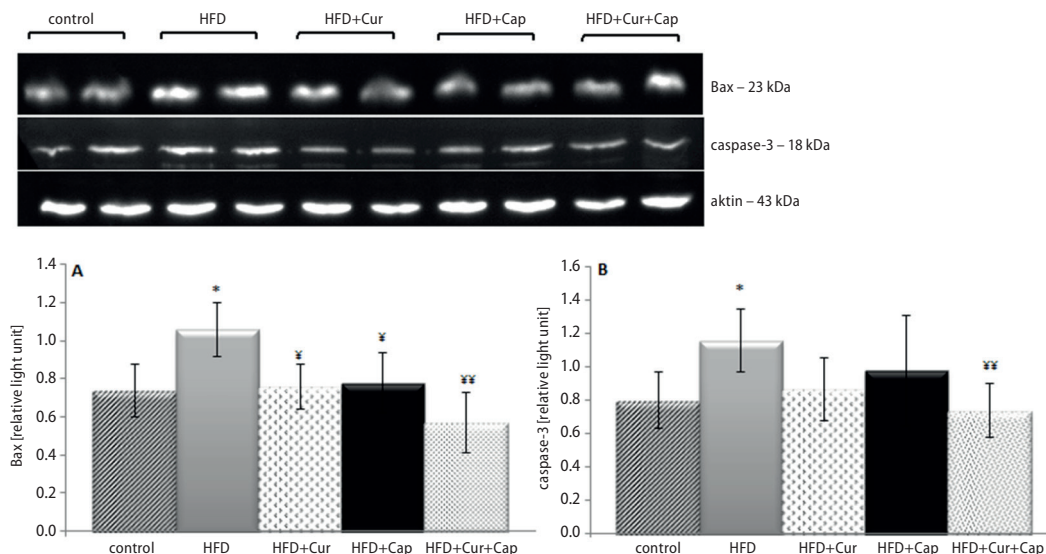
<sup>b1</sup> $p \leq 0.05$ , <sup>b2</sup> $p \leq 0.01$ , <sup>b3</sup> $p \leq 0.001$ ; compared to the HFD group.

Table 2. Hepatic total oxidant status (TOS), total antioxidant status (TAS) and oxidative stress index (OSI) in control rats and rats fed a high-fat diet (HFD). Values are expressed as mean  $\pm$  standard deviation (SD)

Parameter	Control group (n = 8)	HFD group (n = 8)	HFD+CUR group (n = 8)	HFD+CAP group (n = 8)	HFD+CUR+CAP group (n = 8)
TOS [ $\mu\text{mol/L}$ ]	17.7 $\pm$ 2.70	22.9 $\pm$ 2.88 <sup>a2</sup>	20.8 $\pm$ 2.71	19.7 $\pm$ 1.92	19.1 $\pm$ 1.71 <sup>b1</sup>
TAS [ $\mu\text{mol/L}$ ]	1,734 $\pm$ 105.2	1,630 $\pm$ 91.4	1,818 $\pm$ 209	1,698 $\pm$ 58.8	1,912 $\pm$ 96.0 <sup>b1</sup>
OSI [arbitrary units]	1.01 $\pm$ 0.15	1.42 $\pm$ 0.23 <sup>a1</sup>	1.15 $\pm$ 0.20	1.16 $\pm$ 0.13	1.00 $\pm$ 0.07 <sup>b1</sup>

<sup>a1</sup> $p \leq 0.05$ , <sup>a2</sup> $p \leq 0.01$ ; compared to the control group.

<sup>b1</sup> $p \leq 0.01$ ; compared to the HFD group.



**Fig. 2.** Band density analysis of Bax (A) and caspase-3 (B) in liver sections of the experimental groups. Values are expressed as mean ± standard deviation (SD)

\*  $p < 0.01$ , compared to the control group; ‡  $p < 0.05$ , compared to the HFD group.

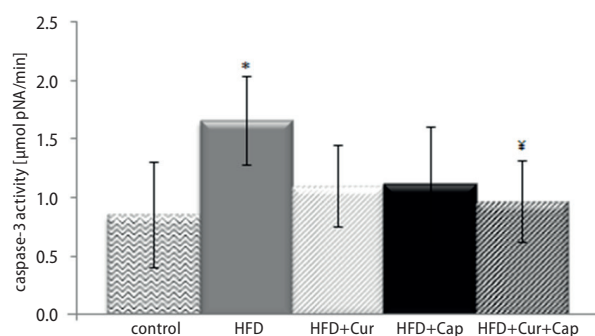


**Fig. 3.** Hepatic caspase-3 activities in the experimental groups. Values are expressed as mean ± standard deviation (SD)

\*  $p < 0.01$ ; compared to the control group; ‡  $p < 0.05$ , compared to the HFD group.

The expression of the antiapoptotic protein Bcl-2 is shown in Fig. 4. The HFD+CAP group had increased Bcl-2 expression as compared to the HFD group ( $p < 0.05$ ); however, Bcl-2 expression was not altered by curcumin treatment (Fig. 4).

As indicated in Fig. 5, there were few TUNEL-positive cells in the control group. The number of TUNEL-positive cells significantly increased in the HFD group compared to the controls ( $p < 0.001$ ). In addition, the number of TUNEL-positive cells in the HFD+CUR+CAP group was similar to that of the control group (Fig. 5E).

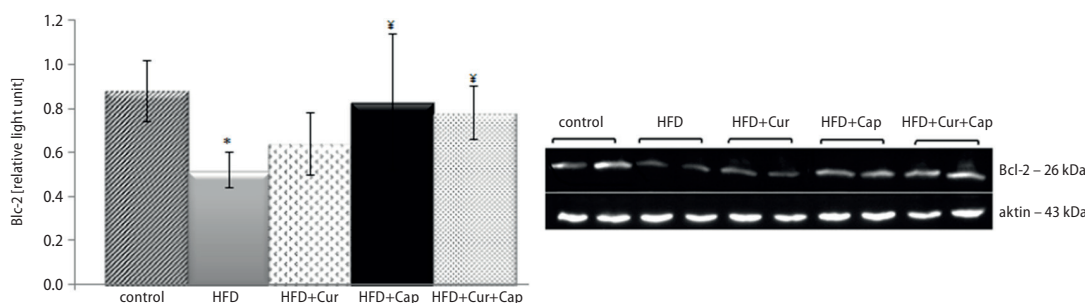


**Fig. 4.** Band density analysis of Bcl-2 expressions. Values are expressed as mean ± standard deviation (SD)

\*  $p < 0.01$ , compared to the control group; ‡  $p < 0.05$ , compared to the HFD group.

The expression of hepatic BAX was negatively correlated with the expression of hepatic Bcl-2 ( $r = -0.565$ ,  $p = 0.004$ ), and was positively correlated with hepatic OSI levels and caspase-3 activities ( $r = 0.477$ ,  $p = 0.018$  and  $r = 0.518$ ,  $p = 0.010$ , respectively). The expression of antiapoptotic Bcl-2 was negatively correlated with the oxidative parameters TOS and OSI ( $r = -0.447$ ,  $p = 0.022$  and  $r = -0.528$ ,  $p = 0.006$ , respectively; Fig. 6A). The expression of hepatic caspase-3 was positively correlated with hepatic caspase-3 activity ( $r = 0.428$ ,  $p = 0.029$ ). Hepatic ROS levels were positively correlated with the expression of hepatic BAX ( $r = 0.492$ ,  $p = 0.011$ ; Fig. 6B) and negatively correlated with TAS ( $r = -0.441$ ,  $p = 0.010$ ).

## Discussion

A HFD has been shown to aid in hepatic fat storage, which is a symptom of fatty liver disease.<sup>27</sup> HFD-induced fatty liver disease is thought to be the cause of some metabolic and biochemical disorders as well as hepatocyte apoptosis.<sup>6,28</sup> Apoptotic cells exhibit various biochemical changes, such as proenzyme activation, protein cleavage or cross-linking, and DNA breakdown.<sup>29</sup> Oxidative stress plays an important role in inducing apoptosis, as well as in the progression of liver injury.<sup>1</sup>

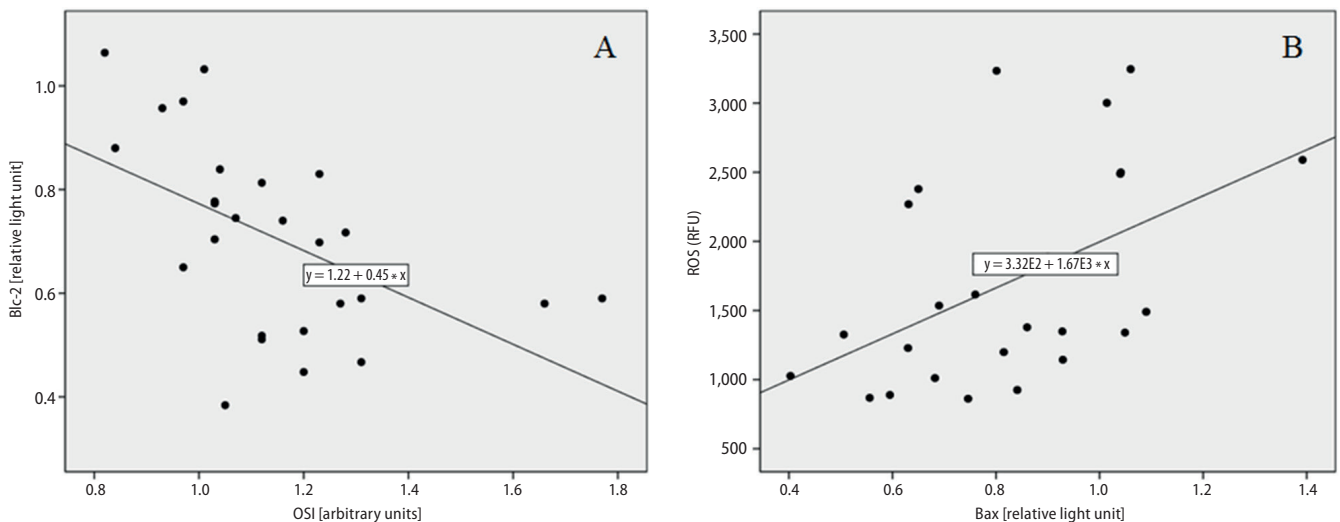
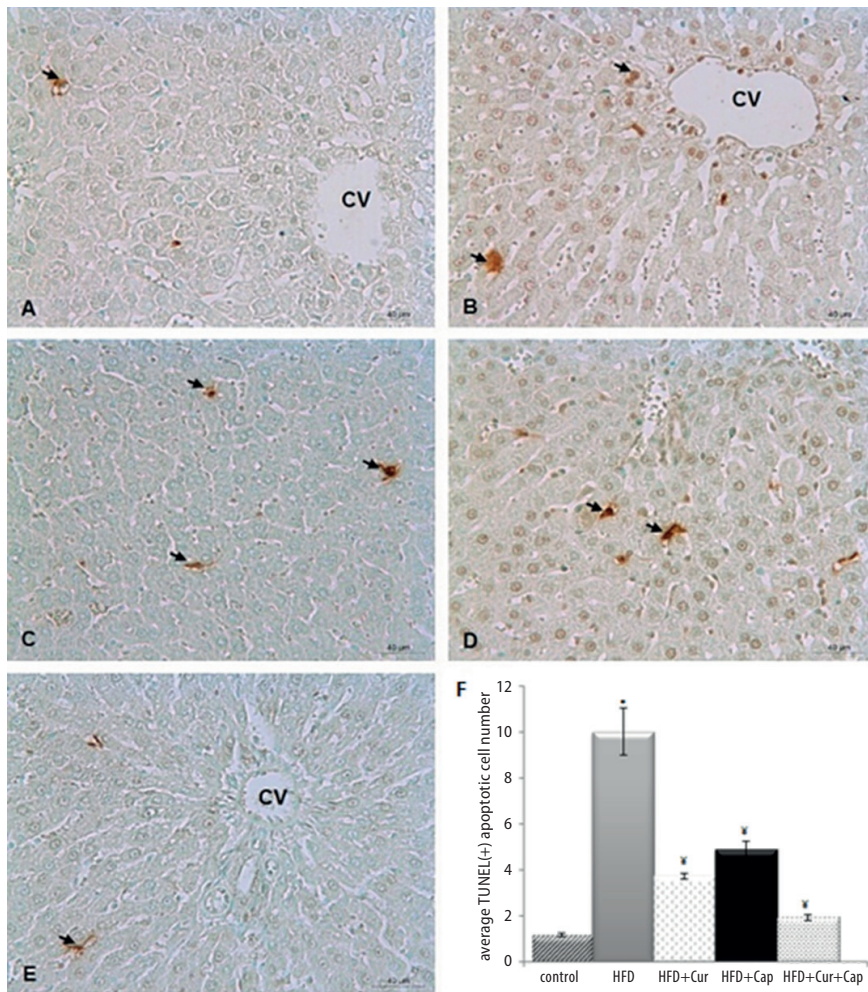


**Fig. 6.** A – regression between hepatic Bcl-2 protein expression and oxidative stress index (OSI) levels ( $n = 32$ ;  $r = 0.528$ ,  $p = 0.006$ ). B – regression between hepatic Bax protein expression and ROS levels in all experimental groups ( $n = 32$ ;  $r = 0.492$ ,  $p = 0.011$ )

In the present study, curcumin and capsaicin were administered either together with the HFD or alone. High-fat diet was premixed with curcumin (1.5 g/kg HFD) and/or capsaicin (0.15 g/kg HFD) and the pellets composed were given to the animals. The bioavailability of curcumin

was reported to be approx. 60–66% of the given dose and after 12 days of oral administration of 400 mg curcumin to rats, respectable amounts of curcumin metabolites were present in their tissues.<sup>30</sup> It was demonstrated that some substances such as alkaloid piperine, a constituent from

black pepper, increased the serum bioavailability of curcumin by 2,000%.<sup>31</sup> Furthermore; it was found that the bioavailability of curcumin was increased 7–8-fold when dissolved in oil or mixed with fatty diet.<sup>32</sup> It was shown that dietary capsaicin administration is rapidly and directly absorbed by the stomach and the intestine. Absorbed capsaicin ranges depend from 50% to 90% associated with the experimental model used.<sup>33</sup> Our experimental diet has been designed in accordance with these studies.

It was recently reported that dietary curcumin and capsaicin have antioxidative and hepatic lipid-reducing effects in rats fed a HFD.<sup>8,11</sup> However, the effect of curcumin and capsaicin on the prevention of hepatocyte apoptosis in fatty liver disease is not clear. In the present study, treatment with dietary curcumin and capsaicin reduced hepatic lipid levels induced by the consumption of HFD. Rats fed a HFD had a nearly 2.6-fold increase in liver TG accumulation over the controls; however, this level returned to that of the control group when these rats were given curcumin or capsaicin, either individually or in combination.

The expression of the hepatic pro-apoptotic proteins BAX and caspase-3 increased, as did caspase-3 activity, while hepatic anti-apoptotic protein Bcl-2 decreased, in rats fed a HFD. Treatment of combined curcumin and capsaicin reversed these effects. Caspase-3 is reported to be the most important enzyme that is activated by any of the initiator caspases (caspase-8, caspase-9 or caspase-10).<sup>34</sup> Caspase-3 also induces the cytoskeletal degeneration of apoptotic cells.<sup>34</sup> In the current study, we measured caspase-3 with biochemical and immunoblotting, and both methods revealed that caspase-3 was suppressed with supplementation of curcumin and capsaicin combination. These 2 spices may prevent apoptosis by inhibiting pro-apoptotic proteins and by inducing anti-apoptotic progression. This hypothesis has been supported by other researchers. In the study of Yu et al., capsaicin inhibits fibrogenesis by suppressing cell proliferation and activation in cultured hepatic stellate cells (HSCs).<sup>35</sup> Galaly et al. reported that curcumin prevents liver injury by regulating apoptosis.<sup>36</sup> Li et al. revealed that chronic dietary capsaicin prevents fatty liver disease by inducing peroxisome proliferator-activated receptor  $\delta$  (PPAR  $\delta$ )-dependent autophagy.<sup>10</sup> Further, Becatti et al. demonstrated that curcumin and capsaicin have inhibitory apoptotic effects, as they increased phosphorylation of ERK in perilesional skin keratinocytes.<sup>14</sup>

Many studies have reported that an increase or decrease in cell death by apoptosis plays an important role in the pathogenesis of many diseases.<sup>37,38</sup> Apoptotic cells are commonly detected around injured tissue. The TUNEL method determines the number of apoptotic cells and the enzymatic endonuclease cleavage products end-labeling the DNA strand breaks.<sup>39</sup> In our current study, the HFD group had a significantly higher number of apoptotic cells than the controls. However, the individual or combined treatment with curcumin and/or capsaicin decreased the number of TUNEL-positive cells compared to the HFD group.

Of note, the protective effect of the combination of curcumin and capsaicin on cell death seems to be more effective than when they are used individually.

Recently published data has shown that mitochondrial dysfunction and cellular stress derived from oxidative stress play an important role as risk factors for the development of hepatocyte apoptosis in NAFLD.<sup>1,6</sup> Mitochondrial dysfunction may also associate with the overproduction of ROS and oxidative stress.<sup>6</sup> In the present study, HFD did not change ROS production. However, in a previous study, we showed that individual or combined treatment with curcumin and/or capsaicin lowered ROS levels.<sup>7</sup> In the current study, ROS levels were measured using a DCFH<sub>2</sub>-DA probe, which has been shown to react with hydrogen peroxide (H<sub>2</sub>O<sub>2</sub>), peroxy nitrite, lipid hydroperoxides, and the superoxide anion.<sup>40</sup> Herein, we found that TOS levels were higher in the HFD group compared to controls. The contradictions in our ROS and TOS measurements may be due to the variations in methodology. The TOS analysis is likely a more sensitive and favorable method for the determination of OSI in a fatty liver experimental model. In the present study, HFD induced OSI levels, which decreased with curcumin and capsaicin treatment. On the other hand, TAS levels were higher with curcumin and capsaicin; this may be due to an adaptive response to the overproduction of TOS. This finding supports that capsaicin, like curcumin, has a direct effect as a radical scavenger. Similar to our results, the study of Joe et al. reported that curcumin and capsaicin diminished the production of ROS in rat peritoneal macrophages.<sup>15</sup> The TAS assay is based on the principle that non-enzymatic antioxidants in the liver tissue reduce the dark blue-green colored 2,2'-azino-bis (3-ethylbenzothiazoline-6-sulphonic acid – ABTS) radical to its colorless reduced form. Both capsaicin and curcumin appear to balance oxidant-antioxidant status by simultaneous regulation in free radical generation and antioxidative defense augmentation.

Based on our current results, curcumin and capsaicin appear to protect HFD-induced liver injury in rats by inhibiting hepatic oxidative stress and apoptosis. The significant negative correlation between anti-apoptotic protein Bcl-2 and OSI levels confirms this assumption. In summary, curcumin and capsaicin exhibit protective effects on HFD-induced liver injury and suppress oxidative stress-related apoptosis. The combination of the 2 spices might offer an alternative choice for protection from fatty liver injury.

## References

1. Cao L, Quan XB, Zeng WJ, Yang XO, Wang MJ. Mechanism of hepatocyte apoptosis. *J Cell Death*. 2016;9:19–29.
2. Pessayre D, Mansouri A, Fromenty B. Nonalcoholic steatosis and steatohepatitis. V. Mitochondrial dysfunction in steatohepatitis. *Am J Physiol Gastrointest Liver Physiol*. 2002;282(2):193–199.
3. Dandona P, Aljada A, Chaudhuri A, Mohanty P, Garg R. Metabolic syndrome: A comprehensive perspective based on interactions between obesity diabetes and inflammation. *Circulation*. 2005;111(11):1448–1454.

4. Vera-Ramirez L, Pérez-Lopez P, Varela-Lopez A, Ramirez-Tortosa M, Battino M, Quiles JL. Curcumin and liver disease. *Biofactors*. 2013; 39(1):88–100.
5. Yuan L, Kaplowitz N. Glutathione in liver diseases and hepatotoxicity. *Mol Aspects Med*. 2009;30(1–2):29–41.
6. Paradies G, Paradies V, Ruggiero FM, Petrosillo G. Oxidative stress cardioprotein and mitochondrial dysfunction in nonalcoholic fatty liver disease. *World J Gastroenterol*. 2014;20(39):14205–14218.
7. Öner-İyidoğan Y, Tanrikulu-Küçük S, Seyithanoğlu M, et al. Effect of curcumin on hepatic heme oxygenase 1 expression in high fat diet fed rats: Is there a triangular relationship? *Can J Physiol Pharmacol*. 2014;92(10):805–812.
8. Seyithanoğlu M, Öner-İyidoğan Y, Doğru-Abbasoğlu S, et al. The effect of dietary curcumin and capsaicin on hepatic fetuin-A expression and fat accumulation in rats fed on a high-fat diet. *Arch Physiol Biochem*. 2016;122(2):94–102.
9. Sharma SK, Vij AS, Sharma S. Mechanisms and clinical uses of capsaicin. *Eur J Pharm*. 2013;720(1–3):55–62.
10. Li Q, Li L, Wang F, et al. Dietary capsaicin prevents nonalcoholic fatty liver disease through transient receptor potential vanilloid 1-mediated peroxisome proliferator-activated receptor  $\delta$  activation. *Pflugers Arch – Eur J Physiol*. 2013;465(9):1303–1316.
11. Manjunatha H, Srinivasan K. Hypolipidemic and antioxidant effects of curcumin and capsaicin in high-fat-fed rats. *Can J Physiol Pharmacol*. 2007;85(6):588–596.
12. Toydemir T, Kanter M, Erboga M, Oguz S, Erenoglu C. Antioxidative, antiapoptotic, and proliferative effect of curcumin on liver regeneration after partial hepatectomy in rats. *Toxicol Ind Health*. 2015;31(2): 162–172.
13. Wang L, Yisong Lv, Huixiang Y, Yin L, Shang J. Curcumin prevents the non-alcoholic fatty hepatitis via mitochondria protection and apoptosis reduction. *Int J Clin Exp Pathol*. 2015;8(9):11503–11509.
14. Becatti M, Prignano F, Fiorillo C, et al. The involvement of Smac/DIABLO p53 NF- $\kappa$ B and MAPK pathways in apoptosis of keratinocytes from perilesional vitiligo skin: Protective effects of curcumin and capsaicin. *Antioxid Redox Signal*. 2010;13(9):1309–1321.
15. Joe B, Lokesh BR. Role of capsaicin curcumin and dietary n-3 fatty acids in lowering the generation of reactive oxygen species in rat peritoneal macrophages. *Biochim Biophys Acta*. 1994;1224(2):255–263.
16. Ejaz A, Wu D, Kwan P, Meydani M. Curcumin inhibits adipogenesis in 3T3-L1 adipocytes and angiogenesis and obesity in C57/BL mice. *J Nutr*. 2009;139(5):919–925.
17. Kang JH, Tsuyoshi G, Le Ngoc H, et al. Dietary capsaicin attenuates metabolic dysregulation in genetically obese diabetic mice. *J Med Food*. 2011;14(3):310–315.
18. Folch J, Lees M, Stanley GHS. A simple method for the isolation and purification of total lipids from animal tissues. *J Biol Chem*. 1957; 226(1):497–509.
19. Aycicek A, Iscan A, Erel O, Akcali M, Selek S. Total antioxidant/oxidant status in meningism and meningitis. *Pediatr Neurol*. 2006;35(6): 382–386.
20. Wang H, Joseph JA. Quantifying cellular oxidative stress by dichlorofluorescein assay using microplate reader. *Free Radic Biol Med*. 1999; 27(5–6):612–616.
21. Kartkaya K, Kanbak K, Oglakci A, Burukoglu D, Ozer MC. Protective effect of calpain inhibitor N-acetyl-L-leucyl-L-leucyl-L-norleucinal on acute alcohol consumption related cardiomyopathy. *Mol Biol Rep*. 2014;41(10):6743–6753.
22. Tunçdemir M, Ertürküne SP, Özçelik D. Investigation of lipid peroxidation and antiapoptotic effects of zinc against liver damage in diabetic rats. *Hum Exp Toxicol*. 2017;36(8):813–822.
23. Peng Y, Rideout DA, Rakita SS, Gower WR Jr, You M, Murr MM. Does LKB1 mediate activation of hepatic AMP-protein kinase [AMPK] and sirtuin1 [SIRT1] after Roux-en-Y gastric bypass in obese rats? *J Gastrointest Surg*. 2010;14(2):221–228.
24. Liu ES, Ye YN, Shin VY, et al. Cigarette smoke exposure increases ulcerative colitis-associated colonic adenoma formation in mice. *Carcinogenesis*. 2003;24(8):1407–1413.
25. Laemmli UK. Cleavage of structural proteins during the assembly of the head of bacteriophage T4. *Nature*. 1970;227(5259):680–685.
26. Soeda J, Miyagawa S, Sano K, Masumoto J, Taniguchi S, Kawasaki S. Cytochrome c release into cytosol with subsequent caspase activation during warm ischemia in rat liver. *Am J Physiol Gastrointest Liver Physiol*. 2001;281(4):1115–1123.
27. Donnelly KL, Smith CI, Schwarzenberg SJ, Jessurun J, Boldt MD, Parks EJ. Sources of fatty acids stored in liver and secreted via lipoproteins in patients with nonalcoholic fatty liver disease. *J Clin Invest*. 2005;115(5):1343–1351.
28. Chiang DJ, McCullough AJ. The impact of obesity and metabolic syndrome on alcoholic liver disease. *Clin Liver Dis*. 2014;18(1):157–163.
29. Hengartner MO. The biochemistry of apoptosis. *Nature*. 2000; 407(6805):770–776.
30. Ravindranath V, Chandrasekhara N. Metabolism of curcumin studies with [3H] curcumin. *Toxicology*. 1981;22(4):337–344.
31. Shoba G, Joy D, Joseph T, Majeed M, Rajendran R, Srinivas PS. Influence of piperine on the pharmacokinetics of curcumin in animals and human volunteers. *Planta Med*. 1998;64(4):353–356.
32. Anand P, Kunnumakkara AB, Newman RA, Aggarwal BB. Bioavailability of curcumin: Problems and promises. *Mol Pharmaceutics*. 2009;4(6): 807–818.
33. Rollyson WD, Stover CA, Brown KC, et al. Bioavailability of capsaicin and its implications for drug delivery. *J Control Release*. 2014;196: 96–105.
34. Elmore S. Apoptosis: A review of programmed cell death. *Toxicol Pathol*. 2007;35(4):495–516.
35. Yu FX, Teng YY, Zhu QD, Zhang QY, Tang YH. Inhibitory effects of capsaicin on hepatic stellate cells and liver fibrosis. *Biochem Cell Biol*. 2014;92(5):406–412.
36. Galaly SR, Ahmed OM, Mahmoud AM. Thymoquinone and curcumin prevent gentamicin-induced liver injury by attenuating oxidative stress inflammation and apoptosis. *J Physiol Pharmacol*. 2014;65(6): 823–832.
37. Thompson CB. Apoptosis in the pathogenesis and treatment of disease. *Science*. 1995;267(5203):1456–1462.
38. Truong-Tran AQ, Grosser D, Ruffin RE. Apoptosis in the normal and inflamed airway epithelium: Role of zinc in epithelial protection and procaspase-3 regulation. *Biochem Pharmacol*. 2003;66(8):1459–1468.
39. Kressel M, Groscurth P. Distinction of apoptotic and necrotic cell death by in situ labelling of fragmented DNA. *Cell Tissue Res*. 1994; 278(3):549–556.
40. Dikalov SI, Li W, Mehranpour P, Wang SS, Zafari AM. Production of extracellular superoxide by human lymphoblast cell lines: Comparison of electron spin resonance techniques and cytochrome C reduction assay. *Biochem Pharmacol*. 2007;73(7):972–980.

# The radiological evaluation of the nasal cavity, conchae and nasal septum volumes by stereological method: A retrospective cone-beam computed tomography study

Begumhan Turhan<sup>1,A-E</sup>, Piraye Kervancioglu<sup>2,A,C-E</sup>, Eda Didem Yalcin<sup>3,A-D</sup>

<sup>1</sup> Department of Physiotherapy and Rehabilitation, Faculty of Health Sciences, Hasan Kalyoncu University, Gaziantep, Turkey

<sup>2</sup> Department of Anatomy, Faculty of Medicine, Gaziantep University, Turkey

<sup>3</sup> Department of Dentomaxillofacial Radiology, Faculty of Dentistry, Gaziantep University, Turkey

A – research concept and design; B – collection and/or assembly of data; C – data analysis and interpretation;

D – writing the article; E – critical revision of the article; F – final approval of the article

Advances in Clinical and Experimental Medicine, ISSN 1899–5276 (print), ISSN 2451–2680 (online)

*Adv Clin Exp Med.* 2019;28(8):1021–1026

## Address for correspondence

Begumhan Turhan

E-mail: begum.aliomanoglu@hku.edu.tr

## Funding sources

None declared

## Conflict of interest

None declared

Received on July 27, 2018

Reviewed on September 27, 2018

Accepted on October 15, 2018

Published online on April 13, 2019

## Abstract

**Background.** The nasal cavity (NC) is the entrance to the respiratory system. Many studies have been conducted on the structure, function and volume of the NC. Only a few studies were performed assessing the volumetric values of NC and conchae.

**Objectives.** The aim of this study was to evaluate the volumetric measurements of the NC, conchae and nasal septum using the stereological method.

**Material and methods.** Cone-beam computed tomography (CBCT) images of 200 individuals (100 females and 100 males) aged 8–59 years were retrospectively evaluated. Inferior nasal concha and middle nasal concha, NC and nasal septum volumes were measured on these images. Measurements were made using point counting method, which is based on the Cavalieri principle. The mean values of the measured structures for 2 age groups and for each gender were obtained. Differences between the groups and genders of all parameters were examined. The volume fractions of measured volumes were calculated.

**Results.** The mean volumes of the nasal septum, left and right NC, left and right inferior nasal conchae, and left and right middle nasal conchae were  $4.99 \pm 1.51 \text{ cm}^3$ ,  $7.44 \pm 2.93 \text{ cm}^3$ ,  $7.68 \pm 2.99 \text{ cm}^3$ ,  $3.10 \pm 1.11 \text{ cm}^3$ ,  $3.04 \pm 1.02 \text{ cm}^3$ ,  $1.32 \pm 0.56 \text{ cm}^3$ , and  $1.28 \pm 0.49 \text{ cm}^3$ , respectively. Gender and age differences were statistically significant in all volumes ( $p < 0.05$ ).

**Conclusions.** The data obtained in this study may assist clinicians in planning treatment, assessing the treatment results of pathological conditions within the NC, and help surgeons in preoperational and postoperational evaluations, especially in dentistry, otorhinolaryngology and plastic surgery.

**Key words:** Cavalieri principle, stereology, nasal cavity volume, cone-beam computed tomography

## Cite as

Turhan B, Kervancioglu P, Yalcin ED. The radiological evaluation of the nasal cavity, conchae and nasal septum volumes by stereological method: A retrospective cone-beam computed tomography study. *Adv Clin Exp Med.* 2019;28(8):1021–1026. doi:10.17219/acem/98960

## DOI

10.17219/acem/98960

## Copyright

© 2019 by Wrocław Medical University

This is an article distributed under the terms of the Creative Commons Attribution Non-Commercial License (<http://creativecommons.org/licenses/by-nc-nd/4.0/>)

## Introduction

The nasal cavity (NC) is the first part of the respiratory system. It opens posteriorly into the nasopharynx through the choanae and the anterior openings are nares. The NC is divided into 2 parts with a compartment which is called the nasal septum. Conchae are prominent bony structures on both lateral walls of the NC, which are covered with mucosa. Also, the conchae are dynamic structures because the area where they are located has the thickest mucous membrane of the NC and intense vascularization. The dynamic nature of the conchae allows the air flow rate and the amount of air to be adjusted.<sup>6,26,27</sup> The volumes of the mentioned structures can be calculated with cross-sectional tomography images using the stereological methods.

Stereological methods provide numerical data, such as volumes, surface areas, as well as densities and lengths of structures objectively and efficiently.<sup>10,16</sup> The Cavalieri principle, a stereological method, is effective in volumetric measurements of anatomical structures. In this principle, parallel and equally thick sections of a structure are taken, the total of section areas multiply by the thickness of section and the volume of the structure is calculated. It is accepted that the Cavalieri principle is the gold standard and provides realistic measurements.<sup>1,2</sup>

The sectional images obtained with conventional computed tomography (CT) and magnetic resonance imaging (MRI) can be used in the calculation of the volume of a structure using the Cavalieri principle.<sup>13</sup> There are only few quantitative studies of NC volumetric analysis performed with cone-beam computed tomography (CBCT).

The most important advantage of CBCT is that the practitioner can obtain 3-dimensional images in sagittal, axial and coronal planes. Three-dimensional reconstruction of CBCT images is also possible. This imaging technique provides valuable information to clinicians and researchers.<sup>23,31</sup>

There is no published study about analyzing the volumes of the NC, conchae and nasal septum using CBCT images with stereological method. In this study, we aimed to calculate the volumes of all these structures on CBCT images with the stereological method.

## Material and methods

### Samples

Patients, admitted to Gaziantep University Faculty of Dentistry in Department of Dentomaxillofacial Radiology for computed tomography examination between January 2015 and February 2017, were retrospectively evaluated. All of the patients had been referred for the diagnosis and treatment planning because of different problems involving the dentomaxillofacial region. All CBCT images were

obtained in the sitting position (scanning time: 14–18 s, collimation height: 13 cm and voxel size: 0.4 mm) using the same device (Planmeca ProMax 3D Mid; Planmeca, Helsinki, Finland). Age groups were established in order to show the differences between the measurements of adults and children. The age limit of 18 years was taken into account which is important for the development and the rapid growth. Images on axial, coronal and sagittal planes of 100 female (50 adults, 50 under 18 years of age) and 100 male (50 adults, 50 under 18 years of age) individuals without craniofacial anomalies and artifacts were evaluated (Fig. 1).

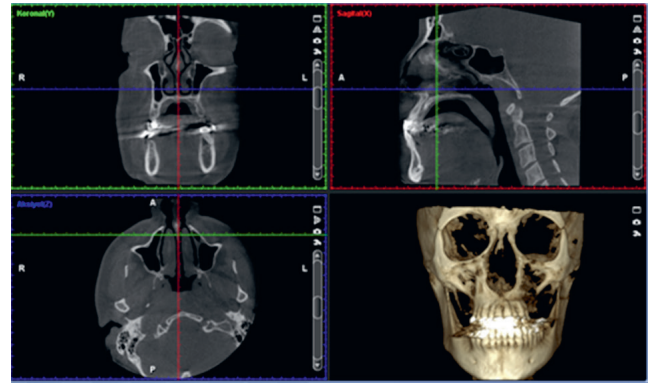


Fig. 1. Display of structures – cone-beam computed tomography (CBCT) in sagittal, axial and coronal planes and 3D reformatted image

### Procedures

A computer-assisted stereological analysis system (Stereoinvestigator v. 8.0, MicroBrightField Bioscience, Williston, USA) was used for the measurements. Ethical approval was obtained from the ethical committee of Gaziantep University (ethics committee decision No: 111/6, date of approval: 12.02.2016).

Volumetric estimations were determined on the coronal images using point-counting (Cavalieri method) approach within stereological methods. All measurements were performed by the same researcher. The volumes of the right and left nasal cavities (RNCV and LNCV) were calculated from the air-filled areas, except for the soft tissue and bony structures. The right and left inferior nasal conchae volumes (RINCV and LINCVCV), right and left middle nasal conchae volumes (RMNCV and LMNCV) and nasal septum volume (NSV) were calculated from the bony structures and the soft tissue lying over them (Fig. 2).

The volume fraction (Vv) representing the proportion of a component in the whole structure was calculated. The volume ratio of each component to the total volume (TV) was determined as a percentage (%).

The volume fraction formula can be written as follows:

$$Vv(a, b) = \frac{\sum a}{\sum b} \times 100$$

(a: each of the components, b: total volume)<sup>17</sup>



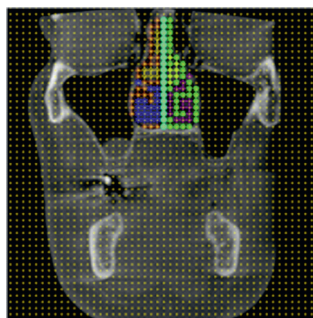


Fig. 2. Calculating the volumes of structures using point counting method

We estimated the volume fraction of the middle nasal conchae, inferior nasal conchae and nasal septum within the TV (RINCV + LINCVC + RMNCVC + LMNCVC + NSV + RNCV + LNCV) with the volume fraction approach, i.e., the MNC volume within the TV volume using the following formula:

$$V_v \text{ (middle nasal conchae, total volume)} = \frac{\sum \text{middle nasal conchae}}{\sum \text{total volume}} \times 100$$

### Statistical analysis

The data was evaluated using SPSS v. 22.0 for Windows (IBM Corp., Armonk, USA) and by analyzing descriptive statistics (frequency, mean and standard deviation (SD)). Before the statistical analysis, Shapiro-Wilk test was used to test for normal distribution of data. All continuous variables were normally distributed. Independent sample t-tests were used to compare the groups. A  $p < 0.05$  was considered statistically significant.

### Results

The mean age of all individuals, females and males was  $26.00 \pm 15.34$ ,  $24.80 \pm 14.69$  and  $27.21 \pm 15.95$ , respectively (Table 1).

Mean RNCV, LNCV, RINCV, LINCVC, RMNCVC, LMNCVC, and NS values of all subjects were  $7.68 \pm 2.99 \text{ cm}^3$ ,  $7.44 \pm 2.93 \text{ cm}^3$ ,  $3.04 \pm 1.02 \text{ cm}^3$ ,  $3.10 \pm 1.11 \text{ cm}^3$ ,  $1.28 \pm 0.49 \text{ cm}^3$ ,  $1.32 \pm 0.56 \text{ cm}^3$ , and  $4.99 \pm 1.51 \text{ cm}^3$ , respectively.

The mean volumes of measured structures of female and male subjects are represented in Table 2. The NC and nasal septum volumes of males were larger than those of females ( $p < 0.05$ ). On the other hand, there was a significant

Table 2. Mean volumes of structures in different gender (n = 200 for each structure)

Structure	Males <sup>a</sup> [cm <sup>3</sup> ]	Females <sup>a</sup> [cm <sup>3</sup> ]	p-value <sup>b</sup>
RNC [cm <sup>3</sup> ]	9.24 ± 2.86	6.13 ± 2.22	0.001
LNC [cm <sup>3</sup> ]	8.78 ± 3.00	6.09 ± 2.17	0.001
RINC [cm <sup>3</sup> ]	3.42 ± 0.95	2.67 ± 0.95	0.001
LINC [cm <sup>3</sup> ]	3.44 ± 1.11	2.76 ± 1.01	0.001
RMNC [cm <sup>3</sup> ]	1.41 ± 0.47	1.14 ± 0.46	0.001
LMNC [cm <sup>3</sup> ]	1.43 ± 0.54	1.21 ± 0.55	0.004
NS [cm <sup>3</sup> ]	5.69 ± 1.05	4.29 ± 1.57	0.001

<sup>a</sup> Values are given as mean ± standard deviation (SD); <sup>b</sup> statistical difference between genders ( $p < 0.05$ : significant); RNC – right nasal cavity; LC – left nasal cavity; RINC – right inferior nasal concha; LINC – left inferior nasal concha; RMNC – right medial nasal concha; LMNC – left medial nasal concha; NS – nasal septum.

Table 3. Mean volumes of structures in adults and children

Structure	Adults <sup>a</sup> (>18 years) (n = 100)	Children <sup>a</sup> (≤18 years) (n = 100)	p-value <sup>b</sup>
RNC [cm <sup>3</sup> ]	9.08 ± 3.17	6.28 ± 2.00	0.001
LNC [cm <sup>3</sup> ]	8.79 ± 3.11	6.08 ± 1.98	0.001
RINC [cm <sup>3</sup> ]	3.36 ± 0.93	2.73 ± 1.01	0.001
LINC [cm <sup>3</sup> ]	3.51 ± 0.96	2.68 ± 1.10	0.001
RMNC [cm <sup>3</sup> ]	1.49 ± 0.48	1.15 ± 0.57	0.001
LMNC [cm <sup>3</sup> ]	1.43 ± 0.47	1.12 ± 0.46	0.001
NS [cm <sup>3</sup> ]	5.62 ± 1.66	4.35 ± 0.99	0.001

<sup>a</sup> Values are given as mean ± standard deviation (SD); <sup>b</sup> statistical difference between genders ( $p < 0.05$ : significant); RNC – right nasal cavity; LC – left nasal cavity; RINC – right inferior nasal concha; LINC – left inferior nasal concha; RMNC – right medial nasal concha; LMNC – left medial nasal concha; NS – nasal septum.

difference between the inferior nasal concha volumes of male and female subjects ( $p < 0.05$ ). Also, there was a significant difference between the 2 genders regarding middle nasal concha volumes ( $p < 0.05$ ) (Table 2).

The mean volumes of measured structures in adults and children are shown in Table 3. The nasal cavities of adults were larger than those of children ( $p < 0.05$ ). Also, the volumes of all structures were larger in adults ( $p < 0.05$ ).

There was no statistically significant difference between the right and the left NC volumes of all individuals ( $p = 0.07$ ). Also, there was no statistically significant difference between the right and the left middle and inferior nasal conchae volumes ( $p = 0.247$  and  $p = 0.449$ , respectively).

The volume fractions (%) of structures in total NC volume are shown in Table 4.

### Discussion

Many studies have been conducted on the structure, function and volume of the NC. In these studies, the structures of the NC, conchae and meatuses, anatomical variations, and air flow in the NC were examined. Radiological imaging,

Table 1. Mean ages in respective groups. Values are given as mean ± standard deviation (SD)

Parameter	Female adults	Female children	Male adults	Male children
Age [years]	36.52 ± 12.23	13.08 ± 2.45	41.00 ± 10.90	13.42 ± 2.66

**Table 4.** Volume fractions of structures in total volume according to age and gender. Values are given as mean  $\pm$  standard deviation (SD)

Volume fraction	Female adults [%]	Female children [%]	Male adults [%]	Male children [%]
RINCV/TV [cm <sup>3</sup> ]	10.59 $\pm$ 2.65	11.01 $\pm$ 2.77	9.59 $\pm$ 1.82	11.11 $\pm$ 2.82
LINCV/TV [cm <sup>3</sup> ]	11.38 $\pm$ 2.50	11.38 $\pm$ 3.35	10.10 $\pm$ 1.89	10.56 $\pm$ 3.38
RMNC/TV [cm <sup>3</sup> ]	4.76 $\pm$ 1.75	4.94 $\pm$ 1.74	4.10 $\pm$ 0.86	4.46 $\pm$ 1.41
LMNC/TV [cm <sup>3</sup> ]	5.01 $\pm$ 1.53	4.97 $\pm$ 2.05	4.17 $\pm$ 1.01	4.50 $\pm$ 1.68
NSV/TV [cm <sup>3</sup> ]	16.81 $\pm$ 3.14	19.56 $\pm$ 3.43	17.68 $\pm$ 4.72	16.91 $\pm$ 2.07
RNCV/TV [cm <sup>3</sup> ]	25.48 $\pm$ 3.81	24.13 $\pm$ 4.27	28.02 $\pm$ 3.09	26.91 $\pm$ 3.45
LNCV/TV [cm <sup>3</sup> ]	25.58 $\pm$ 4.10	23.97 $\pm$ 3.91	26.31 $\pm$ 3.77	25.52 $\pm$ 3.98

TV – total volume; RINCV – right inferior nasal concha volume; LINCV – left inferior nasal concha volume; RMNC – right middle nasal concha volume; LMNC – left middle nasal concha volume; NSV – nasal septum volume; RNCV – right nasal cavity volume; LNCV – left nasal cavity volume.

dissection, measurements on dry bone, acoustic rhinometry, and rhinomanometry methods were used.<sup>5,8,14,20,22,28</sup>

Terheyden et al.<sup>29</sup> accepted that the CT is the gold standard for measuring the NC and its components. Low radiation exposure, multiple display modes in combination with high accurate images, thin thickness of slices, real size analysis, and minimal superimposition make the CBCT ideal for the evaluation of the NC.<sup>9,12,30</sup> The CBCT allows not only the “real-time” images in the axial plane but also 2-dimensional images in the sagittal, coronal and even oblique or curved image planes.<sup>23</sup> Despite the lower cost and less radiation dose compared to conventional CT, studies on CBCT images about calculating the volume of NC and its structures are limited in number.

There are studies that examined some changes before and after rapid maxillary expansion treatment using the CBCT images.<sup>3,4,25,32</sup> In these studies, skeletal changes, changes in the all upper airway volumes, oropharyngeal volume, mandibular position, respiratory performance, and airway resistance were discussed and data obtained from CBCT images was evaluated with 3D software.

In literature, only 2 studies evaluated the volumetric changes of the NC using the stereological method on CT images.<sup>6,7</sup> Also, these studies researched the changes in structures visible on CT images. In this study, we used CBCT images, where the resolution is better than the resolution of CT images.

Emirzeoğlu et al.<sup>6</sup> worked on individuals who were 18–40 years old. Ertekin et al.<sup>7</sup> studied children 8–11 years of age. We conducted this study on a wide range of age groups (8–59 years of age), including the age range of both mentioned studies. This study is a reference study in Turkish population, where wide-scale volumetric calculations are made using stereological method. Also, the volume of the nasal septum was evaluated in this study, unlike in the study conducted by Emirzeoğlu et al.<sup>6</sup>

Ertekin et al.<sup>7</sup> and Emirzeoğlu et al.<sup>6</sup> used CT images with a cross-sectional thickness of 0.6 mm and 3 mm, respectively. Unlike these 2 studies, we examined a 0.4 mm slice of thickness on CBCT images. The mean volumes of structures measured in mentioned studies are given in Table 5 as a comparison of literature.

**Table 5.** Comparison of literature

Parameter	Ertekin et al. <sup>1</sup>		Emirzeoğlu et al. <sup>35</sup>	This study	
Age interval [years]	8–11		18–40	8–59	
Number of cases	342		60	200	
NCV [cm <sup>3</sup> ]	R F: 0.32–1.79 M: 0.45–2.19 (min–max)	L F: 0.31–1.85 M: 0.45–2.20 (min–max)	F: 5.95 $\pm$ 0.10 M: 7.01 $\pm$ 0.18 (4.10–12.71 cm <sup>3</sup> ) (min–max)	R F: 6.13 $\pm$ 2.22 M: 9.24 $\pm$ 2.86	L F: 6.09 $\pm$ 2.17 M: 8.78 $\pm$ 3.00
INCV [cm <sup>3</sup> ]	R F: 0.07–0.68 M: 0.09–0.71 (min–max)	L F: 0.08–0.54 M: 0.08–0.70 (min–max)	F: 1.45 $\pm$ 0.68 M: 1.59 $\pm$ 0.98 (0.41–3.94) (min–max)	R F: 2.67 $\pm$ 0.95 M: 3.42 $\pm$ 0.95	L F: 2.76 $\pm$ 1.01 M: 3.44 $\pm$ 1.11
MNCV [cm <sup>3</sup> ]	R F: 0.03–0.25 M: 0.04–0.30 (min–max)	L F: 0.03–0.25 M: 0.04–0.30 (min–max)	F: 0.56 $\pm$ 0.22 M: 0.67 $\pm$ 0.31 (0.25–1.29) (min–max)	R F: 1.14 $\pm$ 0.46 M: 1.41 $\pm$ 0.47	L F: 1.21 $\pm$ 0.55 M: 1.43 $\pm$ 0.54
NSV [cm <sup>3</sup> ]	F: 0.24–1.00 M: 0.23–1.24 (min–max)		–	F: 6.13 $\pm$ 2.22 M: 5.69 $\pm$ 1.57	

R – right; L – left; F – female; M – male; NSV – nasal septum volume; NCV – right nasal cavity volume; INCV – inferior nasal concha volume; MNC – right middle nasal concha volume.

Similarly as Emirzeoglu et al.<sup>6</sup> and Ertekin et al.,<sup>7</sup> we reported that a significant difference between male and female subjects in the NC measurements. We detected, as in these 2 studies, that the males' NC volumes and other structures' volumes in NC were greater than those in females. According to the obtained data, no significant difference was found in size between the right and left parts of the NC and the conchae.

It is known that nasal conchae are dynamic structures on the lateral wall of the NC. The changes in their sizes and variations of these structures give rise to various clinical consequences. For example, inferior nasal conchae hypertrophy is a kind of variation seen in conchae, resulting in nasal obstruction.<sup>24</sup> Patients with nasal obstruction have difficulties in breathing in general or mouth breathing and suffer from drying in the throat and mouth, sleeping disorders with snoring, and sometimes apnea.<sup>18</sup> Another variation that causes nasal obstruction is the paradoxical development of the middle nasal conchae. The paradoxical middle nasal conchae is defined as the lateral inclination of middle nasal conchae. This condition may cause recurrent infundibular disease when it occurs with ethmoid bulla and uncinata process variations.<sup>19</sup> Also, it is stated that the middle nasal concha and the inferior nasal concha region have a critical prescription in terms of sinus surgery.<sup>21</sup> Evaluation of conchae is important in the treatment of such clinical conditions and also after treatment. Although there are many studies investigating the anatomical variations of nasal conchae, the studies which assess conchae dimensions are rare.

It is clinically important to know the proportions of the structures in the whole volume of the NC. There is only 1 study that shows the proportion of concha volumes in the whole NC volume. According to the study by Ertekin et al.,<sup>7</sup> the volume proportion of inferior nasal concha is in the range of 9–15% of the total volume of the NC. In the same study, the middle nasal concha volume proportion was reported in a range between 19–31% of the total volume of the NC. Despite the fact that the study by Ertekin et al.<sup>7</sup> was conducted on children, the volume ratios of our study are similar.

This study revealed that the volume of the NC, nasal septum and conchae can be accurately calculated with the stereological method on the CBCT images. We believe that the data obtained in this study may assist clinicians in evaluating the treatment of pathological conditions related to the NC and in the planning of treatment as well preoperational and postoperational evaluations, especially in dentistry, otorhinolaryngology and plastic surgery.

## Limitations of the study

In stereological studies, the statistical coefficient error is accepted as 0.05 or less.<sup>15</sup> Similarly, the value of the coefficient error in the volumetric calculations is accepted as 0.05 or below in the present study. However, since the superior nasal concha can be detected in a few sections,

the coefficient error of the volume of this structure is over than 0.05, so superior nasal concha volume cannot be calculated.

## References

1. Acer N, Bayar B, Başaloglu H, Oner E, Bayar K, Sankur S. Unbiased estimation of the calcaneus volume using the Cavalieri principle on computed tomography images. *Ann Anat.* 2008;190(5):452–460.
2. Acer N, Ertekin T, Küçük A, Babaoglu C, Cankaya MN, Camurdanoglu M. 20–25 Yaş Arası Sağlıklı Gençlerde Gri ve Beyaz Cevher Hacimlerinin İncelenmesi: Planimetrik Çalışma. *Kocatepe Tıp Derg.* 2008;9(2): 45–51.
3. Caprioglio A, Meneghel M, Fastuca R, Zecca PA, Nucera R, Nosetti L. Rapid maxillary expansion in growing patients: Correspondence between 3-dimensional airway changes and polysomnography. *Int J Pediatr Otorhinolaryngol.* 2014;78(1):23–27.
4. Cordasco G, Nucera R, Fastuca R, et al. Effects of orthopedic maxillary expansion on nasal cavity size in growing subjects: A low dose computer tomography clinical trial. *Int J Pediatr Otorhinolaryngol.* 2012;76(11):1547–1551.
5. El-Shazly AE, Poirrier AL, Cabay J, Lefebvre PP. Anatomic variations of lateral nasal wall. *Clin Anat.* 2012;25(3):340–346.
6. Emirzeoglu M, Sahin B, Celebi M, Uzun A, Bilgic S, Tontus HO. Estimation of nasal cavity and conchae volumes by stereological method. *Folia Morphol (Warsz).* 2012;71(2):105–108.
7. Ertekin T, Değermenci M, Nisari M, Unur E, Coşkun A. Age-related changes of nasal cavity and conchae volumes and volume fractions in children: A stereological study. *Folia Morphol (Warsz).* 2016;75(1): 38–47.
8. Ghoneima A, Imburgia A, Halum S, Vandis M, Kula K. Three-dimensional airway analysis of trumpet players vs non-trumpet players. *Oral Radiol.* 2015;31(2):105–113.
9. Guijarro-Martinez R, Swennen GR. Cone-beam computerized tomography imaging and analysis of the upper airway: A systematic review of the literature. *Int J Oral Maxillofac Surg.* 2011;40(11):1227–1237.
10. Gundersen HJG. Notes on the estimation of the numerical density of arbitrary profiles: The edge effect. *J Microsc.* 1977;111(2):219–223.
11. Gundersen HJ, Jensen EB. The efficiency of systematic sampling in stereology and its prediction. *J Microsc.* 1987;147(Pt 3):229–263.
12. Hodez C, Griffaton-Taillandier C, Bensimon I. Cone-beam imaging: Applications in ENT. *Eur Ann Otorhinolaryngol Head Neck Dis.* 2011; 128(2):65–78.
13. Kayipmaz S, Sezgin OS, Saricaoglu ST, Bas O, Sahin B, Küçük M. The estimation of the volume of sheep mandibular defects using cone-beam computed tomography images and a stereological method. *Dentomaxillofac Radiol.* 2011;40(3):165–169.
14. Kula K, Jeong AE, Stacey H, Kendall D, Ghoneima A. Three dimensional evaluation of upper airway volume in children with different dental and skeletal malocclusions. *J Biomed Graph Comput.* 2013; 3(4):116.
15. Mouton PR. *Principles and Practices of Unbiased Stereology.* Baltimore, MD: John Hopkins University Press; 2003:5–6.
16. Odaci E, Sahin B, Sonmez OF, Kaplan S, Bas O, Bilgic S. Rapid estimation of the vertebral body volume: A combination of the Cavalieri principle and computed tomography images. *Eur J Radiol.* 2003;48(3): 316–326.
17. Onuk B, Kabak M, Sahin B, Ince NG, Selcuk MB. New method for estimating the volume and volume fractions of the nasal structures in the goose (*Anser anser domesticus*) using computed tomography images. *Br Poult Sci.* 2013;54(4):441–446.
18. Ophir DE, Shapira AA, Marshak GS. Total inferior turbinectomy for nasal airway obstruction. *Arch Otolaryngol.* 1995;111(2):93–95.
19. Orhan İ, Soylu E, Altın G, Yılmaz F, Çalın ÖF, Örmeci T. Paranasal sinüs anatomik varyasyonlarının bilgisayarlı tomografi ile analizi. *Abant Medical Journal.* 2014;3(2):145–149.
20. Patel RM, Pinto JM. Olfaction: Anatomy, physiology and disease. *Clin Anat.* 2014;27(1):54–60.
21. Santos RDP, Habermann W, Hofmann T, Stammberger H. Pre and post functional endoscopic sinus surgery nasal cavity volume assessment by acoustic rhinometry. *Braz J Otorhinolaryngol.* 2006;72(4): 549–553.

22. Samoliński BK, Grzanka A, Gotlib T. Changes in nasal cavity dimensions in children and adults by gender and age. *Laryngoscope*. 2007; 117(8):1429–1433.
23. Scarfe WC, Farman AG, Sukovic P. Clinical applications of cone-beam computed tomography in dental practice. *J Can Dent Assoc*. 2006; 72(1):75–80.
24. Sharma S. Importance of treating compensatory hypertrophy of inferior turbinate in cases of septal deviation causing nasal obstruction. *Journal of Otolaryngology ENT-Research*. 2016;4(3):00097.
25. Smith T, Ghoneima A, Stewart K, et al. Three-dimensional computed tomography analysis of airway volume changes after rapid maxillary expansion. *Am J Orthod Dentofacial Orthop*. 2012;141(5):618–626.
26. Souza RP, Junior JPB, Tornin OS, et al. Sinonasal complex: Radiological anatomy. *Radiologia*. 2006;39(5):367–372.
27. Standring S, ed. *Gray's Anatomy the Basis of Clinical Practice*. 39<sup>th</sup> ed. Barcelona, Spain: Elsevier Ltd.; 2005:547–561.
28. Starbuck JM, Friel MT, Ghoneima A, Flores RL, Tholpady S, Kula K. Nasal airway and septal variation in unilateral and bilateral cleft lip and palate. *Clin Anat*. 2014;27(7):999–1008.
29. Terheyden H, Maune S, Mertens J, Hilberg O. Acoustic rhinometry: Validation by three-dimensionally reconstructed computer tomographic scans. *J Appl Physiol (1985)*. 2000;89(3):1013–1021.
30. Tso HH, Lee JS, Huang JC. Evaluation of the human airway using cone-beam computerized tomography. *Oral Surg Oral Med Oral Pathol Oral Radiol Endod*. 2009;108(5):768–776.
31. White SC, Pharoah MJ. The evolution and application of dental maxillofacial imaging modalities. *Dent Clin North Am*. 2008;52(4):689–705.
32. Zeng J, Gao X. A prospective CBCT study of upper airway changes after rapid maxillary expansion. *Int J Pediatr Otorhinolaryngol*. 2013; 77(11):1805–1810.

# The relationships between glycemic index and glycemic load of diets and nutritional status and antioxidant/oxidant status in the serum of patients with lung cancer

Katarzyna Agnieszka Zabłocka-Słowińska<sup>1,A–D,F</sup>, Katarzyna Skórska<sup>1,A–D,F</sup>, Sylwia Płaczowska<sup>2,B,C,E</sup>, Anna Prescha<sup>1,B</sup>, Konrad Pawełczyk<sup>3,B,E</sup>, Monika Kosacka<sup>4,B,E</sup>, Irena Porębska<sup>4,B,E</sup>, Halina Grajeta<sup>1,E,F</sup>

<sup>1</sup> Department of Food Science and Nutrition, Wrocław Medical University, Poland

<sup>2</sup> Diagnostics Laboratory for Teaching and Research, Wrocław Medical University, Poland

<sup>3</sup> Department and Clinic of Thoracic Surgery, Wrocław Medical University, Poland

<sup>4</sup> Department and Clinic of Pulmonology and Lung Cancers, Wrocław Medical University, Poland

A – research concept and design; B – collection and/or assembly of data; C – data analysis and interpretation;

D – writing the article; E – critical revision of the article; F – final approval of the article

Advances in Clinical and Experimental Medicine, ISSN 1899–5276 (print), ISSN 2451–2680 (online)

*Adv Clin Exp Med.* 2019;28(8):1027–1036

## Address for correspondence

Katarzyna Zabłocka

E-mail: katarzyna.zablocka-slowinska@umed.wroc.pl

## Funding sources

None declared

## Conflict of interest

None declared

Received on July 3, 2018

Reviewed on September 28, 2018

Accepted on October 14, 2018

Published online on March 9, 2019

## Cite as

Zabłocka-Słowińska KA, Skórska K, Płaczowska S, et al.

The relationships between glycemic index and glycemic load of diets and nutritional status and antioxidant/oxidant status in the serum of patients with lung cancer. *Adv Clin Exp Med.* 2019;28(8):1027–1036. doi:10.17219/acem/98952

## DOI

10.17219/acem/98952

## Copyright

© 2019 by Wrocław Medical University

This is an article distributed under the terms of the

Creative Commons Attribution Non-Commercial License

(<http://creativecommons.org/licenses/by-nc-nd/4.0/>)

## Abstract

**Background.** A low glycemic index (GI) and glycemic load (GL) of diets as well as proper nutritional status may partially slow down depletion in antioxidant capacity, and may therefore have an impact on antioxidant/oxidant status in lung cancer patients. However, no studies concerning these associations had previously been conducted.

**Objectives.** The aim of this study was to investigate the association between GI or GL and nutritional status and antioxidant/oxidant status in lung cancer patients.

**Material and methods.** The study was conducted among 180 lung cancer patients (82 women and 98 men) and 171 control subjects (78 women and 93 men). Exclusion criteria for the control subjects included cancers, pro-inflammatory conditions, brain diseases, and psychiatric disorders. All participants were evaluated in terms of their systemic antioxidant/oxidant status, nutritional status (anthropometric parameters), dietary GI and GL and parameters related to circulating glucose: fasting glucose, insulin level and homeostasis model assessment for insulin resistance (HOMA-IR).

**Results.** In women who were lung cancer-positive, associations were observed between total antioxidant status (TAS) and parameters of nutritional status, and between oxidative stress index (OSI) and fasting glucose. In men with lung cancer, we found a positive correlation between total oxidant status (TOS) and GI. In the control group of women, TAS positively correlated with anthropometric parameters, but negatively with dietary fiber and total carbohydrate content. Additionally, TOS and OSI negatively correlated with parameters related to body weight and positively with insulin. In control men, we observed significant negative correlations between parameters related to fasting glucose and TAS and positive ones with TOS and OSI.

**Conclusions.** The results show that in lung cancer oxidative stress is related to GI, while TAS is related to nutritional status. Further investigations performed on a larger cohort are required to better clarify the observed relationships as well as to explain the potential mechanisms involved.

**Key words:** lung cancer, nutritional status, oxidative stress, glycemic load, glycemic index

## Introduction

The most recent global cancer statistics indicate that lung cancer is still the most commonly diagnosed cancer in men in countries of low socioeconomic status. Regardless of the economic status of the country, it remains the most common cause of oncological deaths for both sexes.<sup>1</sup> In Poland, as in the rest of the world, lung cancer is a major cause of cancer-related deaths, although incidences of lung cancer in men are decreasing gradually, in contrast to incidences observed among women, which continue to rise. The National Cancer Register shows that in 2013 more than 14,000 men and almost 7,000 women were diagnosed with lung cancer.<sup>2</sup>

Lung cancer is most effectively prevented by avoiding active and passive smoking.<sup>3</sup> Additional risk factors include environmental pollution, chronic obstructive pulmonary disease and other inflammatory-related respiratory diseases, as well as genetic predisposition. A well-balanced diet rich in vegetable and fruit products, and regular, moderate physical activity may additionally potentiate the prevention of lung cancerogenesis.<sup>4,5</sup>

At the molecular level, oxidative stress plays an important role in lung cancer pathogenesis.<sup>6</sup> Lungs are especially susceptible to pro-oxidative environments caused by factors such as high atmospheric oxygen pressure, the high amount of reactive species generated by pro-inflammatory cells in pulmonary circulation and air xenobiotics, e.g., from air pollution and/or tobacco smoke.<sup>7,8</sup> In lung cancer patients, some mechanisms may induce disturbances in redox homeostasis, e.g., cancer-related chronic inflammation and malnutrition.<sup>9</sup> Oxidative stress in malnourished cancer patients may also be caused by protein, carbohydrate and lipid metabolic alterations, which on the one hand intensify oxidative stress and therefore deplete the antioxidant capacity of the body, but on the other hand impair the synthesis of protein-related reducing agents due to an increased whole body protein turnover.<sup>10,11</sup> Additionally, lessened dietary antioxidant intake and imbalanced dietary habits in general have been demonstrated many times to deepen redox imbalance in healthy people, while data on oncology patients is inconclusive.<sup>12,13</sup> High dietary glycemic index (GI) and glycemic load (GL) may be associated with systemic oxidative stress.<sup>14</sup> A disruption in antioxidant/oxidant status observed under high GI and/or GL may be the result of increased blood glucose concentration and insulin level, which can promote glucose intolerance, insulin resistance, hyperglycemia, and hyperinsulinemia. Hyperglycemia and hyperinsulinemia may lead to oxidative stress independently of other factors.<sup>15</sup>

To the best of our knowledge, no studies concerning the association between the GI and the GL of diets or nutritional status and antioxidant/oxidant status in lung cancer patients have previously been carried out. The authors of this study hypothesize that diets based on low GI and GL and proper nutritional status may partially slow

down depletion in antioxidant capacity and therefore have an impact on antioxidant/oxidant status. Based on the assumptions presented above, finding any potential relationships between GI, GL or nutritional status and antioxidant/oxidant status in lung cancer patients may enhance the management of lung cancer and create an opportunity for more personalized oncological care, including dietary recommendations.

Considering the above, the aim of this study was to investigate the association between GI, GL and nutritional status and antioxidant/oxidant status in lung cancer patients.

## Material and methods

### Material

The study was conducted among 82 women with lung cancer (lung cancer women – LW) at a median age of 66 years (range: 41–82 years) and 98 men with lung cancer (lung cancer men – LM) at a median age of 66 years (range: 41–82 years), before any cancer treatment. All detailed information about the lung cancer patients (clinical stage of the disease, type of cancer, smoking status, and educational level) are presented in Table 1. The clinical stages of disease were evaluated using the TNM classification. The clinical stage and metastases were determined with chest computed tomography (CT), positron emission tomography/CT (PET/CT) and ultrasonography (USG) of the abdominal cavity. Computed tomography/magnetic resonance imaging (CT/MRI) of the central nervous system (CNS) and scintigraphy of bone were performed when necessary. Bronchial fibroscopy was carried out routinely. In the case of enlarged lymph nodes of the mediastinum, an endobronchial ultrasound transbronchial needle aspiration (EBUS-TBNA) was performed. Negative EBUS results were verified in mediastinoscopy. Histological typing of lung cancer was performed by pathologists through microscopic evaluation.

The lung cancer group (LG) was recruited from the Lower Silesian Center of Lung Diseases, Wrocław, Poland. The control group (CG) consisted of 78 women (control women – CW) at a median age of 56 years (range: 24–77 years) and 93 men (control men – CM) at a median age of 59 years (range: 23–98 years), recruited from the Wrocław 3<sup>rd</sup> Age Universities, the Center of Occupational Medicine in Wrocław and from Wrocław Medical University employees. Exclusion criteria for the control group included cancers, pro-inflammatory diseases, autoimmune diseases, gastrointestinal disorders, skin disorders, brain diseases, and psychiatric disorders. The subject's health condition was self-reported. Data on the level of education and smoking status of both the lung cancer patients and the control subjects was also self-reported. The lung cancer patients and control

subjects were asked whether they were current smokers, former smokers (at least 2 weeks without active smoking) or never-smokers.

## Methods

### Blood collection and preparation

The day after a lung cancer patient's admission to hospital, blood samples were collected during a fasting state and the serum was separated and then stored at  $-80^{\circ}\text{C}$  prior to analysis. In the control subjects, blood was collected after overnight fasting at the Diagnostic Laboratory for Teaching and Research or at the Center of Occupational Medicine by a professional (medical analyst). The study protocol was approved by the Ethics Commission of the Wrocław Medical University (approval No. 540/2013), and the study was conducted according to the principles expressed in the Declaration of Helsinki. All participants provided written consent for taking part in the research.

### Biochemical variable measurements in serum

#### Total antioxidant status

Total antioxidant status (TAS) [mmol Trolox equiv./L] was measured in serum by the generation of 2,2'-azino-di-(3-ethylbenzthiazoline sulphonate) (ATBS) radical cation using a commercial TAS kit (Randox Laboratories, Crumlin, UK).

#### Total oxidant status

Total oxidant status (TOS) [ $\mu\text{mol H}_2\text{O}_2/\text{L}$ ] was measured as described by Erel.<sup>16</sup> In this method, the oxidants present in the sample oxidize the ferrous ion-o-dianisidine complex to ferric ion. Ferric ion produces a colored complex with xylenol orange in an acidic medium. The color intensity is related to the total activity of oxidants present in the sample. The assay was calibrated with hydrogen peroxide and the results were expressed in terms of  $\mu\text{mol H}_2\text{O}_2$  equivalent/L of serum.

#### Oxidative stress index

The TOS:TAS ratio was used as the oxidative stress index (OSI), and was calculated as follows<sup>17</sup>:

$$\text{OSI [arbitrary unit]} = \frac{\text{TOS } [\mu\text{mol H}_2\text{O}_2/\text{L}]}{\text{TAS [mmol Trolox equiv./L]}}$$

#### Malondialdehyde

Serum malondialdehyde concentration (MDA) [ $\mu\text{mol/L}$ ] was measured based on a reaction with thiobarbituric acid (TBA) and extraction with 1-butanol after heating in boiling water for 45 min. The absorbance of the pink supernatant was measured at 535 nm, and the results were calculated using the molar coefficient and were expressed in  $\mu\text{mol}$  of MDA/L of serum.

#### Glucose

Glucose concentration (GLC) [mg/dL] was quantified with a commercial kit (cat. No. 981780; Thermo Fisher Scientific, Waltham, USA), based on an enzymatic coupled assay using glucose oxidase and the peroxidase method (GOD-POD).

#### Insulin

Insulin concentration [ $\mu\text{U/mL}$ ] was determined with a DRG Insulin enzyme-linked immunosorbent assay (ELISA) (cat. No. EIA-2935; DRG Instruments GmbH, Marburg, Germany). The test is based on the sandwich principle.

#### Homeostasis model assessment for insulin resistance

Homeostasis model assessment for insulin resistance (HOMA-IR) was calculated using the equation<sup>18</sup>:

$$\text{HOMA-IR} = \frac{(\text{fasting insulin } [\mu\text{U/mL}] \times \text{fasting glucose } [\text{mg/dL}])}{405 \text{ [arbitrary unit]}}$$

#### Nutritional status

Anthropometric parameters were used to assess the nutritional status of the participants. Baseline anthropometric parameters were measured: weight, height, body fat percentage (BFP), waist circumference (WC), hip circumference (HC), waist-hip ratio (WHR), mid-arm circumference (MAC), and calf circumference (CC). Body mass index (BMI) was calculated as the weight in kilograms divided by the square of the height in meters [ $\text{kg/m}^2$ ]. The percentage of body fat was determined using a Body FAT Monitor (Omron BF 306; Omron, Kyoto, Japan).

Fat free mass index (FFMI) was calculated from the following formula<sup>19</sup>:

$$\text{FFMI} = (100\% - \text{BFP})/100 \times \text{weight}/\text{height}^2$$

Waist circumference was measured at the level of the umbilicus, and hip circumference was measured at the trochanter level. The WHR was calculated as the ratio of waist circumference to hip circumference. The MAC was measured with a millimeter tape at the midpoint of the non-dominant arm, between the olecranon and acromion. The CC was measured with wrapping the tape around the widest part of the calf with the patient in a sitting position, left knee raised at a right angle, and the calf uncovered by rolling up the subject's pant leg. All anthropometric measurements were performed twice.

#### Dietary intakes

Dietary data was gathered for all study participants using 72-hour dietary recalls by a trained interviewer.<sup>20</sup> In the case of LG, the interview was carried out on the day of hospital admission. To assess the portion size of food products, the "Album of Photographs of Food Products and Dishes" was used.<sup>21</sup> All dietary recalls were analyzed using

Microsoft Excel 365 (Microsoft Corp., Redmond, USA). The daily energy value of the diets, the amount of total and available carbohydrates and dietary fiber were taken from the “Tables of Composition and Nutritional Value”.<sup>22</sup> The GI values were assigned to individual food items using a method described by Louie et al.<sup>23</sup> The GI values were sourced from one of the following GI databases: the International Tables of Glycemic Index and Glycemic Load Values: 2008 (Atkinson et al. database),<sup>24</sup> the Glycemic Index site of the University of Sydney [www.glycemicindex.com](http://www.glycemicindex.com)<sup>25</sup> and the National Cancer Institute (NCI) database.<sup>26</sup> We used the following equations to calculate GI and GL value:

Glycemic load (GL) of diets<sup>23</sup>:

$$\frac{\text{GI} \times \text{amount (in grams) of available carbohydrate in a serve of that food}}{100}$$

Glycemic index (GI %) of diets<sup>23</sup>:

$$\frac{\text{GL} \times 100\%}{\text{amount (in grams) total carbohydrate in a serve of that food}}$$

### Statistical analysis

The data was analyzed using STATISTICA v. 12.0 (StatSoft Inc., Tulsa, USA). All parameters are presented as a median and range. For all statistical procedures, the significance level was considered to be  $p < 0.05$ . Most of the results obtained did not present normal distribution, as confirmed by the Shapiro–Wilk test. Student’s t-test for parametric data or the Mann–Whitney U test for non-parametric data were performed to evaluate the differences in baseline characteristics, anthropometric parameters, nutrient intakes, and GI and the GL of diets between LG and CG. A  $\chi^2$  test was used to compare the level of education and cigarette smoking status between LG and CG.

The correlations between anthropometric parameters, GI and GL of diets and nutrient intakes, as well as biochemical variables related to serum glucose and antioxidant/oxidant status parameters were assessed using Pearson’s correlation coefficient.

## Results

### Baseline characteristics of lung cancer patients and control subjects

A detailed description of subjects concerning age, histologic types of lung cancer, clinical stages of disease, level of education, and smoking status is presented in Table 1. The majority of LW and LM (88.6% and 89.6%, respectively) suffered from non-small-cell lung cancer (NSCLC). Subjects from LG were diagnosed with different clinical stages of disease – more than half at stages I and IV. The CW subjects were significantly better educated than those from LW; however, no significant differences in self-reported educational level were observed between LM and CM. Both study groups were differentiated by smoking status. A significantly higher percentage of LG regardless of sex were former or current smokers in comparison with CG.

### Dietary intakes, glycemic index and glycemic load of diets

The energy content, carbohydrates, dietary fiber intake, and the GI and GL of diets are presented in Table 2. The energy provided from diets, the total and available carbohydrates, and the ratio of available to total carbohydrates were higher in LW and LM when compared to CW and CM, respectively. The intake of dietary fiber in LM was significantly higher than in CM, but after recalculating per 1,000 kcal, the intake of dietary fiber was significantly

**Table 1.** Baseline characteristics of sex-related groups of lung cancer and control subjects

Variable	n	LW	n	CW	n	LM	n	CM
Age (median (min–max)) [years]	82	<b>66 (41–82)<sup>a</sup></b>	78	<b>56 (24–77)<sup>a</sup></b>	98	<b>64 (38–82)<sup>a</sup></b>	93	<b>59 (23–98)<sup>a</sup></b>
Type of cancer (NSCLC/SCLS) [%]	44	88.6/11.4	78	n/a	58	89.6/10.4	93	n/a
Clinical stage of disease (I/II/IIIa/IIIb/IV) [%]	38	52.6/18.4/7.9/5.3/15.8	78	n/a	51	31.4/13.6/11.8/11.8/31.4	93	n/a
Educational level (primary/secondary/vocational/university) [%]	80	<b>13.8/45.0/22.5/18.8<sup>b</sup></b>	77	<b>3.9/48.0/10.4/37.7<sup>b</sup></b>	96	18.8/29.2/38.5/13.5	91	12.1/35.2/30.8/21.9
Smoking status (former smoker/current smoker/never-smoker) [%]	58	<b>65.5/20.7/13.8<sup>b</sup></b>	78	<b>23.1/17.9/59.0<sup>b</sup></b>	75	<b>78.7/16/5.3<sup>b</sup></b>	91	<b>29.7/29.7/40.6<sup>b</sup></b>

LW – lung cancer women; CW – control women; LM – lung cancer men; CM – control men; <sup>a</sup> – statistically significant differences demonstrated by Student’s t-test or Mann–Whitney U test between sex-related groups of lung cancer and control subjects;  $p < 0.05$ ; <sup>b</sup> – statistically significant differences demonstrated by the  $\chi^2$  test between sex-related groups of lung cancer and control subjects,  $p < 0.05$  (observed significant differences between compared groups are in bold); NSCLC – non-small-cell lung cancer; SCLS – small-cell lung cancer; n/a – not applicable.



**Table 2.** Energy, carbohydrate, dietary fiber intake and dietary GI and GL in the diets of sex-related groups of lung cancer and control subjects: median (min–max)

Variable	n	LW	n	CW	n	LM	n	CM
Energy content [kcal/d]	82	<b>2019.3</b> (1160.1–3196.5)	78	<b>1840.6</b> (1023.4–3018.9)	98	<b>2763.7</b> (1558.1–3978.4)	93	<b>2149.6</b> (1077.0–3995.4)
Total carbohydrate content [g/d]	82	<b>283.4</b> (155.4–477.8)	78	<b>260.7</b> (122.1–431.4)	98	<b>361.7</b> (187.8–561.8)	93	<b>283.7</b> (148.3–598.2)
Total carbohydrate content [g/1,000 kcal]	82	141.2 (99.8–183.2)	78	140.9 (94.2–183.5)	98	128.5 (91.6–165.4)	93	129.4 (90.6–166.6)
Available carbohydrate content [g/d]	82	<b>263.2</b> (139.9–446.1)	78	<b>234.7</b> (111.8–389.2)	98	<b>332.6</b> (165.9–534.4)	93	<b>255.6</b> (125.4–554.0)
Available carbohydrate content [g/1,000 kcal]	82	129.2 (89.9–167.9)	78	128.4 (84.9–166.6)	98	118.1 (82.2–153.7)	93	119.3 (84.8–155.0)
Ratio of available and total carbohydrates [%]	82	<b>92.2</b> (86.1–96.4)	78	<b>91.1</b> (84.6–95.0)	98	<b>92.5</b> (87.7–95.1)	93	<b>91.5</b> (84.5–96.1)
Dietary fiber content [g/d]	82	21.6 (13.1–50.6)	78	22.7 (8.7–45.6)	98	<b>27.6</b> (12.7–46.9)	93	<b>23.5</b> (8.2–54.3)
Dietary fiber content [g/1,000 kcal]	82	<b>11.1</b> (4.7–19.9)	78	<b>12.4</b> (6.3–21.6)	98	<b>9.6</b> (6.6–15.9)	93	<b>10.9</b> (5.0–22.2)
GI [%]	82	<b>52.3</b> (45.5–60.5)	78	<b>50.6</b> (33.0–67.9)	98	<b>53.6</b> (44.1–61.4)	93	<b>54.5</b> (34.6–69.2)
GL [g/d]	82	<b>152.5</b> (72.6–256.9)	78	<b>132</b> (59.2–233.2)	98	<b>198.6</b> (92.3–320.9)	93	<b>155.4</b> (51.3–320.3)
GL/1,000 kcal	82	74.4 (51.5–102.1)	78	69.1 (44.3–93.9)	98	68.4 (45.04–87.70)	93	73.2 (47.6–106.8)

Differences were assessed using the Mann–Whitney U test or Student’s t-test between sex-related groups of lung cancer and control subjects;  $p < 0.05$  (significant differences between compared groups are in bold); LM – lung cancer men; CM – control men; LW – lung cancer women; CW – control women; GI – glycemic index; GL – glycemic load.

lower in LW and LM than in CW and CM. Interestingly, although the GI of diets was significantly higher in LW than in CW, the opposite relationship was observed between LM and CM. Additionally, we found significantly higher GL in the lung cancer women and men when compared to the GL of diets in the control women and men, respectively; however, we did not further observe this difference when recalculating the GL per 1,000 kcal.

## Nutritional status

Data concerning nutritional status was assessed based on anthropometric parameters and are presented in Table 3. The nutritional status of the lung cancer patients was worse than that of the controls, as demonstrated mainly by the significantly lower weight, HC, CC, and MAC in LM compared to CM, and the significantly higher WHR and lower CC in LW in comparison with CW.

## Biochemical measurements regarding antioxidant/oxidant status and circulating glucose

The results concerning biochemical measurements of antioxidant/oxidant status and circulating glucose are presented in Table 4. The analysis revealed significant differences in the antioxidant/oxidant status between the lung cancer patients and the control subjects, demonstrated

by the significantly lower antioxidant capacity (TAS) and the higher oxidative stress (OSI) in LW and LM compared to CW and CM, respectively, and the significantly higher oxidative status (TOS), only in the men. However, no differences in MDA level were observed between lung cancer and control subjects. The LW and LM groups had significantly higher levels of circulating GLC as well as INS, which in turn led to significantly higher values of HOMA-IR compared to CW and CM.

## Correlations between variables related to antioxidant/oxidant status and glucose, anthropometric parameters, nutrient intake, and GI and GL values in the lung cancer and control groups

Correlation analysis revealed various significant relationships between antioxidant/oxidant status and the parameters related to glucose, anthropometric parameters and nutrient intake in sex-differentiated groups of lung cancer and control subjects (Table 5). In LW, we found significant positive correlations between TAS and WC, HC, weight and BMI. Additionally in LW, we observed a significant negative correlation between OSI and energy content and available and total carbohydrate content, as well as a positive correlation between OSI and GLC. Moreover, TAS in CW had a positive association with CC, WC and

**Table 3.** Anthropometric parameters of sex-related groups of lung cancer patients and control subjects: median (min–max)

Variable	n	LW	n	CW	N	LM	n	CM
Weight [kg]	82	65 (40–106)	78	69 (46–98)	97	<b>75</b> <b>(47–146)</b>	82	<b>81</b> <b>(52–118)</b>
BMI [kg/m <sup>2</sup> ]	82	26.2 (16.8–44.1)	78	25.9 (16.8–37.1)	97	25.6 (17.9–51.7)	82	26.3 (18.4–38.7)
FFMI [kg/m <sup>2</sup> ]	53	17.7 (14.1–22.8)	46	17.4 (14.3–25.5)	72	19.4 (13.2–30.0)	55	19.7 (15.2–24.6)
BFP [%]	53	33.8 (11.8–50.0)	46	36.5 (19.7–47.7)	72	24.5 (6.7–44.0)	55	26.1 (6.2–37.7)
WC [cm]	56	94 (62–128)	67	86 (63–119)	73	94.5 (74–141)	73	99 (74–120)
HC [cm]	56	103 (65–141)	67	103 (80–120)	73	<b>98</b> <b>(81–137)</b>	72	<b>102</b> <b>(63–115)</b>
WHR	56	<b>0.899</b> <b>(0.688–1.292)</b>	67	<b>0.832</b> <b>(0.692–1.188)</b>	73	0.967 (0.822–1.138)	72	0.971 (0.768–1.202)
CC [cm]	33	<b>34.0</b> <b>(27.2–42.3)</b>	30	<b>37.8</b> <b>(32.5–42.3)</b>	35	<b>34.3</b> <b>(28.5–41.0)</b>	42	<b>36.0</b> <b>(29.0–46.0)</b>
MAC [cm]	48	29.0 (20.8–36.0)	40	30.0 (24.7–37.0)	68	<b>28.1</b> <b>(23.3–39.1)</b>	53	<b>30.0</b> <b>(22.0–37.0)</b>

Differences were assessed using the Mann–Whitney U test or Student's t-test between sex-related groups of lung cancer patients and control subjects;  $p < 0.05$  (observed significant differences between compared groups are in bold); LW – lung cancer women; CW – control women; LM – lung cancer men; CM – control men; BMI – body mass index; FFMI – fat-free mass index; BFP – body fat percentage; WC – waist circumference; HC – hip circumference; WHR – waist-to-hip ratio; CC – calf circumference; MAC – mid-arm circumference.

**Table 4.** Serum levels of parameters of redox status as well as glucose, insulin and HOMA-IR values in sex-related groups of lung cancer and control subjects: median (min–max)

Variable	n	LW	n	CW	n	LM	n	CM
TAS [mmol Trolox equiv./L]	71	<b>1.51</b> <b>(0.96–2.34)</b>	<b>77</b>	<b>1.64</b> <b>(1.25–2.14)</b>	81	<b>1.62</b> <b>(1.17–2.55)</b>	42	<b>1.85</b> <b>(1.42–2.10)</b>
TOS [ $\mu\text{mol H}_2\text{O}_2$ equiv./L]	69	3.32 (0.27–74.79)	73	2.50 (0.10–48.63)	73	<b>5.22</b> <b>(0.39–52.13)</b>	42	<b>3.14</b> <b>(0.51–74.79)</b>
OSI [arbitrary unit]	62	<b>2.093</b> <b>(0.151–52.301)</b>	73	<b>1.402</b> <b>(0.055–32.691)</b>	69	<b>2.712</b> <b>(0.000–37.773)</b>	42	<b>1.774</b> <b>(0.345–51.938)</b>
MDA [ $\mu\text{mol/L}$ ]	74	1.715 (0.310–4.480)	76	1.553 (0.000–15.625)	82	1.804 (0.559–7.728)	42	1.882 (0.000–6.574)
Glucose [mg/dL]	71	<b>107.1</b> <b>(33.8–296.0)</b>	77	<b>86.5</b> <b>(68.2–231.6)</b>	78	<b>97.8</b> <b>(57.0–286.0)</b>	42	<b>87.0</b> <b>(69.6–296.0)</b>
Insulin [ $\mu\text{U/mL}$ ]	38	<b>16.6</b> <b>(3.9–112.7)</b>	41	<b>10.6</b> <b>(3.8–25.0)</b>	57	<b>18.6</b> <b>(3.1–132.0)</b>	33	<b>10.2</b> <b>(5.4–62.5)</b>
HOMA-IR [arbitrary unit]	38	<b>5.12</b> <b>(0.75–68.29)</b>	41	<b>2.23</b> <b>(0.86–5.74)</b>	57	<b>5.10</b> <b>(0.49–81.58)</b>	33	<b>2.08</b> <b>(1.19–45.71)</b>

Differences between groups were assessed using the Mann–Whitney U test or Student's t-test between lung cancer and control groups (significant differences between compared groups are in bold);  $p < 0.05$ ; LW – lung cancer women; CW – control women; LM – lung cancer men; CM – control men; TAS – total antioxidant status; TOS – total oxidant status; OSI – oxidative stress index; MDA – malondialdehyde; HOMA-IR – homeostasis model assessment for insulin resistance.

weight, but a negative one with dietary fiber and total carbohydrate content. In CW, TOS and OSI had negative correlations with weight and BMI and positive ones with INS. In LM, we only found a positive correlation between TOS and GI. In CM, we observed a significant negative correlation between TAS and GLC as well as HOMA-IR. On the other hand, TOS and OSI correlated positively with GLC, INS and HOMA-IR in this subgroup. For the first time, out of all the subgroups, we found a positive correlation between MDA and BMI as well as weight in CM.

## Discussion

It has been confirmed that antioxidant/oxidant status changes in lung cancer, as well as in many other site-specific cancers, and a depletion of antioxidant capacity has been observed along with tumor progression.<sup>27</sup> Despite this, the mechanisms of redox disturbance in lung cancer patients are still not entirely clear. Cigarette smoking and lung inflammation, as well as systemic inflammation, are recognized as major causes of depletion of antioxidant

**Table 5.** Significant correlations between variables related to concentrations of glucose, anthropometric parameters, nutrient intake, GI, GL, and parameters related to antioxidant/oxidant status in sex-related groups of lung cancer and control subjects

Correlation	N	R	p-value
LW			
TAS vs WC	48	0.2997	0.039
TAS vs HC	48	0.3164	0.028
TAS vs weight	71	0.3317	0.005
TAS vs BMI	71	0.2374	0.046
OSI vs energy content	62	-0.2669	0.036
OSI vs available carbohydrate content	62	-0.2763	0.030
OSI vs total carbohydrate content	62	-0.2737	0.031
OSI vs glucose	57	0.3126	0.018
CW			
TAS vs CC	30	0.3622	0.049
TAS vs WC	66	0.2553	0.039
TAS vs weight	77	0.2322	0.042
TAS vs dietary fiber	77	-0.3032	0.007
TAS vs total carbohydrate content	77	-0.2328	0.042
TOS vs weight	73	-0.2732	0.019
TOS vs BMI	73	-0.2672	0.022
TOS vs insulin	39	0.3326	0.039
OSI vs weight	73	-0.2924	0.012
OSI vs BMI	73	-0.2802	0.016
OSI vs insulin	39	0.3384	0.035
LM			
TOS vs GI	73	0.2460	0.036
CM			
TAS vs glucose	42	-0.3341	0.031
TAS vs HOMA-IR	33	-0.3445	0.050
TOS vs glucose	42	0.8204	<0.001
TOS vs insulin	33	0.8287	<0.001
TOS vs HOMA-IR	33	0.9237	<0.001
OSI vs glucose	42	0.8563	<0.001
OSI vs insulin	33	0.8417	<0.001
OSI vs HOMA-IR	33	0.9527	<0.001
MDA vs weight	42	0.3146	0.042
MDA vs BMI	42	0.5102	0.001

LW – lung cancer women; CW – control women; LM – lung cancer men; CM – control men; TAS – total antioxidant status; WC – waist circumference; HC – hip circumference; BMI – body mass index; OSI – oxidative stress index; TOS – total oxidant status; CC – calf circumference; GI – glycemic index; MDA – malondialdehyde; HOMA-IR – homeostasis model assessment for insulin resistance.

pools.<sup>28</sup> However, other factors may at least partially contribute to this imbalance. Although the link between the GI and GL of diets and oxidative stress is known in the general population,<sup>29</sup> no data concerning this correlation in cancer patients, including lung cancer ones, has been described. The purpose of this study was therefore to assess

the relationship between GI, GL and nutritional status and antioxidant/oxidant status in lung cancer patients.

In this study, we demonstrated elevated systemic oxidative stress and depletion of antioxidant capacity in lung cancer patients when compared to control subjects, which suggests that changes in whole body redox status are at least partially associated with lung cancerogenesis. The disruption of antioxidant/oxidant status in lung tissue has been considered one of the key factors of lung cancerogenesis at the molecular level.<sup>30</sup> However, extensive studies into the detailed mechanisms of systemic alterations in the antioxidant/oxidant status of lung cancer patients have not been conducted. Expanding our knowledge in this area could bring new perspectives into lung cancer pathophysiology. Disruptions in metabolism during cancerogenesis are well-known and are often observed in lung cancer patients, leading to, i.e., malnutrition and altered glucose utilization.<sup>31,32</sup> Elevated circulating glucose (and in consequence, elevated insulin levels) result in a high prevalence of insulin resistance among lung cancer patients. Insulin resistance was proven to be an additional risk factor for lung cancer in 1 study,<sup>28</sup> though the mechanisms concerning the role of insulin resistance in lung cancerogenesis were not studied in that work.<sup>33</sup> In our study, alterations in glucose metabolism were also observed, expressed as higher glucose and insulin concentrations and HOMA-IR levels, in the lung cancer patients than in the control subjects. Evidence presented by Ceriello<sup>34</sup> shows that persistent elevated blood glucose is highly toxic. It induces insulin resistance and impairs insulin secretion by pancreatic  $\beta$ -cells.<sup>34</sup> During chronic hyperglycemia and in the early phase of hyperinsulinemia, free radicals are formed disproportionately and/or impaired antioxidant defenses are observed.<sup>29,35</sup> In addition to metabolic alterations occurring during cancerogenesis, such as a less efficient Cori cycle, hyperglycemia may also result from an imbalanced diet rich in available carbohydrates and with a high GI and/or GL.<sup>36</sup> It would be interesting to see whether dietary intakes with a proven impact on glucose homeostasis are different between the lung cancer and general populations, as this could be an additional factor contributing to glucose alterations. In this study we found that lung cancer patients consumed significantly higher total as well as available carbohydrate content and demonstrated a higher ratio of available to total carbohydrates, while dietary fiber content expressed in g/1,000 kcal of food intake was significantly lower in the lung cancer patients than in the control group. These results suggest that the lung cancer patients' diets were worse than the control subjects' in terms of the quality and quantity of carbohydrates. This resulted in the observed higher GI and GL of the diets of lung cancer patients compared to the control subjects. Melkonian et al. also observed a higher GI of diets and lower dietary fiber intakes by lung cancer patients than control subjects, though there were no differences in the GL of diets or total carbohydrate content.<sup>37</sup>

Moreover, the abovementioned authors found an important association between GI (not GL of diets) and lung cancer risk in the studied group of non-Hispanic whites. Also, a link between high GI or GL and an increased risk of prevalence was observed in other site-specific cancers.<sup>38</sup> On the other hand, a study conducted by Hu et al. found no significant associations between the GI of diets and the risk of lung cancer<sup>39</sup>; therefore, more studies concerning these relationships should be carried out.

Although some studies have been designed to ascertain the impact of GI and/or the GL of diets on the risk of different site-specific cancers,<sup>37,39,40</sup> associations between GI or GL and antioxidant/oxidant status have not been assessed, either in lung cancer patients or in other cancer-related populations. The most frequently described mechanism of cancerogenesis related to a high GI and/or GL of diets is based on the direct mitogenic effect exerted by a high level of insulin and on the indirect effect: by affecting insulin-like growth factors (IGF) and binding proteins (IGFBPs) and by increasing the bioactivity of IGF-I. Circulating insulin as well as IGF-1 may inhibit apoptosis and therefore lead to the immortality of cancer cells.<sup>39</sup> Despite the undeniable role of insulin, IGF and IGFBPs in lung cancerogenesis, an altered antioxidant/oxidant status related to a high GI and/or high GL also seems to be important in lung cancer management, also due to the fact that a large cohort study on a healthy population did not find any association between hs-CRP (an indicator of systemic inflammation) and GI or GL, which showed that another mechanism (other than a pro-inflammatory one) may be linked with metabolic alterations and a high GI or GL of diets.<sup>41</sup> Therefore, finding potential relationships between them in a population with lung cancer may provide additional data on the pathogenesis of this disease.

In this study, we found a significant positive association between GI and TOS, but only in men with lung cancer; however, in women with lung cancer, circulating glucose positively correlated with the index of oxidative stress. These results indicate that a high GI and/or GL may influence the redox balance by intensifying oxidative stress, in addition to other, non-dietary factors, e.g., cancer development and metabolic disturbances. Interestingly, in the control subjects, we observed more relationships between the parameters of antioxidant/oxidant status and biochemical parameters related to circulating glucose. Among the control men, glucose concentration positively correlated with TOS and OSI, which consequently resulted in positive relationships between the parameters of oxidant status and insulin level and HOMA-IR. Moreover, in the control women, these relationships were weaker and observed only with insulin levels, which suggests that the observed dependencies may be strongly related to gender.

High-GI foods are characterized by fast-release carbohydrates and the results of a sharp increase in blood glucose level, including a greater insulin demand.<sup>15</sup> Acute increases in blood glucose concentration may promote

the production of free radicals by non-enzymatic glycation and by an imbalance in the ratio of NADH to NAD<sup>+</sup> induced by glucose in the cells.<sup>14</sup> This is the mechanism most commonly mentioned to account for the relationship between high dietary GI and increased oxidative stress.<sup>42</sup> Hu et al.<sup>14</sup> examined the associations of GI and GL with the plasma oxidative stress markers, MDA and isoprostane (IsoPS) concentration. They found that a low GI, not a low-carbohydrate diet, appears to be beneficial in reducing oxidative stress. In our study of lung cancer patients, we also observed a significant correlation between the parameters of oxidative stress and GI, but not with GL.

In the crossover clinical study by Botero et al., a 10-day low-GI dietary intervention was compared with a high-GI diet in overweight or obese patients.<sup>43</sup> The results showed significantly higher plasma total antioxidant activity under fasting conditions and during the postprandial period on the 7<sup>th</sup> day, but no differences were observed in cardiovascular disease risk biomarkers, such as insulin sensitivity, acute insulin response, total cholesterol, HDL, triglycerides, etc.<sup>43</sup> This study suggests that the parameters of one's antioxidant/oxidant balance are primarily affected by the GI of one's diet, before any other biochemical variables, and may therefore provide a quick answer as to the impact of GI on systemic homeostasis. Moreover, the meta-analysis of the long-term effects of low GI and GL performed by Schwingshackl and Hoffmann showed decreases in C-reactive proteins and fasting insulin concentrations, as well as fat-free mass in obesity subjects, while no changes were observed in the levels of lipid profile biomarkers.<sup>44</sup> In the study by Pittas et al., a beneficial effect on serum CRP concentration was also observed.<sup>45</sup> In our study as in the studies presented above, parameters of circulating glucose significantly correlated with oxidant status; moreover, in the control subjects these correlations were stronger than in the lung cancer patients, probably due to the additional effects of cancerogenesis and cancer-related malnutrition on redox balance among the lung cancer patients. However, we did not find any correlations between fat-free mass index and the parameters of redox status, regardless of the group.

In this study, we observed that the nutritional status of lung cancer patients, mainly women, was associated with total antioxidant capacity rather than with parameters related to oxidative stress: TOS and OSI. This suggests that a reduction in antioxidant capacity may be associated with cancer-related malnutrition. Interestingly, in the control subjects, we found that nutritional status was linked with parameters of antioxidant status and oxidative stress, and that TAS positively correlated with calf circumference, waist circumference and weight; however, more statistically significant relationships were observed between parameters related to body mass and oxidative stress. Based on the observed correlations, we concluded that in healthy people, a high body mass may intensify oxidative stress, while in a population with cancer-related

metabolic alterations of nutritional status, mainly related to muscles, these alterations may be additional factors which influence antioxidant capacity. Indeed, several studies have confirmed at the tissue and molecular level that cancer-related cachexia may negatively affect redox balance.<sup>46,47</sup> Marin-Corral et al. found that malnutrition related to cancer disrupted antioxidant/oxidant status in the muscles and hearts of rats, increasing oxidative modifications of key proteins involved in muscle structure and function.<sup>46</sup> In a study performed on men with severe chronic obstructive pulmonary disease (COPD) and lung cancer, Puig-Vilanova et al. observed that cachectic patients had significantly higher levels of muscle protein oxidation and ubiquitination, and that redox-sensitive signaling pathways like nuclear factor kappa B (NF- $\kappa$ B) and Forkhead box O (FoxO) were activated.<sup>47</sup> Moreover, structural and functional protein levels were lower in the muscles of malnourished patients, regardless of the disease, while levels of autophagy markers were increased only in the muscles of COPD patients and not in healthy subjects. In this study, however, we did not observe any differences in FFMI, an independent parameter of muscle status, between the lung cancer and control groups, nor was any correlation of parameters related to antioxidant/oxidant status with FFMI or BFP found. On the other hand, in control subjects we observed that MDA, a parameter of lipid oxidation, positively correlated with weight as well as BMI. A high body mass is closely related to an altered redox balance. Mechanisms involved in obesity-related disruption in antioxidant status and an increase in ROS resulted in systemic oxidative stress concerning hyperleptinemia, hyperglycemia and hyperlipidemia and an increase of pro-inflammatory cytokine levels, as well as endothelial dysfunction.<sup>48</sup> It is interesting whether sex determines the observed differences in these relationships, since in women, regardless of the occurrence of cancer, parameters of nutritional status were related to a redox state, while in men it was mainly the parameters related to glucose that were linked with parameters of oxidative stress. This could, at least partially, result from differences in the activity of sex hormones. In a study by Barp et al. performed on female and male rats, it was demonstrated that estrogen may have an antioxidant role, while testosterone does not.<sup>49</sup> Moreover, in men (mainly in the control subjects) we observed a higher waist circumference than in women, which could also strengthen correlations with parameters of oxidative stress.<sup>50</sup>

## Conclusions

The results presented in this study show that in lung cancer patients, parameters of oxidative stress are related to GI and alterations in glucose concentration, but not to nutritional status, while total antioxidant status is associated more with nutritional status, but not with parameters

related to glucose concentration or GI and GL of diets. The observed relationships are strongly determined by sex. Further investigations performed on a larger cohort are required to better clarify the observed relationships and to explain the potential mechanisms involved.

## References

1. Torre LA, Bray F, Siegel RL, Ferlay J, Lortet-Tieulent J, Jemal A. Global cancer statistics, 2012. *CA Cancer J Clin*. 2015;65(2):87–108. doi:10.3322/caac.21262
2. Wojciechowska U, Didkowska J. Zachorowania i zgony na nowotwory złośliwe w Polsce. Krajowy Rejestr Nowotworów, Centrum Onkologii – Instytut im. Marii Skłodowskiej-Curie. <http://onkologia.org.pl/raporty/>. Accessed June 23, 2018.
3. Wang A, Kubo J, Luo J, et al. Active and passive smoking in relation to lung cancer incidence in the Women's Health Initiative Observational Study prospective cohort. *Ann Oncol*. 2015;26(1):221–230. doi:10.1093/annonc/mdu470
4. Filaire E, Dupuis C, Galvaing G, et al. Lung cancer: What are the links with oxidative stress, physical activity and nutrition. *Lung Cancer*. 2013;82(3):383–389. doi:10.1016/j.lungcan.2013.09.009
5. Wang Y, Li F, Wang Z, Qiu T, Shen Y, Wang M. Fruit and vegetable consumption and risk of lung cancer: A dose–response meta-analysis of prospective cohort studies. *Lung Cancer*. 2015;88(2):124–130.
6. Misthos P, Katsaragakis S, Milingos N, et al. Postresectional pulmonary oxidative stress in lung cancer patients: The role of one-lung ventilation. *Eur J Cardiothorac Surg*. 2005;27(3):379–383. doi:10.1016/j.ejcts.2004.12.023
7. Rahman I, Biswas SK, Kode A. Oxidant and antioxidant balance in the airways and airway diseases. *Eur J Pharmacol*. 2006;533(1–3):222–239. doi:10.1016/j.ejphar.2005.12.087
8. Gharibvand L, Shavlik D, Ghamsary M, et al. The association between ambient fine particulate air pollution and lung cancer incidence: Results from the AHSMOG-2 study. *Environ Health Perspect*. 2017;125(3):378–384. doi:10.1289/EHP124
9. Saha SK, Lee S Bin, Won J, et al. Correlation between oxidative stress, nutrition, and cancer initiation. *Int J Mol Sci*. 2017;18(7):1544. doi:10.3390/ijms18071544
10. Khare M, Mohanty C, Das BK, Jyoti A, Mukhopadhyay B, Mishra SP. Free radicals and antioxidant status in protein energy malnutrition. *Int J Pediatr*. 2014;2014:1–6. doi:10.1155/2014/254396
11. Mantovani G, Madeddu C, Macciò A. Cachexia and oxidative stress in cancer: An innovative therapeutic management. *Curr Pharm Des*. 2012;18(31):4813–4818. doi:10.2174/138161212803216889
12. Russo GL, Tedesco I, Spagnuolo C, Russo M. Antioxidant polyphenols in cancer treatment: Friend, foe or foil? *Semin Cancer Biol*. 2017;46:1–13. doi:10.1016/j.semcancer.2017.05.005
13. Pitsavos C, Panagiotakos DB, Tzima N, Chrysoshoou C, Economou M. Adherence to the Mediterranean diet is associated with total antioxidant capacity in healthy adults: The ATTICA study. *Am J Clin Nutr*. 2005;82(3):694–699.
14. Hu Y, Block G, Norkus EP, Morrow JD, Dietrich M, Hudes M. Relations of glycemic index and glycemic load with plasma oxidative stress markers. *Am J Clin Nutr*. 2006;84(1):70–77. doi:10.1093/ajcn/84.1.70
15. Dudziak K, Regulska-Ilow B. The importance of glycemic load of the diet in the development of cancer. *Postepy Hig Med Dosw (Online)*. 2013;67:449–462. doi:10.5604/17322693.1050032
16. Erel O. A new automated colorimetric method for measuring total oxidant status. *Clin Biochem*. 2005;38(12):1103–1111. doi:10.1016/j.clinbiochem.2005.08.008
17. Aycicek A, Erel O, Kocyigit A. Decreased total antioxidant capacity and increased oxidative stress in passive smoker infants and their mothers. *Pediatr Int*. 2005;47(6):635–639.
18. Jacobo-Cejudo MG, Valdés-Ramos R, Guadarrama-López AL, Pardo-Morales RV, Martínez-Carrillo BE, Harbig LS. Effect of n-3 polyunsaturated fatty acid supplementation on metabolic and inflammatory biomarkers in type 2 diabetes mellitus patients. *Nutrients*. 2017;9(6):573.
19. Schutz Y, Kyle UUG, Pichard C. Fat-free mass index and fat mass index percentiles in Caucasians aged 18–98 y. *Int J Obes Relat Metab Disord*. 2002;26(7):953–960.

20. Schröder H, Covas MI, Marrugat J, et al. Use of a three-day estimated food record, a 72-hour recall and a food-frequency questionnaire for dietary assessment in a Mediterranean Spanish population. *Clin Nutr.* 2001;20(5):429–437.
21. Szponar L, Rychlik E, Wolnicka K; Instytut Żywności i Żywienia im. Aleksandra Szczygła. *Album fotografii produktów i potraw.* Warszawa, Poland: Instytut Żywności i Żywienia; 2008.
22. Kunachowicz H, Przygoda B, Nadolna I, Iwanow K. *Tabele składu i wartości odżywczej żywności.* Warszawa, Poland: Wydawnictwo Lekarskie PZWL; 2017.
23. Louie JCY, Flood V, Turner N, Everingham C, Gwynn J. Methodology for adding glycemic index values to 24-hour recalls. *Nutrition.* 2011; 27(1):59–64. doi:10.1016/j.nut.2009.12.006
24. Atkinson FS, Foster-Powell K, Brand-Miller JC. International Tables of Glycemic Index and Glycemic Load Values: 2008. *Diabetes Care.* 2008;31(12):2281–2283.
25. The University of Sydney. Glycemic Index Research Service 2007. www.glycemicindex.com. Accessed on April 20, 2018.
26. National Cancer Institute. Diet History Questionnaire Database File 2006. [http://riskfactor.cancer.gov/DHQ/database/dhq1\\_032806.csv](http://riskfactor.cancer.gov/DHQ/database/dhq1_032806.csv)
27. Zabłocka-Słowińska K, Porebska I, Golecki M, et al. Total antioxidant status in lung cancer is associated with levels of endogenous antioxidants and disease stage rather than lifestyle factors: Preliminary study. *Contemp Oncol (Pozn).* 2016;20(4):302–307. doi:10.5114/wo.2016.61850
28. Rahman I, MacNee W. Role of oxidants/antioxidants in smoking-induced lung diseases. *Free Radic Biol Med.* 1996;21(5):669–681. doi:10.1016/0891-5849(96)00155-4
29. Marfella R, Quagliari L, Nappo F, Ceriello A, Giugliano D. Acute hyperglycemia induces an oxidative stress. *J Clin Invest.* 2001;108(4):635–636. doi:10.1172/JCI0113727A
30. Azad N, Rojanasakul Y, Vallyathan V. Inflammation and lung cancer: Roles of reactive oxygen/nitrogen species. *J Toxicol Environ Heal B Crit Rev.* 2008;11(1):1–15. doi:10.1080/10937400701436460
31. Arends J, Baracos V, Bertz H, et al. ESPEN expert group recommendations for action against cancer-related malnutrition. *Clin Nutr.* 2017; 36(5):1187–1196. doi:10.1016/j.clnu.2017.06.017
32. Heber D, Chlebowski RT, Ishibashi DE, Patients C, Herrold JN, Block JB. Abnormalities in glucose and protein metabolism in noncachectic lung cancer patients. *Cancer Res.* 1982;42(11):4815–4819.
33. Petridou ET, Sergentanis TN, Antonopoulos CN, et al. Insulin resistance: An independent risk factor for lung cancer? *Metabolism.* 2011; 60(8):1100–1106. doi:10.1016/j.metabol.2010.12.002
34. Ceriello A. Postprandial hyperglycemia and diabetes complications: Is it time to treat? *Diabetes.* 2005;54(1):1–7. doi:10.2337/DIABETES.54.1.1
35. Rajendran P, Nandakumar N, Rengarajan T, et al. Antioxidants and human diseases. *Clin Chim Acta.* 2014;436(7):332–347. doi:10.1016/j.cca.2014.06.004
36. Klement RJ, Kämmerer U. Is there a role for carbohydrate restriction in the treatment and prevention of cancer? *Nutr Metab.* 2011;8(1):75. doi:10.1186/1743-7075-8-75
37. Melkonian SC, Daniel CR, Ye Y, Pierzynski JA, Roth JA, Wu X. Glycemic index, glycemic load, and lung cancer risk in non-Hispanic whites. *Cancer Epidemiol Biomarkers Prev.* 2016;25(3):532–539. doi:10.1158/1055-9965.EPI-15-0765
38. Romieu I, Ferrari P, Rinaldi S, et al. Dietary glycemic index and glycemic load and breast cancer risk in the European Prospective Investigation into Cancer and Nutrition (EPIC). *Am J Clin Nutr.* 2012;96(2): 345–355.
39. Hu J, La Vecchia C, Augustin LS, et al; Canadian Cancer Registries Epidemiology Research Group. Glycemic index, glycemic load and cancer risk. *Ann Oncol.* 2013;24:245–251. doi:10.1093/annonc/mds235
40. Turati F, Galeone C, Gandini S, et al. High glycemic index and glycemic load are associated with moderately increased cancer risk. *Mol Nutr Food Res.* 2015;59(7):1384–1394. doi:10.1002/mnfr.201400594
41. Griffith JA, Ma Y, Chasan-Taber L, et al. Association between dietary glycemic index, glycemic load, and high-sensitivity C-reactive protein. *Nutrition.* 2008;24(5):401–406.
42. Augustin LSA, Kendall CWC, Jenkins DJA, et al. Glycemic index, glycemic load and glycemic response: An International Scientific Consensus Summit from the International Carbohydrate Quality Consortium (ICQC). *Nutr Metab Cardiovasc Dis.* 2015;25(9):795–815. doi:10.1016/j.numecd.2015.05.005
43. Botero D, Ebbeling CB, Blumberg JB, et al. Acute effects of dietary glycemic index on antioxidant capacity in a nutrient-controlled feeding study. *Obesity (Silver Spring).* 2009;17(9):1664–1670. doi:10.1038/oby.2009.203
44. Schwingshackl L, Hoffmann G. Long-term effects of low glycemic index/load vs. high glycemic index/load diets on parameters of obesity and obesity-associated risks: A systematic review and meta-analysis. *Nutr Metab Cardiovasc Dis.* 2013;23(8):699–706. doi:10.1016/j.numecd.2013.04.008
45. Pittas AG, Roberts SB, Das SK, et al. The effects of the dietary glycemic load on type 2 diabetes risk factors during weight loss. *Obesity (Silver Spring).* 2006;14(12):2200–2209.
46. Marin-Corral J, Fontes CC, Pascual-Guardia S, et al. Redox balance and carbonylated proteins in limb and heart muscles of cachectic rats. *Antioxid Redox Signal.* 2010;12(3):365–380. doi:10.1089/ars.2009.2818
47. Puig-Vilanova E, Rodriguez DA, Lloreta J, et al. Oxidative stress, redox signaling pathways, and autophagy in cachectic muscles of male patients with advanced COPD and lung cancer. *Free Radic Biol Med.* 2015;79:91–108. doi:10.1016/j.freeradbiomed.2014.11.006
48. Savini I, Catani MV, Evangelista D, Gasperi V, Avigliano L. Obesity-associated oxidative stress: Strategies finalized to improve redox state. *Int J Mol Sci.* 2013;14(5):10497–10538. doi:10.3390/ijms140510497
49. Barp J, Araújo ASDR, Fernandes TRG, et al. Myocardial antioxidant and oxidative stress changes due to sex hormones. *Braz J Med Biol Res.* 2002;35(9):1075–1081.
50. Furukawa S, Fujita T, Shimabukuro M, et al. Increased oxidative stress in obesity and its impact on metabolic syndrome. *J Clin Invest.* 2017; 114(12):1752–1761.

# Using laparoscopic ultrasound to delineate dangerous anatomy during difficult laparoscopic cholecystectomies

Maciej Sebastian<sup>A–F</sup>, Maciej Sroczyński<sup>A–F</sup>, Jerzy Rudnicki<sup>A–F</sup>

Department of Minimally Invasive Surgery and Proctology, Wrocław Medical University, Poland

A – research concept and design; B – collection and/or assembly of data; C – data analysis and interpretation; D – writing the article; E – critical revision of the article; F – final approval of the article

Advances in Clinical and Experimental Medicine, ISSN 1899–5276 (print), ISSN 2451–2680 (online)

*Adv Clin Exp Med.* 2019;28(8):1037–1042

## Address for correspondence

Maciej Sebastian  
E-mail: mseba@op.pl

## Funding sources

None declared

## Conflict of interest

None declared

Received on November 17, 2016

Reviewed on February 9, 2017

Accepted on August 8, 2018

Published online on June 14, 2019

## Abstract

**Background.** Bile duct injury (BDI) during laparoscopic cholecystectomy (LC) is not as common now as in the past, but it is still a very debilitating complication. Therefore, there is a very strong need for a method that lowers the number of complications during LC without any additional risks for the patient and the operating team. Laparoscopic ultrasound (LUS), which serves to delineate anatomy, appears to be a very effective and safe technique.

**Objectives.** The aim of this study was to explore the advantages of performing LUS during difficult LC.

**Material and methods.** The study group consisted of 126 patients who underwent surgery between January 2014 and February 2016. All the patients had difficult intraoperative anatomical conditions due to chronic inflammation, previous upper abdominal surgery or biliary pancreatitis in the past. We used a Toshiba PEF-704 LA laparoscopic probe and the Toshiba NemioMX SSA-590A diagnostic ultrasound system (Toshiba Corp., Tokyo, Japan). Doppler sonography was used to differentiate between vascular and biliary structures.

**Results.** Laparoscopic ultrasound ensured a safe plane of dissection and no biliary or vascular complications were observed. Stent insertion into the common bile duct before the operation undoubtedly made the identification of anatomical structures easier. Conversion to an open procedure was deemed necessary in only 6 patients (4.8%).

**Conclusions.** Laparoscopic ultrasound facilitates the successful performance of LCs. It can be used at any time during the operation; it is noninvasive; and there is no need to use X-rays or contrast dye, or to cannulate the cystic duct. The most important advantage of LUS is that it leads to a lower number of conversions and intraoperative complications by identifying anatomical relationships in the plane of dissection.

**Key words:** laparoscopic cholecystectomy, bile duct injury, laparoscopic ultrasound

## Cite as

Sebastian M, Sroczyński M, Rudnicki J. Using laparoscopic ultrasound to delineate dangerous anatomy during difficult laparoscopic cholecystectomies. *Adv Clin Exp Med.* 2019;28(8):1037–1042. doi:10.17219/acem/94077

## DOI

10.17219/acem/94077

## Copyright

© 2019 by Wrocław Medical University

This is an article distributed under the terms of the Creative Commons Attribution Non-Commercial License (<http://creativecommons.org/licenses/by-nc-nd/4.0/>)

## Introduction

Bile duct injury (BDI) during open cholecystectomy occurs in 0.1–0.3% of all cases; in laparoscopic cholecystectomy (LC) this rate ranges from 0.08% to 0.5%.<sup>1,2</sup> According to recent studies, the rates of BDI in LC are approaching the rates in open cholecystectomy, which may reflect better preparation, more sophisticated equipment and more surgical personnel moving beyond the “learning curve”.<sup>1–5</sup> Routine intraoperative cholangiography (IOC) during LC remains a controversial issue and a growing number of surgeons are abandoning it.<sup>6</sup> Preoperative magnetic resonance cholangiopancreatography can be used to detect choledocholithiasis that can be cleared with endoscopic retrograde cholangiopancreatography (ERCP). If choledocholithiasis is detected after a cholecystectomy, ERCP is performed postoperatively.<sup>6</sup> Additionally, most occult bile duct stones detected with routine IOC are clinically insignificant. Bile duct injury is not 100% preventable, and IOC does not provide any information about vascular abnormalities.<sup>7</sup> Therefore, there is a very strong need for a method that will reduce the number of complications without any additional risks for the patient and the operating team. Laparoscopic ultrasound (LUS) appears to be a very effective tool, especially in difficult cases when the inflammatory process changes anatomical relationships, which can lead to disastrous complications if structures are not identified correctly.

## Material and methods

The study group consisted of 126 patients (80 women and 46 men) operated on between January 2014 and February 2016. Written informed consent was obtained from all the participants, and all the procedures performed in this study involving human participants were in accordance with the ethical standards of the 1964 Helsinki Declaration and its later amendments. The indication for the surgery was symptomatic cholelithiasis. The patients selected for the study had difficult intraoperative anatomical conditions due to chronic cholecystitis, previous upper abdominal surgery or biliary pancreatitis (without surgery) in the past (Table 1,2).

The exclusion criteria for the study were acute cholecystitis, acute pancreatitis, gallbladder cancer, and any abdominal operations or acute abdominal conditions within the previous 12 months. The operations were performed on an elective basis by 2 surgeons experienced in LC (>200 LC) and LUS (>100 examinations). We used a Toshiba PEF-704 LA laparoscopic probe (frequency 7.0 MHz) and the Toshiba NemioMX SSA-590A diagnostic ultrasound system (both from Toshiba Corp., Tokyo, Japan). Intraoperative LUS was performed in every patient. The trocar sites were identical to those in standard LC (we used 2 5-mm trocars and 2 10-millimeter trocars). The ultrasound probe was inserted through the epigastrical (transverse

Table 1. Characteristics of the study group

Total number of patients	126
Women/men	80 (63.5%)/46 (36.5%)
Biliary pancreatitis in the past	23 (18%)
Operation for perforation of gastric or duodenal ulcer	10 (8%)
Right hemicolectomy	12 (9.5%)
Chronic inflammation of gallbladder	81 (64%)
Number of conversions	6 (4.8%)
Biliary and/or vascular complications	0 (0%)
Stent insertion to the common bile duct before operation	32 (25.4%)

Table 2. Duration of laparoscopic ultrasound and operation

Time of laparoscopic ultrasound [min]	5.5 (4–9.5)
Time of operation [min] – from skin incision till skin closure	72 (53–130)

view) or umbilical trocar (longitudinal view). The duplex Doppler function facilitated differentiation between vascular and avascular structures. The LUS examination was performed after initial preparation in Calot’s triangle and after shifting the gallbladder to the right. The first structure visualized was the “Mickey Mouse sign” – a characteristic configuration of the bile duct, the proper hepatic artery and the portal vein that resembles the head of Mickey Mouse from Walt Disney movies (Fig. 1A,B). We moved up and down from this point and delineated the anatomy (Fig. 2A–D). Preoperative bile duct stenting (due to massive choledocholithiasis and/or narrowing of the bile duct) made ultrasound interpretation easier, because stents are very easy to identify using ultrasound (Fig. 3A–C, Fig. 4A–C). In our practice, we leave stents throughout the surgery and remove them during a subsequent hospitalization.

Our department is the regional center for ERCP and patients who are qualified for LC after ERCP frequently choose our department, which is the reason for the very high percentage (25.4%) of patients in the study group with stents in the bile duct. During an LC, we cannot touch the tissues and palpate the stents in the bile duct (they are also invisible from the outside), but we can quite easily find them using LUS. We did not observe any complications in the study group associated with the insertion or removal of stents, but it is not a standard procedure before every LC in our department. The indications for inserting stents are massive choledocholithiasis and/or narrowing of the bile duct.

## Results

Conversion to an open procedure was performed in 6 patients (4.8%): 2 men (1 after acute biliary pancreatitis and the other cancer one with chronic cholecystitis, neither



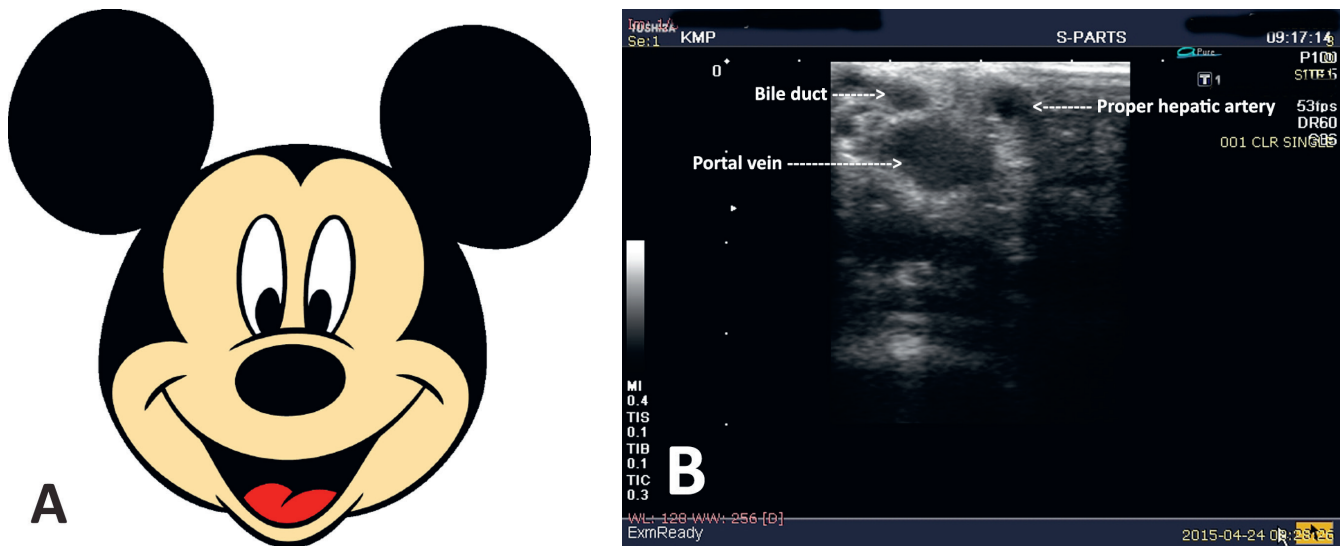


Fig. 1. A – Mickey Mouse; B – the characteristic configuration of the bile duct, the proper hepatic artery and the portal vein in the hepatoduodenal ligament known as the “Mickey Mouse sign”

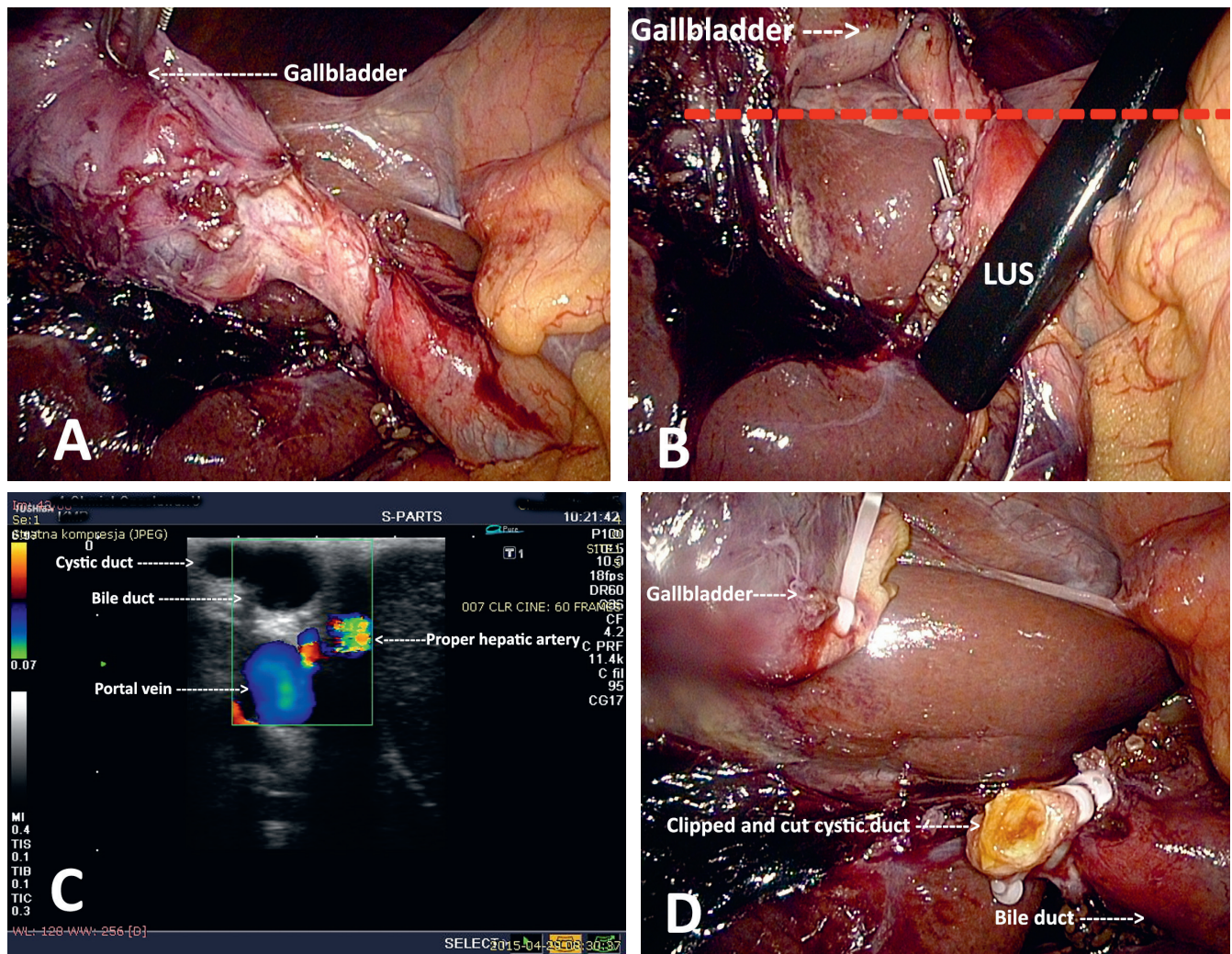


Fig. 2. A – short and wide connection of the cystic duct with the bile duct; chronic cholecystitis; B – LUS defines the correct level of clipping (red line); C – LUS with duplex Doppler function visualizes the connection of the cystic duct with the bile duct, the proper hepatic artery and the portal vein; D – safe clipping and cutting of the cystic duct without narrowing the bile duct

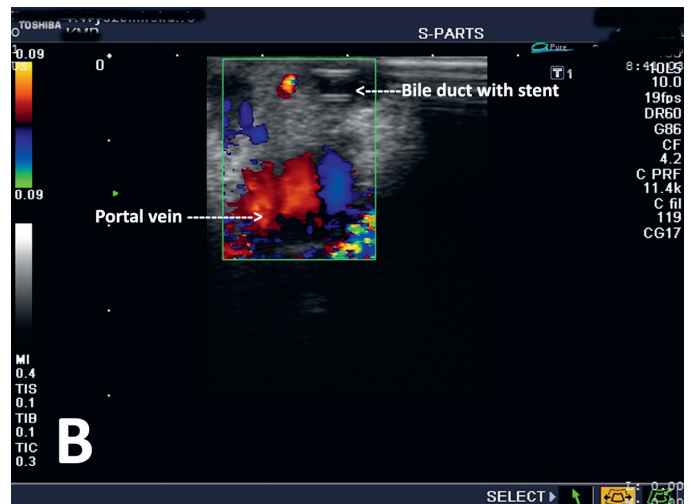
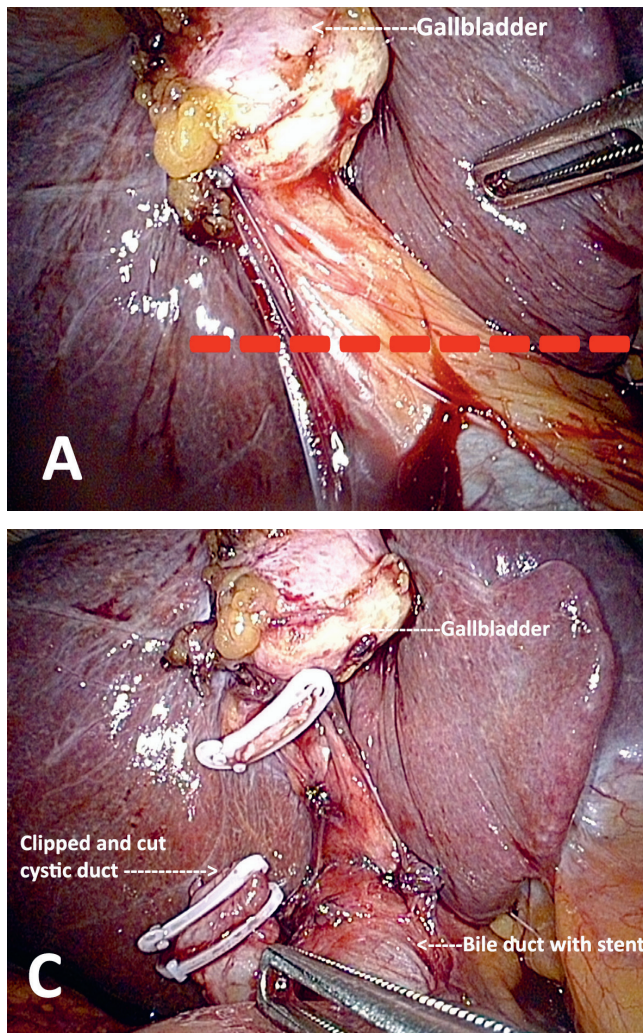


Fig. 3. A – fibrotic and shrunken gallbladder with chronic inflammation; the red line marks the correct level of clipping; B – stent insertion into the bile duct before laparoscopic cholecystectomy (LC) makes ultrasound interpretation easier; C – the cystic duct is safely clipped and cut without narrowing or injuring the bile duct

had stents in the biliary tract) and 4 women (2 after acute biliary pancreatitis and 2 with chronic cholecystitis, also without stents in the biliary tract). The conversions were due to technical problems: because chronic inflammation and hard infiltrations in the region of the hepatoduodenal ligament prevented safe laparoscopic preparation, open cholecystectomies were performed. The conversions were not caused by bleeding from injured vessels in the hepatoduodenal ligament or BDI. We completed LUS in 100% of our patients and did not have to perform IOC. To us, successful LUS meant a safe plane of dissection and no biliary and vascular complications; we do not treat conversion as a failure. Stent insertion into the common bile duct (CBD) before surgery undoubtedly made the identification of anatomical structures easier (there were no conversions in this group of patients).

## Discussion

Laparoscopic ultrasound makes the dreams of many surgeons performing LC come true. It minimizes the level of stress associated with clipping and cutting the cystic

duct and the cystic artery. A major advantage of this method is that it is noninvasive and can be performed at any time during the operation. Laparoscopic ultrasound enables us to differentiate between vascular and avascular structures by duplex Doppler; cannulation of the cystic duct and exposure to radiation and contrast dye is avoided; it can be performed during pregnancy; it is possible to visualize the pancreatic head and possible pathology in this localization.<sup>8</sup> The disadvantages of LUS are undoubtedly the long learning curve, the need for special equipment and limitations to the visualization of the bile ducts.<sup>8</sup> Intraoperative cholangiography allows visualization of the entire biliary tree and finding abnormal anatomic configurations. In comparison to IOC, LUS is less time-consuming and cheaper, but it has comparable sensitivity and specificity in terms of confirmations of anatomical relationships and the presence of bile duct stones.<sup>8</sup> In a study by Teefey et al. IOC confirmed aberrant anatomy in 14% of the patients not found in LUS<sup>9</sup>; in another study LUS detected 82% of anomalies found on IOC.<sup>10</sup> On the other hand, Wysocki's study found that sound surgical judgment combined with a critical view of safety (CVS) are vital to preventing BDI, and routine IOC does not fully protect against major BDI.<sup>11</sup> If the bile duct is mistaken for the cystic duct, IOC can itself lead to an incision causing Strasberg type D BDI.<sup>11–14</sup> A study by Biffl et al. showed that the routine use of LUS was associated with a lack of complications from bile ducts, while 2.5% of the patients who underwent surgery without LUS had bile complications; there were also fewer conversions in the LUS group.<sup>15</sup> Machi et al. reported that in 1,381 LCs with routine use of LUS, no BDI was observed and the conversion rate was lower (6%); additional IOC was necessary in only 2% of the cases.<sup>16</sup> We consider the key to a safe LC

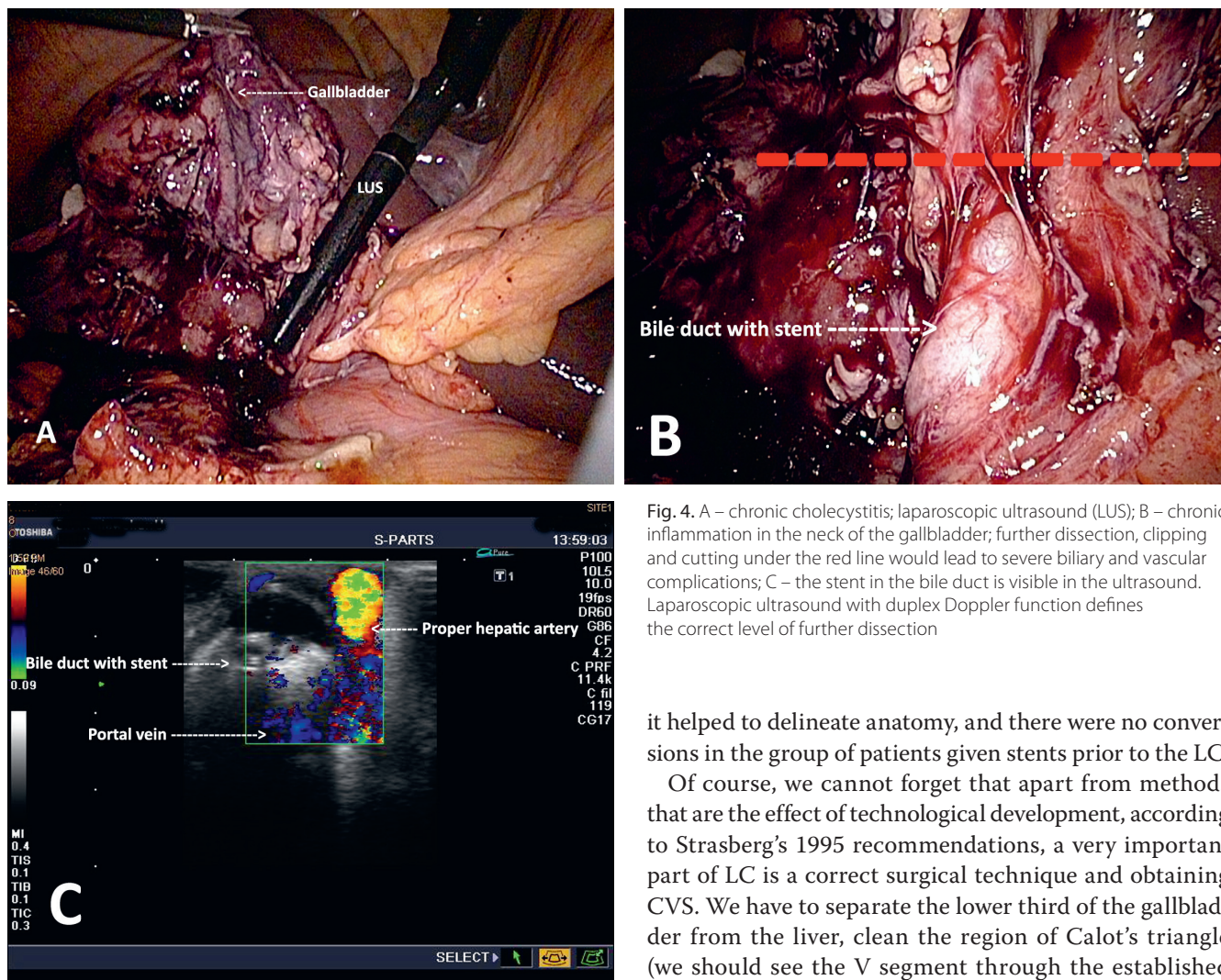


Fig. 4. A – chronic cholecystitis; laparoscopic ultrasound (LUS); B – chronic inflammation in the neck of the gallbladder; further dissection, clipping and cutting under the red line would lead to severe biliary and vascular complications; C – the stent in the bile duct is visible in the ultrasound. Laparoscopic ultrasound with duplex Doppler function defines the correct level of further dissection

is confirmation of the right plane of dissection. We agree with other authors that as a noninvasive, safe, less costly and faster method, LUS should be the primary imaging method during LC, whereas IOC should be used only when any doubts exist.<sup>7,17</sup> Our success rate with LUS was 100% (a safe plane of dissection, no biliary or vascular complications), while the success rate for other authors varied between 95–100% with LUS and 89–97% with IOC (albeit other authors’ definition of “success” was not clear).<sup>18</sup>

The conversion rate from LC to open cholecystectomy varies from 2.6% to 11.9%. Factors associated with a need for conversion are the degree of inflammation, previous upper abdominal surgery, acute cholecystitis, advanced age, male gender, dense adhesions, and obscure anatomy in Calot’s triangle.<sup>19,20</sup> Laparoscopic ultrasound can diminish the rate of conversions without additional risk for the patient by providing exact navigation in the operating field: the decision of whether or not to convert to open surgery is based on visual monitoring of the vessels and the CBD, not on leaking bile and a hole in the portal vein or the hepatic artery. The question of protective bile duct stenting before surgery remains open; in our study

it helped to delineate anatomy, and there were no conversions in the group of patients given stents prior to the LC.

Of course, we cannot forget that apart from methods that are the effect of technological development, according to Strasberg’s 1995 recommendations, a very important part of LC is a correct surgical technique and obtaining CVS. We have to separate the lower third of the gallbladder from the liver, clean the region of Calot’s triangle (we should see the V segment through the established window); the cystic duct and the cystic artery should be the only visible ductal structures left between the gallbladder and the CBD. Sometimes the cystic artery is cut with electrocautery close to the gallbladder, in which case only the cystic duct is visible. If we cannot obtain CVS, we should perform an open cholecystectomy or use additional methods of visualization.<sup>21,22</sup> If we have any doubts, we should use LUS and sigh with relief that we have not followed a misleading route directly to severe complications.

To conclude, LUS as a method of intraoperative guidance during difficult LC helps the surgeon navigate in a hostile environment and allows the procedure to be successfully performed. It enables the surgeon to be certain of the structures being identified, clipped and cut intraoperatively, which is of utmost importance during a difficult LC.

**References**

1. Tropea A, Pagano D, Biondi A, Spada M, Gruttadauria S. Treatment of the iatrogenic lesion of the biliary tree secondary to laparoscopic cholecystectomy: A single center experience. *Updates Surg.* 2016; 68(2):143–148.
2. Halbert C, Pagkratis S, Yang J, et al. Beyond the learning curve: Incidence of bile duct injuries following laparoscopic cholecystectomy normalize to open in the modern era. *Surg Endosc.* 2016;30(6): 2239–2243.

3. Gentileschi P, Di Paola M, Catarci M, et al. Bile duct injuries during laparoscopic cholecystectomy: A 1994–2001 audit on 13,718 operations in the area of Rome. *Surg Endosc.* 2004;18(2):232–236.
4. Nuzzo G, Giulianti F, Giovannini I, et al. Bile duct injury during laparoscopic cholecystectomy: Results of an Italian national survey on 56 591 cholecystectomies. *Arch Surg.* 2005;140(10):986–992.
5. Hamad MA, Nada AA, Abdel-Atty MY, Kawashti AS. Major biliary complications in 2,714 cases of laparoscopic cholecystectomy without intraoperative cholangiography: A multicenter retrospective study. *Surg Endosc.* 2011;25(12):3747–3751.
6. Aziz O, Ashrafian H, Jones C, et al. Laparoscopic ultrasonography versus intra-operative cholangiogram for the detection of common bile duct stones during laparoscopic cholecystectomy: A meta-analysis of diagnostic accuracy. *Int J Surg.* 2014;12(7):712–719.
7. Machi J, Oishi AJ, Tajiri T, Murayama KM, Furumoto NL, Oishi RH. Routine laparoscopic ultrasound can significantly reduce the need for selective intraoperative cholangiography during cholecystectomy. *Surg Endosc.* 2007;21(2):270–274.
8. Yao CC, Huang SM, Lin CC, et al. Assessment of common bile duct using laparoscopic ultrasound during laparoscopic cholecystectomy. *Surg Laparosc Endosc Percutan Tech.* 2009;19(4):317–320.
9. Teefey SA, Soper NJ, Middleton WD, et al. Imaging of the common bile duct during laparoscopic cholecystectomy: Sonography versus videofluoroscopic cholangiography. *AJR Am J Roentgenol.* 1995;165(4):847–851.
10. Röthlin M, Largiadèr F. The anatomy of the hepatoduodenal ligament in laparoscopic sonography. *Surg Endosc.* 1994;8(3):173–180.
11. Wysocki AP. Population-based studies should not be used to justify a policy of routine cholangiography to prevent major bile duct injury during laparoscopic cholecystectomy. *World J Surg.* 2016;41(1):82–89.
12. Beksac K, Turhan N, Karaagaoglu E, Abbasoglu O. Risk factors for conversion of laparoscopic cholecystectomy to open surgery: A new predictive statistical model. *J Laparoendosc Adv Surg Tech A.* 2016;26(9):693–696.
13. Sutcliffe RP, Hollyman M, Hodson J, Bonney G, Vohra RS, Griffiths EA; CholeS study group, West Midlands Research Collaborative. Preoperative risk factors for conversion from laparoscopic to open cholecystectomy: A validated risk score derived from a prospective UK database of 8820 patients. *HPB (Oxford).* 2016;1365-182X(16):31837–31838.
14. Le VH, Smith DE, Johnson BL. Conversion of laparoscopic to open cholecystectomy in the current era of laparoscopic surgery. *Am Surg.* 2012;78(12):1392–1395.
15. Biffl WL, Moore EE, Offner PJ, Franciose RJ, Burch JM. Routine intraoperative laparoscopic ultrasonography with selective cholangiography reduces bile duct complications during laparoscopic cholecystectomy. *J Am Coll Surg.* 2001;193(3):272–280.
16. Machi J, Johnson JO, Deziel DJ. The routine use of laparoscopic ultrasound decreases bile duct injury: A multicenter study. *Surg Endosc.* 2009;23(2):384–388.
17. Jamal KN, Smith H, Ratnasingham K, Siddiqui MR, McLachlan G, Belgaumkar AP. Meta-analysis of the diagnostic accuracy of laparoscopic ultrasonography and intraoperative cholangiography in detection of common bile duct stones. *Ann R Coll Surg Engl.* 2016;98(4):244–249.
18. Perry KA, Myers JA, Deziel DJ. Laparoscopic ultrasound as the primary method for bile duct imaging during cholecystectomy. *Surg Endosc.* 2008;22(1):208–213.
19. Malik AM. Difficult laparoscopic cholecystectomies. Is conversion a sensible option? *J Pak Med Assoc.* 2015;5(7):698–700.
20. Lee NW, Collins J, Britt R. Evaluation of preoperative risk factors for converting laparoscopic to open cholecystectomy. *Am Surg.* 2012;78(8):831–833.
21. Buddingh KT, Nieuwenhuijs VB, van Buuren L, Hulscher JB, de Jong JS, van Dam GM. Intraoperative assessment of biliary anatomy for prevention of bile duct injury: A review of current and future patient safety interventions. *Surg Endosc.* 2011;25(8):2449–2461.
22. Strasberg SM, Hertl M, Soper NJ. An analysis of the problem of biliary injury during laparoscopic cholecystectomy. *Am Coll Surg.* 1995;180(1):101–125.

# Identification of alternative splicing and lncRNA genes in pathogenesis of small cell lung cancer based on their RNA sequencing

Youming Lei<sup>A,D</sup>, Yunfei Shi<sup>A,B</sup>, Jin Duan<sup>B,C</sup>, Yinqiang Liu<sup>C,E</sup>, Guoli Lv<sup>C,E</sup>, Rou Shi<sup>B,E</sup>, Fujun Zhang<sup>B,E</sup>, Qingmei Yang<sup>B,C</sup>, Wei Zhao<sup>A,F</sup>

The First Affiliated Hospital of Kunming Medical University, China

A – research concept and design; B – collection and/or assembly of data; C – data analysis and interpretation; D – writing the article; E – critical revision of the article; F – final approval of the article

Advances in Clinical and Experimental Medicine, ISSN 1899–5276 (print), ISSN 2451–2680 (online)

*Adv Clin Exp Med.* 2019;28(8):1043–1050

## Address for correspondence

Wei Zhao  
E-mail: weizhaowz6@sohu.com

## Funding sources

The study was supported by the Scientific Research Projects of Institutions of Medical and Health Institutions in Yunnan Province The Role of NOD-like Receptors and Inflammatory Bodies in the Development of Xuanwei Lung Cancer (project No. 2016NS017); Number of Training Objects for Leaders of Medical Disciplines in Yunnan Province (project No. D2017013); Doctoral Research Fund of the First Affiliated Hospital of Kunming Medical University The research about PDGFRB functions on lung squamous cell carcinoma progression and its potential usage as a clinical lung squamous cell carcinoma maker.

## Conflict of interest

None declared

Received on July 28, 2017

Reviewed on October 15, 2017

Accepted on August 17, 2018

Published online on August 8, 2019

## Cite as

Lei Y, Shi Y, Duan J, et al. Identification of alternative splicing and lncRNA genes in pathogenesis of small cell lung cancer based on their RNA sequencing. *Adv Clin Exp Med.* 2019;28(8):1043–1050. doi:10.17219/acem/94392

## DOI

10.17219/acem/94392

## Copyright

© 2019 by Wrocław Medical University  
This is an article distributed under the terms of the Creative Commons Attribution Non-Commercial License (<http://creativecommons.org/licenses/by-nc-nd/4.0/>)

## Abstract

**Background.** The molecular mechanisms involved in small-cell lung cancer (SCLC) are largely unknown. Recent studies have suggested that long non-coding RNAs (lncRNAs) are likely to play a critical role.

**Objectives.** There is an urgent need for suitable molecular biomarkers for SCLC diagnosis and for assessing patient prognosis.

**Material and methods.** In this study, we used public databases to identify mRNA-like candidate lncRNAs. A multi-step computational approach was used to construct a functional SCLC lncRNAs-mediated competing with endogenous RNA (ceRNA) network (LMCN) by integrating genome-wide lncRNAs and mRNA expression profiles, miRNA-target interactions, functional analyses, and clinical survival analyses.

**Results.** The results revealed the significance of lncRNAs interactions with ceRNAs in SCLC, indicating that integration of expression profiles and alternative splicing could be used to identify biomarkers and the underlying pathological changes. The following genes: *EPB41L4A-AS1*, *HOXA-AS2*, *XIST*, *DLEU2*, *FGD5-AS1*, *ALMS1-IT1*, *SNHG12*, *MIR17HG*, *MIR4720*, and *SCARNA10* in cluster, as well as shared alternative splicing events, were considered to be critical genes.

**Conclusions.** Olfactory transduction and endocytosis were the top-enriched pathways in SCLC. The selected cluster, including critical genes, might also be a potential pathway of SCLC pathogenesis. As a result, this research provides the perspective information to explore the potential critical genes and its pathways in SCLC therapy.

**Key words:** alternative splicing, small-cell lung cancer (SCLC), critical genes

## Introduction

Small-cell lung cancer (SCLC) is an aggressive neuroendocrine carcinoma. Lung cancer is the leading cause of cancer-related deaths worldwide. About 15% of lung cancer cases are SCLC cases.<sup>1</sup> Its prognosis is poor, and has a trend toward metastasizing to the brain at an early stage, despite advances in treatment modalities that have improved survival.<sup>2</sup> Histological diagnosis can provide information valuable in planning the treatment program, but it is insufficient for predicting clinical outcomes.<sup>3</sup> At present, suitable molecular biomarkers for SCLC diagnosis are needed to assess the patient's prognosis.

Recently, noncoding RNAs (ncRNAs) have received considerable attention due to their key role in affecting shared gene expression programs.<sup>4</sup> These RNAs are usually microRNAs or long-non-coding RNAs (lncRNAs). With the development of high-throughput sequencing technology, ncRNAs have been discovered in a wide range of biological processes. However, the functions of lncRNAs in SCLC are not well characterized and the identification of lncRNA biomarkers is challenging. Typically, lncRNA functions are characterized using a "guilt by association" strategy.<sup>5</sup> Recent studies have demonstrated that lncRNAs compete with endogenous RNAs (ceRNAs) in regulating expression level of other transcripts.<sup>6,7</sup> For example, the lncRNA HULC acts as an endogenous ceRNA and plays an important regulatory role in lung cancer.<sup>8</sup> In addition, a recent study using network analysis identified a lncRNA-associated ceRNA network (across 12 different cancers) and prognostic markers of lncRNAs.<sup>7</sup> Another study proposed that the ceRNA interaction network of SCLC could reveal canonical oncogenic pathways.<sup>9</sup> Collectively, this data underscores the importance of lncRNAs interaction with ceRNAs and indicates that the integration of expression profiles with network analysis could identify the risk of lncRNAs and the underlying tumor pathology.

Current studies have suggested that the alternative splicing of the RNAs, as an essential layer of gene expression regulation that expands the cell proteome, plays complex and critical role in breast cancer.<sup>10</sup> Additionally, the alternative splicing of *EGFR*, *CD44*, *PIK3C3*, *RRAS2*, *MAPKAP1*, and *FGFR2* was shown to raise the risk of stratification in non-small cell lung cancer (NSCLC) patients.<sup>11</sup> Alternative splicing of *S6K1* gene can regulate the mammalian target of rapamycin (mTOR) complex 1 signaling pathway. This has been strongly linked with the onset and progression of NSCLC. Alternative splicing of this gene may, therefore, constitute a relevant and innovative biomarker. The short isoforms of *S6K1* are activated mTORC1, leading to increased 4E-BP1 phosphorylation.<sup>12,13</sup>

In this research, a multi-step computational approach was used for constructing a functional lncRNAs-mediated ceRNA network (LMCN) in SCLC. We utilized the high-throughput profiles of SCLC samples, which were collected from the ArrayExpress database. Intergradations

of alternative splicing, genome-wide lncRNA/mRNA expression profiles, comprehensive miRNA-target interactions, and functional analyses were entailed in the systematic analysis. Based on LMCN, we found that several lncRNAs exhibited specific topological features, which are consistent with coding mRNAs regulatory associated with SCLC pathology. The alternative RNA splicing involved in RNA processing significantly related with cell cycle functions was also identified. Additionally, by exploring a competitive sub-network with in the LMCN we determined that MCM3AP-AS and MIR17HG were involved in a ceRNA regulatory module and synergistically competed with *MATR3*, *XPO1* and *ZCCHC14*. These analyses demonstrated that the integration of alternative splicing profile with cancer-associated lncRNA-mediated ceRNA networks could be used to promote the discovery of molecular biomarkers and SCLC therapeutics.

## Methods

### Data recruitment and preprocess

Sequence data was deposited in Array Express, E-GEOD-60052 (<https://www.omicsdi.org/dataset/arrayexpress-repository/E-GEOD-60052>), including 79 SCLC patients and 7 normal lung tissues. This dataset was processed on the Illumina HiSeq 2000 platform (Illumina, Inc., San Diego, USA). For sequencing, samples for non-coding gene datasets of SCLC patients and controls were prepared using Illumina mRNA-Seq kit (Part #RS-100-0801) (Illumina, Inc.).

For data preprocess, Illumina reads were trimmed for adaptor sequence, and low-complexity or low-quality sequence was removed, then mapped to Human genome reference hg19 via <http://bowtie-bio.sourceforge.net/bowtie2/index.shtml> (data was normalized using DESeq in R package to analyse count data for differential expression (<https://bioconductor.org/packages/release/bioc/html/DESeq.html>)). For data analysis, RNA-seq data was analyzed using the set of open source software programs of the Tuxedo suite: TopHat v. 1.3.3 and Cufflinks (<http://ccb.jhu.edu/software/tophat/tutorial.shtml> and <http://cole-trapnell-lab.github.io/cufflinks/>).<sup>14,15</sup> The R platform available as free software (<http://cran.r-project.org/>) was applied. In brief, PolyAplus RNA (RNA transcripts) was purified from 100 ng of total RNA with oligo-dT beads, and then the samples were fragmented with divalent cations under high temperature. First strand synthesis was performed with random hexamer and reverse transcriptase, and 2<sup>nd</sup> strand synthesis with RNase H and DNA polymerase I. Following cDNA synthesis, the double-stranded products were end-repaired, a single "A" was added and then the Illumina Paired End Adapters ([https://support.illumina.com/content/dam/illumina-support/documents/documentation/chemistry\\_documentation/experiment-design/](https://support.illumina.com/content/dam/illumina-support/documents/documentation/chemistry_documentation/experiment-design/))

illumina-adapter-sequences-1000000002694-09.pdf) were ligated on to the cDNA products. The ligation products were purified using gel electrophoresis. The target size range for these libraries was ~300 bp, such that the final library for sequencing would have cDNA inserts with sizes of ~200 bp long. One run of 2 × 50 bp paired-end sequencing was performed on the HiSeq2000 instrument, using 1 lane per tissue, to produce approx. 80 million read pairs per tissue.

## Reconstructing transcriptomes

To determine splice variants within each tissue, we aligned reads to the hg19 genome using TopHat v. 1.3.3 with an intron database, which extracted from the UCSC Known Genes data set (<http://genome.ucsc.edu>). Aligned reads were then assembled into transcript fragments using Cufflinks software (with parameters '-F 0.05'). Then, the Cuffcompare (<http://cufflinks.cbc.umd.edu/>) was used to compare these transfrags to the Ensembl annotation. After eliminating likely artifacts and assemblies not associated with Ensembl genes, the Cuffdiff was used to redistribute reads with a high-confidence transcript sets obtained.<sup>15,16</sup> Cuffcompare classifies assembled transcripts into multiple categories: the known coding genes, the known noncoding genes, the potentially novel transcripts, and the undefinable transcripts. The potentially novel transcripts and the undefinable transcripts were used for downstream analysis. FPKM expression level for this set was then re-estimated from the original alignments using Cuffdiff.

## Discovery of alternative splicing events

To determine alternative splicing events in the LMCN, we developed a software package that can identify the average shortest (AS) profile and analyse the exons-involved in 1 transcript in the transcripts profiles. We restricted the analysis to Ensembl genes with FPKM ≥ 0.1 re-estimated using Cuffdiff as described above. We define the exon skipping event as the pair between exon-containing splice form and exon-skipping splice form, where the boundaries of flanking introns are required to match precisely. To determine the novel events, the exons and spanning introns were compared against the annotation data sets (UCSC Genes and Ensembl).

## Comparison of alternative splicing events among groups

For each event, we calculated the exon inclusion ratio  $R = \text{FPKMon} / (\text{FPKMon} + \text{FPKMoff})$  for each tissue. To account for minor differences in the annotation of splice junctions, the differentially expressed level of average shortest (AS) mRNA was calculated with limma package in R. All differentially expressed mRNA across groups data were

further screened by limma package based on Bayes method (<http://www.bioconductor.org/>). After processing using the top table method of limma package, the differentially expressed genes were analyzed. Then, they were compared with AS genes. The AS genes and DEG were selected for further network assay. The procedure was as follows: lncRNA, miRNA and mRNA expression profiles were obtained from starBase v. 2.0 (<http://starbase.sysu.edu.cn/starbase2/index.php>). Interactions between miRNA-lncRNAs were identified using existing miRNA target prediction methods. Putative miRNA-lncRNA interactions were identified using the miRanda algorithm with the default parameters. The miRNA target binding sites were predicted on entire lncRNAs. The data of the miRNA-mRNA interactions was downloaded from miRNA reference databases, the TarBase (v. 6, <http://diana.imis.athena-innovation.gr/DianaTools/index.php?r=tarbasev6/index>) and the mirTarBase (v. 4.5, <http://mirtarbase.mbc.nctu.edu.tw/php/download.php>). Both databases store manually curated collections of experimentally supported miRNA targets.

## Functional enrichment analysis

The gene ontology based on gene ontology database and the pathway enrichment analysis based on the database of KEGG pathway were carried out using Fisher's test. P-value <0.05 and false discovery rate (FDR) <0.05 were considered to be statistically significant.

## Results

### Integrated analysis of gene signatures

After preprocessing the expression profile of mRNA datasets, we identified 3,105 differentially expressed genes of SCLA using limma package in R language. Limma is an R/Bioconductor software package that provides an integrated solution for analyzing data from gene expression experiments. Over the past decade, limma has been a popular choice for gene discovery through differential expression analyses of microarray and high-throughput PCR data.<sup>16</sup> Figure 1A shows the log fold changes (log FC) in top 10 gene signatures. Figure 1B shows the volcano plot of these genes (log odds). Log FC value (Fig. 1A) indicated that the upregulated genes were *SNAP25* and *MANEAL*; the downregulated genes were *AGER*, *EPAS1*, *EMP2*, *RP 11-114H24.5*, *HBA2*, *NFKBIA*, *ABCA3*, and *CA4*, and they were considered as suppressor genes in SCLC (Table 1).

### Construction of lncRNAs-mediated ceRNA network

For the network, the Pearson's correlation coefficient of proteins encoded by lncRNA gene signatures and their

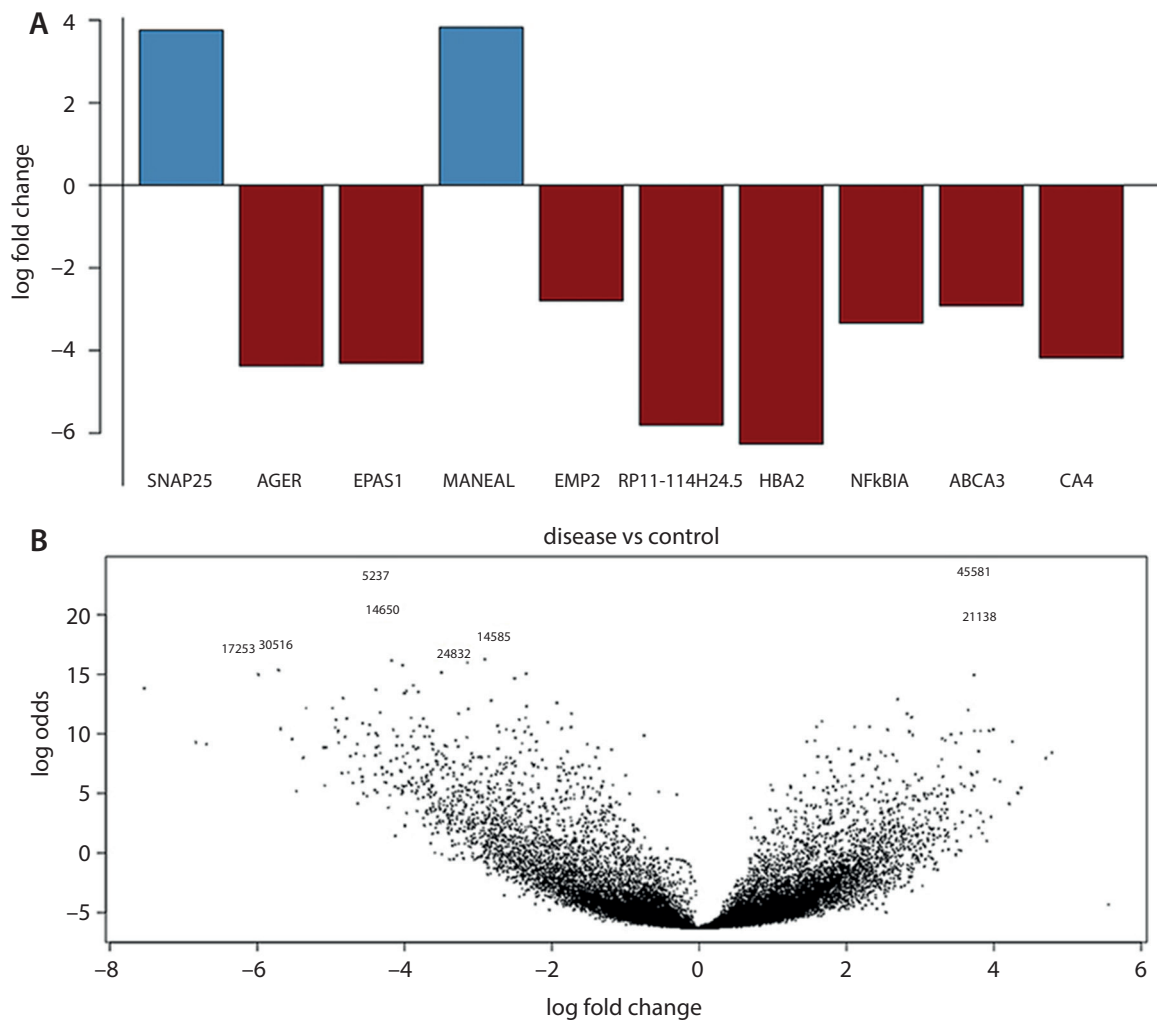


Fig. 1. A – stacked bar plots of fold change for top 10 ranked genes in microarray datasets of small cell lung cancer; B – volcano plot of top 10 ranked genes

mRNA mediated by ceRNA was calculated. The constructed LMCN network (Fig. 2) included 4,987 nodes and 15,579 edges, where nodes represented genes and edges between nodes indicated gene interactions in the network.

## Identification of the cluster in LMCN

While the LMCN could provide a global view of all possible competing ceRNA interactions that could be used to investigate the regulatory properties of the lncRNAs, the partial sub-networks revealed a more detailed pattern of how

Table 1. The top 10 gene signatures identified by gene expression profile in small cell lung cancer

Gene	Log FC	AveExpr	t	p-value	Adjusted p-value	B
<i>SNAP25</i>	3.756787	5.864792	9.581308	3.68E-15	1.38E-10	23.67952
<i>AGER</i>	-4.37513	5.578326	-9.49856	5.40E-15	1.38E-10	23.31936
<i>EPAS1</i>	-4.31265	7.866335	-8.82805	1.23E-13	2.09E-09	20.39216
<i>MANEAL</i>	3.825731	6.030139	8.700969	2.21E-13	2.83E-09	19.83646
<i>EMP2</i>	-2.79616	7.953902	-8.32082	1.30E-12	1.33E-08	18.17466
<i>RP11-114H24.5</i>	-5.80775	2.128777	-8.17396	2.56E-12	2.19E-08	17.53344
<i>HBA2</i>	-6.26852	2.269522	-8.13152	3.12E-12	2.28E-08	17.34829
<i>NFKBIA</i>	-3.33741	6.38071	-7.98145	6.26E-12	4.00E-08	16.69415
<i>ABCA3</i>	-2.91447	7.701587	-7.87974	1.00E-11	5.69E-08	16.25149
<i>CA4</i>	-4.17853	1.285196	-7.84961	1.15E-11	5.88E-08	16.12048

Log FC – logarithmic fold change; AveExpr – the average expression; t – two-sample t-test; B – potential scenario for the statistical test for differential expression.





Fig. 2. LMCN of gene signatures in small cell lung cancer. Purple nodes refer to transcription factors (TFs), red ones refer to the common genes in the cluster

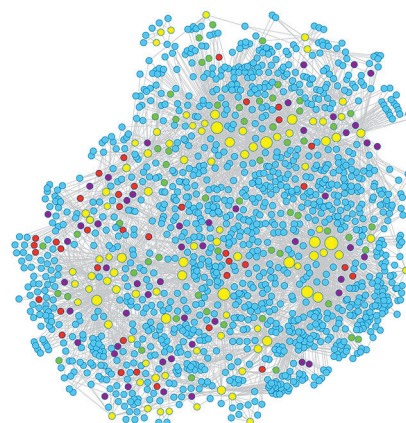


Fig. 3. Gene signatures in the cluster. Purple nodes refer to TFs, red ones refer to the common genes in the cluster 1 and KEGG pathway of oxidative phosphorylation, Parkinson’s disease, Huntington’s disease, and Alzheimer’s disease

the lncRNAs synergized with competing mRNAs. We derived a cluster from the LMCN by applying a Pearson’s correlation coefficient threshold >0.9 (Fig. 3). The genes with a top degree were *EPB41L4A-AS1*, *HOXA-AS2*, *XIST*, *DLEU2*, *FGD5-AS1*, *ALMS1-IT1*, *SNHG12*, *MIR17HG*, *MIR4720*, and *SCARNA10* (Table 2).

### Functional enrichment analysis

Functional enrichment analysis of the obtained gene signatures was carried out, including Gene Ontology (GO) term enrichment and Kyoto Encyclopedia of Genes and Genomes (KEGG) pathway. The GO analysis was carried out in 3 categories, including biological processes (BP), molecular functions (MF) and cellular components (CC). The results of GO analysis showed that cluster genes were significantly enriched in vacuolar transport, Golgi vesicle

transport, mitotic cell cycle phase transition, endosomal transport, and cell cycle phase transition. After the false discovery rate was calculated, the most significant 10 GO terms including BP, MF and CC were presented in Table 3.

For KEGG pathway enrichment, 4 terms were obtained and the most significant ones were Olfactory transduction [PATH:hsa04740], Neuroactive ligand-receptor interaction [PATH:hsa04080], Cell cycle [PATH:hsa04110], Endocytosis [PATH:hsa04144], and Ubiquitin mediated proteolysis [PATH:hsa04120] (Table 4).

### Identification of the hub genes with average shortest events in LMCN

The genes in the LMCN-shared high degree were *HOXA-AS2*, *EPB41L4A-AS1*, *DLEU2*, *XIST*, *MIR17HG*,

Table 2. The average centrality value of cluster

Gene	Degree	Average shortest path length	Closeness centrality	Neighborhood connectivity	Stress	Topological coefficient
<i>NEAT1</i>	38	3.47019424	0.28816831	3.39473684	1481190	0.07483553
<i>FOXP1</i>	6	3.64567984	0.27429726	50.83333333	518298	0.20507545
<i>STX12</i>	5	3.88948426	0.2571035	34.4	310398	0.21410256
<i>KLF7</i>	5	3.68318821	0.27150391	52.8	344072	0.23981481
<i>ITPR1</i>	5	3.55860683	0.28100885	69.2	422280	0.22434211
<i>ATF7IP2</i>	4	3.78767582	0.26401415	52.25	181166	0.29454023
<i>CPEB4</i>	4	3.61888814	0.27632797	71.75	222772	0.26498127
<i>LDLR</i>	4	3.561286	0.28079744	83.25	244082	0.26791531
<i>NCKAP5</i>	4	3.75954454	0.26598967	69	311492	0.29310345
<i>VPS37B</i>	4	3.7635633	0.26570564	59.5	157274	0.28398058
<i>TNKS1BP1</i>	4	3.66175486	0.2730931	73.25	381286	0.27471483
<i>TANC2</i>	4	4.02478232	0.24846064	31.75	46432	0.27702703
<i>CSF1</i>	4	3.73945077	0.26741895	53.75	223642	0.26641414
<i>ADARB1</i>	4	3.81982585	0.26179204	46.5	139536	0.27409639
<i>RBMS1</i>	4	3.71131949	0.26944595	65.75	395634	0.28650442

**Table 3.** Significant terms of GO enrichment

GO ID	Description	Gene ratio	Bg ratio	p-value	Adjusted p-value	Count
GO:0007034	vacuolar transport	129/4397	272/16672	5.20E-14	1.55E-10	129
GO:0048193	Golgi vesicle transport	141/4397	307/16672	8.54E-14	1.55E-10	141
GO:0044772	mitotic cell cycle phase transition	190/4397	450/16672	1.13E-13	1.55E-10	190
GO:0016197	endosomal transport	118/4397	244/16672	1.14E-13	1.55E-10	118
GO:0044770	cell cycle phase transition	198/4397	477/16672	2.45E-13	2.68E-10	198
GO:0006914	autophagy	176/4397	428/16672	1.37E-11	1.24E-08	176
GO:0016482	cytosolic transport	69/4397	131/16672	1.25E-10	9.76E-08	69
GO:0072657	protein localization to membrane	183/4397	478/16672	5.03E-09	3.44E-06	183
GO:0006892	post-Golgi vesicle-mediated transport	37/4397	60/16672	9.30E-09	5.65E-06	37
GO:0000082	G1/S transition of mitotic cell cycle	98/4397	227/16672	2.69E-08	1.47E-05	98

GO ID – Gene Ontology identification; Bg ratio – background ratio indicates the number of target genes regulated by the transcription factor; Count – indicates how many reads map to each feature.

**Table 4.** Significant KEGG pathways

Pathways	p-value	FDR
4740 Olfactory transduction [PATH:hsa04740]	7.88E-48	2.28E-45
4080 Neuroactive ligand-receptor interaction [PATH:hsa04080]	7.15E-16	1.04E-13
4110 Cell cycle [PATH:hsa04110]	7.34E-10	7.10E-08
4144 Endocytosis [PATH:hsa04144]	3.49E-08	2.53E-06
4120 Ubiquitin mediated proteolysis [PATH:hsa04120]	3.61E-07	2.09E-05
5204 Chemical carcinogenesis [PATH:hsa05204]	7.28E-07	3.52E-05
982 Drug metabolism – cytochrome P450 [PATH:hsa00982]	2.92E-06	8.61E-05
4668 TNF signaling pathway [PATH:hsa04668]	2.97E-06	8.61E-05
4114 Oocyte meiosis [PATH:hsa04114]	2.54E-06	8.61E-05
4914 Progesterone-mediated oocyte maturation [PATH:hsa04914]	2.18E-06	8.61E-05

FDR – false discovery rate.

*FGD5-AS1*, *SNHG12*, *ALMS1-IT1*, *ZRANB2-AS2*, and *MIR4720*. In the obtained cluster, the average rank value based on p-value was calculated and genes with the highest value were considered as hub genes. The result was shown in Table 2: genes in a cluster with an average degree value of 6.6 were connected significant. This is consistent with our earlier AS analysis. The average shortest events (AS events) present in several genes (*NEAT1*, *FOXPI*, *STX12*, *KLF7*, *ITPR1*) in the cluster of cell cycle pathways further confirmed the significance of hub genes.

## Discussion

### Pathway analysis of small-cell lung cancer pathogenesis

In the current study, based on LMCN and pathway enrichment of gene signatures, several KEGG pathways were found. Some of these pathways have already been reported by other researchers, such as cell cycle and endocytosis.<sup>17–19</sup> One of the significant pathways was endocytosis

with the p-value of 3.49E-08. Endocytosis is a form of active transport and an important process for the regulation of cell signal transduction, cellular dynamics and cell-to-cell communication. Endocytosis and its counterpart, exocytosis, take place in all cells, which include pinocytosis and phagocytosis. The current study showed that in this pathway ligand-induced endocytosis requires NM IIA to induce the degradation of EGFR, causing the endocytosis process.<sup>20</sup> Our present study verified the endocytosis process in cancer and predicted that the interaction of *ALMS1-IT1* and *VPS37B* as a novel mechanism in trans-Golgi network (Fig. 4). *VPS37B* is located in chromosome 12. This gene binds to *TSG101* at several different sites, which function in vacuolar protein sorting. Several other genes are also in the pathway list, e.g., *GIT2*, *ZFYVE9*, *HSPA6*, *RAB11FIP4*, *CHMP2B*, *TGFB2*, *RAB4A*, *RAB5A*, *RK5*, and others. Some of them are lncRNAs, such as *XIST*, *TRAF3IP2-AS1*, *DLEU2*, *DLEU2*, *MIR4720*, and *SNHG12*. These genes were analyzed via the LMCN, indicating that they were involved in all the 4 main functions (receptor-mediated endocytosis, caveolae, macropinocytosis, and phagocytosis). They were considered as the critical genes. Therefore, endocytosis pathway as well as these genes was thought to be very important in the pathogenesis of SCLC. The map of OXPHOS pathway was shown in Fig. 4.

### Critical genes in pathogenesis of SCLC

The genes in the cluster were considered as critical genes for the pathogenesis of SCLC. These results strongly support *SRSF1* as a prognostic biomarker in SCLC and provide a rationale for personalized therapy in SCLC. The critical genes with AS events in this study included *NEAT1*,

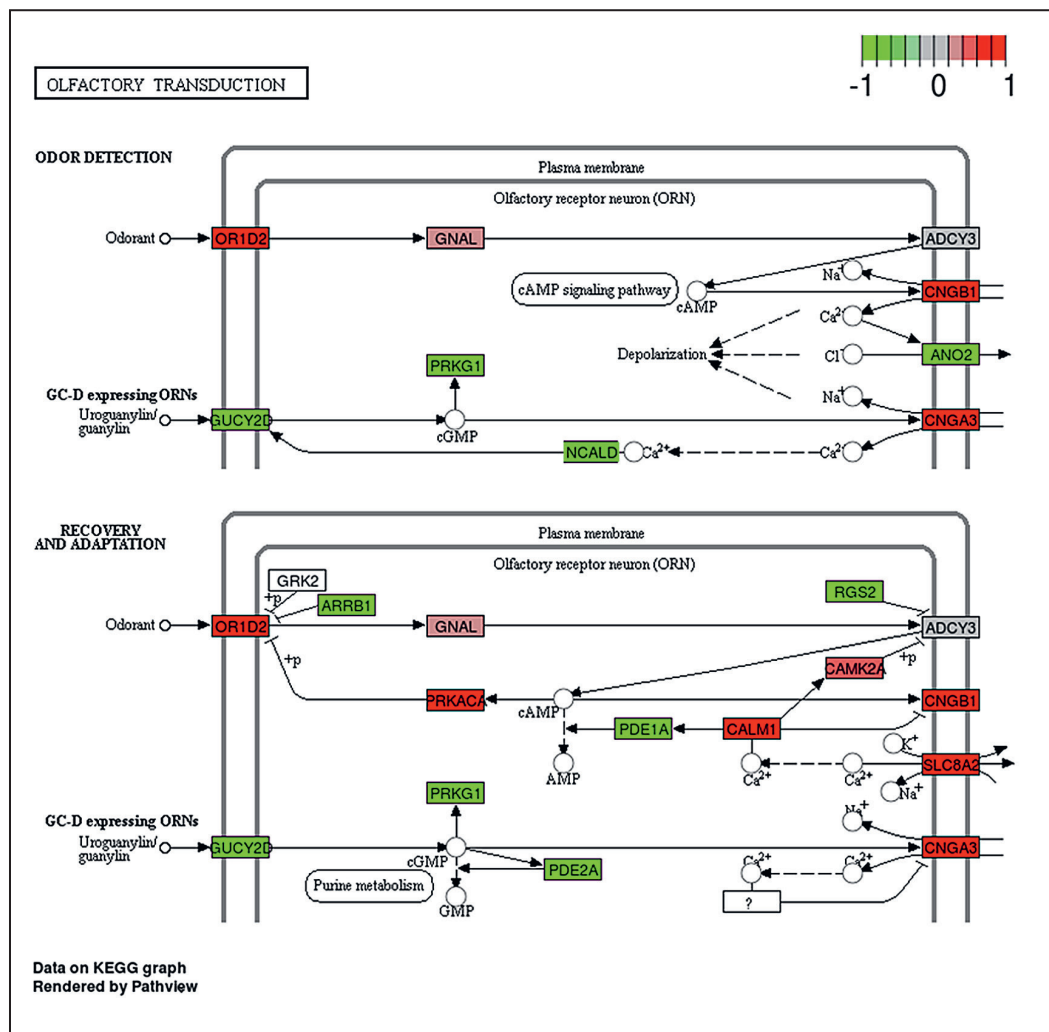


Fig. 4. The map of oxidative phosphorylation pathway

*FOXPI*, *STX12*, *KLF7*, and *ITPR1*. Among these genes, *NEAT1* and *FOXPI* were reported to be associated with cancer. Nuclear-enriched abundant transcript 1 (*NEAT1*, non-protein coding) produces a lncRNA, which is transcribed from the multiple endocrine neoplasia locus. This lncRNA is retained in the nucleus where it forms the core structural component of the paraspeckle sub-organelles. Its high expressions are associated with poor prognosis in different types of solid tumors, such as lung cancer, esophageal cancer, colorectal cancer, and hepatocellular carcinoma.<sup>21</sup> It was aberrantly upregulated and may act as a transcriptional regulator for numerous genes, including some genes involved in unfavorable prognosis in cancer patients.<sup>22</sup> Increased serine/arginine splicing factor 1 (*SRSF1*) DNA copy number and mRNA overexpression has been linked to poor prognosis for SCLC. Functional studies in vitro and in vivo demonstrate that *SRSF1* may play a central role in DNA repair and chemosensitivity.<sup>23</sup> On the other hand, downregulated *NEAT1* promotes leucocyte differentiation in acute promyelocytic leukemia. Our study examined the relationship between *NEAT1* and SCLC and confirmed that the defection of this gene was closely related to the pathogenesis of SCLC.

*FOXPI* gene belongs to the subfamily P of the Forkhead box (FOX) transcription factor family. Forkhead box transcription factors play an important role in the regulation of tissue- and cell type-specific gene transcription during both development and adulthood. This gene may express in several types of human malignant tumors. It also has been reportedly associated with the metastasis and patient prognosis in NSCLC.<sup>24</sup> The expression of *FoxP1* in NSCLC was significantly higher. Since the *FOXPI* protein contains both DNA-binding- and protein-protein binding-domains, it was reported to be a regulator in cancer cells. The low expression of *FOXPI* was independent factors for predicting the poor prognosis for NSCLC.<sup>24</sup> Alternative splicing of *FOXPI* results in multiple transcript variants encoding different isoforms, which is also related to many other cancers.<sup>25</sup> *NEAT1* and *FOXPI* genes connected closely in the cluster and might be another potential way for the pathogenesis of SCLC. The other genes, *STX12*, *KLF7* and *ITPR1*, had not been reported to be in any relationship with SCLC and they need to be investigated further.

In this study, a comprehensive process of data in datasets of SCLC for protein–protein interactions (PPI) network was conducted. Some clusters where the genes connected

closely to SCLC were selected. Then, the function and signaling pathways for SCLC were presented systematically. Finally, the potential pathways and 2 critical genes in SCLC pathogenesis were identified. These may aid in SCLC therapy. However, this study was based on the bioinformatics reports. These results need to be further proven with laboratory tests.

## References

1. Taromi S, Catusse J, Elverfeldt DV, et al. PO-33-Heparin suppresses progression of small cell lung cancer (SCLC) in an orthotopic mouse model. *Thromb Res*. 2016;140(Suppl 1):S188.
2. Liu Y, Liu YS, Wu PF, et al. Brain microvascular endothelium induced-annexin A1 secretion contributes to small cell lung cancer brain metastasis. *Int J Biochem Cell Biol*. 2015;66:11–19.
3. Verhaak RG, Hoadley KA, Purdom E, et al. Integrated genomic analysis identifies clinically relevant subtypes of glioblastoma characterized by abnormalities in PDGFRA, IDH1, EGFR, and NF1. *Cancer Cell*. 2010;17(1):98–110.
4. Guttman M, Donaghey J, Carey BW, et al. lincRNAs act in the circuitry controlling pluripotency and differentiation. *Nature*. 2011;477(7364):295–300.
5. Guo Q, Cheng Y, Liang T, et al. Comprehensive analysis of lncRNA-mRNA co-expression patterns identifies immune-associated lncRNA biomarkers in ovarian cancer malignant progression. *Sci Rep*. 2015;5:17683.
6. Ebert MS, Sharp PA. Emerging roles for natural microRNA sponges. *Curr Biol*. 2010;20(19):R858–R861.
7. Wang P, Ning S, Zhang Y, et al. Identification of lncRNA-associated competing triplets reveals global patterns and prognostic markers for cancer. *Nucleic Acids Res*. 2015;43(7):3478–3489.
8. Wang J, Liu X, Wu H, et al. CREB up-regulates long non-coding RNA, HULC expression through interaction with microRNA-372 in liver cancer. *Nucleic Acids Res*. 2010;38(16):5366–5383.
9. Sumazin P, Yang X, Chiu HS, et al. An extensive microRNA-mediated network of RNA-RNA interactions regulates established oncogenic pathways in glioblastoma. *Cell*. 2011;147(2):370–381.
10. Pradella D, Naro C, Sette C, Ghigna C. EMT and stemness: Flexible processes tuned by alternative splicing in development and cancer progression. *Mol Cancer*. 2017;16(1):8.
11. Li Y, Sun N, Lu Z, et al. Prognostic alternative mRNA splicing signature in non-small cell lung cancer. *Cancer Lett*. 2017;393:40–51.
12. Huertas CS, Dominguez-Zotes S, Lechuga LM. Analysis of alternative splicing events for cancer diagnosis using a multiplexing nanophotonic biosensor. *Sci Rep*. 2017;7:41368.
13. Mei H, Wang Y, Fan J, Lin Z. Alternative splicing of S6K1 promotes non-small cell lung cancer survival. *Tumour Biol*. 2016;37(10):13369–13376.
14. Ghosh S, Chan CK. Analysis of RNA-seq data using TopHat and Cufflinks. *Methods Mol Biol*. 2016;1374:339–361.
15. Trapnell C, Roberts A, Goff L, et al. Differential gene and transcript expression analysis of RNA-seq experiments with TopHat and Cufflinks. *Nat Protoc*. 2012;7(3):562–578.
16. Ritchie ME, Phipson B, Wu D, et al. Limma powers differential expression analyses for RNA-sequencing and microarray studies. *Nucleic Acids Res*. 2015;43(7):e47.
17. Rainero E. Extracellular matrix endocytosis in controlling matrix turnover and beyond: Emerging roles in cancer. *Biochem Soc Trans*. 2016;44(5):1347–1354.
18. Vassie JA, Whitelock JM, Lord MS. Endocytosis of cerium oxide nanoparticles and modulation of reactive oxygen species in human ovarian and colon cancer cells. *Acta Biomater*. 2017;50:127–141.
19. Yu XW, Lin S, Du HZ, et al. Synergistic combination of DT-13 and topotecan inhibits human gastric cancer via myosin IIA-induced endocytosis of EGF receptor in vitro and in vivo. *Oncotarget*. 2016;7(22):32990–33003.
20. Kim JH, Wang A, Conti MA, Adelstein RS. Nonmuscle myosin II is required for internalization of the epidermal growth factor receptor and modulation of downstream signaling. *J Biol Chem*. 2012;287(33):27345–27358.
21. Yu X, Li Z, Zheng H, Chan MT, Wu WK. NEAT1: A novel cancer-related long non-coding RNA. *Cell Prolif*. 2017;50(2). doi:10.1111/cpr.12329
22. Barry G, Briggs JA, Hwang DW, et al. The long non-coding RNA NEAT1 is responsive to neuronal activity and is associated with hyperexcitability states. *Sci Rep*. 2017;7:40127.
23. Jiang L, Huang J, Higgs BW, et al. Genomic landscape survey identifies SRSF1 as a key oncogene in small cell lung cancer. *PLoS Genet*. 2016;12(4):e1005895.
24. Feng J, Zhang X, Zhu H, Wang X, Ni S, Huang J. High expression of FoxP1 is associated with improved survival in patients with non-small cell lung cancer. *Am J Clin Pathol*. 2012;138(2):230–235.
25. Santos ME, Athanasiadis A, Leitao AB, DuPasquier L, Sucena E. Alternative splicing and gene duplication in the evolution of the FoxP gene subfamily. *Mol Biol Evol*. 2011;28(1):237–247.

# Ibrutinib discontinuation in patients with relapsed or refractory chronic lymphocytic leukemia treated in a compassionate use program: A report from the Polish Adult Leukemia Study Group (PALG)

Elżbieta Iskierka-Jażdżewska<sup>1,C,D,F</sup>, Bartosz Puła<sup>2,C,F</sup>, Agnieszka Szeremet<sup>3,B,F</sup>, Marek Hus<sup>4,B,F</sup>, Aleksandra Gołos<sup>2,B,F</sup>,  
Jadwiga Hołojda<sup>5,B,F</sup>, Weronika Piszczek<sup>6,B,F</sup>, Paweł Steckiewicz<sup>7,B,F</sup>, Małgorzata Wojciechowska<sup>8,B,F</sup>, Jan Maciej Zaucha<sup>9,10,B,F</sup>,  
Krzysztof Warzocha<sup>2,E,F</sup>, Krzysztof Jamroziak<sup>2,A,C,D,F</sup>

<sup>1</sup> Department of Hematology, Copernicus Memorial Hospital, Łódź, Poland

<sup>2</sup> Department of Hematology, Institute of Hematology and Transfusion Medicine, Warszawa, Poland

<sup>3</sup> Department of Hematology, Blood Neoplasms and Bone Marrow Transplantation, Wrocław Medical University, Poland

<sup>4</sup> Department of Haematology and Bone Marrow Transplantation, Medical University of Lublin, Poland

<sup>5</sup> Department of Hematology, Specialist District Hospital, Legnica, Poland

<sup>6</sup> Department of Hematology, Copernicus Hospital, Toruń, Poland

<sup>7</sup> Department of Hematology, Holycross Cancer Center, Kielce, Poland

<sup>8</sup> Department of Hematology, Specialist District Hospital, Olsztyn, Poland

<sup>9</sup> Department of Oncological Propaedeutics, Medical University of Gdańsk, Poland

<sup>10</sup> Gdynia Oncology Center, Poland

A – research concept and design; B – collection and/or assembly of data; C – data analysis and interpretation; D – writing the article; E – critical revision of the article; F – final approval of the article

Advances in Clinical and Experimental Medicine, ISSN 1899–5276 (print), ISSN 2451–2680 (online)

*Adv Clin Exp Med.* 2019;28(8):1051–1057

## Address for correspondence

Elżbieta Iskierka-Jażdżewska  
E-mail: elaiskierka@gmail.com

## Funding sources

None declared

## Conflict of interest

None declared

Received on December 19, 2017

Reviewed on May 24, 2018

Accepted on November 21, 2018

Published online on June 14, 2019

## Cite as

Iskierka-Jażdżewska E, Puła B, Szeremet A, et al. Ibrutinib discontinuation in patients with relapsed or refractory chronic lymphocytic leukemia treated in a compassionate use program: A report from the Polish Adult Leukemia Study Group (PALG). *Adv Clin Exp Med.* 2019;28(8):1051–1057. doi:10.17219/acem/99911

## DOI

10.17219/acem/99911

## Copyright

© 2019 by Wrocław Medical University  
This is an article distributed under the terms of the Creative Commons Attribution Non-Commercial License (<http://creativecommons.org/licenses/by-nc-nd/4.0/>)

## Abstract

**Background.** Development of a novel class of drugs, the B-cell receptor-signaling inhibitors, including ibrutinib, has been a major achievement in the therapy of refractory or relapsed chronic lymphocytic leukemia (CLL). However, the CLL patients who have discontinued the ibrutinib treatment in clinical trials have been reported to have poor prognosis.

**Objectives.** In this retrospective study by the Polish Adult Leukemia Group (PALG), we analyzed the reasons for ibrutinib cessation and outcomes after discontinuing ibrutinib in refractory or relapsed CLL patients treated in a compassionate use program in Poland.

**Material and methods.** Polish CLL patients were included if they discontinued ibrutinib for any reason. The clinical data on the course of ibrutinib treatment was collected anonymously using electronic Case Report Forms (CRFs). The causes of discontinuation of ibrutinib as reported by the treating physicians were analyzed.

**Results.** Thirty-seven patients who discontinued ibrutinib were identified. The median duration of ibrutinib treatment in this group was 4.4 months (range: 0.2–25.2). The main reason for discontinuing ibrutinib was adverse events (n = 20, 54%), while 14 (38%) patients discontinued therapy due to disease progression and 3 (8%) due to other causes. The most common treatment complications that led to ibrutinib cessation were severe respiratory tract infections (9 patients, 24%). In the group discontinuing ibrutinib for progressive disease, 11 patients progressed with untransformed CLL, while in 3 patients, a rare type of Richter transformation to Hodgkin's lymphoma was diagnosed. Twenty-nine patients (78%) died during the follow-up period, and median overall survival (OS) reached 2.0 months (95% CI = 0.8–5.5 months). Importantly, no significant survival difference was detected between patients who discontinued ibrutinib due to disease progression and due to adverse events.

**Conclusions.** The results of this analysis indicate that ibrutinib discontinuation in relapsed or refractory CLL is associated with poor prognosis regardless of the reason for ibrutinib cessation.

**Key words:** tyrosine kinase inhibitor, chronic lymphocytic leukemia, ibrutinib

## Acknowledgements

This study was supported by the Polish Adult Leukemia Study Group (PALG). We would like to acknowledge the following clinicians for providing us with information about patients used in our study: Michał Osowiecki MD, PhD; Wanda Knopińska-Posłuszny MD, PhD; Daria Zawirska MD, PhD; Beata Kumiega MD, PhD; Janusz Hałka MD, PhD; Anna Waszczuk-Gajda MD; PhD. We also acknowledge Paulina Wieszczy for her help with statistical analysis.

## Introduction

Chronic lymphocytic leukemia (CLL) is characterized by clonal proliferation and accumulation of mature B-cells, typically co-expressing CD5 and CD23, within the blood, bone marrow, lymph nodes, and spleen.<sup>1</sup> The disease primarily occurs in elderly patients and has a very heterogeneous course.<sup>2</sup> According to current guidelines, patients with an inactive, early stage CLL (Binet A/B or Rai 0–II) should undergo active surveillance, while therapy needs to be started in patients with advanced or active disease.<sup>3</sup>

Until recently, the standard treatment approach to CLL was based on anti-CD20 antibody-containing immunochemotherapy. However, even if prolonged remissions could be initially obtained in a proportion of patients, eventually the disease develops refractoriness to such therapy. Major progress in treating relapsed or refractory CLL has recently been achieved by the development of a novel class of drugs: B-cell receptor signaling inhibitors, including ibrutinib (Imbruvica; Janssen Cilag, Beerse, Belgium). Ibrutinib is a first-in-class, oral, once-daily therapy that inhibits Bruton's tyrosine kinase (BTK).<sup>4</sup> This kinase is a member of the Tec kinase family and a key molecule in the B-cell receptor signaling complex, playing an important role in the survival and spread of normal B cells.<sup>5</sup> It was found that this kinase also affects the maintenance and expansion of various B-cell malignancies, including CLL.<sup>5,6</sup>

Clinical trials on ibrutinib in relapsed or refractory and treatment-naïve CLL patients have been very promising and led to the drug being approved in the USA and EU.<sup>4,7–10</sup> Furthermore, data from several clinical trials has shown that ibrutinib is generally well-tolerated.<sup>4,8–10</sup> The most common adverse events were mostly mild (grade 1–2).<sup>4,7–10</sup> The prevailing ibrutinib-related adverse events included diarrhea, fatigue, cough, edema, upper respiratory tract infections, arthralgia, rash, fever, and mild hematological toxicity. Nonetheless, some unexpected adverse events have also been reported which included mainly hemorrhagic complications and atrial fibrillation.<sup>4,9,10</sup> Bleeding, particularly skin-mucosal hemorrhagic diathesis, was found in 20–40% of patients.<sup>4,8–10</sup> Atrial fibrillation was the 2<sup>nd</sup> unexplained and potentially dangerous side effect, found in 3.5–6.5% of patients treated with ibrutinib (3 times more frequently than in the placebo group).<sup>4,9,10</sup>

Despite the ability of ibrutinib to induce durable responses in the vast majority of patients along with good treatment tolerance, some patient groups treated within clinical trials have had to discontinue their treatment due to disease progression or drug side effects. Recently, it has been reported that those patients have a very poor outcome.<sup>11,12</sup> Understanding the potential reasons for discontinuing a new therapy is vital in clinical practice. Our study has therefore analyzed the causes for discontinuing ibrutinib and the subsequent course of the disease in relapsed or refractory CLL patients treated according

to the ibrutinib compassionate use program and monitored within the observational study of the Polish Adult Leukemia Study Group (PALG).

## Material and methods

### Patients

Polish CLL patients treated within a compassionate ibrutinib use program for relapsed or refractory CLL and monitored within observational study by PALG<sup>13</sup> were included if they discontinued ibrutinib for any reason. The inclusion criteria to the compassionate ibrutinib use program for relapsed or refractory CLL patients in Poland were at least one of the following: a) the deletion of the short-arm of chromosome 17 (17p deletion); b) failure of 2 or more previous treatments (at least 1 with a purine analogue such as fludarabine); c) a progression-free interval of less than 24 months from completing treatment with a nucleoside analogue or a bendamustine-containing regimen in combination with an anti-CD20 monoclonal antibody such as rituximab; d) failure to respond to prior chemotherapy-based treatment; e) stable disease or disease progression on treatment; and f) ineligibility for treatment or re-treatment with a purine analogue-based therapy. The prospective observational study assessing ibrutinib efficacy and toxicity in CLL patients treated in the compassionate use program was designed by PALG and approved by the Ethics Committee at the Institute of Hematology and Transfusion Medicine in Warszawa, Poland.<sup>13</sup> The study was conducted in accordance with the provisions of the Declaration of Helsinki and the International Conference on Harmonization Guidelines for Good Clinical Practice.

The clinical data on the course of ibrutinib treatment was collected anonymously using electronic Case Report Forms (CRFs). The causes of discontinuation of ibrutinib as reported by treating physicians were analyzed. Patients who died while continuing ibrutinib therapy were also included in the analysis irrespective of the cause of death. The criteria of the National Cancer Institute Common Terminology Criteria for Adverse Events v. 4.0 were used to grade toxicity, except for hematologic toxicity cases which were evaluated using the International Workshop Group on CLL (IWCLL) criteria.<sup>14</sup>

### Statistical analysis

The duration of ibrutinib therapy was measured from the starting date of ibrutinib to the date of discontinuing ibrutinib. The overall survival (OS) plots were generated according to the Kaplan–Meier method using time intervals from the date of discontinuing ibrutinib to the date of death or last follow-up. The log-rank test was used to compare survival in groups of patients discontinuing ibrutinib for

different reasons. A p-value below 0.05 was considered statistically significant. All analyses were performed with Prism v. 6.0 software (GraphPad, La Jolla, USA).

## Results

With a data cut-off set at June 2017, 37 (22.4%) of 165 patients monitored in the PALG observational study discontinued compassionate use ibrutinib therapy. The current median follow-up time in the observational study was 26 months. The discontinuation group consisted of 22 male and 15 female patients with a median age of 64 years (range: 46–84). The median time of ibrutinib treatment in this group was 4.4 months (range: 0.2–25.2). Baseline characteristics of these patients at the time of starting ibrutinib and response to ibrutinib are presented in Table 1. Importantly, fluorescent in situ hybridization (FISH) cytogenetics was performed in 20 (65%) patients, of whom the 17p deletion was found in 7 patients (19% of the whole group) as compared to 30 patients (18.4%) in the whole study.

**Table 1.** Baseline characteristics of the 37 patients analyzed at the time of the start of ibrutinib therapy

Characteristic	Number of patients
Median age (range)	64 (46–84)
Male/female sex (ratio)	22/15 (1.47)
ECOG performance status	
0	1 (2.7%)
1	16 (43.3%)
2	13 (35.1%)
3	4 (10.8%)
4	3 (8.1%)
CLL clinical stage (according to Rai classification)	
0	0 (0%)
I	8 (22%)
II	8 (22%)
III	6 (16%)
IV	15 (40%)
17p deletion by FISH	
present	7 (19%)
absent	13 (46%)
not tested	17 (35%)
Previous therapies	
Median (range)	3 (1–10)
≥3 lines of therapy	18 (48.6%)
Duration of ibrutinib therapy	
Median (range)	4.4 months (0.2–25.2)
Best response during therapy with ibrutinib	
CR	1 (2.9)
PR	11 (31.4)
PR with lymphocytosis	5 (14.3)
SD	17 (48.6)
PD	1 (2.9)

ECOG – Eastern Cooperative Oncology Group; CLL – chronic lymphocytic leukemia; FISH – fluorescent in situ hybridization; CR – complete response; PR – partial response; SD – stable disease; PD – progressive disease.

**Table 2.** Reasons for discontinuing ibrutinib therapy in the compassionate use program in Poland

Cause for discontinuing ibrutinib	Number of patients [%]
Adverse events	20 (54)
Pneumonia	6 (16.2)
Upper respiratory tract infection	3 (8.1)
Diarrhea	2 (5.4)
Heart failure	2 (5.4)
Bladder cancer	1 (2.7)
Exacerbation of chronic obstructive pulmonary disease	1 (2.7)
Neutropenia	1 (2.7)
Hyphema	1 (2.7)
Suicide (severe episode of depression)	1 (2.7)
Vomiting	1 (2.7)
Cerebellar ischemic stroke	1 (2.7)
Progressive disease	14 (37.8)
Progression of chronic lymphocytic leukemia	11 (29.7)
Richter’s transformation	3 (8.1)
Patient decision	2 (5.4)
Unknown (patient lost to follow-up)	1 (2.7)

The main reasons for discontinuing ibrutinib included adverse events (n = 20, 54%) and disease progression (n = 14, 38%), while 3 patients (8%) stopped treatment due to other causes (Table 2). Treatment adverse events predominated as being the cause for ibrutinib therapy cessation and consisted of: pneumonia, upper respiratory tract infection, diarrhea, vomiting, neutropenia, hyphema, bladder cancer, heart failure, exacerbation of chronic obstructive pulmonary disease, ischemic cerebellar stroke, and a suicide committed during an episode of major depression (Table 2). The most common adverse event leading to ibrutinib cessation was severe pneumonia observed in 6 patients or 16% of the discontinuation group. The etiology of pneumonia was identified in only 3 patients, while in the remainder blood culture tests were negative or not performed. Among patients with known etiology, there were 2 cases of pneumonia of bacterial origin (*Acinetobacter baumannii* and *Pseudomonas aeruginosa*) and 1 case with highly probable fungal infection (*Candida glabrata* detected in blood culture and the gastrointestinal tract).

In those patients who progressed while on ibrutinib therapy, 2 types of progression could be identified: progression of untransformed CLL and transformation to high grade lymphoma (Richter’s transformation – RT). Interestingly, 2 of the patients who had untransformed CLL experienced rare infiltration of CLL into the central nervous system (CNS) that was confirmed with a biopsy. The 1<sup>st</sup> patient with CNS involvement died 1 day after discontinuing ibrutinib due to pneumonia and progressive disease. The 2<sup>nd</sup> patient with CNS disease failed to respond to further therapy with high-dose methylprednisolone and died 8 months after his ibrutinib therapy was terminated. In the remaining 9 patients with CLL progression without clinical signs of CNS involvement, only 3 received subsequent lines of therapy while a palliative approach

was chosen for the other 6 because of poor general status. Of the former 3 treated patients, 1 achieved partial response after 5 cycles of R-CHOP chemotherapy and has remained alive without signs of disease progression within a follow-up of 7 months. The 2<sup>nd</sup> patient received 1 cycle of chemoimmunotherapy with rituximab, gemcitabine, carboplatin, and dexamethasone with no response, and then was treated with an inhibitor of 3-phosphoinositol kinase idelalisib. Therapy with idelalisib did not, however, prove effective and the patient died due to progressive disease 2 weeks later. The last patient first received 4 cycles of the anti-CD20 monoclonal antibody obinutuzumab in monotherapy with no response. As the second line of treatment, CHOP chemotherapy was administered, but the patient also failed to respond and died 3 months from the day of discontinuing ibrutinib due to CLL progression. Importantly, none of the patients progressing with CLL received venetoclax, as this drug was not available.

Richter's transformation was observed in 3 patients. Interestingly, in all these 3 cases the rare type of transformation to Hodgkin's lymphoma was diagnosed. Two had transformed within the first 4 months of starting ibrutinib. One was treated according to the ABVD chemotherapy regimen but with no response. In the 2<sup>nd</sup> patient, treatment was not initiated because of poor general condition. Both patients died within 6 months after discontinuing ibrutinib therapy. The 3<sup>rd</sup> patient with RT, diagnosed 20 months from starting ibrutinib, has remained alive in remission after high-dose immunochemotherapy and allogeneic stem cell transplantation (alloSCT) at 13 months from discontinuing ibrutinib. A more detailed description of these rare case series is reported elsewhere.<sup>15</sup> Regarding the 3 patients who discontinued ibrutinib for other reasons than CLL progression or adverse events, in 2 the cause was the patient's decision, while in 1 patient the reason for discontinuation was unknown, the patient being lost from follow-up.

By the data cut-off for this report (June 2017), 29 (78.4%) out of 37 patients who discontinued ibrutinib died and 8 have remained alive. The median OS is 2.0 months (95% CI = 0.8–5.5) (Fig. 1). The major causes of death were disease progression and infections. All mortality causes are summarized in Table 3. In order to further investigate the potential differences in outcomes of specific patient groups, we compared the survival of patients after discontinuing ibrutinib due to disease progression (untransformed CLL progression or RT) with that of patients who discontinued ibrutinib due to adverse events or other reasons. Interestingly, the median survival was comparable in these 2 patient groups, being respectively 2.0 months (range: 0.2–10.4) and 1.6 months (range: 0.2–16.7) ( $p = 0.81$ ). (Fig. 2). Furthermore, no significant differences could be found regarding OS of patients who progressed with CLL as compared to those with RT type of progression, although the case numbers are very low (Fig. 3).

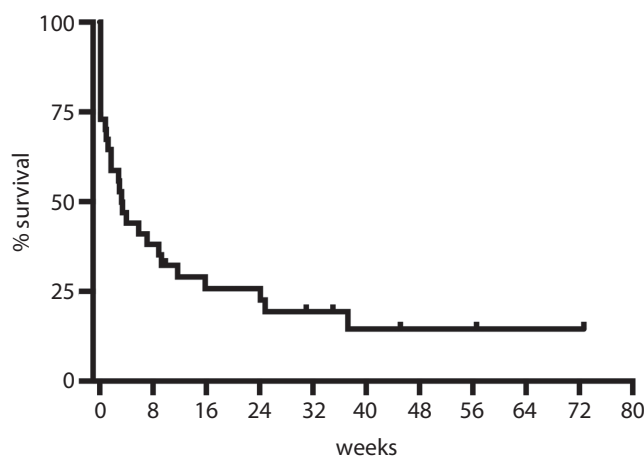


Fig. 1. Kaplan–Meier plot representing the overall survival of all patients who had to discontinue therapy with ibrutinib

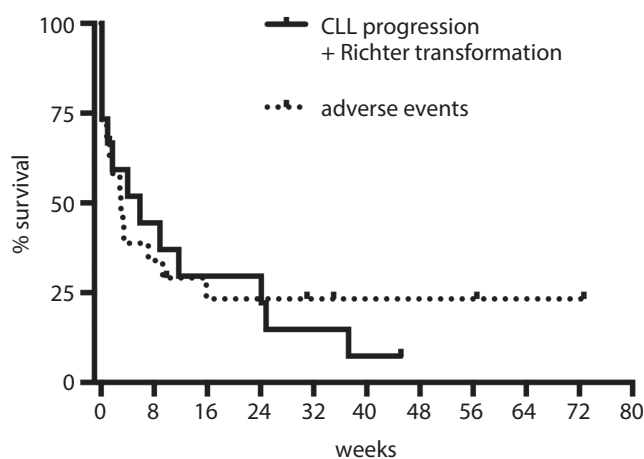


Fig. 2. Comparisons of overall survival in patients after discontinuing ibrutinib due to disease progression with that of patients who discontinued ibrutinib due to adverse events or other reasons. Median survival was comparable in these 2 patients groups, being respectively 2.0 months (range: 0.2–10.4) and 1.6 months (range: 0.2–16.7) ( $p = 0.81$ )

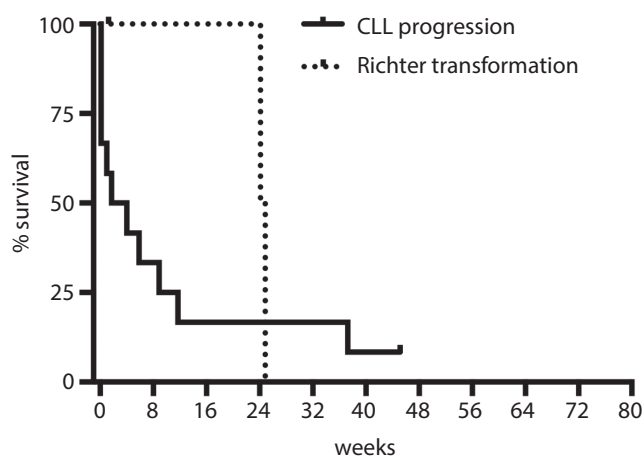


Fig. 3. Survival curves indicate no significant differences in the OS of patients with progression of chronic lymphocytic leukemia as compared to those with a Richter's transformation type of progression ( $p = 0.34$ )



**Table 3.** Causes of death in the CLL patient group studied after ibrutinib discontinuation

Cause of death (n = 29)	Number of patients
Progression of CLL	10
Infections	7
Multi-organ failure	3
Heart failure	3
Gastrointestinal bleeding	1
Cerebellar ischemic stroke	1
Exacerbation of chronic obstructive pulmonary disease	1
Suicide during severe episode of depression	1
Bladder cancer	1
Unknown	1

## Discussion

Knowledge of the patterns of a new anti-cancer therapy discontinuation, including the rate and type of disease progression as well as a profile of severe adverse events, is very important for clinical practice. Herein, we report the outcomes of 37 relapsed or refractory CLL patients who discontinued ibrutinib therapy outside clinical trials. Our analysis confirms a very poor prognosis of such a patient group irrespective of whether the cause of discontinuation was relapse or transformation of CLL or ibrutinib treatment-related complications.

Early reports from clinical trials indicate that the main reasons for discontinuing ibrutinib treatment were severe adverse events and/or confirmation of progressive disease. In a 1b–2 phase, multicenter and open label study, the investigators assessed the safety, efficacy, pharmacokinetics, and pharmacodynamics of ibrutinib<sup>7</sup> which showed that BTK inhibitor therapy had to be halted in 37% of patients. Among the prevailing reasons were progressive disease (13%) and adverse events (8%). Subsequently, 2 reports from single institutions specifically analyzed patient outcomes for those treated with ibrutinib in different clinical trials and who had to discontinue therapy. The 1<sup>st</sup> report presented 33 patients participating in various clinical trials with ibrutinib alone or combined with rituximab at the MD Anderson Cancer Center (Houston, USA).<sup>11</sup> In the 2<sup>nd</sup> one, Maddocks et al.<sup>12</sup> described 76 patients treated in 4 sequential ibrutinib clinical trials at the Ohio State University Comprehensive Cancer Center (USA). These reports showed that the main reasons for discontinuing ibrutinib were adverse events and disease progression. The most common side effects responsible for discontinuing ibrutinib were severe infections. An increased number of RT was also observed in such cases.<sup>11,12</sup>

Our analysis demonstrated that 22.4% (37 out of 165) of patients treated within the compassionate use ibrutinib program discontinued therapy after a median follow-up of 26 months. These findings are comparable to the reports

on patients treated in clinical trials, where ibrutinib was discontinued in 26% and 24.6% of patients, respectively.<sup>11,12</sup> Also consistently with these reports,<sup>11,12,16</sup> the most common reason for ibrutinib cessation was adverse events (54% of patients), where severe infections predominated. Notwithstanding, the Jain et al. study found that the median duration of ibrutinib treatment was significantly longer (13 months vs 4.4 months) than in our findings with no obvious differences in patient characteristics.<sup>11</sup> This could be partially explained by the fact that physicians exercise excessive caution to adverse events when using a new drug outside of clinical trials, as in the case of our report. The cause of severe infections associated with ibrutinib treatment in CLL patients is most probably multifactorial, involving pre-existing immune-suppression associated with the biological mechanisms of CLL and drug-induced susceptibility to infection.<sup>17–19</sup> Interestingly, the results of a recent meta-analysis concerning infectious complications of ibrutinib therapy for hematological malignancies have indicated a significant association between exposure to this drug and an increased risk of serious infections.<sup>19</sup> Therefore, carefully observing fever and other signs and symptoms of infection together with monitoring for neutropenia and searching for potentially responsible pathogens would enable an appropriate anti-infective therapy to be introduced early. Recognizing which CLL patients treated with BTK inhibitors are at a higher risk of developing infectious adverse events could be an important future challenge.

Although not occurring in our study group, a potential reason for discontinuation could also be atrial fibrillation.<sup>20</sup> It should therefore be stressed that discontinuing treatment in patients who develop atrial fibrillation when on ibrutinib therapy is not always necessary. In such situations, a thorough risk assessment for thromboembolic disease should be undertaken. In patients at high risk and where alternatives to ibrutinib are unsuitable, a strictly controlled treatment with anticoagulants should be considered.<sup>21</sup> Appropriate management of adverse events could thereby prevent premature discontinuation of therapy.

Disease progression was the reason for discontinuation in 14 (38%) of our patients including 8 patients (30%) with CLL progression and 3 patients (8%) with RT. It has been found that disease progression in CLL patients treated with ibrutinib has been attributed to the clonal evolution of CLL with acquired mutations in BTK (substitution of cysteine 481 with serine) and phospholipase C- $\gamma$ 2 (PLCG2) (S707Y, R6 65W and L845F) or histologic transformation (RT).<sup>22,23</sup> Unfortunately, we did not assess the occurrence of resistance mutation because the biologic material from the time of relapse was unavailable.

Interestingly, the infiltrations of CLL into the CNS were observed in 2 patients. Central nervous system involvement is a rare complication in CLL and displays heterogeneous neurological symptoms.<sup>24</sup> The therapy for this rare event is still undetermined. Wanquet et al. observed good responses in patients with CLL infiltration of the CNS who were

treated with ibrutinib (5-year OS was respectively 72% and 48% for treatment-naïve and previously treated patients).<sup>24</sup> Patients with relapsed or refractory CLL and confirmed CNS involvement during ibrutinib therapy had limited therapeutic options. However, prognosis seemed to be related to CLL characteristics rather than to the CNS infiltration itself.<sup>24</sup>

The 2<sup>nd</sup> type of progression that was observed in 3 of our patients was RT, which is generally found in about 2–10% of CLL patients.<sup>25</sup> Interestingly, it was reported that in patients treated with ibrutinib who progressed, RT may be particularly common.<sup>23</sup> It is still unclear if ibrutinib increases the risk of RT or if patients included in ibrutinib therapy constitute groups with poorer prognoses than the general population suffering from CLL. Current observations indicate that during ibrutinib therapy, progressive CLL occurred later than RT. In the Ahn et al. study, histologic transformation was limited to the first 15 months when on ibrutinib while progression due to CLL was diagnosed at a median of 38 months.<sup>26</sup> Maddocks et al.<sup>12</sup> likewise found the estimated rates of cumulative RT incidence at 12 months to be 4.5% (95% CI = 2.0–7.0%) and the estimated rates of the cumulative incidence of progressive disease due to CLL at 12 months to be 0.3% (95% CI = 0–1.0%). Our results are thus comparable, with 2 out of 33 patients with RT diagnosed in the 4<sup>th</sup> month of ibrutinib therapy. In contrast to the majority of RT cases under ibrutinib, the RT in the 3<sup>rd</sup> patient was diagnosed after almost 2 years of ibrutinib treatment.

Interestingly, in our analysis, all 3 RT patients were diagnosed with a Hodgkin variant of RT, a rare form accounting for 0.4–2.3% of CLL cases.<sup>27</sup> However, 2 recent case reports on patients with the Hodgkin variant of RT during ibrutinib therapy have been published.<sup>28,29</sup> Their outcomes of therapy are superior to those of the more common RT in diffusing large B-cell lymphoma.<sup>30</sup> Nevertheless, patients with Hodgkin's lymphoma and RT who had received purine nucleoside analogs for CLL have very short survivals if treated with HL-type therapy.<sup>31,32</sup> Interestingly, one of our RT patients responded favorably to intensive chemotherapy consolidated with alloSCT and remains alive at 13 months after transplantation.

Our data suggests that the survival of relapsed/refractory CLL patients who discontinued ibrutinib is poor. The median OS was 2.0 months (95% CI = 0.8–5.5) and did not differ significantly between patients who progressed and those who discontinued ibrutinib due to other causes. The results of available studies also confirm the unfavorable outcomes of this category of CLL patients.<sup>11,12,16</sup> However, in contrast to our findings, the largest study from the MD Anderson Cancer Center indicated that survival was significantly influenced by the reason of ibrutinib discontinuation. Patients who had progressive CLL had better survival compared with those who had disease transformation.<sup>16</sup> Additionally, Jain et al. suggested that one of the possible reasons for the poor salvage ability of patients who discontinued ibrutinib was a higher

proportion of patients having 17p deletion (58% vs 25%) and unmutated IGHV (94% vs 74%) compared with patients who continued receiving ibrutinib therapy.<sup>11</sup> Also, our group contained a relatively high proportion of 17p deleted patients (7 out of 20 tested patients, 35%), but unfortunately the IGHV mutational status was not examined in any of the patients included.

Importantly, recent studies on new therapeutic options for this patient group have been performed. Patients who discontinued ibrutinib due to progression or toxicity had improved outcomes if they received venetoclax (ORR 79%) or idelalisib (ORR 46%) compared to immunotherapy.<sup>33</sup> Venetoclax, a selective BCL-2 inhibitor, was approved by the Food and Drug Administration in the USA in April 2016 for patients with previously treated del17p CLL on the basis of a single-arm, multicenter, phase II trial.<sup>33</sup> Based on the positive results of subsequent studies, extension for indicating its use is to be expected.<sup>34–37</sup> Unfortunately, our patients did not have access to venetoclax.

Our analysis has confirmed that discontinuing ibrutinib therapy in patients with relapsed or refractory CLL is associated with poor prognosis. Elucidating the biological mechanisms of resistance in CLL as well as investigating new targeted therapeutic options such as venetoclax, are thus needed to improve treatment outcomes for this patient group.

## References

1. Swerdlow SH, Campo E, Harris NL, et al. *WHO Classification of Tumours of Haematopoietic and Lymphoid Tissues*. 4<sup>th</sup> ed. Lyon, France: International Agency for Research on Cancer; 2008.
2. Pulte D, Redaniel MT, Bird J, Jeffreys M. Survival for patients with chronic leukemias in the US and Britain: Age-related disparities and changes in the early 21<sup>st</sup> century. *Eur J Haematol*. 2015;94(6):540–545.
3. Eichhorst B, Robak T, Montserrat E, et al; ESMO Guidelines Committee. Chronic lymphocytic leukaemia: ESMO Clinical Practice Guidelines for diagnosis, treatment and follow-up. *Ann Oncol*. 2015;26(Suppl 5):78–84.
4. Byrd JC, Brown JR, O'Brien S, et al; for the RESONATE Investigators. Ibrutinib versus ofatumumab in previously treated chronic lymphoid leukemia. *N Engl J Med*. 2014;371:213–223.
5. Burger JA, Chiorazzi N. B cell receptor signaling in chronic lymphocytic leukemia. *Trends Immunol*. 2013;34(12):592–601.
6. Ponader S, Chen SS, Buggy JJ, et al. The Bruton tyrosine kinase inhibitor PCI-32765 thwarts chronic lymphocytic leukemia cell survival and tissue homing in vitro and in vivo. *Blood*. 2012;119(5):1182–1189.
7. Byrd JC, Furman RR, Coutre SE, et al. Targeting BTK with ibrutinib in relapsed chronic lymphocytic leukemia. *N Engl J Med*. 2013;369(1):32–42.
8. Byrd JC, Furman RR, Coutre SE, et al. Three-year follow-up of treatment-naïve and previously treated patients with CLL and SLL receiving single-agent ibrutinib. *Blood*. 2015;125(16):2497–2506.
9. Chanan-Khan A, Cramer P, Demirkan F, et al; HELIOS Investigators. Ibrutinib combined with bendamustine and rituximab compared with placebo, bendamustine, and rituximab for previously treated chronic lymphocytic leukaemia or small lymphocytic lymphoma [HELIOS]: A randomised, double-blind, phase 3 study. *Lancet Oncol*. 2016;17(2):200–211.
10. Burger JA, Tedeschi A, Barr PM, et al; for the RESONATE-2 Investigators. Ibrutinib as initial therapy for patients with chronic lymphocytic leukemia. *N Engl J Med*. 2015;373:2425–2437.
11. Jain P, Keating M, Wierda W, et al. Outcomes of patients with chronic lymphocytic leukemia after discontinuing ibrutinib. *Blood*. 2015;125(13):2062–2067.

12. Maddocks KJ, Ruppert AS, Lozanski G, et al. Etiology of ibrutinib therapy discontinuation and outcomes in patients with chronic lymphocytic leukemia. *JAMA Oncol.* 2015;1(1):80–87.
13. Iskierka-Jazdzewska E, Hus M, Giannopoulos K, et al. Efficacy and toxicity of compassionate ibrutinib use in relapsed/refractory chronic lymphocytic leukemia in Poland: Analysis of the Polish Adult Leukemia Group (PALG). *Leuk Lymphoma.* 2017;58(10):2485–2488.
14. Hallek M, Cheson BD, Catovsky D, et al; International Workshop on Chronic Lymphocytic Leukemia. Guidelines for the diagnosis and treatment of chronic lymphocytic leukemia: A report from the International Workshop on Chronic Lymphocytic Leukemia updating the National Cancer Institute-Working Group 1996 guidelines. *Blood.* 2008;111(12):5446–5456.
15. Jamroziak K, Szymczyk A, Hus M, et al. A series of chronic lymphocytic leukemia patients with Hodgkin variant Richter's transformation during ibrutinib therapy: A report from the Polish Adult Leukemia Group (PALG). *Eur J Haematol.* 2018. doi: 10.1111/ejh.13016
16. Jain P, Thompson PA, Keating M, et al. Long-term outcomes for patients with chronic lymphocytic leukemia who discontinue ibrutinib. *Cancer.* 2017;123(12):2268–2273.
17. Williams AM, Baran AM, Meacham PJ, et al. Analysis of the risk of infection in patients with chronic lymphocytic leukemia in the era of novel therapies. *Leuk Lymphoma.* 2018;59(3):625–632.
18. Winqvist M, Palma M, Heimersson K, et al. Dual targeting of Bruton tyrosine kinase and CD52 induces minimal residual disease-negativity in the bone marrow of poor-prognosis chronic lymphocytic leukaemia patients but is associated with opportunistic infections: Results from a phase I study. *Br J Haematol.* 2018;182(4):590–594.
19. Tillman BF, Pauff JM, Satyanarayana G, Talbott M, Warner JL. Systematic review of infectious events with the Bruton tyrosine kinase inhibitor ibrutinib in the treatment of hematologic malignancies. *Eur J Haematol.* 2018;100(4):325–334.
20. Thorp BC, Badoux X. Atrial fibrillation as a complication of ibrutinib therapy: Clinical features and challenges of management. *Leuk Lymphoma.* 2018;59(2):311–320.
21. Chai KL, Rowan G, Seymour JF, Burbury K, Carney D, Tam CS. Practical recommendations for the choice of anticoagulants in the management of patients with atrial fibrillation on ibrutinib. *Leuk Lymphoma.* 2017;58(12):2811–2814.
22. Furman RR, Cheng S, Lu P, et al. Ibrutinib resistance in chronic lymphocytic leukemia. *N Engl J Med.* 2014;370(24):2352–2354.
23. Sharma S, Galanina N, Guo A, et al. Identification of a structurally novel BTK mutation that drives ibrutinib resistance in CLL. *Oncotarget.* 2016;7(42):68833–68841.
24. Wanquet A, Birsén R, Bonnet C, et al. Management of central nervous system involvement in chronic lymphocytic leukaemia: A retrospective cohort of 30 patients. *Br J Haematol.* 2017;176(1):37–49.
25. Jamroziak K, Tadmor T, Robak T, Polliack A. Richter syndrome in chronic lymphocytic leukemia: Updates on biology, clinical features and therapy. *Leuk Lymphoma.* 2015;56(7):1949–1958.
26. Ahn IE, Underbayev C, Albitar A, et al. Clonal evolution leading to ibrutinib resistance in chronic lymphocytic leukemia. *Blood.* 2017;129(11):1469–1479.
27. Tsimberidou AM, O'Brien S, Kantarjian HM, et al. Hodgkin transformation of chronic lymphocytic leukemia: The M.D. Anderson Cancer Center experience. *Cancer.* 2006;107(6):1294–1302.
28. Glavey S, Quinn J, McCloy M, et al. Emergence of Bruton's tyrosine kinase-negative Hodgkin lymphoma during ibrutinib treatment of chronic lymphocytic leukaemia. *Eur J Haematol.* 2017;99(4):378–380.
29. Sachanas S, Pangalis GA, Moschogiannis M, et al. Hodgkin lymphoma transformation of chronic lymphocytic leukemia under ibrutinib therapy: Chance association or therapy-related? *Anticancer Res.* 2017;37(6):3277–3280.
30. Jamroziak K, Grzybowska-Lzydorczyk O, Jesionek-Kupnicka D, Gora-Tybor J, Robak T. Poor prognosis of Hodgkin variant of Richter transformation in chronic lymphocytic leukemia treated with cladribine. *Br J Haematol.* 2012;158(2):286–288.
31. Brecher M, Banks PM. Hodgkin's disease variant of Richter's syndrome: Report of eight cases. *Am J Clin Pathol.* 1990;93(3):333–339.
32. Bockorny B, Codreanu I, Dasanu CA. Hodgkin lymphoma as Richter transformation in chronic lymphocytic leukaemia: A retrospective analysis of world literature. *Br J Haematol.* 2012;156(1):50–66.
33. Mato AR, Hill BT, Lamanna N, et al. Optimal sequencing of ibrutinib, idelalisib, and venetoclax in chronic lymphocytic leukemia: Results from a multicenter study of 683 patients. *Ann Oncol.* 2017;28(5):1050–1056.
34. Stilgenbauer S, Eichhorst B, Schetelig J, et al. Venetoclax in relapsed or refractory chronic lymphocytic leukaemia with 17p deletion: A multicentre, open-label, phase 2 study. *Lancet Oncol.* 2016;17(6):768–778.
35. Seymour JF, Ma S, Brander DM, et al. Venetoclax plus rituximab in relapsed or refractory chronic lymphocytic leukaemia: A phase 1b study. *Lancet Oncol.* 2017;18(2):230–240.
36. Roberts AW, Davids MS, Pagel JM, et al. Targeting BCL2 with Venetoclax in relapsed chronic lymphocytic leukemia. *N Engl J Med.* 2016;374(4):311–322.
37. Jones JA, Wierda WG, Choi MY, et al. Venetoclax activity in CLL patients who have relapsed after or are refractory to ibrutinib or idelalisib. *J Clin Oncol.* 2016 34(15 Suppl):7519–7519.



# Effect of PI3K/PKB signal pathway inhibitor wortmannin pretreatment on intestinal barrier function in severe acute pancreatitis rats

Qinqing Tang<sup>C,D</sup>, Hengyi Wang<sup>B,C</sup>, Xingyu Wang<sup>C</sup>, Maoyong Fang<sup>E</sup>, Hong Zhang<sup>A,F</sup>

Department of Emergency, First Affiliated Hospital of Anhui Medical University, Hefei, China

A – research concept and design; B – collection and/or assembly of data; C – data analysis and interpretation; D – writing the article; E – critical revision of the article; F – final approval of the article

Advances in Clinical and Experimental Medicine, ISSN 1899–5276 (print), ISSN 2451–2680 (online)

*Adv Clin Exp Med.* 2019;28(8):1059–1066

## Address for correspondence

Hong Zhang

E-mail: zhanghong20070703@163.com

## Funding sources

This work was supported by grants from the International Education Project of Anhui Medical University (grant No. gjjyxm201525) of China; the Training Program of the National Natural Science Foundation of The First Affiliated Hospital of Anhui Medical University of China (grant No. 2013kj08); the Research Foundation of Anhui Medical University (grant No. 2015xkj089); and by Anhui Province Public Welfare Linkage Plan Project (grant No. 1604f0804022).

## Conflict of interest

None declared

Received on March 19, 2018

Reviewed on August 1, 2018

Accepted on November 21, 2018

Published online on August 12, 2019

## Cite as

Tang Q, Wang H, Wang X, Fang M, Zhang H. Effect of PI3K/PKB signal pathway inhibitor wortmannin pretreatment on intestinal barrier function in severe acute pancreatitis rats.

*Adv Clin Exp Med.* 2019;28(8):1059–1066.

doi:10.17219/acem/99910

## DOI

10.17219/acem/99910

## Copyright

© 2019 by Wrocław Medical University

This is an article distributed under the terms of the Creative Commons Attribution Non-Commercial License (<http://creativecommons.org/licenses/by-nc-nd/4.0/>)

## Abstract

**Background.** It is well-known that severe acute pancreatitis (SAP) due to infection is mainly caused by intestinal bacterial translocation. The intestinal barrier is tasked with preventing intestinal pathogenic bacteria and toxins from reaching the parenteral tissues through the intestinal wall. Therefore, maintaining intestinal barrier function may be the key to preventing damage from acute pancreatitis (AP). The phosphatidylinositol 3-kinase/protein kinase B pathway (PI3K/PKB) plays a role in AP. However, the exact effect of PI3K/PKB on injury associated with SAP has not yet been found.

**Objectives.** The present study was aimed at investigating the impact of wortmannin (WT), a PI3K/PKB inhibitor, on intestinal barrier function in SAP rats.

**Material and methods.** The rats were divided into 3 groups: 1) the Sham Surgery group (SS), whose duodenum and pancreas were flipped 3 times ( $n = 18$ ); 2) the pancreatitis group (SAP), who were injected through retrograde pancreatic duct injection with 5% sodium taurocholate ( $n = 18$ ); and 3) the WSAP intervention group (SAP+WT). Serum alpha-amylase levels, plasma endogenous endotoxin, hematoxylin-eosin (H&E) staining, intestinal mucosa electron microscopy, intestinal permeability, and expression of p-PKB (phosphorylated protein kinase B) were measured.

**Results.** In our findings under an electron microscope, the SAP group presented cell edema and mitochondrial vacuolated degeneration, sparsely arranged microvilli, tight junction damage, and widening, while the WSAP group exhibited less change and lower pancreas scores ( $7.4 \pm 1.14$ ,  $10.2 \pm 1.48$  and  $12.0 \pm 1.58$  for 3 h, 6 h and 12 h, respectively) ( $p < 0.05$ ). Furthermore, the plasma endogenous endotoxin levels and Evans blue content of the WSAP group was significantly lower at all timepoints than in the SAP group ( $p < 0.05$ ). Western blotting showed that p-PKB expression was lower in the WSAP group than in the SAP group ( $p < 0.05$ ). Our study suggests that WT relieves intestinal permeability changes in SAP rats and may be dose-dependent.

**Conclusions.** The PI3K/PKB signal pathway may involve SAP-related intestinal injuries and WT may relieve SAP intestinal injuries through the PI3K/PKB pathway.

**Key words:** intestinal barrier, alpha-amylase, endotoxin, acute pancreatitis, signal pathway, wortmannin

## Introduction

Severe acute pancreatitis (SAP) not only causes the death of the pancreas itself, but also leads to failure of the other organs, with a fatality rate of 30%.<sup>1,2</sup> Severe acute pancreatitis patients suffer from local tissue necrosis and systemic inflammatory response, often complicated by a bacterial infection of the pancreatic tissue and by the systemic inflammatory response syndrome associated with infection and multiple organ dysfunction syndrome.

Clinical data and animal studies show that most pancreatic and peripancreatic infections are enterogenic infections caused by the translocation of intestinal bacteria and bacterial endotoxin.<sup>3,4</sup> Severe acute pancreatitis due to infection is mainly caused by intestinal bacterial translocation, and often is closely related to therapeutic effect.<sup>5</sup>

Many studies have shown that destruction of the intestinal barrier is the basis of enterogenic SAP infection.<sup>6–8</sup> Damage of the intestinal mucosa barrier can lead to a more permeable intestinal mucosa, bacterial and endotoxin translocation, the release of inflammatory cytokines, systemic inflammatory response syndrome, and multiple organ dysfunction syndrome.<sup>9</sup>

The intestinal barrier is tasked with preventing intestinal pathogenic bacteria and toxins from reaching the par-enteral tissues through the intestinal wall. The integrity of the intestinal mucosa barrier depends on the intestinal mucosa epithelial cells and the integrity of the close connection in the intestinal mucosa barrier. The tight junction between the cells surrounds the top of the intestinal epithelial cells. Furthermore, a close connection also closes the 20-nanometer gap existing between the cells, prevents bacteria and toxins in the lumen from entering the body, and maintains a stable internal environment. Severe trauma, burn, infections, major surgery, stress, and ischemia hypoxia can lead to reduced functioning of the intestinal mucosal barrier.<sup>10</sup>

Phosphatidylinositol 3-kinase (PI3K) is a 2<sup>nd</sup> messenger related to intracellular signal transduction. The phosphatidylinositol 3-kinase/protein kinase B pathway (PI3K/PKB) is an important signal transduction system which mediates extracellular signals and induced cellular responses, and plays an important role in inflammatory cell activation, chemotaxis, tumorigenesis, and ischemia reperfusion injury. In recent years, more and more attention has been paid to the relationship between the PI3K/PKB signaling pathway and pancreatitis. The PI3K/PKB signal transduction pathway is activated when acute pancreatitis (AP) occurs, which further activates downstream factor NF kappa B and promotes the production of a variety of inflammatory factors. This creates a cascade effect named the “inflammatory cytokines storm” which induces a systemic inflammatory response and multiple organ failure. Phosphorylated protein kinase B (p-PKB) reflects the activation level of the PI3K/PKB signal pathway.

Wortmannin (WT), a potent and selective inhibitor of PI3K, was applied to inhibit the activation of PI3K and thus to prevent the activation of PKB.<sup>11,12</sup> Evidence indicates that WT may decrease inflammatory cytokines in SAP rats and suggests its regulatory mechanisms may involve the suppression of NF- $\kappa$ B and p38MAPK activity.<sup>13</sup>

The aims of the study were: 1) to investigate intestinal barrier function through intestinal permeability changes; 2) to study the relationship between PI3K/PKB signal transduction pathway and SAP intestinal injuries by measuring the expression levels of P-PKB and PKB in intestinal tissue; and 3) to observe the role of WT in intestinal injury in SAP rats, as to study its possible mechanism.

## Material and methods

### Experiment design

All the animal use experimental protocols were approved by the Animal Care and Use Committee of Anhui Medical University (Hefei, China) and the experiments were performed in accordance with the guidelines of the committee.

Pathogen-free male Wistar rats weighing 200–300 g were provided by the Laboratory Animal Center of Anhui Medical University. The animals were housed in cages at a controlled temperature of 24°C and under 12-hour light–dark cycles. The animals had free access to water and food. The rats were housed 5 per cage.

The animals fasted overnight, except for free access to water, before the operation. Anesthesia (10% chloral hydrate) was injected ip.

The rats were divided into 3 groups: 1) the Sham Surgery group (SS), in which duodenum and pancreas were flipped 3 times (n = 18); 2) the pancreatitis group (SAP), in which animals were injected through retrograde pancreatic duct injection with 5% sodium taurocholate (n = 18); and 3) the WSAP intervention group (SAP+WT). The WT was dissolved in dimethyl sulfoxide and stored at –20°C. The intraperitoneal (i.p.) injection of WT (0.35 mg/kg) was performed 4 h before the SAP model was established. Each group was randomly divided into 3 subgroups (3 h, 6 h and 12 h) with 6 rats in each subgroup.

The operation was carried out in a sterile environment in the laboratory equipped with a super clean bench. Ten percent chloral hydrate (3 mL/kg) was i.p. injected into the rats at 3-hour, 6-hour and 12-hour timepoints. Three milliliters of inferior vena cava blood was collected in coagulation promoting tubes. After that, it stood at room temperature for 1 h and was centrifuged at 3,000 rpm at 4°C for 15 min. The serum samples were cryopreserved at –20°C for serum alpha-amylase detection. Next, 1 mL of venous blood was collected in anticoagulation tubes and left standing at room temperature for 1 h. The sample was then centrifuged at 3,000 rpm at 4°C for 15 min and the plasma was cryopreserved at –20°C for detection of endotoxins.

## Biochemical assays

The assays of amylase activity in alpha-amylase were performed according to the guidelines of the alpha-amylase assay kit manufacturer (Jiancheng Technology, Shenzhen, China). Sodium taurocholate from Sigma-Aldrich (St. Louis, USA) was used.

Serum samples were taken from a refrigerator set to  $-20^{\circ}\text{C}$  and placed into a water bath at  $37^{\circ}\text{C}$  for 10 min, the serum using automatic biochemical analyzer. One milliliter of inferior vena blood was placed into the anticoagulation tube and then centrifuged for 15 min at 4,000 rpm in order to separate the plasma. This detection procedure was in strict accordance with the instructions from the Limulus Amebocyte Lysate (LAL) endotoxin detection kit (Associates of Cape Cod, East Falmouth, USA), and plasma endogenous endotoxin content was determined using the endpoint chromogenic method.

A 6-centimeter section of the small intestine was prepared and gently rinsed with saline. Then, one end of the small intestine was closed and ligated; a gavage needle was inserted at the other end. The intestinal tissue was then injected with 0.2 mL of Evans blue dye through a 1-milliliter syringe and placed into a 20-milliliter Krebs liquid beaker, under 95%  $\text{O}_2$  and in a  $37^{\circ}\text{C}$  water bath. The sac tissue was removed 30 min later and saline intestine until the flushing fluid clarification. It was allowed to dry for 24 h at  $37^{\circ}\text{C}$ ; then, 1 mL of formamide solution was added and it was incubated at  $50^{\circ}\text{C}$  for 24 h. The intestinal tissue was removed and the solution was centrifuged. Supernatant was detected using a UV spectrophotometer at a wavelength of 655 nm. The Evans blue content was measured in the intestinal tissue according to the Evans blue standard curve.

## Histopathological examination

The same parts of the pancreas and the end of the ileum tissue were taken and fixed with 4% polyformaldehyde for hematoxylin & eosin (H&E) staining. Ileum tissue 10 cm away from the blind valve was taken and the mesentery was removed. It was then washed with phosphate-buffered saline solution (PBS) and immediately put into liquid nitrogen and stored at  $-80^{\circ}\text{C}$ . Histological examination was performed by a pathologist on sections which were assigned random numbers for blinding. The severity of pancreatitis was documented with scoring edema, hemorrhage, leukocyte infiltration, parenchymal necrosis, and fatty tissue necrosis according to Spormann's scoring system.<sup>14</sup>

## Electron microscopy

The samples, about 0.5 cm in length, were quickly cut with a sharp scalpel from the ileocecal ileum, placed on a pre-cooled glass slide, and rapidly received 4 drops of glutaraldehyde solution at  $4^{\circ}\text{C}$ . They were then cut into small

pieces (0.5–1 mm<sup>2</sup> in area) and fixed at  $4^{\circ}\text{C}$  in a 2.5% glutaraldehyde solution for 6 h. After washing with PBS, 1% osmium tetroxide was added at  $4^{\circ}\text{C}$  for 2 h. The solution was dehydrated by graded alcohol washes, soaked in propylene oxide for 30 min and then soaked in a mixture with the equivalent content of propylene oxide and resin for 2 h. The samples were soaked in pure resin for 2 h and then soaked in resin-containing solution. Next, they were placed in a  $60^{\circ}\text{C}$  incubator and processed for 48 h. The samples were then cut into ultrathin sections (70 nm) and studied under transmission electron microscope (TEM) after being washed with water and dried.

## Western blot analysis of p-PKB

The tissue protein extracts were prepared as follows. Approximately 200–300 mg of ileal tissue was removed from the mesentery and non-target tissues, and then minced on ice. The tissue had 1 mL of lysis buffer added to it and was placed in a glass homogenizer in ice 30–50 times. Next, the tissues were placed on ice for cooling. The homogenate was transferred to a chilled centrifuge tube and centrifuged at  $4^{\circ}\text{C}$  at 3,000 rpm for 10 min, in order to extract a pellet. The supernatant was then transferred to a new pre-cooled centrifuge tube at  $4^{\circ}\text{C}$  and centrifuged at 14,000 rpm for 30 min. The resulting supernatant was transferred into new tubes, packed and stored frozen.

The protein content was determined with Coomassie Blue G-250 (ThermoFisher, Waltham, USA). The proteins were separated using sodium dodecyl sulfate–polyacrylamide gel electrophoresis (SDS-PAGE). After electrophoresis, the proteins in PAGE gel were transferred with electroblotting to nitrocellulose membranes ( $40^{\circ}\text{C}$ ). An electrochemiluminescent agent was added when the strip was fully colored (about 1–2 min). The film was immediately filled with dry filter paper and wrapped in plastic wrap into the rear intensifying screen. It was exposed in a darkroom for between 30 s and 10 min. The X-rays were then developed.

The scan density analysis was performed as follows. The ImageJ v. 1.40 software (National Institutes of Health, Bethesda, USA) was used for quantitative analysis on the results of the western blotting. *GADPH* was selected as an internal reference. The gray percentages of p-PKB, *GADPH*, PKB, and *GADPH* were calculated.

## Statistical methods

All data was processed with SPSS v. 13.0 software (SPSS Inc., Chicago, USA) and tested for normality of distribution using the Kolmogorov–Smirnov test. Normally distributed data was expressed as mean  $\pm$  standard deviation (SD). Comparisons between control and treatment groups were made with one-way analysis of variance (ANOVA) tests and then post-hoc tests. A p-value  $<0.05$  was considered statistically significant.

## Results

### Serum alpha-amylase detection

The levels of serum alpha-amylase had increased, confirming the diagnosis of AP. Table 1 shows the different values of alpha-amylase in each group. Animals from the SAP group had higher levels of alpha-amylase than those in the other groups. According to the statistical analysis, there was a significant difference between the SAP group and the SS group ( $p < 0.05$ ). However, after the rats were treated with WT, their level of alpha-amylase decreased significantly (Table 1).

**Table 1.** Serum alpha-amylase of SAP rats ( $n = 6$  for each timepoint,  $\bar{x} \pm s$ ). The SAP group had higher levels of alpha-amylase when compared to that of the other groups. According to the statistical analysis, there was significant difference between the SAP group and the control group ( $p < 0.05$ ). However, after wortmannin treatment, their level of alpha-amylase decreased significantly

Groups	Alpha-amylase [U/L]		
	3 h	6 h	12 h
SS	982 $\pm$ 125	970 $\pm$ 130	983 $\pm$ 137
SAP	1,422 $\pm$ 102*	1,785 $\pm$ 176*	1,986 $\pm$ 204*
WSAP	1,268 $\pm$ 106*	1,143 $\pm$ 88 <sup>#</sup>	1,157 $\pm$ 143 <sup>#</sup>

\* $p < 0.05$ , compared to the control group; <sup>#</sup> $p < 0.05$ , compared to the SAP group.

### Changes of plasma endotoxin levels at different time points

The plasma endotoxin levels in the SS group at the 3-hour, 6-hour and 12-hour timepoints were 0.071  $\pm$ 0.009 EU/mL, 0.075  $\pm$ 0.022 EU/mL and 0.056  $\pm$ 0.008 EU/mL, respectively. The levels in the SAP group were 0.250  $\pm$ 0.015 EU/mL, 0.300  $\pm$ 0.014 EU/mL and 0.460  $\pm$ 0.026 EU/mL, respectively. The levels in the WSAP group were 0.162  $\pm$ 0.018 EU/mL, 0.226  $\pm$ 0.015 EU/mL and 0.238  $\pm$ 0.023 EU/mL, respectively. There were no significant differences between the different timepoints in the SS group. However, the plasma endotoxin levels of the SAP group and the WSAP group at each timepoint were significantly higher than those of the SS group ( $p < 0.05$ ) and they gradually increased over time. Also, the endotoxin levels of the WSAP group were significantly lower at all timepoints than in the SAP group ( $p < 0.05$ ) (Table 2).

### Pathological changes

Under light microscopy, the SS group was observed to have complete lobular structures, no bleeding or necrosis, and no inflammatory cell infiltration (Fig. 1A). The SAP 3 h subgroup exhibited hemorrhaging (Fig. 1B). As time elapsed, the damage to the pancreas gradually increased, with edema, hemorrhaging, parenchymal

**Table 2.** The plasma levels of endotoxins in pancreatic rats (EU/mL,  $\bar{x} \pm s$ ,  $n = 6$ ). The plasma endotoxin levels among the SAP and WSAP groups at all timepoints were significantly higher than those of the SS group ( $p < 0.05$ ), and they gradually increased with time. The endotoxin levels of the WSAP group were significantly lower at all timepoints compared with the SAP group ( $p < 0.05$ )

Groups	Plasma endotoxin levels (EU/mL)		
	3 h	6 h	12 h
SS	0.071 $\pm$ 0.009	0.075 $\pm$ 0.022	0.056 $\pm$ 0.008
SAP	0.250 $\pm$ 0.015 <sup>#</sup>	0.300 $\pm$ 0.014 <sup>#</sup>	0.460 $\pm$ 0.026 <sup>#</sup>
WSAP	0.162 $\pm$ 0.018*	0.226 $\pm$ 0.015*	0.238 $\pm$ 0.023*

<sup>#</sup> $p < 0.05$ , compared to the control group; \* $p < 0.05$ , compared to the SAP group.

necrosis, and infiltrating inflammatory cells being observed (Fig. 1C). However, the WSAP group showed milder pancreatic pathological damage than the SAP group, with less hemorrhaging (Fig. 1D). The pathological tissue scores are shown in Table 3. Compared with the SAP groups, the WSAP groups had significantly lower histopathological scores at 3 h, 6 h and 12 h ( $p < 0.05$ ). The morphological changes of the pancreas, including pancreatic edema, necrosis, hemorrhaging, and inflammation, were scored according to Spormann's criteria.<sup>14</sup> We also found histopathological changes in the ileum, including irregular villi, edema and infiltration of inflammatory cells (Fig. 1F,G), while the SS group did not display those changes (Fig. 1E).

**Table 3.** Pancreatic tissues scores ( $\bar{x} \pm s$ ). Compared to the SAP group ( $n = 6$ ), the WSAP group ( $n = 6$ ) had significantly lower histopathological scores at 3 h, 6 h and 12 h ( $p < 0.05$ ). The morphological changes of the pancreas, including pancreatic edema, necrosis, hemorrhage, and inflammation, were scored according to Spormann's criteria<sup>14</sup>

Group	Timepoint		
	3 h	6 h	12 h
SAP	10.0 $\pm$ 1.58	12.8 $\pm$ 1.92	15.4 $\pm$ 1.14
WSAP	7.4 $\pm$ 1.14*	10.2 $\pm$ 1.48*	12.0 $\pm$ 1.58*

\* $p < 0.05$ , compared to the SAP group.

### Ultrastructural changes of the intestinal mucosa

The ileal epithelial cells were observed under TEM. The epithelial cell structure of the SS group was arranged in neat rows, with intracellular organelles, mitochondria and endoplasmic reticulum structure intact (Fig. 2A). Compared with the control group, the SAP group were observed after 6 h to present mitochondrial vacuolated degeneration and sparsely arranged microvilli (Fig. 2B). The SAP group were observed after 12 h to have cell edema, mitochondrial vacuolated degeneration, sparsely arranged microvilli, tight junction damage, and widening (Fig. 2C). However, the WSAP group exhibited less change than the SAP group (Fig. 2D,E), with neatly arranged microvilli, tight junction narrowing and less edema.



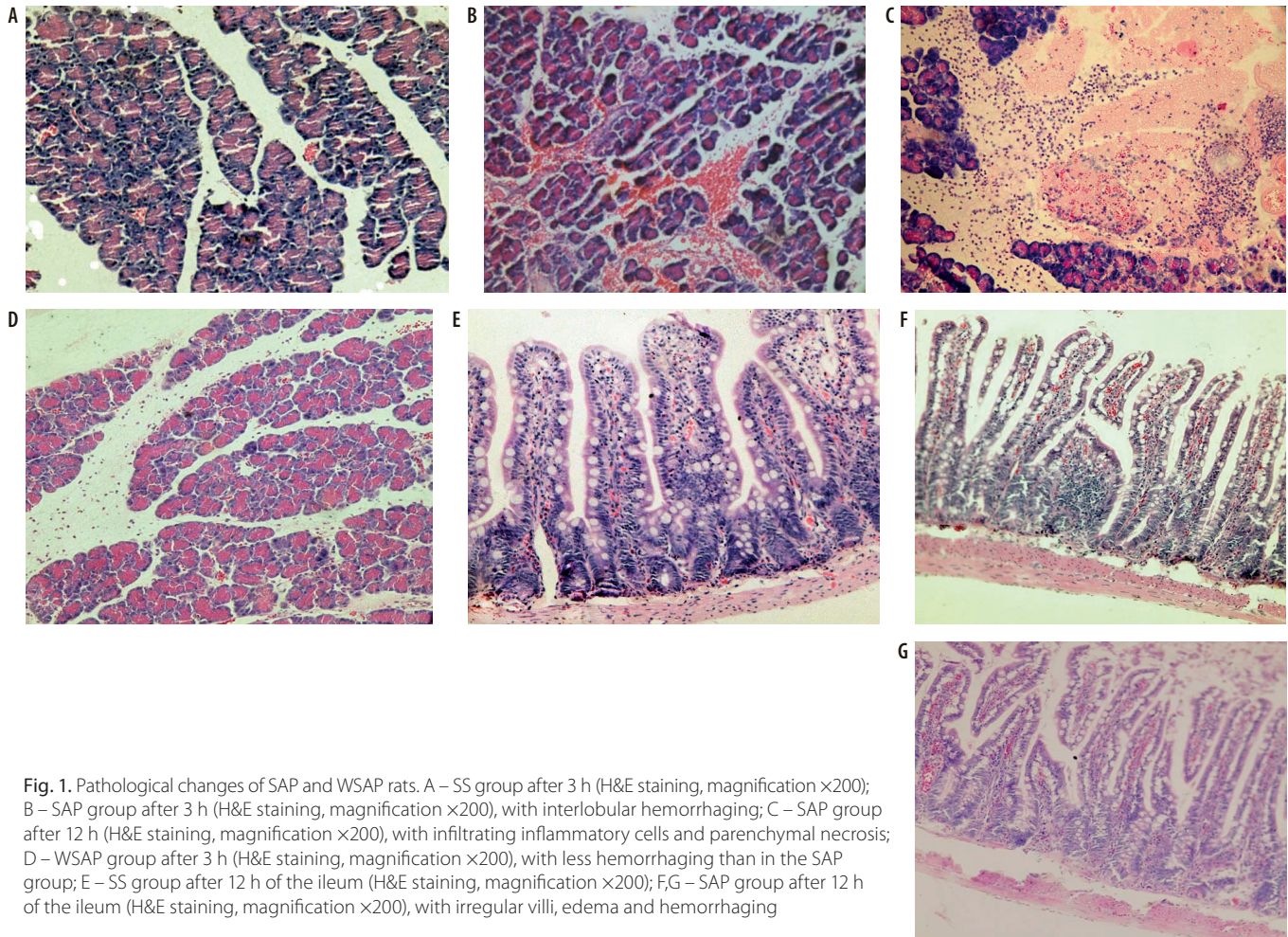


**Fig. 1.** Pathological changes of SAP and WSAP rats. A – SS group after 3 h (H&E staining, magnification ×200); B – SAP group after 3 h (H&E staining, magnification ×200), with interlobular hemorrhaging; C – SAP group after 12 h (H&E staining, magnification ×200), with infiltrating inflammatory cells and parenchymal necrosis; D – WSAP group after 3 h (H&E staining, magnification ×200), with less hemorrhaging than in the SAP group; E – SS group after 12 h of the ileum (H&E staining, magnification ×200); F,G – SAP group after 12 h of the ileum (H&E staining, magnification ×200), with irregular villi, edema and hemorrhaging

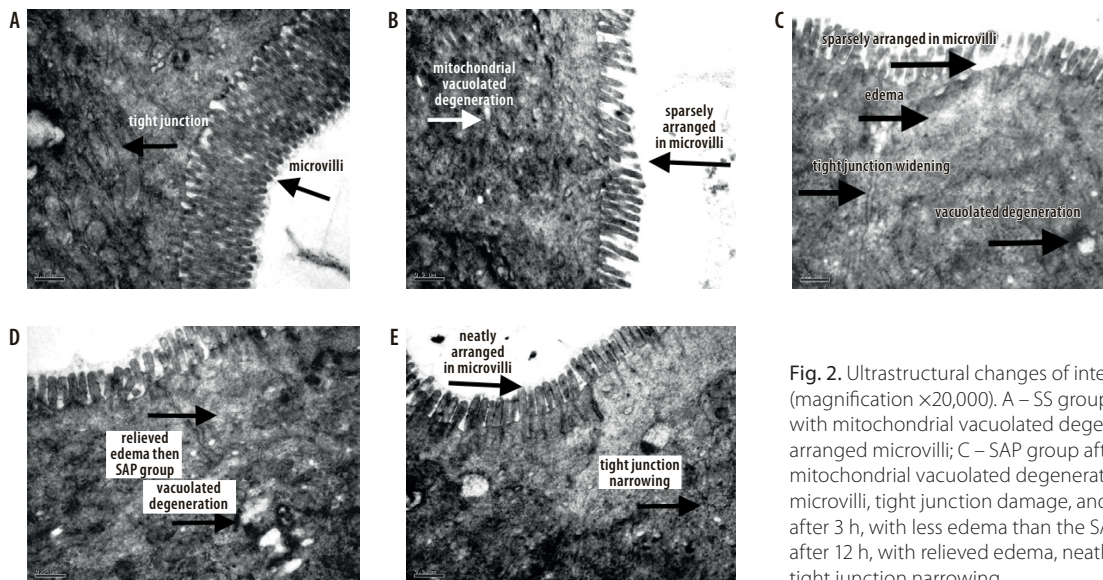


**Fig. 2.** Ultrastructural changes of intestinal mucosa (magnification ×20,000). A – SS group; B – SAP group after 6 h, with mitochondrial vacuolated degeneration and sparsely arranged microvilli; C – SAP group after 12 h, with cell edema, mitochondrial vacuolated degeneration, sparsely arranged microvilli, tight junction damage, and widening; D – WSAP group after 3 h, with less edema than the SAP group; E – WSAP group after 12 h, with relieved edema, neatly arranged microvilli and tight junction narrowing

### The intestinal Evans blue results

The SAP group ileal tissue Evans blue content was higher than the SS group ( $92.06 \pm 5.24 \mu\text{g/g}$ ) ( $p < 0.01$ ), showing increased intestinal mucosal permeability in the SAP

group. However, compared with the SAP group, the Evans blue content was significantly lower in the WSAP group:  $225.95 \pm 6.45 \mu\text{g/g}$ ,  $168.45 \pm 6.84 \mu\text{g/g}$  and  $108.47 \pm 6.68 \mu\text{g/g}$  after 3 h, 6 h and 12 h, respectively. This suggests that WT changes to intestinal permeability may be dose-dependent.

## Western blot

The total PKB protein expression was abundant in all 3 study groups. The differences were not statistically significant and did not change over time. The levels of p-PKB were higher in the SAP group than in the SS group and they rose steadily from 3 h to 12 h after the procedure. However, PKB phosphorylation was significantly inhibited in the WSAP group, as in the 3 h, 6 h and 12 h subgroups. The content of p-PKB was lower in the WSAP group than in the SAP group and the difference was significant ( $p < 0.05$ ) (Fig. 3, Table 4).

## Discussion

The pathogenesis of SAP is still poorly understood and has not been completely elucidated. Increasing evidence has demonstrated that the production and release of inflammatory mediators and other bioactive substances may play a significant role in systemic manifestations of SAP and is associated with remote organ dysfunction.<sup>15</sup>

PI3K is present in the cell, and its biological effects are extensive. It has been shown that PI3K can be activated to participate in signal transduction by a variety of inflammatory factors in inflammation, and that PKB is an important protease located downstream of PI3K, closely related to PI3K. PI3K can combine with the PH domain of PKB,

phosphorylate it and cause further changes in the target genes in the nucleus; it regulates neutrophil activation and migration and the expression of inflammatory factors. Therefore, phosphorylation of PKB can be used as an activity indicator of PI3K.<sup>16</sup> Fully active PKB/Akt mediates numerous cellular functions, including angiogenesis, metabolism, growth, proliferation, survival, protein synthesis, transcription, and apoptosis.<sup>17</sup> PI3K pathway activation is required for G1/S and G2/M phase progression, and constitutive activation of PI3K or PKB leads to reduced cyclin B synthesis and interferes with timely degradation of cyclin B1.<sup>18</sup>

A genetic or pharmacological blockade of the PI3K/PKB pathway in experimental animals can protect normal tissues against damage caused by inflammation.<sup>19</sup> Inhibition of the PI3K/PKB pathway with a PI3K/PKB inhibitor decreased serum cytokine levels and increased the survival of mice subjected to sepsis.<sup>20</sup> Research by Zhu et al. offers evidence that IPostC mediates cardioprotection in the remodeled rat myocardium, primarily via activation of the PI3K–PKB/Akt reperfusion injury salvage kinase pathway.<sup>21</sup> PI3Ks are also involved in the pathogenesis of AP. Activation of the PI3K signaling pathway, and in particular of the class IB PI3K $\gamma$  isoform, plays a significant role in those events which are necessary for the initiation of acute pancreatic injury.<sup>18</sup> Downregulation of the CSE/H2S system plays an important role in SAP development and progression and in preconditioning the H2S donor with NaHS-induced anti-inflammatory activity in SAP.

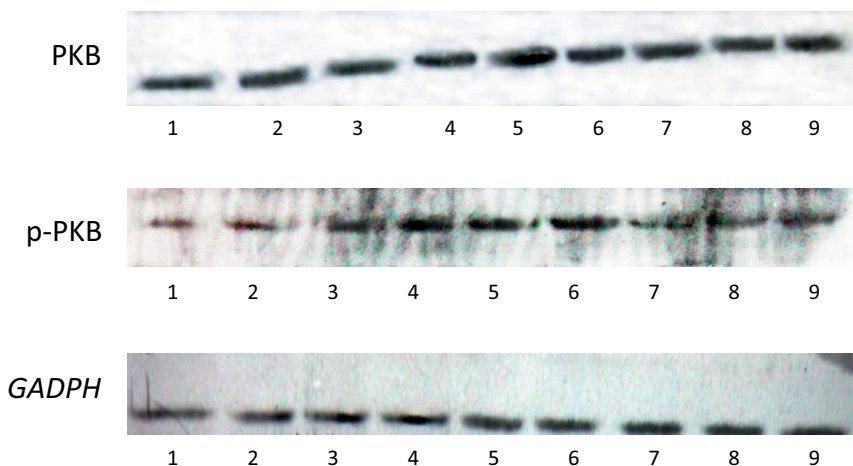


**Fig. 3.** The expression of PKB and p-PKB in the intestines of all study groups at different timepoints. The p-PKB levels were higher in the SAP group than in the SS group and they rose steadily between 3 h and 12 h after the operation. However, PKB phosphorylation was significantly inhibited in the WSAP group, as in its 3 h, 6 h and 12 h subgroups

1: SS group after 3 h; 2: SS group after 6 h; 3: SS group after 12 h; 4: SAP group after 3 h; 5: SAP group after 6 h; 6: SAP group after 12 h; 7: WSAP group after 3 h; 8: WSAP group after 6 h; 9: WSAP group after 12 h.

**Table 4.** The expression of PKB and p-PKB compared with *GADPH* in the intestines of all trial study groups at different timepoints. The levels of p-PKB content was higher in the SAP group than in the SS group, and continued to rise steadily from 3 h to 12 h after the operation. However, PKB phosphorylation was significantly inhibited in the WSAP group, also in 3 h, 6 h and 12 h subgroups. The content levels of p-PKB were lower in the WSAP group than in the SAP group, and the difference was significant ( $p < 0.05$ )

Group \ Pathway	3 h		6 h		12 h	
	PKB/ <i>GADPH</i>	p-PKB/ <i>GADPH</i>	PKB/ <i>GADPH</i>	p-PKB/ <i>GADPH</i>	PKB/ <i>GADPH</i>	p-PKB/ <i>GADPH</i>
SS	1.54 ± 0.61	0.68 ± 0.09	1.42 ± 0.63	0.82 ± 0.20	1.46 ± 0.72	0.78 ± 0.30
SAP	1.65 ± 0.54	1.25 ± 0.33 <sup>#</sup>	1.48 ± 0.62	1.62 ± 0.54 <sup>#</sup>	1.52 ± 0.66	1.77 ± 0.62 <sup>#</sup>
WSAP	1.49 ± 0.80	0.98 ± 0.21 <sup>**</sup>	1.55 ± 0.47	0.98 ± 0.36 <sup>**</sup>	1.58 ± 0.73	1.18 ± 0.41 <sup>**</sup>

<sup>#</sup> $p < 0.05$ , compared to the control group; <sup>\*\*</sup> $p < 0.05$ , compared to the SAP group.

This protective effect was associated with PI3K/PKB phosphorylation inhibition.<sup>22</sup>

The fungal metabolite WT and the synthetic compound LY294002 are the 2 currently known inhibitors that show a fairly high specificity for PI3K. It has been shown that WT causes 95% inhibition of PI3K and that the concentration required to induce apoptosis of cells maintained in growth factors correlates closely with that required for PI3K inhibition.<sup>23</sup>

Wortmannin is a commonly used cell biology reagent and has been previously used to inhibit DNA repair, receptor-mediated endocytosis and cell proliferation.<sup>24</sup> Wortmannin has been shown to be effective in decreasing serum cytokine levels and increasing the survival of mice subjected to sepsis.<sup>20</sup> It has also been shown to markedly reduce the subcellular redistribution of cathepsin B in an AP rat model.<sup>25</sup> Doses of WT markedly reduced trypsinogen activation in vitro and in vivo during the early stages of secretagogue-induced pancreatitis.<sup>16</sup> Furthermore, WT treatment decreases inflammatory cytokines in SAP.<sup>26</sup> Ng et al.<sup>27</sup> found that dosages of 0.175 mg/kg, 0.35 mg/kg or 0.7 mg/kg of WT inhibited PKB/Akt phosphorylation in a time- and dose-dependent manner, reaching a plateau at 4 h and at 0.7 mg/kg. Abliz et al.<sup>28</sup> demonstrated that 2 mg/kg of WT attenuates the thyroid injury associated with SAP in rats. Findings of Xu et al. showed that 1 mg/kg of WT decreases inflammatory cytokines in SAP rats.<sup>13</sup> Ding's study<sup>29</sup> suggests that a dosage of 0.35 mg/kg of WT is better for SAP rats than 1.4 mg/kg because of toxicity; thus, we chose a dosage of 0.35 mg/kg of WT to induce SAP in the WSAP rats.

Intestinal barrier dysfunction is now considered to be a major cause of complications such as bacterial translocation and MODS in SAP. Infection of pancreatic and peripancreatic tissues is considered to originate from the intestine.<sup>30,31</sup>

Samel et al.<sup>32</sup> demonstrated that bacterial translocation occurs within 3 h of the induction of pancreatitis in rats. Meriläinen et al. found that claudins mostly seem to remain unaltered during the early phase of the disease, but there is evidence of decreased claudin-3, claudin-4 and claudin-7 in acute necrotic pancreatitis, which may lead to tight junction disruption and bacterial translocation during the late course of the disease.<sup>6</sup> Tian et al. demonstrated that tumor necrosis factor  $\alpha$  (TNF- $\alpha$ )-regulated miR-155 overexpression inhibits apical junction complex (AJC) component protein syntheses of ZO-1 and E-cadherin by downregulating post-transcriptional RhoA expression, and that it disrupts the intestinal epithelial barrier in experimental SAP.<sup>8</sup> Thus, tight junction disruption and intestinal bacterial translocation are important factors that lead to SAP.

In our study, the SS group was observed under H&E staining to have complete lobular structures, no bleeding or necrosis, and no inflammatory cell infiltration. The SAP rats displayed hemorrhaging, edema, parenchymal necrosis, and infiltrating inflammatory cells. However,

the WSAP group showed milder pancreatic pathological damage than the SAP group, with significantly lower histopathological scores after 3 h, 6 h and 12 h ( $p < 0.05$ ). The morphological changes of the pancreas, including pancreatic edema, necrosis, hemorrhaging, and inflammation, were scored according to Spormann's criteria.<sup>14</sup> The WSAP group also exhibited lighter ultrastructural changes to the intestinal mucosa compared with the SAP group, which suggests that WT relieves the damage in SAP rats. The SAP group displayed mitochondrial vacuolated degeneration, sparsely arranged microvilli, cell edema, and tight junction widening. However, the WSAP group rats were observed to have neatly arranged microvilli, tight junction narrowing and less edema.

In addition, the intestinal mucosal permeability was higher in the SAP group. However, the Evans blue content was significantly lower in the WSAP group than in the SAP group. This suggests that WT changes to intestinal permeability may be dose-dependent. A microbiological evaluation of bacterial translocation in SAP may directly support our findings.

The results of western blotting showed that PKB phosphorylation was significantly inhibited in the WSAP group, as in its 3 h, 6 h and 12 h subgroups, and that the content of p-PKB was lower in the WSAP group than in the SAP group. Our study suggests that WT relieves intestinal permeability changes in SAP rats. The results of western blotting show that the levels of p-PKB were lower in the WSAP group than in the SAP group. It is possible that the PI3K/PKB signal transduction pathway may involve SAP intestinal injuries and that WT may relieve SAP intestinal injuries through the PI3K/PKB pathway.

## References

- Zhao G, Zhang JG, Wu HS, et al. Effects of different resuscitation fluid on severe acute pancreatitis. *World J Gastroenterol.* 2013;19(13):2044–2052.
- Fritz S, Hackert T, Hartwig W, et al. Bacterial translocation and infected pancreatic necrosis in acute necrotizing pancreatitis derives from small bowel rather than from colon. *Am J Surg.* 2010;200(1):111–117.
- Sun X, Shao Y, Jin Y, et al. Melatonin reduces bacterial translocation by preventing damage to the intestinal mucosa in an experimental severe acute pancreatitis rat model. *Exp Ther Med.* 2013;6(6):1343–1349.
- Li JP, Yang J, Huang JR, et al. Immunosuppression and the infection in patients with early SAP. *Front Biosci.* 2013;18:892–900.
- Liang HY, Chen T, Yan HT, Huang Z, Tang LJ. Berberine ameliorates severe acute pancreatitis induced intestinal barrier dysfunction via a myosin light chain phosphorylation dependent pathway. *Mol Med Rep.* 2014;9(5):1827–1833.
- Meriläinen S, Mäkelä J, Koivukangas V, et al. Intestinal bacterial translocation and tight junction structure in acute porcine pancreatitis. *Hepatogastroenterology.* 2012;59(114):599–606.
- Tian R, Tan JT, Wang RL, Xie H, Qian YB, Yu KL. The role of intestinal mucosa oxidative stress in gut barrier dysfunction of severe acute pancreatitis. *Eur Rev Med Pharmacol Sci.* 2013;17(3):349–355.
- Tian R, Wang RL, Xie H, Jin W, Yu KL. Overexpressed miRNA-155 dysregulates intestinal epithelial apical junctional complex in severe acute pancreatitis. *World J Gastroenterol.* 2013;19(45):8282–8291.
- Sharma B, Srivastava S, Singh N, Sachdev V, Kapur S, Saraya A. Role of probiotics on gut permeability and endotoxemia in patients with acute pancreatitis: A double-blind randomized controlled trial. *J Clin Gastroenterol.* 2011;45(5):442–448.

10. Deitch EA, Senthil M, Brown M, et al. Trauma-shock-induced gut injury and the production of biologically active intestinal lymph is abrogated by castration in a large animal porcine model. *Shock*. 2008; 30(2):135–141.
11. Luo J, Huang B, Zhang Z, Liu M, Luo T. Delayed treatment of propofol inhibits lipopolysaccharide-induced inflammation in microglia through the PI3K/PKB pathway. *Neuroreport*. 2018;29(10):839–845.
12. Qiao X, Gai H, Su R, et al. PI3K-AKT-GSK3 $\beta$ -CREB signaling pathway regulates anxiety-like behavior in rats following alcohol withdrawal. *J Affect Disord*. 2018;235:96–104.
13. Xu P, Wang J, Yang ZW, Lou XL, Chen C. Regulatory roles of the PI3K/Akt signaling pathway in rats with severe acute pancreatitis. *PLoS One*. 2013;8(11):e81767.
14. Spormann H, Sokolowski A, Letko G. Effect of temporary ischemia upon development and histological patterns of acute pancreatitis in the rat. *Pathol Res Pract*. 1989;184(5):507–513.
15. Bhatia M, Neoptolemos JP, Slavin J. Inflammatory mediators as therapeutic targets in acute pancreatitis. *Curr Opin Investig Drugs*. 2001;2(4):496–501.
16. Lin CH, Yeh SH, Lin CH. A role for the PI-3 kinase signaling pathway in fear conditioning and synaptic plasticity in the amygdale. *Neuron*. 2001;31(5):841–851.
17. Hemmings BA, Restuccia DF. PI3K-PKB/Akt pathway. *Cold Spring Harb Perspect Biol*. 2012;4(9):a011189.
18. Liang J, Slingerland JM. Multiple roles of the PI3K/PKB (Akt) pathway in cell cycle progression. *Cell Cycle*. 2003;2(4):339–345.
19. Cantley LC. The phosphoinositide 3-kinase pathway. *Science*. 2002; 296(5573):1655–1657.
20. Yadav UC, Naura AS, Aguilera-Aguirre L, et al. Aldose reductase inhibition prevents allergic airway remodeling through PI3K/AKT/GSK-3 $\beta$  pathway in mice. *PLoS One*. 2013;8(2):e57442.
21. Zhu M, Feng J, Lucchinetti E, et al. Ischemic postconditioning protects remodeled myocardium via the PI3K-PKB/Akt reperfusion injury salvage kinase pathway. *Cardiovasc Res*. 2006;72(1):152–162.
22. Rao CY, Fu LY, Hu CL, et al. H2S mitigates severe acute pancreatitis through the PI3K/AKT-NF- $\kappa$ B pathway in vivo. *World J Gastroenterol*. 2015;21(15):4555–4563.
23. Yao R, Cooper GM. Requirement for phosphatidylinositol 3-kinase in the prevention of apoptosis by nerve growth factor. *Nature*. 1995; 267(5206):2003–2006.
24. Liu Y, Shreder KR, Gai W, Corral S, Ferris DK, Rosenblum JS. Wortmannin, a widely used phosphoinositide 3-kinase inhibitor, also potently inhibits mammalian polo-like kinase. *Chem Biol*. 2005;12(1):99–107.
25. Kim SH, Jang YW, Hwang P, Kim HJ, Han GY, Kim CW. The renoprotective effect of a phosphoinositide 3-kinase inhibitor wortmannin on streptozotocin-induced proteinuric renal disease rats. *Exp Mol Med*. 2012;44(1):45–51.
26. Rogers Lynette K, Xu P, Wang J, Yang ZW, Lou XI, Chen C. Regulatory roles of the PI3K/Akt signaling pathway in rats with severe acute pancreatitis. *PLoS One*. 2013;8(11):e81767.
27. Ng SS, Tsao MS, Nicklee T, Hedley DW. Wortmannin inhibits pkb/akt phosphorylation and promotes gemcitabine antitumor activity in orthotopic human pancreatic cancer xenografts in immunodeficient mice. *Clin Cancer Res*. 2001;7(10):3269–3275.
28. Abliz A, Deng W, Sun R, Guo W, Zhao L, Wang W. Wortmannin, PI3K/Akt signaling pathway inhibitor, attenuates thyroid injury associated with severe acute pancreatitis in rats. *Int J Clin Exp Pathol*. 2015;8(11): 13821–13833.
29. Ding RK. *The Role of PI3K/PKB Signal Pathway and its Inhibitor Wortmannin in Renal Injuries Induced by Severe Acute Pancreatitis in Rats*. PhD dissertation 2011, Hebei Medical University, China.
30. Schwarz M, Thomsen J, Meyer H, Buchler MW, Beger HG. Frequency and time course of pancreatic and extrapancreatic bacterial infection in experimental acute pancreatitis in rats. *Surgery*. 2000;127(4): 427–432.
31. Chen J, Huang C, Wang J, et al. Dysbiosis of intestinal microbiota and decrease in paneth cell antimicrobial peptide level during acute necrotizing pancreatitis in rats. *PLoS One*. 2017;12(4):e0176583.
32. Samel S, Lanig S, Lux A, et al. The gut origin of bacterial pancreatic infection during acute experimental pancreatitis in rats. *Pancreatology*. 2002;2(5):449–455.

# Correlation of rs749292 and rs700518 polymorphisms in the aromatase gene (*CYP19A1*) with osteoporosis in postmenopausal Polish women

Adam Kamiński<sup>1,A,D,E</sup>, Anna Bogacz<sup>2,3,C,E</sup>, Małgorzata Górską-Paukszta<sup>2,B,C</sup>,  
Agnieszka Seremak-Mrozikiewicz<sup>4,5,A,E</sup>, Bogusław Czerny<sup>2,6,A,F</sup>

<sup>1</sup> Department of Orthopedics and Traumatology, Independent Public Clinical Hospital No. 1, Pomeranian Medical University, Szczecin, Poland

<sup>2</sup> Department of Stem Cells and Regenerative Medicine, Institute of Natural Fibers and Medicinal Plants, Plewiska, Poland

<sup>3</sup> Department of Histocompatibility with Laboratory of Genetic Diagnostics, Regional Blood Center, Poznań, Poland

<sup>4</sup> Division of Perinatology and Women's Diseases, Poznan University of Medical Sciences, Poland

<sup>5</sup> Department of Pharmacology and Phytochemistry, Institute of Natural Fibres and Medicinal Plants, Plewiska, Poland

<sup>6</sup> Department of Pharmacology and Pharmacoeconomics, Pomeranian Medical University, Szczecin, Poland

A – research concept and design; B – collection and/or assembly of data; C – data analysis and interpretation;  
D – writing the article; E – critical revision of the article; F – final approval of the article

Advances in Clinical and Experimental Medicine, ISSN 1899–5276 (print), ISSN 2451–2680 (online)

*Adv Clin Exp Med.* 2019;28(8):1067–1071

## Address for correspondence

Adam Kamiński  
E-mail: adam.kaminski.848@gmail.com

## Funding sources

The study was supported with statutory projects from the Institute of Natural Fibres and Medicinal Plants and the Pomeranian Medical University in Szczecin, Poland.

## Conflict of interest

None declared

Received on November 20, 2017

Reviewed on May 20, 2018

Accepted on February 7, 2019

Published online on March 11, 2019

## Cite as

Kamiński A, Bogacz A, Górską-Paukszta M, Seremak-Mrozikiewicz A, Czerny B. Correlation of rs749292 and rs700518 polymorphisms in the aromatase gene (*CYP19A1*) with osteoporosis in postmenopausal Polish women. *Adv Clin Exp Med.* 2019;28(8):1067–1071. doi:10.17219/acem/103803

## DOI

10.17219/acem/103803

## Copyright

© 2019 by Wrocław Medical University  
This is an article distributed under the terms of the Creative Commons Attribution Non-Commercial License (<http://creativecommons.org/licenses/by-nc-nd/4.0/>)

## Abstract

**Background.** The aromatase gene (*CYP19A1*) is responsible for the aromatization of androgenic precursors to estrogens in peripheral tissues – including bone – after menopause.

**Objectives.** The aim of this study was to evaluate the genotypes and allele frequencies of the rs749292 and rs700518 polymorphisms of the *CYP19A1* gene in Polish postmenopausal women with osteopenia and osteoporosis. The potential correlations between genetic polymorphisms, bone mineral density (BMD), risk for bone fractures, and other clinical parameters were analyzed.

**Material and methods.** The study included 675 unrelated women (109 women with osteopenia, 333 women with osteoporosis, and 233 healthy women). Genomic DNA was extracted from the blood samples and the *CYP19A1* polymorphisms were determined using the polymerase chain reaction restriction fragment length polymorphism (PCR-RFLP) method. Bone mineral density at the lumbar spine (L1–L4) was measured with dual energy X-ray absorptiometry (DEXA).

**Results.** The analysis of the *CYP19A1* rs749292 polymorphism showed that there were no statistically significant differences in the distribution of genotypes between the study groups with osteoporosis and osteopenia and the control group. However, it was noted that the GG genotype occurred more often in the group with osteopenia (35.8%; OR = 1.44) than in the control group (27.9%). Also, a difference was noted in the distribution of genotypes in women with osteoporosis. In addition, it can be assumed that the G allele may lead to an increased susceptibility to osteopenia and osteoporosis. The analysis of the *CYP19A1* rs700518 polymorphism showed that heterozygotes were more common in the group with osteoporosis (58.3%) than in the control group (52.8%).

**Conclusions.** Our results suggest that the rs749292 polymorphism of the *CYP19A1* gene may contribute to an elevated risk for fractures in postmenopausal Polish women.

**Key words:** postmenopausal osteoporosis, gene polymorphism, bone mineral density, *CYP19A1*

## Introduction

Osteoporosis is a common disease in postmenopausal women and is characterized by reduced bone mass resulting in an increased risk of fractures. Furthermore, it has been demonstrated that bone mass is highly dependent on genetic and environmental factors.<sup>1</sup> Sex steroid hormones also have an important influence on bone mass.<sup>2</sup> The main source of estrogens in women after menopause is the aromatization of androgenic precursors. The conversion of androgens to estrogens is catalyzed in a variety of tissues and aromatase (*CYP19A1*) is the key enzyme in this transformation.<sup>3,4</sup> It is known that the loss of bone mass occurs due to the age-related loss of gonadal function. The *CYP19A1* gene is located on 15q21.2 and contains 10 exons; exons 2 to 10 are transcribed and translated to create the aromatase enzyme.<sup>5–8</sup>

Importantly, it has been demonstrated that the various polymorphisms in the *CYP19A1* gene may positively or negatively correlate with aromatase activity, sex hormone levels, bone mineral density (BMD) values, and fractures.<sup>9–14</sup> Therefore, polymorphisms of genes regulating hormone production and metabolism may potentially explain the etiology of osteoporosis. The aim of this study was to examine the potential effects of the rs749292 and rs700518 polymorphisms in the *CYP19A1* gene on osteoporosis in postmenopausal women. To our knowledge, there are no studies on the relationship between the *CYP19A1* rs749292 polymorphism and osteoporosis development in postmenopausal women.

## Material and methods

### Patients

The study was comprised of 675 unrelated Polish women, including 109 women with osteopenia, 333 women with osteoporosis, and 233 healthy women. All of the women were in a postmenopausal age. During an interview with each patient, data on the occurrence of diseases, the age of first and last menstruation, the number of pregnancies, birth weight, and current height and weight were collected. Then, the body mass index (BMI) was calculated for each patient. The inclusion criteria for genetic research included the following: the onset of menopause at least 1 year prior to the study and the lack of hormone replacement therapy (HRT) or medications that affect bone mass – such as selective estrogen receptor modulators (SERMs), calcitonin, bisphosphates, heparin, steroids, thyroid hormones, antiepileptics, GnRH analogues, or tibolone. Patients with diseases which influence bone metabolism – such as endocrine and metabolic disorders, hematological diseases, cancer, connective tissue diseases, and autoimmune disorders – were excluded from the study. Additionally, the postmenopausal patients did not suffer from hypoestrogenism

at reproductive age or the premenopausal period. This study also disqualified patients who had undergone bilateral ovariectomy and patients with premature ovarian insufficiency (POI). Moreover, vitamin D and calcium intake either in the diet or as a supplement was advised per current clinical practice, but their use was not recorded among the patients studied.

The BMD measurements were performed at the Laboratory of Densitometry in Clinical Hospital No. 1 of the Pomeranian Medical University in Szczecin, Poland. Bone mineral density was measured at the lumbar vertebrae and the femoral neck using the dual-energy x-ray absorptiometry method (DEXA) and a LUNAR DPX 100 densitometer (Lunar Corp., Madison, USA). All subjects underwent DEXA screening of lumbar vertebrae 2 to 4 (L2–L4). Bone mineral density values are presented as T-scores and Z-scores. Based on these measurements, the women were classified into 3 groups: those with osteopenia ( $-2.5 < \text{T-score} < -1$ ), those with osteoporosis ( $\text{T-score} < -2.5$ ) and those with a normal T-score ( $\text{T-score} > -1$ ).

Among the patients studied, we did not observe the occurrence of any fractures, though – based on the BMD and bone turnover values in some patients – there was a risk of fracture. In addition, serum estradiol levels were not measured in the patients because the study assumed that postmenopausal patients with osteoporosis would have decreased levels of estrogen. The characteristics of the study population (postmenopausal women with osteopenia, osteoporosis or normal T-scores) are presented in Table 1.

The study was approved by the Local Bioethical Committee of the Pomeranian Medical University in Szczecin, Poland. All patients were informed about the purpose of the study and provided written informed consent.

### Analysis of *CYP19A1* polymorphisms

Blood samples were collected in the Department of Orthopedics and Traumatology at the Pomeranian Medical University. The analysis of *CYP19A1* gene polymorphisms was conducted at the Department of Stem Cell and Regenerative Medicine at the Institute of Natural Fibers and Medicinal Plants in Poznań, Poland. Genomic DNA was extracted from peripheral blood using a QIAamp Blood Kit (Qiagen GmbH, Hilden, Germany) according to the manufacturer's instructions.

*CYP19A1* rs749292 (A>G, TaqI) and rs700518 (G>A, RsaI) variants were determined by polymerase chain reaction restriction fragment length polymorphism (PCR-RFLP). The following primers were used for PCR: *CYP19A1*TaqIF: 5'-GCC ACC TGT CTC TCA TTC CA-3', *CYP19A1*TaqIR: 5'-CTC CGT GAT TTG TCA GCT CTT-3' (386 bp), *CYP19A1*RsaIF: 5'-AGT AAC ACA GAA CAG TTG CA-3', and *CYP19A1*RsaIR: 5'-TCC AGA CTC GCA TGA ATT CTC CGT A-3' (188 bp). The polymorphic sites were defined using restriction enzymes for the *CYP19A1* gene, such as TaqI

**Table 1.** Characteristics of the study population (postmenopausal women with osteopenia, osteoporosis, or a normal T-score)

Patients' characteristics	Osteopenia mean ( $\pm$ 95% CI)	Osteoporosis mean ( $\pm$ 95% CI)	Controls, mean ( $\pm$ 95% CI)	p-value
Age [years]	53.2377 ( $\pm$ 1.4553)	56.0643 ( $\pm$ 1.4760)	53.3788 ( $\pm$ 2.0206)	0.54 <sup>a</sup> 0.014 <sup>b</sup>
Height [cm]	162.6311 ( $\pm$ 0.8926)	160.2527 ( $\pm$ 1.0504)	163.0758 ( $\pm$ 1.4701)	0.08 <sup>a</sup> 0.01 <sup>b</sup>
Weight [kg]	65.1721 ( $\pm$ 1.9699)	61.2088 ( $\pm$ 1.8626)	68.7273 ( $\pm$ 2.9815)	0.026 <sup>a</sup> 0.001 <sup>b</sup>
BMI	24.6445 ( $\pm$ 0.7077)	23.7879 ( $\pm$ 0.6314)	25.8802 ( $\pm$ 1.1117)	0.04 <sup>a</sup> 0.04 <sup>b</sup>
Birth weight [g]	3226.7857 ( $\pm$ 159.3961)	3141.2500 ( $\pm$ 285.7844)	3628.9474 ( $\pm$ 231.7143)	0.026 <sup>a</sup> 0.005 <sup>b</sup>
Reproductive years	36.2000 ( $\pm$ 1.2743)	35.6154 ( $\pm$ 1.2418)	36.3750 ( $\pm$ 1.9291)	0.724 <sup>a</sup> 0.528 <sup>b</sup>
Age of first menstruation [years]	13.1167 ( $\pm$ 0.6184)	12.9385 ( $\pm$ 0.5362)	13.3750 ( $\pm$ 0.6776)	0.636 <sup>a</sup> 0.754 <sup>b</sup>
Age of last menstruation [years]	49.2099 ( $\pm$ 0.9868)	48.1585 ( $\pm$ 1.0905)	50.1707 ( $\pm$ 1.3847)	0.069 <sup>a</sup> 0.058 <sup>b</sup>
Number of pregnancies	1.8852 ( $\pm$ 0.1945)	1.9560 ( $\pm$ 0.2687)	1.9394 ( $\pm$ 0.2984)	0.869 <sup>a</sup> 0.902 <sup>b</sup>
Years after menopause	7.1833 ( $\pm$ 1.5562)	10.6308 ( $\pm$ 1.4245)	7.0313 ( $\pm$ 2.0156)	0.854 <sup>a</sup> 0.001 <sup>b</sup>
BMD L2–L4 [g/cm <sup>2</sup> ]	0.9674 ( $\pm$ 0.0398)	0.9752 ( $\pm$ 0.0296)	0.9694 ( $\pm$ 0.0439)	0.986 <sup>a</sup> 0.944 <sup>b</sup>
BMD L2–L4 YA [%]	80.9022 ( $\pm$ 3.4153)	81.2783 ( $\pm$ 2.4579)	81.0204 ( $\pm$ 3.5647)	0.965 <sup>a</sup> 0.982 <sup>b</sup>
BMD L2–L4 AM [%]	89.1304 ( $\pm$ 3.6295)	89.5043 ( $\pm$ 2.4379)	89.7755 ( $\pm$ 3.8959)	0.989 <sup>a</sup> 0.968 <sup>b</sup>
T-score	-1.8520 ( $\pm$ 0.0552)	-3.1640 ( $\pm$ 0.1118)	0.0779 ( $\pm$ 0.2261)	<0001 <sup>b</sup>
Z-score	-0.8448 ( $\pm$ 0.1694)	-3.5691 ( $\pm$ 3.8881)	0.6425 ( $\pm$ 0.4002)	0.117 <sup>a</sup> <0001 <sup>b</sup>

<sup>a</sup> – comparison between the group with osteopenia and the control group; <sup>b</sup> – comparison between the group with osteoporosis and the control group; 95% CI – 95% confidence interval; BMI – body mass index; BMD – bone mineral density; BMD L2–L4 – bone mineral density of lumbar vertebrae 2 to 4; BMD-AM L2–L4 – age-matched bone mineral density of lumbar vertebrae 2 to 4; BMD L2–L4 YA – young-adults bone mineral density of lumbar vertebrae 2 to 4.

(AA: 327 bp, 59 bp; GG: 172bp, 155 bp, 59 bp) and RsaI (GG: 164 bp, 24 bp; AA: 188 bp). The PCR-RFLP products were separated by electrophoresis according to their size in 3% agarose gel with ethidium bromide and viewed under UV light.

## Statistical analysis

Data analysis was performed using SPSS Statistics v. 17.0 software (SPSS Inc., Chicago, USA). The results are presented as mean values. The odds ratios (OR) are given with the respective 95% confidence intervals (95% CI). The observed frequencies were compared with the expected frequencies and tested for Hardy-Weinberg equilibrium. The distribution of variables was evaluated with the Shapiro–Wilk test. The homogeneity of variances was assessed using the Levene test. Quantitative variables were compared with one-way analysis of variances (ANOVA) with post hoc contrast comparison tests. Ordinal data were compared with a  $\chi^2$  test.

## Results

Our analysis of the *CYP19A1* rs749292 polymorphism showed that there were no statistically significant differences in the distribution of genotypes between women with osteoporosis or osteopenia and the control group ( $p = 0.109$ ). However, it is noticeable that the mutant GG genotype occurred more often in the group with osteopenia (35.8%; OR = 1.44) than in the control group (27.9%). Also, a difference was observed in the distribution of genotypes among the women with osteoporosis. Despite a lack of statistical significance between the groups, the wild homozygote (AA) occurred more frequently among the control group (23.2%) than among the patients with osteopenia (21.1%) or those with osteoporosis (17.7%) (Table 2). There was only 1 statistically significant difference among the clinical parameters – the correlation between BMI and genotype in the osteopenia group ( $p = 0.049$ ) – although this was not observed in the patients with osteoporosis. On the basis of these results, it can be assumed that

**Table 2.** Distribution of the CYP19A1 (rs749292) polymorphism in women with osteopenia, osteoporosis, and normal T-scores

Genotype	Osteopenia		Osteoporosis		Control		Statistical analysis		
	observed values n [%]	expected values [%]	observed values n [%]	expected values [%]	observed values n [%]	expected values [%]	OR	95% CI	p-value
AA	23 (21.1)	18.2	59 (17.7)	20.8	54 (23.2)	22.6	0.89 <sup>a</sup> 0.71 <sup>b</sup>	0.49–1.58 <sup>a</sup> 0.46–1.11 <sup>b</sup>	0.39 <sup>a</sup> 0.07 <sup>b</sup>
AG	47 (43.1)	48.9	186 (55.9)	49.6	114 (48.9)	49.9	0.79 <sup>a</sup> 1.32 <sup>b</sup>	0.49–1.28 <sup>a</sup> 0.93–1.87 <sup>b</sup>	0.19 <sup>a</sup> 0.06 <sup>b</sup>
GG	39 (35.8)	32.9	88 (26.4)	29.6	65 (27.9)	27.5	1.44 <sup>a</sup> 0.92 <sup>b</sup>	0.86–2.40 <sup>a</sup> 0.63–1.37 <sup>b</sup>	0.09 <sup>a</sup> 0.38 <sup>b</sup>
Total	109 (100)	100.00	333 (100)	100.00	233 (100)	100.00	–	–	–
Alleles									
A	93 (42.7)	–	304 (45.6)	–	222 (47.6)	–	0.82 <sup>a</sup> 0.92 <sup>b</sup>	0.58–1.15 <sup>a</sup> 0.72–1.18 <sup>b</sup>	0.13 <sup>a</sup> 0.27 <sup>b</sup>
G	125 (57.3)	–	362 (54.4)	–	244 (52.4)	–	1.22 <sup>a</sup> 1.08 <sup>b</sup>	0.87–1.71 <sup>a</sup> 0.85–1.38 <sup>b</sup>	0.13 <sup>a</sup> 0.27 <sup>b</sup>
Total	218 (100.00)	–	666 (100.00)	–	466 (100.00)	–	–	–	–

<sup>a</sup> – comparison between the group with osteopenia and the control group; <sup>b</sup> – comparison between the group with osteoporosis and the control group; OR – odds ratio; 95% CI – 95% confidence interval.

**Table 3.** Distribution of the CYP19A1 (rs700518) polymorphism in women with osteopenia, osteoporosis, and normal T-scores

Genotype	Osteopenia		Osteoporosis		Control		Statistical analysis		
	observed values n [%]	expected values [%]	observed values n [%]	expected values [%]	observed values n [%]	expected values [%]	OR	95% CI	p-value
AA	27 (24.8)	25.9	83 (24.9)	29.3	65 (27.9)	29.5	0.85 <sup>a</sup> 0.85 <sup>b</sup>	0.48–1.47 <sup>a</sup> 0.58–1.28 <sup>b</sup>	0.32 <sup>a</sup> 0.24 <sup>b</sup>
AG	57 (52.3)	50.0	194 (58.3)	49.7	123 (52.8)	49.6	0.98 <sup>a</sup> 1.25 <sup>b</sup>	0.61–1.58 <sup>a</sup> 0.88–1.77 <sup>b</sup>	0.51 <sup>a</sup> 0.11 <sup>b</sup>
GG	25 (22.9)	24.1	56 (16.8)	21.0	45 (19.3)	20.9	1.24 <sup>a</sup> 0.84 <sup>b</sup>	0.68–2.23 <sup>a</sup> 0.53–1.34 <sup>b</sup>	0.26 <sup>a</sup> 0.25 <sup>b</sup>
Total	109 (100)	100.00	333 (100)	100.00	233 (100)	100.00	–	–	–
Alleles									
A	111 (50.9)	–	360 (54.1)	–	253 (54.3)	–	0.87 <sup>a</sup> 0.99 <sup>b</sup>	0.62–1.22 <sup>a</sup>	0.22 <sup>a</sup>
G	107 (49.1)	–	306 (45.9)	–	213 (45.7)	–	1.15 <sup>a</sup> 1.01 <sup>b</sup>	0.82–1.60 <sup>a</sup> 0.77–1.26 <sup>b</sup>	0.22 <sup>a</sup> 0.49 <sup>b</sup>
Total	218 (100.00)	–	666 (100.00)	–	466 (100.00)	–	–	–	–

OR – odds ratio; 95% CI – 95% confidence interval.

the G allele (mutant) may lead to an increased susceptibility to osteopenia and osteoporosis.

In our analysis of the CYP19A1 rs700518 polymorphism, there were no statistically significant differences in the distribution of genotypes between the groups with osteoporosis and osteopenia and the control group ( $p = 0.520$ ). It was observed that heterozygotes were more common among the women with osteoporosis (58.3%) than in the control group (52.8%), but the difference was not statistically significant (Table 3). There were some statistically significant differences between clinical parameters and genotypes. Correlations were observed between genotype and BMI ( $p = 0.049$ ), age ( $p = 0.035$ ), and years after menopause ( $p = 0.012$ ) in the patients with osteopenia. Osteopenia

occurred at an earlier age (49.9 years) in the patients with the mutant AA genotype than in those with the GG (53.1 years) and GA (54.9 years) genotypes ( $p = 0.035$ ). Also, a statistically significant difference was observed between genotype and age-matched bone mineral density (BMD-AM) ( $p = 0.042$ ). The lowest BMD-AM was observed in patients with the recessive AA genotype. The BMD-AM values were higher among the women with the GG and GA genotypes. These results indicate a trend of a higher probability of osteopenia in the recessive homozygotes.

There were no statistically significant differences in genotype frequency among patients with osteoporosis, but a correlation did appear between the genotype and reproductive years ( $p = 0.042$ ).



## Discussion

In this study, we observed no statistically significant effects of CYP19A1 polymorphisms on the occurrence of osteopenia and osteoporosis. No differences were noted in the distribution of the CYP19A1 rs749292 genotype between patients and controls. However, the GG genotype occurred more often in women with osteopenia than in the control group. Available studies indicate that genetic variations of the CYP19A1 gene, including rs749292, are associated with hormone levels in postmenopausal women with breast cancer.<sup>15,16</sup> At the same time, while no data is available (according to our knowledge and literature review) on the allele and genotype frequencies for CYP19A1 rs749292 in postmenopausal women with osteopenia/osteoporosis compared to controls, results similar to ours were obtained by Yilmaz et al.<sup>17</sup> The authors of that study investigated the frequencies of the CYP19A1 rs700518 polymorphism in patients with osteoporosis and a control group from the Turkish population. They did not observe a relationship between the studied polymorphism and the occurrence of osteoporosis, though they did report a higher occurrence of the AG genotype (63%) among the control group. This relationship could have resulted from the limited size of the study group. They also pointed out the lower frequency of AA and AG genotypes among the patients. In our study, the AA genotype also occurred less frequently in osteoporotic patients (16.8%) compared with the control group (19.3%). However, the differences were not statistically significant (OR = 0.84; 95% CI = 0.53–1.34; p = 0.25).

Furthermore, Geng et al. found no significant effect of the rs700518 polymorphism on BMD in the Chinese population among postmenopausal women.<sup>18</sup> Similarly, in our study the GA genotype (44.5%) occurred most frequently, while the homozygous GG and AA genotypes accounted for 19.5% and 36%, respectively. The CYP19A1 rs700518 polymorphism was also reported to be associated with differences in BMD and hormone levels in men (n = 1068). Lorentzon et al. showed that men with the GG genotype had higher BMD values than carriers of the AG and AA genotypes.<sup>1</sup> Similar statistically significant results (p = 0.010) were obtained by Riancho et al.<sup>11</sup> Total hip BMD was the highest in patients with the GG genotype (0.823 g/cm<sup>3</sup>) and was accordingly lower in those with the GA (0.807 g/cm<sup>3</sup>) and AA (0.795 g/cm<sup>3</sup>) genotypes.

In our study, we also observed the same relationship between genotype and AM-BMD values (p = 0.042) among female patients with osteopenia (89.3 for GG, 91.9 for GA and 78.9 for AA). Napoli et al.<sup>14</sup> conducted a study on women taking the aromatase inhibitor during breast cancer therapy and showed that patients with the AA genotype developed significant bone loss relative to patients carrying the G allele (GA and GG genotypes). These findings may suggest that the A allele leads to more susceptibility to bone loss during therapy and that the GG genotype has a protective influence.

## Conclusions

Our results suggest that the rs749292 polymorphism of the CYP19A1 gene may contribute to an elevated risk for fractures in Polish postmenopausal women.

## References

- Lorentzon M, Swanson C, Eriksson AL, Mellström D, Ohlsson C. Polymorphisms in the aromatase gene predict areal BMD as a result of affected cortical bone size: The GOOD study. *J Bone Miner Res.* 2006;21(2):332–339.
- Carson JA, Manolagas SC. Effects of sex steroids on bones and muscles: Similarities, parallels, and putative interactions in health and disease. *Bone.* 2015;80:67–78.
- Riancho JA, Valero C, Naranjo A, Morales DJ, Sanudo C, Zarrabeitia MT. Identification of an aromatase haplotype that is associated with gene expression and postmenopausal osteoporosis. *Clin Endocrinol Metab.* 2007;92(2):660–665.
- Shimodaira M, Nakayama T, Sato N, et al. Association study of aromatase gene (CYP19A1) in essential hypertension. *Int J Med Sci.* 2008;5(1):29–35.
- Bulun SE, Sebastian S, Takayama K, Suzuki T, Sasano H, Shozu M. The human CYP19 (aromatase P450) gene: Update on physiologic roles and genomic organization of promoters. *J Steroid Biochem Mol Biol.* 2003;86(3–5):219–224.
- Leelawattana R, Ziambaras K, Roodman-Weiss J, et al. The oxidative metabolism of estradiol conditions postmenopausal bone density and bone loss. *J Bone Miner Res.* 2000;15(12):2513–2520.
- Masi L, Becherini L, Gennari L, et al. Polymorphism of the aromatase gene in postmenopausal Italian women: Distribution and correlation with bone mass and fracture risk. *J Clin Endocrinol Metab.* 2001;86(5):2263–2269.
- Somner J, McLellan S, Cheung J, et al. Polymorphisms in the P450 c17 (17-hydroxylase/17,20-Lyase) and P450 c19 (aromatase) genes: Association with serum sex steroid concentrations and bone mineral density in postmenopausal women. *J Clin Endocrinol Metab.* 2004;89(1):344–351.
- Gennari L, Masi L, Merlotti D, et al. A polymorphic CYP19 TTTA repeat influences aromatase activity and estrogen levels in elderly men: Effects on bone metabolism. *J Clin Endocrinol Metab.* 2004;89(6):2803–2810.
- Riancho JA, Zarrabeitia MT, Valero C, et al. Aromatase gene and osteoporosis: Relationship of ten polymorphic loci with bone mineral density. *Bone.* 2005;36(5):917–925.
- Riancho JA, Sanudo C, Valero C, et al. Association of the aromatase gene alleles with BMD: Epidemiological and functional evidence. *J Bone Miner Res.* 2009;24(10):1709–1718.
- Zarrabeitia MT, Hernández JL, Valero C, et al. A common polymorphism in the 5'-untranslated region of the aromatase gene influences bone mass and fracture risk. *Eur J Endocrinol.* 2004;150(5):699–704.
- Tofteng CL, Kindmark A, Brändström H, et al; Danish Osteoporosis Prevention Study. Polymorphisms in the CYP19 and AR genes – relation to bone mass and longitudinal bone changes in postmenopausal women with or without hormone replacement therapy: The Danish Osteoporosis Prevention Study. *Calcif Tissue Int.* 2004;74(1):25–34.
- Napoli N, Rastelli A, Ma C, et al. Genetic polymorphism at Val80 (rs700518) of the CYP19A1 gene is associated with aromatase inhibitor associated bone loss in women with ER + breast cancer. *Bone.* 2013;55(2):309–314.
- Kopp TI, Jensen DM, Ravn-Haren G, et al. Alcohol-related breast cancer in postmenopausal women: Effect of CYP19A1, PPARG and PPARG-C1A polymorphisms on female sex-hormone levels and interaction with alcohol consumption and NSAID usage in a nested case-control study and a randomized controlled trial. *BMC Cancer.* 2016;16:283.
- Flote VG, Furberg AS, McTiernan A, et al. Gene variations in estrogen pathways, CYP19A1, daily 17β-estradiol and mammographic density phenotypes in premenopausal women. *Breast Cancer Res.* 2014;16:499.
- Yilmaz MB, Pazarbasi A, Guzel AI, et al. Association of serum sex steroid levels and bone mineral density with CYP17 and CYP19 gene polymorphisms in postmenopausal women in Turkey. *Genet Mol Res.* 2011;10(3):1999–2008.
- Geng L, Yao ZW, Luo JY, Han LL, Lu Q. Association between Val80 polymorphism of the CYP19 gene, A163G polymorphism of the OPG gene and bone mineral density in post-menopausal Chinese women [in Chinese]. *Yi Chuan.* 2007;29(11):1345–1350.



# The titanium-made growth-guidance technique for early-onset scoliosis at minimum 2-year follow-up: A prospective multicenter study

Grzegorz Mięksiak<sup>1,8,A–F</sup>, Krzysztof Kołtowski<sup>2,3,A,B,E,F</sup>, Piotr Menartowicz<sup>3,A,B,F</sup>, Zygmunt Oleksik<sup>4,B,C,F</sup>, Dariusz Kotulski<sup>4,A–C,F</sup>, Tomasz Potaczek<sup>5,A–C,E,F</sup>, Martin Repko<sup>6,A,B,E,F</sup>, Milan Filipovič<sup>6,A,B,E,F</sup>, Anna Danielewicz<sup>7,A,C,E,F</sup>, Marek Fatyga<sup>7,A,B,E,F</sup>, Michał Latański<sup>7,A–F</sup>

<sup>1</sup> Department of Neurosurgery, University Hospital in Opole, Poland

<sup>2</sup> Department of Pediatric Surgery and Urology, Wrocław Medical University, Poland

<sup>3</sup> St. Hedwig of Silesia Hospital, Trzebnica, Poland

<sup>4</sup> Department of Orthopedics, University Children's Hospital of Kraków, Poland

<sup>5</sup> Department of Orthopedics and Rehabilitation, Jagiellonian University Medical College, Kraków, Poland

<sup>6</sup> Orthopedic Department of University Hospital Brno, Czech Republic

<sup>7</sup> Department of Pediatric Orthopedics, Medical University of Lublin, Poland

<sup>8</sup> Institute of Medicine, Opole University, Poland

A – research concept and design; B – collection and/or assembly of data; C – data analysis and interpretation; D – writing the article; E – critical revision of the article; F – final approval of the article

Advances in Clinical and Experimental Medicine, ISSN 1899–5276 (print), ISSN 2451–2680 (online)

*Adv Clin Exp Med.* 2019;28(8):1073–1077

## Address for correspondence

Grzegorz Mięksiak  
E-mail: gmiekisiak@gmail.com

## Funding sources

None declared

## Conflict of interest

None declared

## Acknowledgements

The authors would like to thank Ms. Ewelina Brunicka for her commitment in all stages of the study.

Received on October 2, 2018

Reviewed on October 16, 2018

Accepted on December 21, 2018

Published online on June 18, 2019

## Cite as

Mięksiak G, Kołtowski K, Menartowicz P, et al. The titanium-made growth-guidance technique for early-onset scoliosis at minimum 2-year follow-up: A prospective multicenter study. *Adv Clin Exp Med.* 2019;28(8):1073–1077. doi:10.17219/acem/102269

## DOI

10.17219/acem/102269

## Copyright

© 2019 by Wrocław Medical University

This is an article distributed under the terms of the Creative Commons Attribution Non-Commercial License (<http://creativecommons.org/licenses/by-nc-nd/4.0/>)

## Abstract

**Background.** The management of early-onset scoliosis (EOS) remains a serious challenge in pediatric orthopedics. The growth-guidance system (GGS) is a surgical option that allows continuous growth along a rod, averting the need for repeated operative lengthening.

**Objectives.** The objective of this study was to evaluate the outcomes of the GGS in the treatment of EOS.

**Material and methods.** A prospective study, including 81 patients from 4 departments treated with this method from 2013 to 2015, was conducted with a minimum follow-up period of 24 months. The follow-up data of 57 patients was available, thus the drop-out rate was 29.63%. There were 44 girls with a mean age of 10.03 years and 13 boys with a mean age of 8.04 years.

**Results.** The mean preoperative Cobb angle was 65.3° (range 36°–139°) was corrected to 23.7° (2°–94°), and at the end of the 2-year follow-up increased to 30.7° (8°–93°). The predominant proximal level of instrumentation was T5 and the distal was L1. The combined length of T1–T12 and T12–S1 increased on average by 33.19 mm in 24 months. The overall rate of serious complications was 43.86%. The most prevalent device-related complications were: the dislodgement of top screws because of the short length of the rod (14 cases), the implant failure (11 cases) and loss of correction (9 cases).

**Conclusions.** The results show that the GGS used in this study allows for a good and stable correction while preserving the ability of the spine to grow in at least a 2-year follow-up. The complication rate is acceptable and comparable with other growth-friendly techniques. To date, this is the largest successful study on the use of titanium-made GGSs.

**Key words:** early-onset scoliosis, scoliosis, spine, titanium

## Introduction

Early-onset scoliosis (EOS) is a very serious, potentially life-threatening clinical condition,<sup>1</sup> which develops in young children under the age of 10. Patients with progressive thoracic scoliosis tend to develop, as a part of natural history, restrictive lung disease and possibly cardiac disease associated with early mortality.<sup>1–3</sup>

Despite progress in the field of spinal disorders, managing EOS remains a serious challenge. The first line of treatment consisting of conservative methods, such as bracing and casting, is often unsuccessful and is often used to buy time for skeletal maturity.<sup>4</sup> Early attempts to utilize a classical fusion technique, according to the belief that a short and straight spine was superior to a long and deformed one, failed miserably.<sup>5</sup> Studies have reported that early fusion leads to pulmonary compromise and poor overall quality of life,<sup>6,7</sup> as it is crucial to allow for accommodation of developing lungs. Campbell et al.<sup>8</sup> defined the term “thoracic insufficiency syndrome” as the inability of the thorax to allow effective respiration and growth of lungs. One of the most appealing concepts of surgical treatment, besides distraction-based methods, is the growth-guidance system (GGs), which was first introduced as the Luque trolley,<sup>9</sup> and further improved into the Shilla method.<sup>10</sup> This technique uses stainless steel rods and specially modified locking nuts that allow for fairly unrestricted sliding motion. Early results have shown good results with an acceptable complication rate.<sup>11</sup> The system described in the present study is based on a similar principle, though it is made of titanium. The purpose of this study was to analyze the results and complications in a group of patients with a minimum 24-months follow-up.

## Material and methods

An approval No. DS240/2013 was obtained from the ethics committee of the Medical University of Lublin, Poland. In a prospective uncontrolled multicenter study, 81 EOS patients from 4 departments of 2 countries (Poland and Czech Republic) were enrolled. They underwent index surgery from 2013 to 2015. The 24-months follow-up data was available for 57 patients and they were included in this study. Thus, the overall follow-up rate was 70.37%. The demographics and basic characteristics are shown in Table 1. There were 44 girls and 13 boys; boys were significantly younger. The majority of the patients, 76.79%, belonged to Risser 0 grade; the difference between the sexes was not statistically significant. The median proximal end of deformity was T5 in both the sexes; the median distal end was L1 and T12 for females and males, respectively. The majority of the patients (76.09%) had single curve deformities, 80% in females and 63.64% in males; the difference between the sexes was statistically insignificant. Eighteen patients were syndromic. In all but 7 cases surgical treatment was preceded by unsuccessful conservative treatment (rehabilitation and bracing).

Table 1. Demographics and basic characteristics

Variables	Female	Male
Number of patients	44	13
Age at index surgery $\pm$ SD	10.03 $\pm$ 4.82*	8.04 $\pm$ 3.65*
Percentage of Risser 0 patients (the rest Risser 1)	81.82	61.54
Predominant proximal end level of scoliosis	T5	T5
Predominant distal end level of scoliosis	L1	T12
Percentage of patients with a single curve	80.00	63.64
Median number of instrumented levels (range)	12 (9–16)	11 (10–16)

\*p < 0.05; SD – standard deviation.

## Surgery

All the subjects underwent a 3-plane correction of scoliosis and instrumentation with Socore GGS (Novaspine, Salouël, France) pedicle screws. The spine was exposed in a standard subperiosteal fashion near the apex. In the apical zone, the rods were tightly fixed to screws using classical locking caps. A fusion-promoting environment was created to allow for 2–3 level spondylodesis. The goal was to make the apical level as neutral as possible. The transverse connector was used on a case-by-case basis. At both ends of the instrumentation, extraperiosteal dissection was used along with specially designed locking caps that enabled relatively unconstrained sliding movement of the rod inside the screw head (Fig. 1). The purpose was to convert the grow-friendly stabilization into rigid spondylodesis after some 2–3 years at the surgeon's discretion, when sufficient vertebral column growth has been achieved.

The patients did not use external stabilization such as bracing and/or casting. Radiographic analysis was

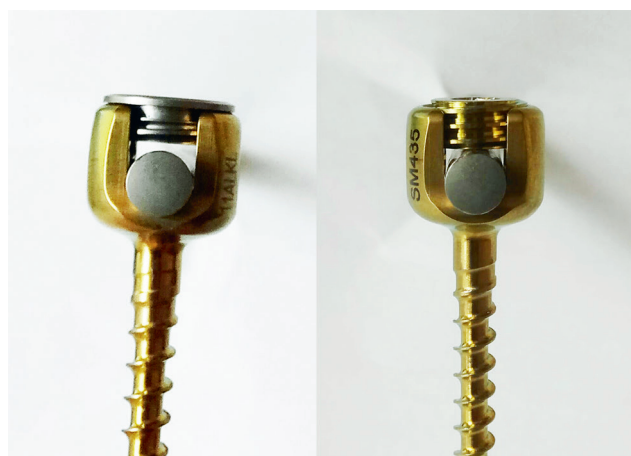


Fig. 1. Comparison of the sliding GGS screw cap (left) and a traditional locking cap (right)

**Table 2.** Device-related complications according to the classification system by Smith et al.<sup>14</sup>

Grade	Description	Number of cases
I	Does not require unplanned surgery	32
II	Requires unplanned surgery/surgeries	17
III	Requires abandoning growth-friendly strategy	8
IV	Death	0
Total		57

performed with taking standard standing X-rays just before and soon after the surgery, and at the follow-up. Besides the Cobb angle, the apical vertebral rotation (AVR) was evaluated using the Nash and Moe method,<sup>12</sup> which classifies the degree of rotation into one of the 5 groups (0–IV). The differences in mean values of Cobb angle were compared using the paired Student’s t-test, while median values of AVR were evaluated using the Wilcoxon test.

The changes in the lengths from the point located right between the pedicles of the T1 and T12 vertebrae as well as between T12 and S1 were calculated and evaluated using the paired Student’s t-test. The implant-related complications were categorized according to the classification system described by Smith et al.,<sup>13</sup> which is shown in Table 2.

## Results

As shown in Fig. 2, the average angle of the major curve was 65.3° ±17.6° before surgical treatment, 23.7° ±15.77° immediately after surgery and 30.7° ±17.56° after 24 months of surgery. The changes in measurement were statistically significant at p < 0.01. The T1–T12 and T12–S1 lengths increased at each time point: they measured 197.7 ±27.33 mm and 136.93 ±21.14 mm before the surgery, 218.7 ±27.39 mm and 149.53 ±21.74 mm immediately after surgery, and

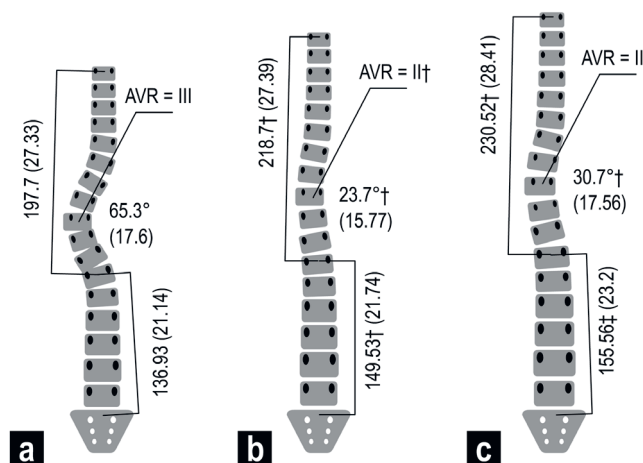


**Fig. 2.** Schematic diagram of the parameters before (a), soon after (b) and 2 years after (c) surgery

\* p < 0.0001; † p < 0.01, SD – standard deviation (in parentheses).

230.52 ±28.41 mm and 155.56 ±23.2 mm 24 months after surgery, respectively. The differences were statistically significant at p < 0.0001.

The mean total length, measured by adding up both the lengths, was 325.11 ±61.62 mm before the surgery and increased by 26.38 mm on average after the surgery (351 ±73.03 mm). In the 2-year follow-up, it increased by further 33.19 mm to 384.66 ±42.03 mm. The differences were statistically significant (p < 0.0001) at every time point of measurement. The AVR decreased after the surgery from grade III to II (p < 0.01). This value was maintained at the 24-month follow-up.

The dropout rate from the study was also analyzed. The mean age and the mean values for the largest Cobb angle of the study participants and drop-outs were 9.65 and 8.38 years, and 66.37° and 60.43°, respectively. Both the differences were statistically insignificant.

A total of 57 device-related complications occurred (Table 2). The majority of the complications were minor, not requiring unplanned surgery. In 17 cases, unplanned surgeries were required, and in 8 cases, the growth-friendly technique had to be abandoned. Thus, the rate of serious complications was 43.86%. The most prevalent device-related complication was associated with the length of the rod, which was too short, leading to the dislodgement of top screws (14 cases), followed by implant failure in 11 cases and loss of correction in 9 cases. All the complications are summarized in Table 3.

**Table 3.** Details of complications

Description	Number of cases
Rod too short	14
Implant failure/fracture	11
Loss of correction	10
Implant migration	9
Infection	3
Other	10
Total	57

## Discussion

Early-onset scoliosis is one of the most challenging problems in the field of spine surgery as the reasons are multi-faceted. The curves are often big and stiff; the patients frequently suffer from significant comorbidities, are underweight with poorly developed subcutaneous tissue, and are often osteopenic.<sup>14</sup> Early trials with definite, single-stage fusion techniques failed, and the only reliable measure was repeated surgery.<sup>14</sup> An obvious solution, considering the pathomechanism of EOS, would be to create a growth-friendly non-fusion method.<sup>5,15</sup>

Over the years, several different approaches have been attempted. Skaggs et al.<sup>16</sup> divided the non-fusion surgical

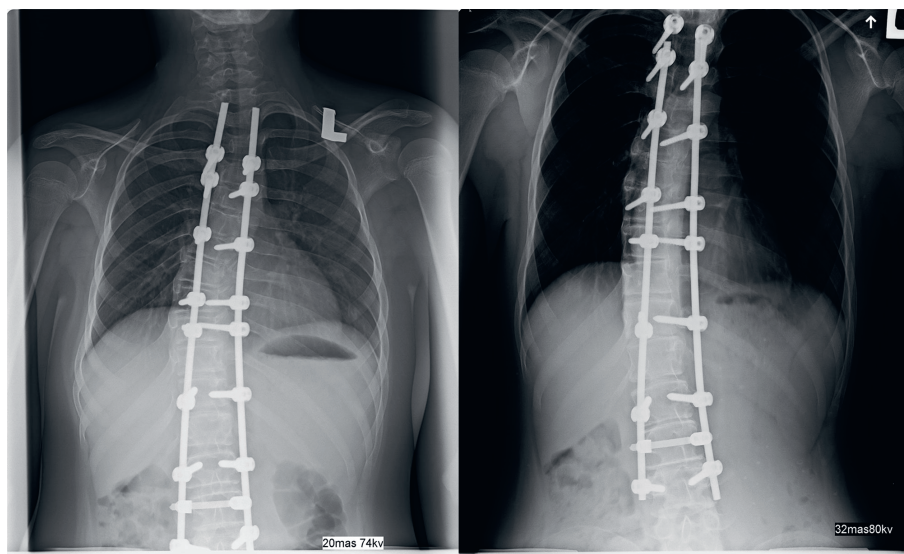


Fig. 3. The rod was too short for growth which occurred in 2 years after the index surgery (left to right)

techniques used in EOS into 3 groups: distraction-based systems, compression-based systems and GGSs. The latter is built around the idea of directing the growth of spine along rigid rods. The first GGS was the Luque trolley, introduced in 1977.<sup>17</sup> The trolley comprised multiple sublaminar wires placed along rigid rods. The driving force was the spine itself, as it maintained its growth potential, despite the deformity. The results were generally unfavorable,<sup>15,18</sup> and the main problem was premature fusion secondary to heterotopic ossification caused by periosteal stripping.<sup>11</sup> As a result, the technique fell into disuse.

The Shilla system was introduced by McCarthy et al.<sup>19</sup> It represents a major improvement over the trolley principle. The biggest advantage was the use of pedicle screws, instead of laminar wires, which allowed 3D manipulation of the curve. Furthermore, in theory, the lack of subperiosteal dissection for the placement of guide screws should limit the risk of premature fusion. Initial results were promising, and the authors were able to demonstrate the satisfactory growth of the trunk as well as good deformity correction, which was maintained after 2 years.<sup>11</sup>

The system described in the present study operates on the same principle as Shilla, the main difference being that titanium was used instead of stainless steel. This is particularly important in the case of sliding constructs as one of the major reported problems is metallosis,<sup>20</sup> a deposition of metallic debris in the vicinity of the sliding rod. Although the significance of this phenomenon is yet to be studied, it has been associated with several side effects, such as implant failure, loosening and local tissue necrosis.<sup>21</sup> Titanium metallosis is less studied, yet its toxicity requires extremely high circulating concentrations of the elements which are unlikely to occur from the degradation of an implant.<sup>22</sup> In the present study, the deposition of metal debris was apparent in each and every re-operation (including final fusion) case. The significance of this phenomenon in the setting of GGS is yet to be evaluated.<sup>11</sup>

The first publication on the use of Socore GGS used in present study was published by Latalski et al. in 2013.<sup>23</sup> In the present study, we were able to demonstrate good correction in the coronal plane, with only modest loss, over the period studied. In the present study, the loss of correction was near 7°, similar to the study using the Shilla system.<sup>11</sup> Ample derotation has been observed after initial surgery as AVR decreased from III to II, which was maintained over the 24-month period. To our knowledge, this is the first time this value has been reported for the guided growth technique.

The overall growth of T1–T12 + T12–S1 was 33.19 mm. This value is within the same ballpark as the data from studies on the growth of a normal spine, where the annual increase is roughly 1 cm and 1.8 cm/year between age of 5 and 10, and age of 10 and skeletal maturity, respectively.<sup>24</sup> As the majority of children in this study were around 10 years of age, the growth of the vertebral column seems almost unrestricted. Similar results were reported for magnetic MAGEC rods, with a comparable increase in the spinal growth; T1–S1 6 mm/year in primary, and 12 mm/year in revision cases.<sup>25</sup> In a similar article to this on Shilla system by McCarthy et al.,<sup>11</sup> instead of changes in absolute length, the relative growth of 13% was reported. It must be noted that in our case, instead of direct T1–S1 length, we used a combined length of T1–T12 and T12–S1; however, with the mean Cobb angle of 30.7°, this difference becomes irrelevant.

Our complication rate of 43.86% seems high for general standards of spinal surgery, but the EOS surgery is inevitably associated with high complication rates, even as high as 84%, particularly in syndromic children.<sup>26</sup> In a study comparing growth using magnetic rods and conventional rods, the overall complication rate was 76%.<sup>27</sup> On the other hand, 17 unplanned surgeries are far more acceptable than repeated lengthening surgeries required every 6 months. The most prevalent complication, i.e., the dislodgement of screws of rods that are too short, is a serious drawback

(Fig. 3). The length of the rod is decided by the surgeon during surgery; too long rods may cause extensive skin and subcutaneous tissue irritation on the top of the construct, and damage to facet joints at the bottom.


This study has certain limitations. Long-term follow-ups until skeletal maturity is required. Although we assumed that all patients require a definite fusion by means of replacing the locking caps and spondylodesis, it is yet to be determined if this step is required in each case. Our study lacks data on the sagittal profile, in particular, on the upper T-spine kyphosis and proximal junctional kyphosis. Last but not the least, the presence of metallosis is yet to be studied.


## Conclusions

To our knowledge, this is the largest study with a titanium-based GGS, and the interim results are encouraging. We were able to demonstrate good growth while maintaining the proper level of correction. Despite the limitations, we hope this study would contribute to the management of EOS, as not much work has been done using the modern GGSs.

### ORCID iDs

Grzegorz Miękiśiak  <https://orcid.org/0000-0001-6781-7013>

Tomasz Potaczek  <https://orcid.org/0000-0001-9019-8644>

Michał Latałski  <https://orcid.org/0000-0002-7919-0294>

### References

- Pehrsson K, Larsson S, Oden A, Nachemson A. Long-term follow-up of patients with untreated scoliosis: A study of mortality, causes of death, and symptoms. *Spine (Phila Pa 1976)*. 1992;17(9):1091–1096.
- Goldberg CJ, Gillic I, Connaughton O, et al. Respiratory function and cosmesis at maturity in infantile-onset scoliosis. *Spine (Phila Pa 1976)*. 2003;28(20):2397–2406.
- Fernandes P, Weinstein SL. Natural history of early onset scoliosis. *J Bone Joint Surg Am*. 2007;89(Suppl 1):21–33.
- Hasler CC. Early-onset scoliosis: Contemporary decision-making and treatment options. *J Pediatr Orthop*. 2018;38(Suppl 1):S13–S20.
- Tis JE, Karlin LI, Akbarnia BA, et al; Growing Spine Committee of the Scoliosis Research Society. Early onset scoliosis. *J Pediatr Orthop*. 2012;32(7):647–657.
- Vitale MG, Matsumoto H, Bye MR, et al. A retrospective cohort study of pulmonary function, radiographic measures, and quality of life in children with congenital scoliosis: An evaluation of patient outcomes after early spinal fusion. *Spine (Phila Pa 1976)*. 2008;33(11):1242–1249.
- Karol LA, Johnston C, Mladenov K, Schochet P, Walters P, Browne RH. Pulmonary function following early thoracic fusion in non-neuromuscular scoliosis. *J Bone Joint Surg Am*. 2008;90(6):1272–1281.
- Campbell RM, Smith MD, Mayes TC, et al. The characteristics of thoracic insufficiency syndrome associated with fused ribs and congenital scoliosis. *J Bone Joint Surg Am*. 2003;85-A(3):399–408.
- Luque ER. Paralytic scoliosis in growing children. *Clin Orthop Relat Res*. 1982;(163):202–209.
- McCarthy RE, Sucato D, Turner JL, Zhang H, Henson MAW, McCarthy K. Shilla Growing rods in a caprine animal model: A pilot study. *Clin Orthop Relat Res*. 2010;468(3):705–710.
- McCarthy RE, Luhmann S, Lenke L, McCullough FL. The Shilla growth guidance technique for early-onset spinal deformities at 2-year follow-up. *J Pediatr Orthop*. 2014;34(1):1–7.
- Nash CL, Moe JH. A study of vertebral rotation. *J Bone Joint Surg Am*. 1969;51(2):223–229.
- Smith JT, Johnston C, Skaggs D, Flynn J, Vitale M. A new classification system to report complications in growing spine surgery: A multi-center consensus study. *J Pediatr Orthop*. 2015;35(8):798–803.
- Fletcher ND, Bruce RW. Early onset scoliosis: Current concepts and controversies. *Curr Rev Musculoskelet Med*. 2012;5(2):102–110.
- Mardjetko SM, Hammerberg KW, Lubicky JP, Fister JS. The Luque trolley revisited. Review of nine cases requiring revision. *Spine (Phila Pa 1976)*. 1992;17(5):582–589.
- Skaggs DL, Akbarnia BA, Flynn JM, Myung KS, Sponseller PD, Vitale MG; Chest Wall and Spine Deformity Study Group; Growing Spine Study Group; Pediatric Orthopaedic Society of North America; Scoliosis Research Society Growing Spine Study Committee. A classification of growth friendly spine implants. *J Pediatr Orthop*. 2014;34(3):260–274.
- Luque E, Cardoso A. Treatment of scoliosis without arthrodesis or external support: Preliminary report. *Orthop Trans*. 1977;119:276.
- Pratt RK, Webb JK, Burwell RG, Cummings SL. Luque trolley and convex epiphysiodesis in the management of infantile and juvenile idiopathic scoliosis. *Spine (Phila Pa 1976)*. 1999;24(15):1538–1547.
- McCarthy RE, McCullough F, Luhmann SJ LL. *Greater than two years follow-up Shilla growth enhancing system for the treatment of scoliosis in children*. In: 2<sup>nd</sup> Annual International Conference on Early Onset Scoliosis (ICEOS). Montreal, Canada; 2008.
- Yang JH, Ham CH, Hwang YG, Suh SW. Metallosis: A complication in the guided growing rod system used in treatment of scoliosis. *Indian J Orthop*. 2017;51(6):714–718.
- Neumann DRP, Thaler C, Hitzl W, Huber M, Hofstädter T, Dorn U. Long-term results of a contemporary metal-on-metal total hip arthroplasty: A 10-year follow-up study. *J Arthroplasty*. 2010;25(5):700–708.
- Merritt K, Rodrigo JJ. Immune response to synthetic materials. Sensitization of patients receiving orthopaedic implants. *Clin Orthop Relat Res*. 1996;(326):71–79.
- Latałski M, Fatyga M, Kołtowski K, Menartowicz P, Repko M, Filipović M. Guided-growth implants in the treatment of early onset scoliosis. A pilot study. *Ortop Traumatol Rehabil*. 2013;15(1):23–29.
- Dimeglia A, Canavese F. The growing spine: How spinal deformities influence normal spine and thoracic cage growth. *Eur Spine J*. 2012;21(1):64–70.
- Hickey BA, Towriss C, Baxter G, et al. Early experience of MAGEC magnetic growing rods in the treatment of early onset scoliosis. *Eur Spine J*. 2014;23(Suppl 1):S61–65.
- Phillips JH, Knapp DR, Herrera-Soto J. Mortality and morbidity in early-onset scoliosis surgery. *Spine (Phila Pa 1976)*. 2013;38(4):324–327.
- Teoh KH, Winson DMG, James SH, et al. Do magnetic growing rods have lower complication rates compared with conventional growing rods? *Spine J*. 2016;16(Suppl 4):S40–S44.





# Transcatheter closure of atrial septal communication: Impact on quality of life in mid-term follow-up

Maria Lelakowska<sup>1,A–D</sup>, Paweł Tomasz Matusik<sup>2,C–E</sup>, Piotr Stanisław Podolec<sup>3,F</sup>, Maria Olszowska<sup>3,E</sup>,  
Jadwiga Maria Nessler<sup>1,E</sup>, Natalia Podolec<sup>4,B</sup>, Tadeusz Przewłocki<sup>3,B</sup>, Monika Komar<sup>3,A,B</sup>

<sup>1</sup> Department of Coronary Disease and Heart Failure, John Paul II Hospital, Kraków, Poland

<sup>2</sup> Department of Electrocardiology, Institute of Cardiology, Jagiellonian University Medical College, John Paul II Hospital, Kraków, Poland

<sup>3</sup> Department of Cardiac and Vascular Diseases, Institute of Cardiology, Jagiellonian University Medical College, John Paul II Hospital, Kraków, Poland

<sup>4</sup> Faculty of Medicine, Jagiellonian University Medical College, Kraków, Poland

A – research concept and design; B – collection and/or assembly of data; C – data analysis and interpretation;

D – writing the article; E – critical revision of the article; F – final approval of the article

Advances in Clinical and Experimental Medicine, ISSN 1899–5276 (print), ISSN 2451–2680 (online)

*Adv Clin Exp Med.* 2019;28(8):1079–1085

## Address for correspondence

Monika Komar  
E-mail: monniik@interia.pl

## Funding sources

None declared

## Conflict of interest

None declared

Received on July 26, 2018

Reviewed on November 25, 2018

Accepted on December 30, 2018

Published online on June 18, 2019

## Abstract

**Background.** Atrial septal defect (ASD) and patent foramen ovale (PFO) are specific types of atrial septal communications (ASC).

**Objectives.** We aimed to assess quality of life (QoL) in patients before and after percutaneous closure of ASC and determine the factors influencing QoL in this group of patients.

**Material and methods.** We performed a clinical assessment and conducted an SF-36 questionnaire, electrocardiography and echocardiography studies in patients before and 6 months after percutaneous ASC closure.

**Results.** Patients with ASD ( $n = 56$ ) had a lower SF-36 total score than those with PFO ( $n = 73$ ), before and after percutaneous ASC occlusion (both  $p < 0.001$ ). After the procedure, the improvement of SF-36 total score in patients with ASD or atrial fibrillation was greater ( $p < 0.001$  and  $p = 0.005$ , respectively). We observed correlations between improvement of QoL and baseline supraventricular extrasystolic beats ( $r_s = 0.28$ ;  $p = 0.002$ ), but not ventricular extrasystolic beats ( $r_s = 0.03$ ;  $p = 0.76$ ). Quality of life improvement was predicted in patients with ASD by higher baseline tricuspid annular plane systolic excursion (TAPSE) and right ventricular longitudinal dimension  $R^2 = 0.38$ ;  $p < 0.001$ . However, in patients with PFO, this was predicted by TAPSE, lack of arterial hypertension and usage of angiotensin-converting enzyme inhibitors,  $R^2 = 0.30$ ;  $p < 0.001$ .

**Conclusions.** Patients with ASD have lower QoL than those with PFO before and after percutaneous ASC occlusion. Six months after the procedure, the improvement of QoL in patients with ASD was higher than in those with PFO. The change in QoL self-assessed by patients after the procedure was associated with episodes of arrhythmia and was predicted with echocardiographic and clinical parameters.

**Key words:** quality of life, patent foramen ovale, atrial septal defect, transcatheter closure

## Cite as

Lelakowska M, Matusik PT, Podolec PS, et al. Transcatheter closure of atrial septal communication: Impact on quality of life in mid-term follow-up. *Adv Clin Exp Med.* 2019;28(8):1079–1085. doi:10.17219/acem/102440

## DOI

10.17219/acem/102440

## Copyright

© 2019 by Wrocław Medical University

This is an article distributed under the terms of the Creative Commons Attribution Non-Commercial License (<http://creativecommons.org/licenses/by-nc-nd/4.0/>)

## Introduction

Atrial septal communications (ASC) include ostium secundum atrial septal defect (ASD) and patent foramen ovale (PFO). The ASD is one of the most common congenital heart defects, while PFO is an anatomical variant. Those with ASD and PFO are considered as 2 different patient populations. The PFO is the most prevalent ASC and is diagnosed in about 26% (17–35%) of the population. A right-to-left shunt through PFO usually occurs during a temporary or permanent increase in right atrial pressure. On the other hand, PFO with concomitant valvular regurgitation and/or stenosis may be associated with left-to-right shunt. The PFO may lead to paradoxical embolism, usually in circulation related to the central nervous system.<sup>1–3</sup> The ASD comprises about 10% of all congenital heart defects diagnosed after birth.<sup>4–8</sup> According to European Society of Cardiology guidelines, ASD with a hemodynamically significant shunt (signs of right ventricular volume overload) and pulmonary vascular resistance <5 Wood units should be closed. Moreover, closure of ASD and PFO should be considered in cases of previous paradoxical systemic embolism.<sup>1,4</sup>

The importance of a quality of life (QoL) assessment in patients undergoing various types of medical interventions became apparent in the 1970s. With the advancement of medicine, therapeutic goals are not only set to remove the disease, which in many cases is not possible, but also to improve patient's functioning in society, fulfillment of social roles and restoration of well-being.<sup>9–12</sup>

The aim of the study was to assess QoL in patients before and after percutaneous closure of ASC (ASD and PFO) and to determine the factors influencing QoL in this group of patients.

## Material and methods

### Patients

The methodology of the study has been previously described in detail.<sup>13</sup> Briefly, we included consecutive patients with ASD or PFO.

Inclusion criteria:

1) Presence of ASD or PFO planned for percutaneous closure.

2) Consent to undergo transthoracic echocardiography (TTE), transesophageal echocardiography (TEE), 24-hour Holter electrocardiogram (ECG) monitoring and percutaneous ASC closure, and to perform a clinical assessment including the SF-36 questionnaire, before and 6 months after the procedure.

Exclusion criteria:

1) Chronic atrial fibrillation (AF).  
2) Patients after cardiac surgery, AF ablation or cardiovascular implantable electronic device placement.

3) The presence of significant valvular heart disease and/or other congenital cardiovascular defects and/or cardiomyopathy.

4) Left ventricular ejection fraction (LVEF) below 50% or dementia.

5) The presence of a significant leak around the implanted septal occluder.

6) Sub-optimal imaging on echocardiography and poorly visible P-waves in ECG (non-echogenicity and poor ECG recording quality).

7) Incomplete SF-36 questionnaire.

We excluded patients with chronic AF and poorly visible P-waves because P-wave dispersion analysis was performed as a part of our study.<sup>13</sup> From our study, we excluded 3 patients with chronic AF, 1 patient who did not complete the SF-36 questionnaire and 3 patients who did not return it. Furthermore, 1 patient was excluded due to a significant leak around the implanted occluder.

Clinical history assessment and physical examination (including assessment of cardiovascular complaints and comorbidities) were performed before percutaneous closure of the ASD and PFO and 6 months after the procedure.

### TTE, TEE and 24-hour Holter ECG monitoring

Transthoracic and transesophageal echocardiography studies were performed according to recommendations from international guidelines.<sup>13–19</sup> using the Toshiba Power Vision system (Toshiba, Tokyo, Japan) and an ultrasound probe with a frequency from 2.5 MHz to 3.5 MHz. M-mode imaging, 2-dimensional (2D) imaging, pulse-wave Doppler, continuous wave Doppler, and color flow Doppler imaging were used. Two-dimensional imaging was used to assess the location and size of the ASC from standard views: parasternal cross-sectional view at the level of large vessels, apical 4-chamber, apical 5-chamber, and subcostal views. The morphology of the atrial septum was assessed during TEE in the bicaval view and high longitudinal view.<sup>16,17</sup> Basic parameters of cardiac chamber quantification and valvular functions were assessed. Moreover, right ventricular pressure and pulmonary to systemic blood flow ratio (Qp/Qs) were calculated. Assessment of the Holter ECG monitoring results was performed as previously described.<sup>13</sup>

### Quality of life assessment

Assessment of QoL was based on a self-assessment of patients using a 36-item SF-36 questionnaire. The SF-36 questionnaire used in our study was composed of 11 points including 36 questions, which consisted of 8 subscales for the assessment of: SF1 – physical functioning (PF); SF2 – limitations due to physical health, role-physical (RP); SF3 – social functioning (SF); SF4 – bodily pain (BP); SF5 – mental health (MH); SF6 – role limitations due to emotional problems, role-emotional (RE); SF7 – vitality (VT);

SF8 – general health (GH). In the final assessment, QoL index was calculated (SF-36 total score). In the interpretation of results, higher scores in the self-assessment of patients indicated better QoL.<sup>9–12</sup>

Written consent was given by all patients to perform studies and procedures according to Polish/European Society of Cardiology (ESC) standards and to perform the QoL assessment. Approval for the study was provided by the Bioethics Committee of the Jagiellonian University Medical College.

## Statistical analysis

Quantitative variables were described with the mean  $\pm$  standard deviation (SD) and/or median and/or range and/or interquartile range (IQR). Qualitative variables were presented as number and/or frequency. Hypotheses about the normal distribution of the quantitative variables analyzed were verified using the Shapiro–Wilk test. Differences in quantitative variables between the 2 groups were tested with independent samples using the Student t-test or Mann–Whitney U test. An assessment of differences between qualitative variables was performed using the  $\chi^2$  test or Fisher’s exact test. An analysis of changes in quantitative variables, before and after procedure, was performed using the Wilcoxon matched-pairs test, while qualitative (dichotomous) variables were analyzed with McNemar’s test for repeated measures. Relations between SF-36 total score and its change and other variables were tested using Spearman’s rank test ( $r_s$ ). Selected variables associated with a change in SF-36 total score ( $p < 0.05$ ) in univariate statistical analysis, which did not substantially correlate (including correlation coefficient  $\geq 0.6$ ) with other independent variables, were included into a multiple linear regression analysis. The selection of variables which significantly influenced the dependent variable, was performed using stepwise backward regression.  $R^2$  was calculated and an assessment of model adequacy using the  $F_{k,n-k-1}$  test was performed, where “k” is the number of variables in a model and “n” is the number of patients in a group. Statistical analyses were performed with STATISTICA v. 12 software (StatSoft, Tulsa, USA).

## Results

### Baseline patient characteristics

The study group included 129 patients (70 female), with a mean age of  $44.5 \pm 13.4$  (19–76) years, scheduled for percutaneous closure of ASD ( $n = 56$ ) or PFO ( $n = 73$ ). Patients undergoing percutaneous closure of ASD were older and were predominantly female when compared to those undergoing closure of PFO (Table 1). There were 10 patients with PFO and a history of stroke, while there was no history of stroke in patients with ASD. None of the patients

included in the study had significant neurological deficits. When compared to patients with PFO, those with ASD more commonly suffered from episodes of palpitations (37.5% vs 10.9%), dyspnea (32.1% vs 9.6%), arterial hypertension (30.4% vs 4.1%), and pulmonary hypertension (33.9% vs 0%) before the procedure ( $p < 0.001$  for all comparisons between the 2 groups, Table 1). These ASD patients also more often used calcium channel blockers (CCB),  $\beta$ -blockers and angiotensin-converting enzyme inhibitors (ACE-I) when compared with the remainder of the patients in the study group. On the other hand, patients with PFO, when compared with ASD patients, more commonly experienced migraine episodes (Table 1). Ventricular extrasystolic and supraventricular extrasystolic beats were more prevalent in the ASD patients when compared to the remainder of patients (median (IQR): 2 (1–900) vs 1 (0–3) ventricular extrasystolic beats/day,  $p = 0.017$  and 178 (42–540) vs 8 (0–200) supraventricular extrasystolic beats/day,  $p < 0.001$ ). Detailed characteristics of the study group are shown in Table 1.

### Baseline QoL assessment

There were differences in almost all the SF-36 scores between patients with ASD and PFO (Table 1). In both groups of patients with ASC, age negatively correlated with SF-36 total score (Table 2). Moreover, SF-36 total score correlated inversely with New York Heart Association (NYHA) class and positively with LVEF in patients with ASD (Table 2). We observed correlations between SF-36 total score after PFO closure and radiation absorbed dose ( $r_s = 0.31$ ;  $p = 0.009$ ) and right ventricular longitudinal dimension ( $r_s = 0.25$ ;  $p = 0.041$ ). Additionally, a correlation was seen between SF-36 total score after ASD closure and mid-cavity right ventricular linear dimension ( $r_s = 0.29$ ;  $p = 0.034$ ). These correlations, however, were not seen in the other groups studied or before the procedure. Left ventricular diastolic dimension, left ventricular systolic dimension, proximal right ventricular outflow tract (RVOT prox), and basal right ventricular linear dimension did not correlate with SF-36 total score before or after ASC closure in patients with ASD or PFO considered separately. Quality of life, reflected by SF-36 total score, in patients with ASD was lower than in patients with PFO (Table 1). Patients with history of stroke had a tendency towards lower SF-36 total score than the remaining subjects (95.0 (87–108) vs 120 (88–132);  $p = 0.057$ ).

### Procedures performed

The septal occluders were successfully implanted in 124 patients. In 5 patients, the procedure was not performed (Table 1). The diameter of the implanted septal occluders ranged from 7 mm to 34 mm (median: 25; 25–28 mm). The ASC occlusion, as reflected by fluoroscopy time and radiation absorbed dose, appeared more

**Table 1.** Clinical characteristics of patients undergoing closure of atrial septal communication

Variable	ASD (n = 56)	PFO (n = 73)	p-value
Age, mean $\pm$ SD [years]	49.8 $\pm$ 13.3	40.5 $\pm$ 12.0	<0.001
Male sex, n (%)	12 (21.4)	47 (64.4)	<0.001
Comorbidities and CVD risk factors, n (%)			
Arterial hypertension	17 (30.4)	3 (4.1)	<0.001
Pulmonary hypertension	19 (33.9)	0 (0.0)	<0.001
Hyperlipidemia	15 (26.8)	7 (9.6)	0.010
Diabetes mellitus	4 (7.1)	1 (1.4)	0.166
Obesity	3 (5.4)	2 (2.7)	0.652
Smoking	14 (25.0)	9 (12.3)	0.062
Anemia	0 (0.0)	1 (1.4)	0.999
Migraine	0 (0.0)	11 (15.1)	0.002
Vasovagal syndrome	1 (1.8)	3 (4.1)	0.632
Stroke/TIA	4 (7.1)	24 (32.9)	<0.001
Atrial fibrillation	17 (30.4)	8 (11.0)	0.006
Quality of life assessed using SF-36 questionnaire, at baseline			
SF-36 total score	99 (68–129)	124 (96–132)	<0.001
Physical functioning	41 (29–46)	44 (41–48)	0.001
Limitations due to physical health	5 (0–10)	10 (5–20)	<0.001
Social functioning	5 (4–7)	6 (5–8)	0.005
Bodily pain	6 (4–9)	8 (6–9)	0.084
Mental health	15 (11–18)	17 (11–19)	0.348
Role limitations due to emotional problems	5 (0–15)	15 (5–15)	0.006
Vitality	11 (9–16)	13 (8–17)	0.159
General health	11 (9–15)	12 (10–15)	0.079
Echocardiographic parameters, n (%)			
Left-to-right shunt	54 (96.4)	41 (56.2)	<0.001
Interatrial septal aneurysm	11 (19.6)	50 (68.5)	<0.001
Enlarged LA	35 (62.5)	14 (19.2)	<0.001
Enlarged RA	37 (66.1)	14 (19.2)	<0.001
Enlarged right ventricle	33 (58.9)	16 (21.9)	<0.001
Myocardial hypertrophy	9 (16.1)	4 (5.5)	0.074
Device, n (%)			
Cardia Ultrasept ASD occluder	4 (7.1)	0 (0.0)	
Cardia Ultrasept PFO occluder	0 (0.0)	69 (94.5)	
Memopart ASD occluder	51 (91.1)	0 (0.0)	-
No implanted device	1 (1.8)	4 (5.5)	
Procedure, n (%)			
Without complications	55 (98.2)	69 (94.5)	
Stopped due to complications	0 (0.0)	1 (1.4)	NS
Unsuccessful	1 (1.8)	3 (4.1)	
Medications, n (%)			
CCB	18 (32.1)	1 (1.4)	<0.001
Beta-blocker	17 (30.4)	10 (13.7)	0.021
ACE-I	17 (30.4)	5 (6.8)	<0.001

ACE-I – angiotensin-converting enzyme inhibitor; ASD – atrial septal defect; CCB – calcium channel blocker; CVD – cardiovascular disease; LA – left atrium; N – number; NS – nonsignificant; PFO – patent foramen ovale; RA – right atrium; SD – standard deviation; SF-36 – 36-item SF-36 questionnaire; TIA – transient ischemic attack. Values are presented as mean  $\pm$ SD or median (interquartile range) or number and percentage.

difficult in patients with ASD when compared to patients with PFO (fluoroscopy time: 7.4 (4–15) vs 4 (3–6) min,  $p < 0.001$ ; radiation absorbed dose: 29 (18–113) vs 16 (10–36) mGy,  $p < 0.001$ ). In 1 (0.8%) case, a transient rhythm disorder was observed. There were no serious complications, no fractures of the device and no device embolizations. All patients remained well with no complications or new symptoms at the 6-month follow-up.

## Patient characteristics and quality of life after ASC closure

Six months after the procedure, reduction of episodic palpitations, dyspnea and AF, as well as an increase in NYHA class were observed, and in these terms ASD patients did not significantly differ from patients with PFO.

In addition, 6 months after the procedure, higher SF-36 total scores were noted in patients with ASD and PFO (Table 3). There were differences in almost all the SF-36 scores between patients with ASD and PFO, except for the SF, BP, MH, and vitality subscales (Table 4). In patients with ASD, significant improvement in the QoL parameters were noted, with the exception of the BP subscale ( $p = 0.675$ ). On the other hand, in patients with PFO after the procedure, a significant improvement in SF-36 QoL parameters was observed, except for the SF ( $p = 0.253$ ) and BP subscales ( $p = 0.166$ ). After percutaneous ASC occlusion, the mean improvement in QoL was higher in patients with ASD when compared to patients with PFO (Table 3). Increased change in SF-36 total score was associated with presence of arterial hypertension ( $p = 0.013$ ), episodes of dyspnea ( $p = 0.034$ ), palpitations ( $p = 0.048$ ), and use of CCB ( $p = 0.001$ ),  $\beta$ -blockers ( $p = 0.040$ ) and ACE-I ( $p = 0.003$ ), presence of interatrial septal aneurysm ( $p = 0.016$ ), and myocardial hypertrophy ( $p = 0.018$ ) before the procedure. Importantly, patients with AF had a higher improvement in SF-36 total score (14 (7–22) vs 6 (1–16);  $p = 0.005$ ). Those with AF episode reduction, when compared to the remainder, were also characterized by a higher change in SF-36 total score (16 (7–32) vs 7 (1–18);  $p = 0.03$ ). We also observed correlations between an increase in change of the SF-36 total score (difference between 6 months after ASC occlusion and baseline) and baseline supraventricular extrasystolic beats (SVEB;  $r_s = 0.28$ ;  $p = 0.002$ ). However, correlations were not observed between increase in the change of SF-36 total score and ventricular extrasystolic beats (VEB;  $r_s = 0.03$ ;  $p = 0.76$ ). Patients with ASD had a higher improvement in SF-36 total score (14 (6–26) vs 5 (1–13);  $p = 0.003$ ). Importantly, increase in the change of SF-36 total score correlated with baseline RVOT prox ( $r_s = 0.20$ ;  $p = 0.03$ ), basal right ventricular linear dimension (RVD1) ( $r_s = 0.31$ ;  $p < 0.001$ ), mid-cavity right ventricular linear dimension

**Table 2.** Spearman's correlations ( $r_s$ ) between quantitative variables and SF-36 total score at baseline and after closure of atrial septal communication

Variable	SF-36 total score before ASC closure $r_s$ (p-value)			SF-36 total score after ASC closure $r_s$ (p-value)		
	ASC	ASD	PFO	ASC	ASD	PFO
Age [years]	-0.34 (<0.001)	-0.28 (0.038)	-0.32 (0.005)	-0.32 (<0.001)	-0.34 (0.010)	-0.28 (0.022)
NYHA class	-0.31 (<0.001)	-0.29 (0.030)	-0.19 (0.113)	-0.32 (<0.001)	-0.37 (0.006)	-0.13 (0.302)
Echocardiography						
LVEF [%]	0.22 (0.014)	0.59 (<0.001)	-0.01 (0.944)	0.37 (<0.001)	0.71 (<0.001)	0.21 (0.090)
TAPSE [mm]	-0.29 (0.001)	-0.38 (0.004)	-0.10 (0.342)	-0.04 (0.662)	-0.18 (0.189)	0.21 (0.077)
LA area [cm <sup>2</sup> ]	-0.20 (0.025)	-0.29 (0.029)	0.09 (0.426)	-0.13 (0.165)	-0.26 (0.053)	0.17 (0.168)
RA area [cm <sup>2</sup> ]	-0.21 (0.016)	-0.29 (0.030)	0.04 (0.752)	-0.10 (0.257)	-0.19 (0.173)	0.13 (0.296)
Qp/Qs ratio	-0.33 (<0.001)	-0.23 (0.094)	*	-0.34 (<0.001)	-0.19 (0.161)	*
Procedure						
Fluoroscopy time [min]	-0.31 (<0.001)	-0.31 (0.022)	-0.04 (0.711)	-0.30 (0.001)	-0.35 (0.009)	0.10 (0.402)

ASD – atrial septal defect; ASC – atrial septal communication; LVEF – left ventricular ejection fraction; NYHA – New York Heart Association; PFO – patent foramen ovale; RA – right atrium; TAPSE – tricuspid annular plane systolic excursion; LA – left atrium; Qp/Qs ratio – pulmonary to systemic blood flow ratio; SF-36 – 36-item SF-36 questionnaire. \*Qp/Qs ratio = 1 in all patients.

**Table 3.** Changes in SF-36 total score before and 6 months after successful closure of atrial septal communication

Variable	SF-36 total score					
	ASC before (n = 124)	ASC 6-m FU	ASD before (n = 55)	ASD 6-m FU	PFO before (n = 69)	PFO 6-m FU
Median	111	121	98	117	120	131
Interquartile range	87.5–131.0	102.5–139.0	56–129	82–136	96–132	121–140
p-value	<0.001*		<0.001*		<0.001*	

6-m FU – 6-month follow-up; ASD – atrial septal defect; ASC – atrial septal communication; PFO – patent foramen ovale; SF-36 – 36-item SF-36 questionnaire. Values are presented as median (interquartile range). \*p-value for comparison of patients before and after the procedure.

(RVD2) ( $r_s = 0.35$ ;  $p < 0.001$ ), longitudinal right ventricular dimension (RVD3) ( $r_s = 0.38$ ;  $p < 0.001$ ), and TAPSE ( $r_s = 0.42$ ;  $p < 0.001$ ), but not LVEF ( $r_s = -0.005$ ;  $p = 0.95$ ). Additionally, correlations between increase in the change of SF-36 total score and baseline left and right atrial area

were observed ( $r_s = 0.21$ ;  $p = 0.02$  and  $r_s = 0.30$ ;  $p < 0.001$ , respectively). We also observed correlations between increase in the change of SF-36 total score and decrease in SVEB ( $r_s = 0.19$ ;  $p = 0.04$ ), but not VEB ( $r_s = -0.05$ ;  $p = 0.55$ ).

**Table 4.** Comparison of quality of life assessed with SF-36 between patients after atrial septal communication occlusion (ASD, PFO)

Variable	ASD* (n = 55)	PFO* (n = 69)	p-value
SF-36 total score	117 (82–136)	131 (121–140)	<0.001
Physical functioning	40 (31–44)	48 (44–48)	<0.001
Limitations due to physical health	10 (0–15)	15 (8–20)	0.005
Social functioning	6 (5–8)	6 (5–8)	0.844
Bodily pain	8 (5–8)	8 (6–9)	0.215
Mental health	17 (12–21)	17 (12–21)	0.957
Role limitations due to emotional problems	15 (5–15)	15 (15–15)	0.009
Vitality	13 (9–16)	16 (9–17)	0.092
General health	13 (9–15)	14 (12–17)	0.011

ASD – atrial septal defect; PFO – patent foramen ovale; SF-36 – a 36-item SF-36 questionnaire. Values are presented as median (interquartile range). \*In 5 patients the procedure was not performed (in 4 patients with PFO and in 1 patient with ASD).

Change in SF-36 total score in patients with ASD was predicted by TAPSE and RVD3, while in patients with PFO this was predicted by TAPSE, lack of arterial hypertension and ACE-I use (Table 5).

## Discussion

In patients with ASD, the most commonly reported symptoms are exertional dyspnea, limitation of physical condition and paroxysmal palpitations. Among the causes of gradual deterioration of clinical status of patients with ASD are age-dependent decline in left ventricular diastolic compliance, which increases left-to-right shunt, the development of pulmonary hypertension, and the appearance of AF (30.4% of our patients with ASD), which often initiates right ventricular heart failure.<sup>3</sup> On the other hand, the presence of PFO is associated with an increased risk of crossed (paradoxical) embolism, which may cause a cryptogenic stroke.<sup>1,2</sup> In our study, stroke/TIA occurred in 32.9% of patients with PFO.

**Table 5.** Multiple regression analysis of predictors of change in SF-36 total score (difference between 6 months after atrial septal communication occlusion and baseline), which reflects general increase in SF-36 total score

Multiple regression analysis	Variables	Standardized coefficients $\beta$	Unstandardized coefficients B	95% CI for B		p-value
				lower	upper	
ASC ( $R^2 = 0.35$ ; $F_{4,119} = 15.99$ ; $p < 0.001$ )	TAPSE [mm]	0.40	3.14	1.93	4.35	<0.001
	RVD3 [mm]	0.26	0.63	0.26	1.00	0.001
	arterial hypertension	-0.38	-10.18	-20.00	-0.38	0.042
	ACE-I	0.42	10.54	1.28	19.79	0.026
ASD ( $R^2 = 0.38$ ; $F_{2,52} = 15.8$ ; $p < 0.001$ )	TAPSE [mm]	0.38	2.76	1.04	4.48	0.002
	RVD3 [mm]	0.36	1.05	0.37	1.73	0.003
PFO ( $R^2 = 0.30$ ; $F_{3,65} = 9.48$ ; $p < 0.001$ )	TAPSE [mm]	0.38	3.41	1.51	5.30	0.001
	arterial hypertension	-0.34	-16.38	-28.12	-3.64	0.013
	ACE-I	0.44	13.90	5.59	22.2	0.001

95% CI – 95% confidence interval; ACE-I – angiotensin-converting enzyme inhibitor; ASD – atrial septal defect; NS – not significant; PFO – patent foramen ovale; SF-36 – 36-item SF-36 questionnaire; RVD3 – longitudinal right ventricular dimension; TAPSE – tricuspid annular plane systolic excursion.

The results of percutaneous ASC closure are very promising,<sup>13</sup> but the procedure is not free of potential complications.<sup>20–22</sup> Percutaneous occlusion does not lead to postoperative scarring on the chest, which is a significant advantage from the patient's perspective. This may have a major impact on the QoL, especially that of young women.<sup>11</sup> The assessment of health status after correction of the ASC is based primarily on the results of echocardiographic, radiological and laboratory studies.<sup>7</sup> However, they do not always reflect a satisfactory level of QoL. In this study, it was shown that the QoL between patients before percutaneous occlusion of ASD and PFO differs. Special attention is drawn to a subjectively low grade in the assessment of RP (limitations in performing roles and/or in work ability), SF (social life, meetings with family) and RE (anxiety, bad mood, lack of work) subscales, but not the MH (nervousness, depression, unhappiness, and sadness) and VT (willingness to live, tiredness, lack of energy) subscales. On the other hand, in the self-assessment reflecting GH, a trend towards lower QoL was observed in patients with ASD. After ASC occlusion, QoL in all subscales improved, except for sense of pain. Deterioration of patient functioning (performing roles) due to physical health (limitation in work ability) at the 6-month follow-up after ASD occlusion may result from restrictions recommended by doctors and suggestions by the patient's family members before the procedure. Such situations are very common and unfortunately are also transferred to the post-procedural period.<sup>11,12</sup> Asymptomatic patients or those with mild symptoms (a majority of patients with PFO) may not experience such a significant improvement after the procedure when compared to patients with ASD, in whom effective occlusion of the defect is associated with resolution of significant ailments. Quality of life between patients with ASD and PFO before the procedure did not differ in the subscales of BP, MH, VT, and GH. The existence of comorbidities, such as arterial hypertension, episodes of AE, dyspnea and palpitations, as well as the use

of medications (CCB,  $\beta$ -blockers, and ACE-I), influences QoL. Significant associations of change in SF-36 total score with a reduction of the abovementioned symptoms after ASC occlusion were noted. Patients after ASD and PFO occlusion did not differ in regard to SF, BP, MH, and VT. Similarly, after percutaneous ASD closure, Komar et al.<sup>4</sup> observed a significant improvement in the clinical condition of patients and reduction in the frequency of dyspnea, palpitations and resolution of right heart volume overload. This was reflected by a decrease in right atrial area and right ventricular size (diastolic and systolic dimension as well as right ventricular area) and a significant improvement in QoL. On the other hand, Siudalska et al.<sup>11</sup> observed decreased overall QoL and physical health in patients after surgical correction of ASD than in the control group. At the same time, there were no differences in mental health between the groups. The only category significantly differentiating the compared groups was social functioning, which was worse in patients who had undergone surgical correction of ASD. Somatic disorders were significantly more common in surgical patients. In our study, we have shown that the procedure-related change in self-assessed QoL by patients was associated with right ventricular and atrial dimensions. In patients with ASD, change in SF-36 total score was predicted by TAPSE and RVD3, while in patients with PFO, this change was predicted by TAPSE, lack of arterial hypertension and ACE-I use. Therefore, in both groups, patients with better right ventricular function (TAPSE) before percutaneous closure of ASC may benefit the most, in terms of QoL improvement, from ASC occlusion. In patients with ASD, increased longitudinal right ventricular dimension plays an important role, while in patients with PFO, lack of arterial hypertension and ACE-I use are important factors. These observations are in line with previous studies in different groups of patients.<sup>23,24</sup>

Our study has several limitations, including the observational character of the study, a relatively short follow-up and


a small group of patients investigated. However, the changes described are significant. On the other hand, longer Holter ECG monitoring could increase detection and provide more detailed characteristics of arrhythmias.


## Conclusions


Patients with atrial septal defect have a lower QoL than patients with patent foramen ovale, both before and after percutaneous ASC occlusion. Improvement of quality of life in patients with atrial septal defect is higher than in those with patent foramen ovale. The change in self-assessed QoL after the procedure was associated with episodic arrhythmia and predicted by echocardiographic and clinical parameters. Patient education on potential role limitations should be considered in patients with ASC, especially those with ASD.

### ORCID iDs


Maria Lelakowska  <https://orcid.org/0000-0003-4456-5954>


Paweł Tomasz Matusik  <https://orcid.org/0000-0001-5788-575X>


Piotr Stanisław Podolec  <https://orcid.org/0000-0001-6101-2935>

Maria Olszowska  <https://orcid.org/0000-0003-3037-0400>

Jadwiga Maria Nessler  <https://orcid.org/0000-0002-5076-5816>

Natalia Podolec  <https://orcid.org/0000-0003-0192-7310>

Tadeusz Przewłocki  <https://orcid.org/0000-0002-9575-7270>

Monika Komar  <https://orcid.org/0000-0001-5341-2947>

### References

- Komar M, Podolec P, Przewłocki T, et al. Transoesophageal echocardiography can help distinguish between patients with “symptomatic” and “asymptomatic” patent foramen ovale. *Kardiol Pol.* 2012;70(12):1258–1263.
- Hari P, Pai RG, Varadarajan P. Echocardiographic evaluation of patent foramen ovale and atrial septal defect. *Echocardiography.* 2015;32(Suppl 2):S110–124.
- Sabiniewicz R. Interventional, percutaneous closure of interatrial communication: Atrial septal defect and patent foramen ovale. *Ann Acad Med Gedan.* 2012;62 (Suppl. 4):1–219.
- Komar M, Przewłocki T, Olszowska M, Sobień B, Podolec P. The benefit of atrial septal defect closure in elderly patients. *Clin Interv Aging.* 2014;9:1101–1107.
- Komar M, Przewłocki T, Olszowska M, Sobień B, Tomkiewicz-Pająk L, Podolec P. Is it worth closing the atrial septal defect in patients with insignificant shunt? *Postepy Kardiol Interwencyjnej.* 2014;10(2):78–83.
- Komar M, Przewłocki T, Olszowska M, et al. Conduction abnormality and arrhythmia after transcatheter closure of atrial septal defect. *Circ J.* 2014;78(10):2415–2421.
- Podolec P, Przewłocki T, Pieculewicz M, et al. Early haemodynamic changes after transcatheter closure of atrial septal defect [in Polish]. *Przegl Lek.* 2004;61(6):640–643.
- Fang F, Luo XX, Lin QS, et al. Characterization of mid-term atrial geometrical and electrical remodeling following device closure of atrial septal defects in adults. *Int J Cardiol.* 2013;168(1):467–471.
- Lelakowska-Pieła M, Pudło J, Rydlewska A, Senderek T, Lelakowski J. Quality of life in patients after anti-arrhythmic devices implantation [in Polish]. *Pol Merkur Lekarski.* 2013;35(210):331–338.
- Liszniński P, Pudło J, Lelakowska-Pieła M, Nowak J, Lelakowski J. Analysis of RF ablation treatment on quality of life in patients with cardiac arrhythmias [in Polish]. *Przegl Lek.* 2015;72(1):1–5.
- Siudalska H, Lipczyńska M, Leszczyńska K, et al. Quality of life in patients following atrial septal defect surgical repair. *Folia Cardiol.* 2004;11(8):599–606.
- Cieślak B. Influence of the heart diseases on quality of life – literature review [in Polish]. *Acta Bio-Opt Inf Med Biomed Eng.* 2014;20(2):101–118.
- Lelakowska M, Komar M, Matusik PT, Nessler J, Podolec P, Olszowska M. Transcatheter closure of atrial septal communication: Impact on P-wave dispersion, duration and arrhythmia in mid-term follow-up. *Kardiol Pol.* 2018;76(10):1465–1473.
- Warnes CA, Williams RG, Bashore TM, et al. ACC/AHA 2008 Guidelines for the Management of Adults with Congenital Heart Disease: a report of the American College of Cardiology/American Heart Association Task Force on Practice Guidelines (writing committee to develop guidelines on the management of adults with congenital heart disease). *Circulation.* 2008;118(23):714–833.
- Rudski LG, Lai WW, Afalalo J, et al. Guidelines for the echocardiographic assessment of the right heart in adults: A report from the American Society of Echocardiography endorsed by the European Association of Echocardiography, a registered branch of the European Society of Cardiology, and the Canadian Society of Echocardiography. *J Am Soc Echocardiogr.* 2010;23(7):685–713.
- Lang RM, Badano LP, Tsang W, et al; American Society of Echocardiography; European Association of Echocardiography. EAE/ASE recommendations for image acquisition and display using three-dimensional echocardiography. *J Am Soc Echocardiogr.* 2012;25(1):3–46.
- Lang RM, Badano LP, Mor-Avi V, et al. Recommendations for cardiac chamber quantification by echocardiography in adults: An update from the American Society of Echocardiography and the European Association of Cardiovascular Imaging. *J Am Soc Echocardiogr.* 2015;28(1):1–39.
- Błażejowski J, Sinkiewicz W. Echocardiographic assessment of the right heart – 2015 expert guidelines in clinical practice. *Folia Cardiol.* 2017;12:171–178.
- Pepi M, Evangelista A, Nihoyannopoulos P, et al; European Association of Echocardiography. Recommendations for echocardiography use in the diagnosis and management of cardiac sources of embolism: European Association of Echocardiography (EAE) (a registered branch of the ESC). *Eur J Echocardiogr.* 2010;11(6):461–476.
- Gutiérrez-Barrios A, Laca-Peña JM, Vignau-Cano JM, et al. Silent early migration of a Figulla® septal occluder into the left ventricle. *Kardiol Pol.* 2017;75(7):724.
- Cottini M, Pergolini A, Musumeci F. Atrial septal defect occluder dislocation engaged through the tricuspid valve: Surgical removal via right thoracotomy. *Kardiol Pol.* 2017;75(3):279.
- Goreczny S, Bedair R, Bilka K, Morgan G. Retrieving a large embolised atrial septal occluder – hooked... and landed. *Kardiol Pol.* 2017;75(3):277.
- Wolfel EE. Effects of ACE inhibitor therapy on quality of life in patients with heart failure. *Pharmacotherapy.* 1998;18(6):1323–1334.
- Trevisol DJ, Moreira LB, Kerckhoff A, Fuchs SC, Fuchs FD. Health-related quality of life and hypertension: A systematic review and meta-analysis of observational studies. *J Hypertens.* 2011;29(2):179–188.





# Genetic polymorphisms in pattern recognition receptors are associated with allergic diseases through gene–gene interactions

Anna Dębińska<sup>A–E</sup>, Hanna Danielewicz<sup>A,C,E</sup>, Anna Drabik-Chamerska<sup>B,C</sup>, Danuta Kalita<sup>B,C</sup>, Andrzej Boznański<sup>A,E,F</sup>

1<sup>st</sup> Department and Clinic of Pediatrics, Allergology and Cardiology, Wrocław Medical University, Poland

A – research concept and design; B – collection and/or assembly of data; C – data analysis and interpretation; D – writing the article; E – critical revision of the article; F – final approval of the article

Advances in Clinical and Experimental Medicine, ISSN 1899–5276 (print), ISSN 2451–2680 (online)

*Adv Clin Exp Med.* 2019;28(8):1087–1094

## Address for correspondence

Anna Dębińska  
E-mail: [anna.debinska@umed.wroc.pl](mailto:anna.debinska@umed.wroc.pl)

## Funding sources

None declared

## Conflict of interest

None declared

## Acknowledgements

The authors would like to thank Professor Torben Sigsgaard from the Department of Public Health in the University of Aarhus for kindly providing us with the DNA samples which were used in our PCR reactions as positive controls.

Received on March 29, 2018

Reviewed on August 12, 2018

Accepted on February 18, 2019

Published online on August 9, 2019

## Cite as

Dębińska A, Danielewicz H, Drabik-Chamerska A, Kalita D, Boznański A. Genetic polymorphisms in pattern recognition receptors are associated with allergic diseases through gene–gene interactions. *Adv Clin Exp Med.* 2019;28(8):1087–1094. doi:10.17219/acem/104538

## DOI

10.17219/acem/104538

## Copyright

© 2019 by Wrocław Medical University

This is an article distributed under the terms of the Creative Commons Attribution Non-Commercial License (<http://creativecommons.org/licenses/by-nc-nd/4.0/>)

## Abstract

**Background.** There is evidence that suggests variation in gene encoding pattern recognition receptors, the essential components of innate immunity, might be associated with atopic diseases. However, results have been inconclusive.

**Objectives.** The aim of the study was to determine the individual associations and possible interactive effects of the *CD14* (cluster of differentiation 14), *TLR4* (toll-like receptor 4) and *TLR2* (toll-like receptor 2) polymorphisms on allergic diseases.

**Material and methods.** The *CD14 C-159T*, *TLR4 +896A/G* and *TLR2 A-16934T* polymorphisms were identified in 115 children aged from 6 to 17 years. All subjects were selected using a detailed questionnaire which included questions on symptoms and each one underwent skin prick testing. All single-nucleotide polymorphisms (SNPs) were determined using real-time polymerase chain reaction (PCR) assays.

**Results.** There was no statistically significant correlation between the 3 polymorphisms (*CD14 C-159T*, *TLR4 +896A/G* and *TLR2/-16934A/T*) and either asthma, allergic rhinitis or atopy. We observed that children who were heterozygous or homozygous for both the *CD14/-159T* and *TLR2/-16934A* alleles had a 4-fold lower risk for asthma than children who were carriers of the T allele of *CD14* but non-carriers of the A allele of *TLR2*, and an almost 3-fold lower risk for asthma when compared to all other groups. Concerning allergic rhinitis, a similar trend was observed. In addition, the presence of at least 1 A allele in the *TLR2/-16934* polymorphism reduced the risk for asthma and allergic rhinitis, but only in children who were homozygous for the common A allele in the *TLR4 +896* polymorphism.

**Conclusions.** Our study supports the idea that the *CD14*, *TLR2* and *TLR4* polymorphisms may not be directly involved in the development of atopic diseases. However, our results suggest that their impact on the risk of asthma and allergic rhinitis might be modulated by gene–gene interactions.

**Key words:** single nucleotide polymorphisms, asthma, innate immunity, atopy, gene–gene interactions

## Introduction

Toll-like receptors (TLRs) and cluster of differentiation 14 (CD14) are pattern recognition receptors (PRRs) that are critically involved in activating innate immunity and in inducing subsequent adaptive immune responses. These receptors are expressed in a wide variety of innate immune cells, including epithelial cells, macrophages, mast cells, eosinophils, and dendritic cells. Toll-like receptors and CD14 recognize and respond to diverse microbial molecules that are often referred to as pathogen-associated molecular patterns (PAMPs).<sup>1,2</sup> Experimental studies have largely implicated TLRs and CD14 in both the development and control of the allergic reaction.<sup>3,4</sup> The role of these receptors in the pathogenesis of allergic diseases results from the biological role that they play in activating and regulating the immune response.<sup>2,4</sup> Toll-like receptors and CD14 stimulation via microbial products activates antigen-presenting cells, influences the function of T regulatory cells (T<sub>reg</sub>), determines the Th<sub>1</sub>/Th<sub>2</sub> balance and Th<sub>17</sub> cell differentiation, and controls cytokine production in mast cells and eosinophil activation.<sup>2,4,5</sup> The discovery of TLRs and their signaling pathways provides an immunological basis for the hygiene hypothesis, which suggests that allergic diseases develop because of changes in microbial exposure and PPR stimulation early in life.<sup>6,7</sup>

Because toll-like receptor 2 (TLR2), toll-like receptor 4 (TLR4) and CD14 are so centrally involved in the recognition of the microbial environment, it has been speculated that genetic changes in these molecules may modulate responsiveness to lipopolysaccharides (LPSs) and other PAMPs, leading to inadequate immune responses and thus playing a role in the development of atopy and other allergic diseases.<sup>8</sup> There is growing evidence coming from functional studies that polymorphisms in genes which encode TLR2, TLR4 and CD14 significantly influence transcriptional activity, gene expression and/or receptor function, making them biologically plausible candidate genes for asthma and allergic diseases.<sup>9–11</sup>

TLR2 is a key component in linking microbial products, apoptosis and host defense mechanisms. It identifies elements of the cell walls of gram-positive and gram-negative bacteria, protein components of viruses, and molecules of bacillus, fungi and parasites.<sup>3,4,12</sup> The *TLR2*-16934A/T polymorphism is located in a region that significantly influences the process of transcription of the *TLR2* gene. A much higher level of transcription of the TLR2 receptor has been demonstrated on monocytes of healthy volunteers with the homozygotic genotype TT, in comparison with monocytes of the wild allele A carriers.<sup>9</sup>

TLR4 is the principal receptor for recognizing LPSs – the main component of the cell walls of gram-negative bacteria – and it plays a critical role in the innate immune response to both gram-negative pathogens and respiratory syncytial virus.<sup>3,4,12</sup> Arbour et al. confirmed that the presence of the *TLR4*+896A/G polymorphism

is associated with hyporesponsiveness to inhaled endotoxin, reduced density of TLR4 in airway epithelium and reduced production of inflammatory cytokines in response to endotoxins.<sup>10</sup> Another experimental study showed that the *TLR4*+896A/G polymorphism is associated with a blunted systemic inflammatory response to inhaled lipopolysaccharides.<sup>13</sup>

The *CD14* gene encodes a protein that functions as a co-receptor for TLR4 and is one of the major components in the innate immunity response. The CD14 receptor is multifunctional with a high specificity for LPSs, and together with TLR4 forms the complex that activates the innate immune system through various pathways.<sup>1,14</sup> The *CD14* gene is located on chromosome 5q31.3, a region associated with asthma in a genome-wide linkage study.<sup>15</sup> Functional research has shown that the *CD14*-159C/T polymorphism significantly influences the intensity of transcription and expression of the gene.<sup>11</sup> This data is reflected in numerous clinical studies confirming that the *CD14*-159C/T polymorphism is connected with a higher concentration of sCD14 in blood serum and a lower concentration of total immunoglobulin E (IgE).<sup>16–21</sup> Based on these results of functional studies, it was hypothesized that polymorphisms within *TLR2*, *TLR4* and *CD14* genes – by changing the gene expression and/or the function of the receptor – may modify the immunological response towards microbiological factors and influence the risk of allergy development. Numerous studies have implicated polymorphisms of the *TLR2*, *TLR4* and *CD14* genes in the pathogenesis of asthma and allergies. Among the reported studies, most found that these polymorphisms were associated with asthma and allergic diseases, though the reports are contradictory.<sup>22–25</sup> In the ALEX study, the wild-type *TLR2*-16934T allele was found to be associated with fewer asthma diagnoses, symptoms and atopy among German and Austrian farmers' children, but this relationship was not observed in children who did not live on a farm.<sup>26</sup> The *TLR4*+896A/G variant was found to be associated with 4-fold higher prevalence of asthma and a 7-fold higher prevalence of atopic asthma in a population of Swedish children.<sup>27</sup> Another study found that asthmatic people with the *TLR4*+896A/G polymorphism have more severe atopy.<sup>28</sup> However, subsequent studies on *TLR4* polymorphisms as a risk factor for atopy and asthma in adults or children have reported conflicting results.<sup>20,26,27,29</sup> Some studies found the *CD14*-159T allele was associated with lower IgE levels and/or a reduced risk of atopy,<sup>17,18</sup> while other studies found no association<sup>19,30</sup> or an increased risk of atopy and higher IgE levels in subjects with the *CD14*-159T allele.<sup>31–33</sup> A large meta-analysis of the *CD14*-159C/T promoter polymorphism and atopic asthma found a significant protective effect for carriers of the TT and CT genotype as compared with the CC genotype.<sup>25</sup> On the other hand, a recent review concluded that there is still no convincing evidence of *CD14* and *TLRs* polymorphisms playing a role in childhood asthma among

Caucasians.<sup>22</sup> Since the results of available published association studies are heterogeneous, further population studies are warranted. Moreover, in the case of complex diseases, the predisposition might be better explained by a combined effect of the variations in multiple genes within the same functional pathway.

Therefore, the aim of this case-control study was to determine the individual associations and possible interactive effect of the *CD14/-159C/T*, *TLR4/+896A/G* and *TLR2/-16934A/T* polymorphisms with respect to atopy, asthma and allergic rhinitis in a population of Polish children

## Material and methods

### Study population

A total of 115 unrelated children (57 males and 58 females) ranging in age from 6 to 17 years (mean age: 11.8 years) were enrolled in the study. All study participants were of Caucasian ethnicity. The study subjects were recruited from patients who had visited the Outpatient Allergy Clinic for Children in Wrocław, Poland, and from the general population. The healthy control subjects were recruited from the general population through community-based approaches. We distributed flyers at local schools, pediatricians' and family doctors' offices, and during health fairs. Interested parents were instructed to contact the research coordinator via telephone. All participants, case subjects and controls were selected with the help of a detailed questionnaire that included questions regarding overall health status, symptoms of asthma and allergic rhinitis, sociodemographic information, and family history of allergic diseases.

All subjects, including the positive and negative controls, underwent skin prick testing (SPT) for a panel of 6 common inhalant allergens: house dust mites (*Dermatophagoides pteronyssinus* and *Dermatophagoides farinae*), cat dander, grass pollen (a mix of 6 species), tree pollen I (a mix of 5 species), and tree pollen II (a mix of 4 species) (Allergopharma, Reinbek, Germany). The concentration of total serum IgE was measured using the commercially available IMMULITE 2000 Total IgE kit (Diagnostic Products Corporation, Los Angeles, USA).

Diagnoses of atopy and its related diseases were made according to the following criteria:

Atopy was defined as a positive skin prick test reaction – determined with a wheal 3 mm in diameter – to 1 or more of the 6 common inhalant allergens. Additionally, atopic patients had had symptoms of asthma and/or allergic rhinitis during the previous 12 months.

Asthma was defined using the questionnaire answers along with a physician's diagnosis of asthma, according to the Global Initiative For Asthma (GINA) criteria.<sup>34</sup> Asthma was confirmed by a history of coughing, wheezing

and chest tightness during the previous 12 months as well as by positive results of the reversibility tests: >12% reversibility of FEV<sub>1</sub> after  $\beta_2$ -agonist inhalation.

Diagnoses of allergic rhinitis were based on reports of a doctor's diagnosis of allergic rhinitis and/or the occurrence of 2 or more symptoms (nasal obstruction, rhinorrhea, sneezing, or itchy nose) in the absence of a common cold during the previous 12 months, plus sensitization against common inhalant allergens.

The control group, matched with the case group for age and gender, included healthy children who met the following criteria: an absence of symptoms of asthma, allergic rhinitis or other allergic diseases, a negative SPT result, and a negative family history of allergic diseases.

### Genotyping

The samples of the 115 subjects were genotyped for the *CD14 C-159T*, *TLR4 +896 A/G* and *TLR2 A-16934T* polymorphisms. Genomic DNA was obtained from ethylenediaminetetraacetic acid (EDTA) whole blood samples using a QIAamp DNA Blood Mini Kit (Qiagen GmbH, Hilden, Germany). All SNPs were determined with real-time polymerase chain reaction (PCR) assays with subsequent melting curve analysis using SimpleProbe<sup>®</sup> probes (TibMolbiol, Berlin, Germany) which were complementary to the wild-type sequences. Initial PCR amplifications and melting analyses were carried out with various oligonucleotide concentrations and ratios. Melting peaks were optimized when asymmetric PCR conditions (unequal amounts of primers) were used. The reactions were performed on a Light Cycler 1.5 platform (Roche Applied Science, Mannheim, Germany) as described in Table 1. For quality control of the genotyping procedures, positive and negative controls for each genotype were included in each reaction.

### Statistical analysis

Hardy–Weinberg equilibrium was tested for using the  $\chi^2$  goodness-of-fit test to compare the observed genotype frequencies with the expected frequencies among the controls. Differences in genotype frequencies or demographic characteristics between the case and control groups were evaluated using the  $\chi^2$  test or the Fisher's exact test, as appropriate. Correlations of genotypes or alleles with patient groups vs control subjects without atopic diseases were determined by computing the odds ratio (OR), its 95% confidence interval (95% CI) and p-values using logistic regression analysis for crude ORs (and adjusted ORs when adjusting for age and gender). Three different genetic models were tested separately in the comparison of genotypes and atopic diseases in this study. A  $\chi^2$  test or Fisher's exact test was used to determine the combined effect of genotype pairs. Gene–gene interaction was investigated using logistic regression models for atopy, asthma and allergic

**Table 1.** Primer and probe sequences used for genotyping SNPs in the *CD14*, *TLR4* and *TLR2* genes and PCR conditions

Polymorphism	SNP ID	Specific primers	Probes
CD14/-159C/T	rs 2569190	f:5'- CTTCggCTgCCTCTgACAgTT r:5'- ggTgCCAACAgATgAggTTCAC	5'- TTCCTgTXITACggCCCCCT--PH
Reaction mix		2.5 µL of DNA at a concentration of 15–60 ng/µL, 1.0 µL forward primer (5 µmol/L), 1.0 µL reverse primer (2.5 µmol/L), 1.0 µL probe (2 µmol/L), 2.0 µL of LightCycler®TaqMan®Master	
PCR		12 min 95°C – 55 cycles (10 s 95°C – 20 s 55°C – 20 s 72°C), ramping rate 20°C/s – 45–90°C with 0.1°C/s	
TLR4/+896A/G	rs 4696480	f:5'- AACAgAAATTATCCATTCATgT r:5'- AgCAGTTTATgTgAATgAgTTT	5'- CCAgAXITgACCCTCACCAgATgC--PH
Reaction mix		2.5 µL of DNA at a concentration of 15–60 ng/µL, 1.0 µL forward primer (5 µmol/L), 1.0 µL reverse primer (5 µmol/L), 1.0 µL probe (2 µmol/L), 2.0 µL of LightCycler®TaqMan®Master	
PCR		12 min 95°C – 50 cycles (10 s 95°C – 20 s 55°C – 20 s 72°C), ramping rate 20°C/s – 40–80°C with 0.1°C/s	
TLR2/-16934A/T	rs 4986790	f:5'- CCAAgAAgTTTgAACTCATgTAA r:5'- ATTTAAAgAAATTAggCTTCATAAgCT	5'- ACTACCTCgATgATATTATXITgACTTATT--PH
Reaction mix		2.5 µL of DNA at concentration of 15–60 ng/µL, 1.0 µL forward primer (5 µmol/L), 1.0 µL reverse primer (1 µmol/L), 1.0 µL probe (2 µmol/L), 2.0 µL of LightCycler®TaqMan®Master	
PCR		12 min 95°C – 50 cycles (10 s 95°C – 20 s 55°C – 20 s 72°C), ramping rate 20°C/s – 40–90°C with 0.1°C/s	

PCR – polymerase chain reaction; SNP – single nucleotide polymorphism; TLR – toll-like receptor.

rhinitis with interaction terms. Both parametric (t-test and analysis of variance – ANOVA) and non-parametric (Mann–Whitney U test and Kruskal–Wallis test) analyses were performed to study the phenotypic differences in each genotype group, depending on the normality of the distribution of the variables. Statistical significance was set at a p-value <0.05. The statistical analyses were carried out using STATISTICA v. 9.0 (StatSoft, Inc., Tulsa, USA) and the SPSS Statistics v. 11.1 (SPSS Inc., Chicago, USA). A p-value <0.05 was considered statistically significant and all statistical tests were 2-sided.

The study was approved by the Ethics Committee of the Wrocław Medical University and informed written consent – including consent for genetic studies – was obtained from all of the subjects prior to testing.

## Results

The baseline characteristics of the study population are presented in Table 2. The allele and genotype distributions for the *CD14/-159C/T*, *TLR4/+896A/G* and *TLR2/-16934A/T* polymorphisms among the case subjects and controls are shown in Table 3. Because the GG genotype of the *TLR4/+896A/G* was rare, we combined the AG and GG genotypes for *TLR4* when calculating p-values. The genotype frequencies of the 3 SNPs studied were in agreement with Hardy–Weinberg equilibrium in all groups, as indicated by the  $\chi^2$  values at p-values >0.05 shown in Table 4.

No significant differences in genotype or allelic frequencies for the *CD14/-159C/T*, *TLR4/+896A/G* and *TLR2/-16934A/T* polymorphisms could be observed when the children with atopy, asthma or allergic rhinitis were compared to non-atopic controls. Furthermore, there were no significant

**Table 2.** Characteristics of the study groups. Polysensitization is a positive skin prick tests against at least 3 allergens. Descriptive data is presented as observation count, percent, mean, and standard deviation or median and range

Variable	Cases (n = 67)	Controls (n = 48)
Age [years]	12.4 ±3	11.0 ±2.7
Gender [male/female]	38/29	19/29
Atopy	67 (100.0)	0
Asthma	33 (49.2)	0
Allergic rhinitis	59 (88.0)	0
Number of positive skin tests	3 (1–6)	0
Polysensitization	43 (64.2)	0
Atopic hereditary	37 (55.2)	0
Asthma	18 (26.8)	0
Allergic rhinitis	26 (38.8)	0
Total serum IgE [IU/mL]	603 ±801	0

IgE – immunoglobulin E.

correlations between the *CD14/-159C/T*, *TLR4/+896A/G* and *TLR2/-16934A/T* alleles and/or genotypes and total IgE level or the number of positive skin prick tests in all studied groups (data not shown).

Next, we examined if there was a connection between the studied phenotypes and coinheritance of the studied polymorphisms. We observed that children who were heterozygous or homozygous for both the *CD14/-159T* and *TLR2/-16934A* alleles had a 4-fold lower risk for asthma than children who were carriers of the T allele of *CD14* but non-carriers of the A allele of *TRL2* and an almost 3-fold lower risk for asthma when compared to all other groups. Concerning allergic rhinitis, a similar trend was observed: a 3-fold lower risk of having nasal allergies was seen in carriers of the A allele of *TRL2* who were also carriers of the T allele of the *CD14* gene when compared

**Table 3.** Genotype and allele frequencies of CD14, TLR4 and TLR2 polymorphisms in the study groups. To study a co-dominant model, the 3 genotype groups were analyzed separately using wild-type homozygotes as a reference group. To test a dominant model, wild-type homozygotes were compared with heterozygotes and homozygotes for minor alleles. In a multiplicative model, genotypes were coded as a 3-level variable for the number of minor alleles

Genotype	Control n [%]	Atopy			Asthma			Allergic rhinitis		
		n [%]	p-value	OR (95% CI)	n [%]	p-value	OR (95% CI)	n [%]	p-value	OR (95% CI)
CD14/-159C/T										
CC	13 (27.1)	20 (29.8)	0.945	1.00 (ref)	10 (30.3)	0.848	1.00 (ref)	17 (28.8)	0.832	1.00 (ref)
CT	22 (45.8)	30 (44.8)		0.90 (0.35÷2.34)	13 (39.4)		0.70 (0.22÷2.21)	29 (4.2)		1.09 (0.41÷2.93)
TT	13 (27.1)	17 (25.4)		1.04 (0.35÷3.10)	10 (30.3)		0.87 (0.24÷3.20)	13 (22.0)		1.03 (0.32÷3.33)
CT + TT	35 (72.9)	47 (70.2)	0.461	0.94 (0.39÷2.25)	23 (69.7)	0.948	0.75 (0.26÷2.15)	42 (71.2)	0.100	1.05 (0.43÷2.60)
T	48 (50.0)	64 (47.8)	0.841	1.00 (0.59÷1.72)	33 (50.0)	0.873	0.94 (0.50÷1.76)	55 (46.6)	0.722	0.99 (0.55÷1.92)
TLR4/+896A/G										
AA	44 (91.7)	59 (88.1)	0.758	1.00 (ref)	28 (84.8)	0.475	1.00 (ref)	51 (86.4)	0.541	1.00 (ref)
AG + GG	4 (8.3)	8 (11.9)		1.81 (0.47÷6.93)	5 (15.2)		2.15 (0.49÷9.39)	8 (13.6)		2.13 (0.55÷8.24)
G	4 (4.2)	9 (6.7)	0.591	1.94 (0.57÷6.54)	6 (9.1)	0.319	2.40 (0.66÷8.65)	9 (7.6)	0.392	2.23 (0.65÷7.65)
TLR2/-16934A/T										
TT	11 (22.9)	26 (38.8)	0.184	1.00 (ref)	14 (42.4)	0.158	1.00 (ref)	23 (39.0)	0.206	1.00 (ref)
TA	21 (43.8)	25 (37.3)		0.44 (0.16÷1.17)	12 (36.4)		0.35 (0.10÷1.14)	22 (37.3)		0.49 (0.18÷1.35)
AA	16 (33.3)	16 (23.9)		0.38 (0.13÷1.08)	7 (21.2)		0.31 (0.08÷1.12)	14 (23.7)		0.39 (0.13÷1.17)
TA + AA	37 (77.1)	41 (61.2)	0.110	0.46 (0.19÷1.10)	19 (57.6)	0.105	0.40 (0.15÷1.08)	36 (61.1)	0.117	0.44 (0.18÷1.10)
A	43 (44.8)	57 (42.5)	0.116	0.64 (0.38÷1.06)	26 (39.4)	0.070	0.58 (0.31÷1.10)	50 (42.4)	0.083	0.61 (0.35÷1.05)

ref – reference; TLR – toll-like receptor; OR – odds ratio; CI – confidence interval.

**Table 4.** Hardy–Weinberg equilibrium values in the study groups.  $\chi^2$  test or Fisher’s exact test\*,  $p > 0.05$

Genotype	Control	Atopy	Asthma	Allergic rhinitis
CD14/-159C/T	p = 0.563	p = 0.400	p = 0.223	p = 0.924
TLR2/16934A/T	p = 0.424	p = 0.053	p = 0.170	p = 0.069
TLR4/+896A/G	p = 1.000*	p = 0.250*	p = 0.219*	p = 0.280*

TLR – toll-like receptor.

to the reference group and to all other genotype combinations. In addition, the presence of at least 1 A allele at the *TLR2/-16934* polymorphism significantly correlated with a decreased risk for asthma and allergic rhinitis, but only in children who were homozygous for the common A allele at the *TLR4/+896* polymorphism. No significant correlation of the *TLR2/-16934A/T* with either asthma or allergic rhinitis was seen in the cases with at least one G allele at the *TLR4/+896* polymorphism. As shown in Table 5, the odds ratios (ORs) and p-values for asthma

and allergic rhinitis suggest the presence of a gene–gene interaction, though when modeling for interactions, the interaction coefficient was not significant for either genotype combination (p-value for interaction >0.05). No significant difference in the prevalence of asthma or allergic rhinitis was detected for the combination of the *CD14/-159C/T* and *TLR4/+896A/G*. No epistatic effect was found in the case of atopic phenotype (data not shown).

## Discussion

In this study, we found that the *CD14/-159C/T*, *TLR4/+896A/G*, and *TLR2/-16934A/T* polymorphisms did not affect either atopy or allergic disease susceptibility in a population of Polish children. To date, there have been no association studies investigating these polymorphisms within *TLR2* and *TLR4* genes in this population, and only 3 studies investigated *CD14* polymorphisms in relation to asthma.<sup>35–37</sup> To the best of our knowledge, this is also the first study in this population that attempts

**Table 5.** Association between CD14, TLR4 and TLR2 genotype combinations and asthma and allergic rhinitis

Genotype combinations	Control n [%]	Asthma			Allergic rhinitis		
		n [%]	p-value	OR (95% CI)	n [%]	p-value	OR (95% CI)
CD14 CC + TLR2 TT	2 (4.2)	1 (3.0)	1.000	1.00 (ref) –	1 (3.0)	0.565	1.00 (ref) –
CD14 CC + TLR2 TA/AA	11 (22.9)	9 (27.3)		2.08 (0.09÷46.2)	9 (27.3)		2.90 (0.23÷36.1)
CD14 CT/TT + TLR2 TT	9 (25.7)	13 (56.5)	0.037*	1.00 (ref) –	13 (56.5)	0.032*	1.00 (ref) –
CD14 CT/TT + TLR2 TA/AA	26 (74.3)	10 (43.5)		0.25* (0.07÷0.87)	10 (43.5)		0.31* (0.11÷0.88)
TLR4 AA + TLR2 TT	9 (18.8)	13 (39.4)	0.038*	1.00 (ref) –	13 (39.4)	0.030*	1.00 (ref) –
TLR4 AA + TLR2 TA/AA	35 (72.9)	15 (45.5)		0.27* (0.08÷0.85)	15 (45.5)		0.35* (0.13÷0.95)
TLR4 AG/GG + TLR2 TT	2 (50.0)	1 (20.0)	0.524	1.00 (ref) –	1 (20.0)	0.547	1.00 (ref) –
TLR4 AG/GG + TLR2 TA/AA	2 (50.0)	4 (80.0)		0.67 (0.03÷16.38)	4 (80.0)		1.83 (0.06÷54.9)

\* statistically significant results; ref – reference; OR – odds ratio; CI – confidence interval.

to understand the gene–gene interactions based on polymorphisms. Among the large number of SNPs currently identified in the studied genes, we decided to cover SNPs that have proven and relevant functional consequences.<sup>9–11</sup> Although the correlations between polymorphisms in the *TLR2*, *TLR4* and *CD14* genes in allergic diseases have received considerable attention in recent years, the results are still contradictory.

The first hints that variations in genes which encode receptors of innate immunity may modulate the risk of allergy actually came from studies on *CD14*, but the results of the association studies remain controversial. Baldini et al.<sup>17</sup> reported an association of the *CD14-159/TT* genotype with higher sCD14 expression, lower total serum IgE and fewer mean positive SPTs in atopic patients. Numerous studies have replicated the results from the initial Tucson study, but no correlation between the *CD14-159C/T* polymorphism and atopic diseases has been observed.<sup>18–20,30</sup> The lack of association between *CD14* genotypes and atopic diseases in our research is in line with the results of these studies. However, we could not find any association between *CD14* polymorphism and total serum IgE level or the number of positive SPTs. Similar results were obtained in a previous study on Polish children.<sup>36</sup> In addition, no such associations were found in either the Asian or Caucasian populations.<sup>21,27,38–41</sup> A significant correlation between the *CD14-159C/T* polymorphism and asthma was not observed in another recent study among the Puerto Rican population, the population that exhibits the highest asthma prevalence of any racial or ethnic group.<sup>42</sup> On the other hand, other authors have reported a correlation of the *CD14-159/TT* genotype with a lower risk of developing asthma<sup>17,31,35,43</sup> or have even reported the opposite results.<sup>32,33,44</sup>

In the present study, the genotype and allele frequency of the *TLR4/+896A/G* polymorphism did not significantly

differ between the allergic patients and the controls. Our results are consistent with studies in populations from Denmark,<sup>30</sup> Tunisia,<sup>31</sup> Egypt,<sup>45</sup> Korea,<sup>46</sup> and Japan<sup>47</sup> that did not find an effect of the *TLR4/+896A/G* polymorphism on the risk of asthma or atopy-related traits. In addition, similar results were obtained in both the Puerto Rican population<sup>42</sup> and a heterogeneous American cohort.<sup>29</sup> The lack of association between the *TLR4/+896A/G* polymorphism and asthma has also been confirmed by the latest meta-analysis.<sup>23</sup> In contrast, a previous meta-analysis of 8 studies showed a marginal association of *TLR4/+896A/G* with asthma risk, indicating that the major A allele might protect against asthma.<sup>24</sup> This is in agreement with a study among Swedish children suggesting that the AG genotype was associated with an increased risk of asthma, especially atopic asthma.<sup>27</sup> Yang et al.<sup>28</sup> observed a positive correlation of the *TLR4/+896A/G* allele with atopy severity in an asthmatic population, whereas another analysis of Turkish children showed that the heterozygosity of the *TLR4/+896A/G* polymorphism is associated with milder forms of asthma.<sup>20</sup>

When it comes to the *TLR2/-16934A/T* polymorphism, a large European study showed that farmers' children carrying a T allele in *TLR2/-16934* were less likely to have a diagnosis of asthma, atopic sensitization or hay fever symptoms.<sup>26</sup> In this study, we did not find any significant correlation between the *TLR2/-16934A/T* polymorphism and either atopy or the development of asthma/allergic rhinitis. This finding is in agreement with a study conducted on a population of young Danish farmers which did not demonstrate any effect of the *TLR2* polymorphisms on the risk of new-onset asthma and atopy.<sup>30</sup> Similarly, no association between the *TLR2/-16934A/T* polymorphism and asthma were found in the Puerto Rican population.<sup>42</sup> Interestingly, Kerkhof et al. showed in their PIAMA cohort study that children with at least 1 A allele in *TLR2/-16934*

had a significantly lower risk of doctor-diagnosed asthma.<sup>48</sup> A similar, but statistically insignificant trend was observed in our analysis for atopy as well as for asthma and allergic rhinitis.

One characteristic feature in the genetics of complex diseases is the low reproducibility and contradictory results of association studies. These conflicting results can be attributed to a lack of statistical power, differences in ethnicity and age, genetic heterogeneity, and environmental exposure. Multiple gene–gene interactions are also likely to contribute to such discrepancies. Gene–gene interactions seem to be biologically plausible, especially with regard to the genes which encode PRRs, form functional heterodimer networks, and take part in complex mechanisms of human innate and adaptive immunity. Reijmerink et al.<sup>49</sup> identified gene–gene interactions of TLR4-related pathway genes in connection with the development of asthma and atopy. Interestingly, significant gene–gene interactions were identified even with SNPs that did not demonstrate an effect on their own. Another study demonstrated that genes involved in the development and functioning of regulatory T cells, specifically IL2RA, TLR2, TGFBR2, and FOXP3, are associated with atopy and asthma when looking at gene–gene interaction.<sup>50</sup>

Therefore, we examined the possibility of a combined effect between the *CD14/-159C/T*, *TLR4/+896A/G* and *TLR2/-16934A/T* polymorphisms in relation to atopy-related traits. Interestingly, our results revealed that children heterozygous or homozygous for the *TLR2/-16934A* and *CD14/-159T* alleles had a significantly lower risk of asthma and allergic rhinitis than children carrying the same genotype for *CD14* who were homozygous for the *TLR2/-16934T* allele. Similar patterns were observed when looking at the combination of *TLR4* and *TLR2* polymorphisms: the co-occurring homozygous genotype for the wild-type *TLR4* allele and at least 1 *TLR2/-16934A* allele was associated with a reduced risk for asthma and allergic rhinitis. These findings suggest some possible epistatic effect of these polymorphisms on asthma and allergic rhinitis, because we could not find any significant correlations in the single-SNP analyses. Thus, it is possible that each variant has a small effect which is not strong enough by itself to cause such a complex disease as asthma or atopy. Our results provide support for our initial hypothesis that the combination of functional SNPs in more than one gene which encodes receptors of innate immunity may magnify the impact of disease or may indicate a new association.

A potential limitation of our study, typical for all case-control studies, is the relatively small sample size and, consequently, rather low statistical power, which may lead to false negative or fortuitous false positive results. An interaction analysis requires a large population; hence, our results should be interpreted with caution. However, the biological plausibility of the interactions between the genes for PRRs lends credibility to our results.

## Conclusions

In summary, our study and the others mentioned above support the notion that the polymorphisms we tested may not play a crucial and decisive role in the development of atopic diseases by themselves, but our preliminary results suggest that their impact on the risk of asthma and allergic rhinitis might be modulated by gene–gene interactions. Further studies to confirm such interactions must be well-designed with adequate sample sizes in order to ensure enough statistical power. We conclude that some genetic associations might remain unnoticed when gene–gene interactions are not considered and we recommend that future studies examine combined genetic effects as well as primary ones.

## References

1. Arancibia SA, Beltrán CJ, Aguirre IM, et al. Toll-like receptors are key participants in innate immune responses. *Biol Res.* 2007;40(2):97–112.
2. Iwamura C, Nakayama T. Toll-like receptors in the respiratory system: Their roles in inflammation. *Curr Allergy Asthma Rep.* 2008;8(1):7–13.
3. Bauer S, Hangel D, Yu P. Immunobiology of toll-like receptor in allergic disease. *Immunobiology.* 2007;212(6):521–533.
4. Goldman M. Translational mini-review series on Toll-like receptors: Toll-like receptor ligands as novel pharmaceuticals for allergic disorders. *Clin Exp Immunol.* 2007;147(2):208–216.
5. Liu G, Zhang L, Zhao Y. Modulation of immune responses through direct activation of toll-like receptors to T cells. *Clin Exp Immunol.* 2010;160(2):168–175.
6. Garn H, Renz H. Epidemiological and immunological evidence for hygiene hypothesis. *Immunobiology.* 2007;212(6):441–452.
7. von Mutius E. Allergies, infection and the hygiene hypothesis: The epidemiological evidence. *Immunobiology.* 2007;212(6):433–439.
8. Tesse R, Pandey RC, Kabesch M. Genetic variations in toll-like receptor pathway genes influence asthma and atopy. *Allergy.* 2011;66(3):307–316.
9. Dalvi MS, Halonen MA. A polymorphism in TLR2 (–16934A/T) influences TLR2 surface expression on human monocytes. *Proc Am Thorac Soc.* 2005;2:A736.
10. Arbour NC, Lorenz E, Schutte BC, et al. TLR4 mutation are associated with endotoxin hyporesponsiveness in humans. *Nat Genet.* 2000;25(2):187–191.
11. LeVan TD, Bloom JW, Bailey TJ, et al. A common single nucleotide polymorphism in the CD14 promoter decreases the affinity of Sp protein binding and enhances transcriptional activity. *J Immunol.* 2001;167(10):5838–5844.
12. Kaisho T, Akira S. Toll-like receptor function and signaling. *J Allergy Clin Immunol.* 2006;117(5):979–987.
13. Michel O, LeVan TD, Stern D, et al. Systemic responsiveness to lipopolysaccharide and polymorphisms in the toll-like receptor 4 gene in human beings. *J Allergy Clin Immunol.* 2003;112(5):923–929.
14. Wright SD, Ramos RA, Tobias PS, Ulevitch RJ, Mathison JC. CD14, a receptor for complexes of lipopolysaccharide (LPS) and LPS binding protein. *Science.* 1990;249(4975):1431–1433.
15. Postma DS, Bleeker ER, Amelung PJ, et al. Genetic susceptibility to asthma-bronchial hyperresponsiveness co-inherited with a major gene for atopy. *N Engl J Med.* 1995;333(14):894–900.
16. LeVan TD, Michel O, Dentener M, et al. Association between CD14 polymorphisms and serum soluble CD14 levels: Effect of atopy and endotoxin inhalation. *J Allergy Clin Immunol.* 2008;121(2):434–440.
17. Baldini M, Lohman IC, Halonen M, Erickson RP, Holt PG, Martinez FD. A polymorphism in the 5' flanking region of the CD14 gene is associated with circulating soluble CD14 levels and with total serum immunoglobulin E. *Am J Respir Cell Mol Biol.* 1999;20(5):976–983.
18. Koppelman GH, Reijmerink NE, Colin Stine O, et al. Association of a promoter polymorphism of the CD14 gene and atopy. *Am J Respir Crit Care Med.* 2001;163(4):965–969.

19. Leung TF, Tang NL, Sung YM, et al. The C-159T polymorphism in the CD14 promoter is associated with serum total IgE concentration in atopic Chinese children. *Pediatr Allergy Immunol.* 2003;14(4):255–260.
20. Sackensen C, Karaaslan C, Keskin O, et al. The effect of polymorphisms at the CD14 promoter and the TLR4 gene on asthma phenotypes in Turkish children with asthma. *Allergy.* 2005;60(12):1485–1492.
21. Kabesch M, Hasemann K, Schickinginger V, et al. A promoter polymorphism in the CD14 gene is associated with elevated levels of soluble CD14 but not with IgE or atopic diseases. *Allergy.* 2004;59(5):520–525.
22. Klaassen EM, Thönissen BE, van Eys G, Dompeling E, Jöbsis Q. A systemic review of CD14 and toll-like receptors in relation to asthma in Caucasian children. *Allergy Asthma Clin Immunol.* 2013;9(1):10.
23. Zhao J, Shang H, Cao X, et al. Associations in polymorphisms in TLR2 and TLR4 with asthma risk. *Medicine (Baltimore).* 2017;96(35):e7909.
24. Tizaoui K, Kaabachi W, Hamzaoui K, Hamzaoui A. Association in single nucleotide polymorphisms in Toll-like receptor genes with asthma risk: A systemic review and meta-analysis. *Allergy Asthma Immunol Res.* 2015;7(2):130–140.
25. Zhao L, Bracken MB. Association of CD14 -260 (-159) C>T and asthma: A systematic review and meta-analysis. *BMC Med Genet.* 2011;12:93–103.
26. Eder W, Klimecki W, Lizhi Y, et al; ALEX Study Team. Toll-like receptor 2 as a major genes for asthma in children of European farmers. *J Allergy Clin Immunol.* 2004;113(3):482–488.
27. Fagerås Böttcher M, Hmani-Aifa M, Lindström A, et al. A TLR4 polymorphism is associated with asthma and reduction lipopolysaccharide-induced interleukin-12 (p70) responses in Swedish children. *J Allergy Clin Immunol.* 2004;114(3):561–567.
28. Yang IA, Barton SJ, Rorke S, et al. Toll-like receptor 4 polymorphism and severity of atopy in asthmatics. *Genes Immun.* 2004;5(1):41–45.
29. Raby BA, Klimecki WT, Laprise C, et al. Polymorphisms in Toll-like receptor 4 are not associated with asthma or atopy-related phenotypes. *Am J Respir Crit Care Med.* 2002;166(11):1449–1456.
30. Smit LAM, Bongers SIM, Ruven HJT, et al. Atopy and new-onset asthma in young Danish farmers and CD14, TLR2 and TLR4 genetic polymorphisms: A nested case-control study. *Clin Exp Allergy.* 2007;37(11):1602–1608.
31. Lachheb J, Dhifallah IB, Chelbi H, Hamzaoui K, Hamzaoui A. Toll-like receptors and CD14 genes polymorphisms and susceptibility to asthma in Tunisian children. *Tissue Antigens.* 2008;71(5):417–425.
32. Han D, She W, Zhang L. Association of the CD14 gene polymorphism C-159T with allergic rhinitis. *Am J Rhinol Allergy.* 2010;24(1):e1–3.
33. Woo JG, Assa'ad A, Heizer AB, et al. The -159 C->T polymorphism of CD14 is associated with nonatopic asthma and food allergy. *J Allergy Clin Immunol.* 2003;112:438–444.
34. Bateman ED, Hurd SS, Barnes PJ, et al. Global strategy for asthma management and prevention: GINA executive summary. *Eur Respir J.* 2008;31(1):143–178.
35. Kowal K, Bodzenta-Lukaszyk A, Pampuch A, et al. Analysis of -675 4g/5G SERPINE1 and C-159T CD14 polymorphisms in house dust mite-allergic asthma patients. *J Invest Allergol Clin Immunol.* 2008;18(4):284–292.
36. Lis G, Kostyk E, Sanak M, Pietrzyk JJ. Badania molekularne w populacji dzieci chorych na astmę oskrzelową. Cz.1. Polimorfizm regionu promotorowego genu CD14. *Pneumonol Alergol Pol.* 2001;69(5–6):265–272.
37. Zabrowski T, Wojas-Krawczyk K, Krawczyk P, et al. The effect of CD14 and TLR4 gene polymorphisms on the occurrence of atopic and non-atopic asthma. *Adv Clin Exp Med.* 2011;20(4):413–421.
38. Rennie DC, Karunanayake CP, Chen Y, et al. CD14 gene variants and their importance for childhood croup, atopy and asthma. *Dis Markers.* 2013;35(6):765–771.
39. Sengler C, Haider A, Sommerfeld C, et al; German Multicenter Allergy Study Group. Evaluation of the CD14 C-159T polymorphism in the German Multicenter Allergy Study cohort. *Clin Exp Allergy.* 2003;33(2):166–169.
40. Liang XH, Cheung W, Heng CK, et al. CD14 promoter polymorphisms have no functional significance and are not associated with atopic phenotypes. *Pharmacogenet Genomics.* 2006;16(4):229–236.
41. Nishimura F, Shibasaki M, Ichikawa K, Arinami T, Noguchi E. Failure to find an association between CD14-159C/T polymorphism and asthma: A family-based association test and meta-analysis. *Allergol Int.* 2006;55(1):55–58.
42. Ortiz-Martinez MG, Frias-Belen O, Nazario-Jimenes S, et al. A case-control study of innate immunity pathway gene polymorphisms in Puerto Ricans reveals association of toll-like receptor 2 +596 variant with asthma. *BMC Pulm Med.* 2016;16:112–122.
43. Zambelli-Weiner A, Ehrlich E, Stockton ML, et al. Evaluation of the CD14/-260 polymorphism and house dust endotoxin exposure in the Barbados Asthma Genetics Study. *J Allergy Clin Immunol.* 2005;115(6):1203–1209.
44. De Faria ICJ, de Faria EJ, Toro AADC Ribeiro JD, Bertuzzo CS. Association for TGF- $\beta_1$ , CD14, IL-4, IL-4R and ADAM33 gene polymorphisms with asthma severity in children and adolescents. *J Pediatr (Rio J).* 2008;84(3):203–210.
45. Hussein YM, Hanan AA, Shalaby SM, Ali AA, Alzahrani SS. Toll-like receptor 2 and Toll-like receptor 4 polymorphisms and susceptibility to asthma and allergic rhinitis: A case-control analysis. *Cell Immunol.* 2012;274(1–2):34–38.
46. Kang I, Oh YK, Lee SH, Jung HM, Chae SC, Lee JH. Identification of polymorphisms in the Toll-like receptor gene and the association with allergic rhinitis. *Eur Arch Otorhinolaryngol.* 2010;267(3):385–389.
47. Noguchi E, Nishimura F, Fukai H, et al. An association study of asthma and total serum immunoglobulin E levels for Toll-like receptor polymorphisms in Japanese population. *Clin Exp Allergy.* 2004;34(2):177–183.
48. Kerkhof M, Postma DS, Brunekreef B, et al. Toll-like receptor 2 and 4 genes influence susceptibility to adverse effects of traffic-related air pollution on childhood asthma. *Thorax.* 2010;65(8):690–697.
49. Reijmerink NE, Bottema RWB, Kerkhof M, et al. TLR-related pathway analysis: Novel gene-gene interaction in the development of asthma and atopy. *Allergy.* 2010;65(2):199–207.
50. Bottema RWB, Kerkhof M, Reijmerink NE, et al. Gene-gene interaction in regulatory T-cell function in atopy and asthma development in childhood. *J Allergy Clin Immunol.* 2010;126(2):338–344.



# Comparing radioactive tracers $^{18}\text{F}$ -FDG and $^{18}\text{F}$ -FLT in the staging of diffuse large B-cell lymphoma by PET/CT examination: A single-center prospective study

\*Justyna Rybka<sup>1,B–F</sup>, \*Bogdan Małkowski<sup>2,A–F</sup>, Monika Olejniczak<sup>3,B,C</sup>, Ewa Chmielowska<sup>3,B,C</sup>, Ewelina Sokołowska<sup>4,C</sup>, Kazimierz Kuliczkowski<sup>1,B,E,F</sup>, Tomasz Wróbel<sup>1,A–F</sup>

<sup>1</sup> Department of Hematology, Blood Neoplasms and Bone Marrow Transplantation, Wrocław Medical University, Poland

<sup>2</sup> Department of Positron Emission Tomography and Molecular Imaging, Collegium Medicum, Nicolaus Copernicus University, Toruń, Poland

<sup>3</sup> Department of Oncology, Oncology Centre, Bydgoszcz, Poland

<sup>4</sup> Department of Corporate Finance, University of Gdańsk, Poland

A – research concept and design; B – collection and/or assembly of data; C – data analysis and interpretation; D – writing the article; E – critical revision of the article; F – final approval of the article

Advances in Clinical and Experimental Medicine, ISSN 1899–5276 (print), ISSN 2451–2680 (online)

*Adv Clin Exp Med.* 2019;28(8):1095–1099

## Address for correspondence

Justyna Rybka  
E-mail: rybka.justyna@o2.pl

## Funding sources

None declared

## Conflict of interest

None declared

\* Both authors contributed equally to the work

Received on October 30, 2016  
Reviewed on January 20, 2017  
Accepted on February 18, 2019

Published online on June 18, 2019

## Cite as

Rybka J, Małkowski B, Olejniczak M, et al. Comparing radioactive tracers  $^{18}\text{F}$ -FDG and  $^{18}\text{F}$ -FLT in the staging of diffuse large B-cell lymphoma by PET/CT examination: A single-center prospective study. *Adv Clin Exp Med.* 2019;28(8):1095–1099. doi:10.17219/acem/104558

## DOI

10.17219/acem/104558

## Copyright

© 2019 by Wrocław Medical University  
This is an article distributed under the terms of the Creative Commons Attribution Non-Commercial License (<http://creativecommons.org/licenses/by-nc-nd/4.0/>)

## Abstract

**Background.** Positron emission tomography in combination with computer tomography (PET/CT) is a very important method of imaging patients with non-Hodgkin lymphomas (NHLs). It is used to define the initial grade of the disease and to assess early response to treatment and after chemotherapy. The most commonly used radioactive tracer is  $^{18}\text{F}$ -FDG, but  $^{18}\text{F}$ -FLT seems to be more specific.

**Objectives.** The aim of our study was to compare the staging of diffuse large B-cell lymphoma (DLBCL) with PET/CT examination using  $^{18}\text{F}$ -FLT and  $^{18}\text{F}$ -FDG.

**Material and methods.** The study included 33 patients with newly diagnosed DLBCL (17 women and 16 men). The median age of the patients was 57 years. In each patient, 2 PET/CT examinations were performed before treatment, one using  $^{18}\text{F}$ -FLT and the second using  $^{18}\text{F}$ -FDG.

**Results.** The average maximum  $^{18}\text{F}$ -FDG uptake in the whole group of patients was higher than the average maximum of  $^{18}\text{F}$ -FLT. This was also true of individual patients; however, 3 patients with an aggressive disease course had greater FLT uptake than the other patients.

**Conclusions.** Our analysis suggests that PET/CT exams using  $^{18}\text{F}$ -FLT may be a useful diagnostic tool in patients with DLBCL.

**Key words:** diffuse large B-cell lymphoma, positron emission tomography,  $^{18}\text{F}$ -FLT

## Introduction

Positron emission tomography in combination with computer tomography (PET/CT) is a very important method of imaging patients with lymphomas. It is used to define the initial grade of the disease and to assess early response to treatment and after chemotherapy.<sup>1,2</sup> The most commonly used radiopharmaceutical is 2-deoxy-2-(<sup>18</sup>F) fluorine-D-glucose (<sup>18</sup>F-FDG). It is taken up in all metabolically active tissues, which are distinguished by increased uptake of glucose. After the transport of <sup>18</sup>F-FDG to a cell, phosphorylation to glucose-6-phosphate occurs and <sup>18</sup>F-FDG gathers in the cellular cytoplasm without undergoing further reactions. Malignant cells show increased FDG uptake, especially those proliferating fast.<sup>2</sup> Because of this, PET/CT examination is particularly useful in patients with aggressive lymphomas with a high proliferation rate, such as diffuse large B-cell lymphoma (DLBCL).<sup>3</sup> An undoubted shortcoming of <sup>18</sup>F-FDG is that it is not only taken up by malignant cells. Increased glucose metabolism also appears in the course of inflammatory or infectious lesions, which can lead to false-positive results. This of particular clinical importance in the assessment of a patients' response to treatment in both the early assessment and after chemotherapy. In the case of a false-positive PET/CT examination result, a patient can be unnecessarily qualified for treatment intensification.<sup>4,5</sup> In light of this, other radioactive tracers are being sought which can reduce the risk of false-positive results. Test results have indicated that (<sup>18</sup>F)-fluoro-3'-deoxy-3'-L-fluorothymidine (<sup>18</sup>F-FLT) may be a more specific tracer. It is transported to the cells and, as a result of a reaction with thymidine kinase type 1 (TK1), it undergoes phosphorylation to monophosphate and is used in DNA synthesis. This makes <sup>18</sup>F-FLT a good cell proliferation tracer, in contrast with <sup>18</sup>F-FDG, which reflects only increased glucose uptake.<sup>6–8</sup> There is not much clinical data concerning the use of <sup>18</sup>F-FLT in PET/CT imaging of lymphomas.

The aim of our study was to compare the staging of DLBCL with PET/CT examination using <sup>18</sup>F-FLT and <sup>18</sup>F-FDG.

## Material and methods

The study included 33 patients with newly diagnosed DLBCL (17 women and 16 men). The median age of the examined group was 57 years (range: 20–74 years). Nine patients (27%) were at stage I according to Ann Arbor staging; 13 patients (40%) were at stage II; 6 (18%) were at stage III; and 5 (15%) at stage IV. In 10 patients a bulky mass tumor (>7 cm) was found. Two PET/CT scans were performed on each patient before treatment: one of them using <sup>18</sup>F-FLT and the other with <sup>18</sup>F-FDG. The interval between PET/CT scans did not exceed 7 days. Each patient gave written consent to take part in this study. The study

Table 1. The patients' clinical data

Number of patients	33
Sex	17 females 16 males
Age	57 (range: 20–74)
Ann Arbor stage	I: 9 patients II: 13 patients III: 6 patients IV: 5 patients
B symptoms	15 patients
International Prognostic Index	low: 17 low-intermediate: 3 high-intermediate: 8 high: 5
Median of antigen Ki 67(%)	80 (range: 30–99)
Median D-lactate dehydrogenase level [U/L]	391.5 (range: 240–1,199)
Median beta-2 microglobulin level [mg/dL]	3.0 (1.3–4.9)
Bulky mass	10 patients
Bone marrow involvement	2 patients

protocol was approved by the Wroclaw Medical University Bioethics Commission.

The patients' clinical data is presented in Table 1.

## PET-FDG and PET-FLT examinations

PET/CT examinations using <sup>18</sup>F-FDG were performed in patients who had fasted for 6 h; the concentration of glucose in the blood serum was under 150 mg/dL. Imaging from the cranial base to the upper third of the thighs was performed using Biograph 6 and Biograph mCT scanners (Siemens AG, Munich, Germany) 60 ±10 min after injecting FDG intravenously in doses of 5–7 MBq/kg of body mass. The procedure for the PET/CT using <sup>18</sup>F-FLT was the same: The patients had not eaten for at least 6 h; imaging was performed with Biograph 6 and Biograph mCT scanners 60 ±10 min after administering 350 MBq/kg of FLT. Whole-body CT scanning was used for attenuation correction and anatomical localization. Standard CT scans were undertaken at 120 kV, 100 mAs, 0.8 s rotation with a 1.25-mm slice width, and with no contrast injection. Image interpretation was performed using the Syngovia application and the MI Oncology workstation (Siemens AG).

## PET/CT examination assessment

To ensure proper interpretation, nuclear medicine and radiology specialists read the scans. Any discrepancies in interpretation were resolved by consensus. The tumors were localized according to the CT scans. Increased focal uptake was detected in the tumor and assessed by measuring the maximum standardized uptake value (SUV<sub>max</sub>). Ellipsoidal volumes of interest (VOIs) with the diameter of the particular lesion were placed

in the chosen areas of the highest uptake affected by lymphomas. The  $SUV_{max}$  from these VOIs was calculated according to the standard formula ( $Bq/g \times \text{body weight [g]} / \text{injected activity in Bq}$ ).

FLT uptake was compared with FDG uptake for a particular lesion (lesion-to-lesion analysis). Next, the mean SUV values of individual patients were calculated to eliminate any influence connected with the number of lesions in particular patients. The mean  $SUV_{max}$  values for FLT and FDG in individual patients were compared (patient-to-patient analysis).

The results were analyzed statistically using STATISTICA v. 8.0 software (StatSoft Inc., Tulsa, USA). The statistical analysis was included the Mann–Whitney U test, Student’s t-test, and Pearson and Spearman correlation methods. Differences were considered statistically significant at the  $p < 0.05$  level.

## Results

The first PET examination performed on all the patients was the scan using  $^{18}F$ -FLT, followed by the one using  $^{18}F$ -FDG. The time between tests was from 2 to 7 days. In the whole examined group, a total of 450 avid lesions were revealed. The  $^{18}F$ -FLT PET scan found 28 lesions

in 3 patients that were not avid during the test using  $^{18}F$ -FDG. In the  $^{18}F$ -FDG PET examination, 17 lesions were found in 7 patients that were invisible in the  $^{18}F$ -FLT PET exam. The differences between the lesions discovered with the use of  $^{18}F$ -FDG and  $^{18}F$ -FLT did not entail any changes in the assessments of the degree of disease progression.

### The correlation between FLT and FDG activity

The average  $SUV_{max}$  of F-FDG uptake in the whole group of patients was 11.56 (median 8.6), which was significantly higher than the value of the average  $SUV_{max}$  of F-FLT uptake, which was 8.62 (median 8.4). There was a statistically significant correlation between the F-FDG and F-FLT uptake values (Pearson product–moment correlation coefficient = 0.37). The results are presented in Fig. 1 and Fig. 2.

### Comparison of FDG and FLT uptakes in particular patients

Comparing the average maximum FLT and FDG uptakes between particular patients, it turned out that they were significantly higher in the FDG PET examination than in the FLT PET scan (14.908 vs 7.73) ( $p < 0.05$ ).

### Individual FLT uptake

In 3 patients, the average FLT value was significantly higher ( $p = 0.029$ ) than in other patients. Also, the initial  $SUV_{max}$  of FLT in these 3 patients was clearly higher than their FDG  $SUV_{max}$  ( $7.84 \pm 3.36$  vs  $5.6 \pm 4.67$ ). In all 3 patients with an increased FLT uptake, the disease course was more aggressive than in the rest of the participants. These patients died during treatment. Our results may point to a relationship between intensified F-FLT uptake and a poor clinical course of the disease.

### Correlations between FDG and FLT SUV values and selected factors

In the entire patient population, an analysis was performed of correlations between FDG and FLT activity and D-lactate dehydrogenase (D-LDH) activity, beta-2 microglobulin concentration, International Prognostic Index (IPI) value, and the value of the proliferation marker Ki-67. We found

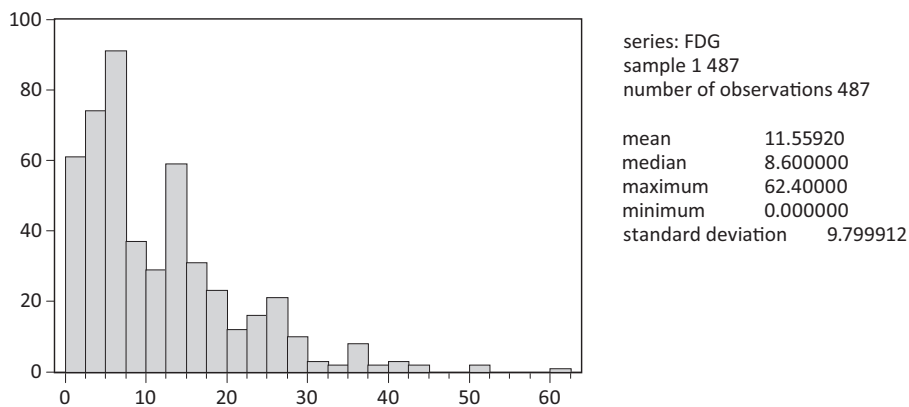


Fig. 1. FDG activity in the entire patient population

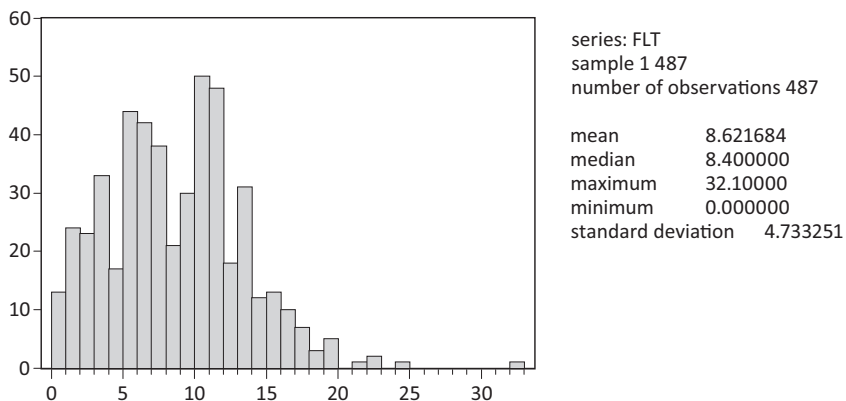


Fig. 2. FLT activity in the entire patient population

**Table 2.** Pearson correlation index for FDG, FLT and selected factors

Factor	FDG	FLT	IPI	Ki67	LDH	B2M
FDG	1.000000	0.581476	-0.172185	0.163427	-0.074044	-0.194903
FLT	0.581476	1.000000	0.267783	0.037243	0.107746	-0.064273
IPI	-0.172185	0.267783	1.000000	-0.108016	0.644455	0.396296
Ki67	0.163427	0.037243	-0.108016	1.000000	-0.049231	-0.229803
LDH	-0.074044	0.107746	0.644455	-0.049231	1.000000	-0.172268
B2M	-0.194903	-0.064273	0.396296	-0.229803	-0.172268	1.000000

FDG – fluorine-D-glucose; FLT – fluoro-deoxy-L-fluorothymidine; IPI – International Prognostic Index; Ki67 – antigen Ki67; LDH – lactate dehydrogenase; B2M – beta-2 microglobulin.

a statistically significant positive correlation between FDG and FLT activity. A positive correlation was also found between FLT and D-LDH activity, although that connection was not statistically significant.

The results are presented in Table 2.

### FLT activity in relation to gender

The tests found a statistically significant difference between the FLT uptake value in women and in men: FLT uptake was higher in women than in men ( $p = 0.0011$ ).

### FDG and FLT activity in the assessment of bone marrow involvement

Each patient in the study population had a bone marrow biopsy performed before the start of chemotherapy. In 2 patients, bone marrow infiltration by lymphoma cells was found in the histopathological examination, although neither the FDG nor the FLT PET exams revealed any bone marrow involvement in either case.

## Discussion

PET-CT examination is at present the imaging standard in aggressive non-Hodgkin lymphomas (NHL), both before the start of a therapy and in assessments after the end of treatment.<sup>3</sup> In high-grade NHL like DLBCL, the true negative rate of the PET-CT results is confirmed after the end of chemotherapy.<sup>9</sup> <sup>18</sup>F-FDG is a radioactive tracer that is commonly used in PET-CT examinations, but due to the non-specificity of FDG uptake, compounds that could decrease the probability of false-positive results are being sought. <sup>18</sup>F-FLT, which was used for the first time by Shields et al., seems to be such a radioactive tracer.<sup>10</sup> That study showed that <sup>18</sup>F-FLT PET results correlate with the cell proliferation degree in solid neoplasms and in lymphomas.<sup>5,11,12</sup> In a group of 20 patients with small cell lung cancer, Everitt et al. conducted <sup>18</sup>F-FLT PET and <sup>18</sup>F-FDG PET scans before the start of treatment and during therapy. It turned out that <sup>18</sup>F-FLT PET was more sensitive test than <sup>18</sup>F-FDG PET.<sup>13</sup> In a study of 20 patients with

breast cancer, <sup>18</sup>F-FLT PET was performed before the start of the treatment and before the second chemotherapy cycle.<sup>14</sup> The  $SUV_{max}$  <sup>18</sup>F-FLT PET value before the treatment significantly correlated with Ki-67 activity, which suggested the role of FLT in defining neoplasm proliferation activity. After the end of chemotherapy a significant decrease in the <sup>18</sup>F-FLT PET  $SUV_{max}$  value was observed in connection with the reduction of the tumor mass.<sup>14</sup> Cho et al. conducted a study using <sup>18</sup>F-FLT PET and <sup>18</sup>F-FDG PET scans in patients with cervical and vaginal cancer before therapy and after the end of chemo- and radiotherapy.<sup>15</sup> The FLT  $SUV_{max}$  value was significantly lower than the FDG  $SUV_{max}$  in the first examination. After treatment, the FLT  $SUV_{max}$  value was much lower regardless of the presence of the inflammatory response after radiotherapy. The study results point to the possibility of monitoring gynecological neoplasm treatment results with <sup>18</sup>F-FLT PET.

The use of <sup>18</sup>F-FLT PET in imaging lymphoid tumors is not a diagnostic standard and there are very few data concerning the use of this method in this group of patients. Lee et al. assessed the role of early <sup>18</sup>F-FLT PET scans as a prognostic index in a group of 61 patients with NHL.<sup>16</sup> The population examined included patients with DLBCL, mantle cell lymphoma (MCL), follicular lymphoma (FL), Burkitt lymphoma, natural killer cell lymphoma, and T-cell lymphoma. <sup>18</sup>F-FLT PET scans were performed before the treatment, after the first chemotherapy cycle and after the treatment. The patients with a positive result in the early <sup>18</sup>F-FLT PET examination had shorter progression-free survival (PFS) and shorter overall survival (OS) in comparison to the patients with negative PET results (PFS 52% vs 80.7% and OS 56.2% vs 81.4%).<sup>16</sup> In a group of 17 patients with FL and FL transformation, Wondergem et al. compared the  $SUV_{max}$  values for <sup>18</sup>F-FLT PET and <sup>18</sup>F-FDG PET. In patients with FL transformation, the  $SUV_{max}$  values for both <sup>18</sup>F-FLT and <sup>18</sup>F-FDG were significantly higher than in the group of patients with FL without transformation. In the population with FL transformation, <sup>18</sup>F-FDG PET revealed higher  $SUV_{max}$  values than <sup>18</sup>F-FLT PET, and the authors of the study therefore suggested that imaging with <sup>18</sup>F-FDG PET is a better diagnostic option in cases of FL transformation.<sup>17</sup>

In the group of 33 untreated DLBCL patients in our study, we compared  $^{18}\text{F}$ -FLT PET and  $^{18}\text{F}$ -FDG PET examinations. In the whole population and also in individual patients,  $\text{SUV}_{\text{max}}$  values for  $^{18}\text{F}$ -FDG were higher than for  $^{18}\text{F}$ -FLT. In 3 patients with an especially aggressive disease course, 28 avid lesions were found in the  $^{18}\text{F}$ -FLT PET examinations that were not visible in the  $^{18}\text{F}$ -FDG PET examination. The  $\text{SUV}_{\text{max}}$  values for  $^{18}\text{F}$ -FLT PET in those patients were significantly higher than their  $^{18}\text{F}$ -FDG PET SUV values. These results suggest that  $^{18}\text{F}$ -FLT PET-CT can be used as an indicator of an aggressive clinical course in patients with DLBCL. In the population we assessed, the  $^{18}\text{F}$ -FLT PET examinations were conducted before the start of therapy. Herrmann et al. conducted  $^{18}\text{F}$ -FLT PET scans in patients with DLBCL before the treatment and a week after the first chemotherapy cycle (rituximab, cyclophosphamide, doxorubicin, vincristine, prednisone).<sup>18</sup> The reduction of  $\text{SUV}_{\text{max}}$  values for  $^{18}\text{F}$ -FLT after the first chemotherapy cycle was significantly higher in patients who achieved complete remission after chemotherapy. It seems that early  $^{18}\text{F}$ -FLT PET examinations can be useful in assessing the efficacy of treatment.<sup>18</sup> In aggressive NHLs such as DLBCL, a negative PET test result has a confirmed predictive value after the end of treatment. However, early  $^{18}\text{F}$ -FDG PET scans can carry a risk of false-positive results in connection with the immunochemotherapy used, which can lead to reactive changes caused by treatment itself.

We also noticed that in our study group  $^{18}\text{F}$ -FLT values were significantly higher in the females than in the males. This observation requires further analysis in a larger patient population.

## Conclusions

The results of our study suggest that  $^{18}\text{F}$ -FLT PET-CT can be a useful diagnostic method in the assessment of patients with DLBCL. Data from the available literature also indicates this. Our analysis concerned a small group of patients and the results are preliminary, requiring confirmation in a larger population of patients.

## References

1. Kirby AM, Mikhaeel NG. The role of FDG-PET in the management of lymphoma: Practical guidelines. *Nucl Med Commun.* 2007;28(5): 355–357.
2. Been LB, Suurmeijer A, Cobben D, Jager PL, Hoekstra HJ, Elsinga PH. ( $^{18}\text{F}$ ) FLT-PET in oncology: Current status and opportunities. *Eur J Nucl Med Mol Imaging.* 2004;31(12):1659–1672.
3. Moskowitz CH. Interim PET-CT in the management of diffuse large B-cell lymphoma. *Hematology Am Soc Hematol Educ Program.* 2012; 2012:397–401.
4. Allen-Auerbach M, de Vos S, Czernin J. PET/computed tomography and lymphoma. *Radiol Clin North Am.* 2013;51(5):833–844.
5. Buck AK, Bommer M, Stilgenbauer S, et al. Molecular imaging of proliferation in malignant lymphoma. *Cancer Res.* 2006;66(22): 11055–11061.
6. Barthel H, Cleij MC, Collingridge DR, et al. 3'-deoxy-3'-( $^{18}\text{F}$ ) fluorothymidine as a new marker for monitoring tumor response to antiproliferative therapy in vivo positron emission tomography. *Cancer Res.* 2003;63(13):3791–3798.
7. Wang R, Zhu H, Chen Y, et al. Standardized uptake value based evaluation of lymphoma by FDG and FLT PET/CT. *Hematol Oncol.* 2014; 32(3):126–132.
8. Omid S, Shields T, Shields AF. PET imaging of proliferation with pyrimidines. *J Nucl Med.* 2013;54(6):903–912.
9. Tilly H, Dreyling M. Diffuse large B-cell lymphoma: ESMO Clinical Practice Guidelines for diagnosis, treatment and follow up. *Ann Oncol.* 2010;21:172–174.
10. Shields AF, Grierson JR, Kozawa SM, Zheng M. Development of labeled thymidine analogs for imaging tumor proliferation. *Nucl Med Biol.* 1996;23(1):17–22.
11. Bading JR. Kinetic analysis of  $^{18}\text{F}$ -FLT PET in lung tumors. *J Nucl Med.* 2012;53(3):506–507.
12. Eckel F, Herrmann K, Schmidt S, et al. Imaging of proliferation in hepatocellular carcinoma with the in vivo marker  $^{18}\text{F}$ -fluorothymidine. *J Nucl Med.* 2009;50(9):1441–1447.
13. Everitt SJ, Ball DL, Hicks RJ, et al. Differential  $^{18}\text{F}$ -FDG and  $^{18}\text{F}$ -FLT uptake on serial PET/CT imaging before and during definitive chemoradiation for non-small cell lung cancer. *J Nucl Med.* 2014;55(7): 1069–1074.
14. Woolf DK, Beresford M, Li SP, et al. Evaluation of FLT-PET-CT as an imaging biomarker of proliferation in primary breast cancer. *Br J Cancer.* 2014;110(12):2847–2854.
15. Cho LP, Kim CK, Viswanathan AN. Pilot study  $^{18}\text{F}$ -fluorothymidine PET/CT in cervical and vaginal cancers before and after external beam radiation. *Gyn Oncol Rep.* 2015;14:34–37.
16. Lee H, Kim S, Kim Y, et al. Early determination of prognosis by interim  $^{39}\text{deoxy-}^{39}\text{F}$ -fluorothymidine PET in patients with non-Hodgkin lymphoma. *J Nucl Med.* 2014;55(2):216–222.
17. Wondergem MJ, Rizvi SNF, Jauw Y, et al.  $^{18}\text{F}$ -FDG or 3'-deoxy-3'- $^{18}\text{F}$ -fluorothymidine to detect transformation of follicular lymphoma. *J Nucl Med.* 2015;56(2):216–221.
18. Herrmann K, Buck AK, Schuster T, et al. Week one FLT-PET response predicts complete remission to R-CHOP and survival in DLBCL. *Oncotarget.* 2014;5(12):4050–4059.



# IgG plasma cells initiate changes in the protein C system in mouse ulcerative colitis through CD14<sup>+</sup>CD64<sup>+</sup> macrophage activation

Xu Hong Lin<sup>1,D</sup>, Hui Chao Wang<sup>2,B</sup>, Yong Yu Li<sup>3,E</sup>, Jun Ling Guo<sup>4,C</sup>, Yu Xia Li<sup>1,B</sup>, Guan Chang Cheng<sup>4,A</sup>, Dan Dan Wei<sup>1,F</sup>, Rui Lin Yang<sup>1,C</sup>, Jun Jie Zhang<sup>5,F</sup>, De Sheng Yang<sup>6,B</sup>, Bin Wang<sup>1,B</sup>, Xue Qun Ren<sup>5,A</sup>

<sup>1</sup> Department of Clinical Laboratory, Translational Medicine Center, Huaihe Hospital Affiliated to Henan University, Kaifeng, China

<sup>2</sup> Department of Nephrology, First Affiliated Hospital of Henan University, Kaifeng, China

<sup>3</sup> Department of Pathophysiology, Tongji University School of Medicine, Shanghai, China

<sup>4</sup> Department of Cardiovascular Medicine, Huaihe Hospital Affiliated to Henan University, Kaifeng, China

<sup>5</sup> Department of General Surgery, Huaihe Hospital Affiliated to Henan University, Kaifeng, China

<sup>6</sup> Department of Gastroenterology, Huaihe Hospital Affiliated to Henan University, Kaifeng, China

A – research concept and design; B – collection and/or assembly of data; C – data analysis and interpretation;

D – writing the article; E – critical revision of the article; F – final approval of the article

Advances in Clinical and Experimental Medicine, ISSN 1899–5276 (print), ISSN 2451–2680 (online)

*Adv Clin Exp Med.* 2019;28(8):1101–1110

## Address for correspondence

Xue Qun Ren

E-mail: 800726lxh@tongji.edu.cn

## Funding sources

This work was supported with grants from the National Natural Science Foundation of China (grant No. 81500430 to Dr. Xu Hong Lin, No. U1304802 to Dr. Xu Hong Lin and No. 31571181 to Prof. Yong Yu Li).

## Conflict of interest

None declared

## Acknowledgements

The authors are grateful to the National Natural Science Foundation of China for grants that supported this work.

Received on July 11, 2017

Reviewed on October 24, 2017

Accepted on August 9, 2018

Published online on August 8, 2019

## Cite as

Lin XH, Wang HC, Li YY, et al. IgG plasma cells initiate changes in the protein C system in mouse ulcerative colitis through CD14<sup>+</sup>CD64<sup>+</sup> macrophage activation. *Adv Clin Exp Med.* 2019;28(8):1101–1110. doi:10.17219/acem/94160

## DOI

10.17219/acem/94160

## Copyright

© 2019 by Wrocław Medical University

This is an article distributed under the terms of the Creative Commons Attribution Non-Commercial License (<http://creativecommons.org/licenses/by-nc-nd/4.0/>)

## Abstract

**Background.** Inhibition of the protein C system (PCS) might be one of the mechanisms of ulcerative colitis (UC).

**Objectives.** The aim of the study was to explore the role of IgG plasma cells in changes in the PCS in UC.

**Material and methods.** Dextran sulfate sodium (DSS) was chosen to induce mouse UC. Inflammation was assessed using hematoxylin & eosin (H&E) staining and immunofluorescence. The profiling of colonic plasma cells and macrophages from colitis mice was analyzed with flow cytometry. After stimulation of macrophages with IgG type immune complex (IgG-IC), western blot was used to determine tumor necrosis factor  $\alpha$  (TNF- $\alpha$ ) and interleukin 6 (IL-6) protein levels. After co-incubation of colonic mucosa microvascular endothelial cells (MVECs) with TNF- $\alpha$  or IL-6, mitogen-activated protein kinase (MAPK) expression was detected.

**Results.** The DSS-colitis mice showed higher inflammatory indexes ( $p < 0.05$  or  $p < 0.01$ ), accompanied by greater infiltration of CD38<sup>+</sup>IgG<sup>+</sup> plasma cells ( $p < 0.01$ ), CD14<sup>+</sup>CD64<sup>+</sup> macrophages ( $p < 0.01$ ) and IgG-IC than healthy mice. Enhancement of TNF- $\alpha$  and IL-6 protein expression was demonstrated in this subset of macrophages when stimulated by IgG-IC ( $p < 0.01$ ). After MVECs were incubated with TNF- $\alpha$  or IL-6, the expression of  $\beta$ -arrestin1, pP38 MAPK and pJNK MAPK exhibited an increase ( $p < 0.05$  or  $p < 0.01$ ), but downregulation of endothelial protein C receptor (EPCR) expression was observed ( $p < 0.05$  or  $p < 0.01$ ); this inhibition of EPCR expression was reversed by SB203580, SP600125 or U0126 ( $p < 0.05$  or  $p < 0.01$ ). In addition, changes in activated protein C (APC) presented results similar to those for EPCR expression ( $p < 0.05$  or  $p < 0.01$ ).

**Conclusions.** These results reveal that the PCS is inhibited during UC processing. There is a possibility that the interaction between IgG plasma cells and CD14<sup>+</sup>CD64<sup>+</sup> macrophages, as well as further secretion of cytokines from CD14<sup>+</sup>CD64<sup>+</sup> macrophages by the formation and stimulation of IgG-IC, subsequently influence MVECs through the  $\beta$ -arrestin-MAPK pathway. Enhancement of PCS activity may represent a novel approach for treating UC.

**Key words:** macrophages, ulcerative colitis, MAPK, protein C system, plasma cells

Ulcerative colitis (UC), the primary type of inflammatory bowel disease (IBD), is a recurrent, chronic intestinal inflammation of unknown cause, and a high risk of cancer is known to be associated with this disease.<sup>1</sup> Recently, the incidence of UC in China has rapidly increased, and as a consequence has gained more attention from researchers. Because of its unknown etiology, long course and the variety in the presentation of the lesions, it is often difficult to cure, and has become a very common treatment-resistant digestive disease.

The pathogenesis of UC is not fully understood. Recent research has revealed that IBD-induced pathogenesis extends beyond typical immune cells; however, non-immune cells, for example colonic mucosal microvascular endothelial cells (MVECs), are also involved in the pathological process.<sup>2</sup> Because the development of UC entails an interaction between the coagulation system and inflammation, hypercoagulation is a complication often found in patients. This complication manifests as microthrombus formation and microcirculation disturbance,<sup>3</sup> which develop into the primary disease. Damage to endothelial cells plays a vital role in the process of coagulation activation in UC patients, while the protein C system (PCS) is a major mediator of endothelial cell function. Recent studies have shown that the PCS plays a regulative role both in human MVECs and murine colitis.<sup>4,5</sup> Therefore, an imbalance of the PCS may induce the mediators of pathogenesis in UC patients. Our previous research showed that colon mucosal macrophages acted on mucosal MVECs by secreting pro-inflammatory cytokines and further inhibiting the PCS.<sup>6</sup>

At present, it is unclear what precisely is the initiator of PCS inhibition by macrophages. Studies have shown that redundant activation of humoral immunity is closely related to the pathological process of UC,<sup>7</sup> and acute UC is accompanied by activation of the humoral immune response. Lamina propria lymphocytes (mainly activated B cell subtypes) have been found to be an important source of immunoglobulins and autoantibodies. Plasma cells are the terminal effector cells derived from the development and differentiation of B lymphocytes in the connective tissue. Plasma cells have the important function of synthesizing and secreting antibodies, which they distribute mainly to the mucosa. Our previous research found that a large number of plasma cells accumulated in the colonic mucosa of DSS-colitis mice,<sup>6</sup> while neither the profiling of plasma cells involved in UC nor the interaction between plasma cells and macrophages in inhibiting the PCS have been elucidated. Therefore, exploring the changes and mechanisms of the PCS in UC pathology, as well as finding new drug targets, are of great importance.

In order to investigate the relationship and mechanisms between the PCS and UC, we used a DSS-induced model of colitis for this study. Topics covered in the discussion section primarily include the role of regulative signals of inflammation-coagulation, further elucidation of the pathological mechanism of UC *in vivo* and *in vitro*,

the pathway of plasma cells-IgG-IC-macrophages-pro-inflammatory cytokines-MVECs-PCS during UC, as well as theoretical and experimental evidence for elucidating the mechanism and exploring new drugs for UC treatment.

## Material and methods

### The animals

C57BL/6J mice, 6–8 weeks old, half male and female (22–24 g,  $n = 70$ ), were provided by the Laboratory Animal Center of Henan Province, Zhengzhou, China (Certificate No. SCXK (YU) 2015-0004). The mice were housed in a standard environment for 1 week ( $24 \pm 1^\circ\text{C}$ , natural light-dark cycle) and were granted free access to normal tap water and standard rodent chow. The mice were fasted for 12 h before the experiment, and were randomly assigned to their respective groups. In the present study, 5 experiments were performed: 1) for histological evaluation and plasma cells (both the control group ( $n = 8$ ) and the UC group ( $n = 8$ )); 2) for macrophages both at the histological level and at the cellular level (both the control group ( $n = 8$ ) and the UC group ( $n = 8$ )); 3) for immune complex (both groups; ( $n = 8$  each)); 4) for macrophage isolation and stimulation (only non-UC mice were used ( $n = 8$ ), and were divided into control group and IgG-IC group); 5) for MVEC isolation and stimulation (only non-UC mice were used ( $n = 8$ ), and were divided into control group, tumor necrosis factor  $\alpha$ /interleukin 6 (TNF- $\alpha$ /IL-6) group, SB203580 group, SP600125 group, and U0126 group). All the animal experimental procedures complied with international principles for the care and use of laboratory animals. The procedures were conducted in accordance with guidelines from the Animal Ethics Committee of the Henan University School of Medicine, Kaifeng, China.

### Induction of experimental murine colitis

Experimental ulcerative colitis was induced in 30 mice by providing them with 4% DSS (Sigma-Aldrich, St. Louis, USA) as the sole source of drinking water for 7 consecutive days, according to the method described by Schicho et al.<sup>8</sup> During these 7 days, the weight, general physical condition, stool characteristics, and gross and occult blood of the mice were measured daily. The death rate in the DSS-induced UC group left 8 mice in each experiment (1, 2 and 3) by the end of this period; at the end, all the surviving mice were sacrificed by cervical dislocation. Plasma was prepared by centrifugation of blood samples at 12,000 g,  $4^\circ\text{C}$ , for 10 min, then frozen at  $-80^\circ\text{C}$ . A colon segment was cut longitudinally 1 cm above the anus, carefully rinsed with normal saline, and then weighed and measured for length and macroscopic scoring. The detached colon was separated into several parts. Some tissues were used for



the isolation of plasma cells and macrophages, some tissues were immediately fixed in 10% neutral-buffered formalin for histological analysis and immunofluorescence, while others were preserved at  $-80^{\circ}\text{C}$  for F4/80 staining.

## Macroscopic scoring

The macroscore was documented based on the evaluation system devised by Hartmann et al.,<sup>9</sup> namely: 1) body weight loss from baseline (0 points: none, 1 points: 1–5%, 2 points: 5–10%, 3 points: 10–20%, 4 points: more than 20%); 2) stool consistency (0 points for normal stools, 2 points for loose and pasty stools that failed to stick to the anus, 4 points for liquid stools that remained adhesive to the anus); 3) bleeding (0 points for a negative hemocult test, 2 points for a positive one, 4 points for any gross bleeding from the rectum). A total clinical score ranging from 0 (healthy) to 4 (the maximum score for DSS-induced colitis) was obtained by dividing the sum of the above scores by 3.

## Histology evaluation

Colon segments were fixed as described above and then dehydrated and embedded in paraffin. The tissue was sliced into 5- $\mu\text{m}$  slices, stained with hematoxylin and eosin (H&E), and observed under a microscope to evaluate the degree of tissue damage. An experienced blinded researcher evaluated 5 sections for each colon sample and scored them as described by Kihara et al.<sup>10</sup> Each score was assessed as follows: 1) inflammation severity (0 points: none; 1 points: mild; 2 points: moderate; 3 points: severe); 2) inflammation extent (0 points: none; 1 points: mucosa; 2 points: submucosa; 3 points: transmural); 3) crypt damage (0 points: none; 1 points: basal 1/3 damage; 2 points: basal 2/3 damage; 3 points: crypt lost, surface epithelium present; 4 points: crypt and surface epithelium lost); 4) percent involvement (0 points: 0%; 1 points: 1–25%; 2 points: 26–50%; 3 points: 51–75%; 4 points: 76–100%). The total histologic score, ranging from 0 to 14, was obtained by adding the 4 subscores.

## Isolation and identification of the phenotype of mouse colonic plasma cells

The immunomagnetic bead technique was used to purify CD54<sup>+</sup> cells (BD Pharmingen, Heidelberg, Germany) as described by Medina et al.<sup>11</sup> Using this method, lamina propria cells were obtained and stained with anti-CD54<sup>+</sup> antibody for 10 min, followed by adjustment to a concentration of  $1 \times 10^7/\text{mL}$ . Dynabeads<sup>TM</sup> Goat Anti-Mouse IgG (Invitrogen, Thermo Fisher Scientific, Waltham, USA) were applied to isolate plasma cells through a magnetic separator. The phenotype of the plasma cells was tested using flow cytometry with anti-IgA, IgG, IgM, and CD38 antibody, respectively.

## Macrophage evaluation in colonic smooth muscle

Macrophages were visualized using F4/80 staining according to the method described by Li et al.<sup>12</sup> Briefly, the staining was performed by pre-incubation of whole-mount preparations of colonic smooth muscle in 10% normal goat serum (NGS) in phosphate-buffered saline (PBS) for 1 h at room temperature, followed by incubation with the primary antibody (F4/80, rat anti-mouse MCA 497, 1:1 in PBS) overnight at  $4^{\circ}\text{C}$ . The specimens were incubated with a secondary antibody – Alexa Fluor 488 donkey anti-rat, 1:100 in PBS (Invitrogen) – for 1 h at room temperature, and were then mounted in Eukitt<sup>®</sup> quick-hardening mounting medium (Sigma-Aldrich). Phosphate-buffered saline was used as negative control, and the macrophages in the colonic smooth muscle strips were counted.

## Isolation and identification of mouse colonic macrophages

Mouse colonic macrophages were isolated and cultured in accordance with the method described by Chen et al.<sup>13</sup> In brief, the mouse colon was cut longitudinally, quickly placed into Hanks solution containing 1 g/L ethylenediaminetetraacetic acid (EDTA) at  $37^{\circ}\text{C}$  for 60 min, and then subjected to further digestion with 1 g/L collagenase for 2 h. The cell suspensions were resuspended in ISO osmotic fluid and the precipitation was collected. After staining with CD14 monoclonal fluorescent antibody (BD Pharmingen), intestinal macrophages were identified with flow cytometry.

## Determination of macrophage type using flow cytometry

To determine the properties of the macrophages that participate in the pathogenesis of UC, the macrophage receptors were tested as previously described.<sup>14</sup> In brief, the cell concentration was adjusted to  $1 \times 10^6/\text{mL}$ , and labeled antibodies CD16/32 (eBioscience, Thermo Fisher Scientific) or CD64 (BioLegend, San Diego, USA) were added and incubated with the samples. The cells were resuspended in PBS and centrifuged; after resuspension with PBS, the samples were subjected to flow cytometry.

## IgA, IgM or IgG type immune complex in colonic tissue using immunofluorescence

After routine dewaxing and hydration, antigens were retrieved through the use of immunohistochemistry. Next, 5% bovine serum albumen (BSA) was used to block the specimens, after which primary antibodies anti-IgA, anti-IgM and anti-IgG (Southern Biotech, Birmingham, USA) were added and then incubated for 1 night at  $4^{\circ}\text{C}$ . Next, the slides were incubated for 1 h with

fluorescent-labeled secondary antibodies protected from light, followed by 4',6-diamidino-2-phenylindole (DAPI) staining and glycerol mounting.

## TNF- $\alpha$ and IL-6 protein expression in the macrophages

IgG type immune complex (IgG-IC) was mimicked with the plate-immobilized IgG method as described by Uo et al.<sup>14</sup> Isolated macrophages from normal mice, stimulated with IgG-IC or soluble human IgG (hIgG), were collected and the protein concentration in the supernatant was tested. Colonic macrophages were collected and prepared in lysis buffer for western blotting in accordance with the method described previously.<sup>15</sup> Primary antibodies – rabbit anti-TNF- $\alpha$  and rabbit anti-IL-6 (both from Abcam, Cambridge, UK) – were used at a concentration of 1:500, and the  $\beta$ -actin antibody (Abcam) was used at a concentration of 1:1,000. Then the secondary antibody, Pierce<sup>®</sup> Goat Anti-Rabbit IgG (H+L) (Thermo Fisher Scientific), was added at a concentration of 1:10,000 and incubated for 1.5 h at room temperature. Photos were taken with the Bio-Rad ChemiDoc XRS+ imaging system (Bio-Rad Laboratories, Hercules, USA) and analyzed using an image analysis system in order to determine the optical density of the bands.

## Isolation and culture of colonic mucosa MVECs

Colonic mucosa MVECs were isolated using the method described by Scaldaferrri et al.<sup>16</sup> Murine colonic tissues were digested enzymatically (37°C, 0.25% trypsin, 1 mL) and then cultured for 96 h in MCDB 131 medium containing 20% serum,  $1 \times 10^5$  IU/L penicillin, heparin, 0.1 g/L streptomycin, endothelial cell growth factor, and 0.584 g/L glutamine. After digestion, the cell suspension was collected and cultured in fresh medium for 72 h. The purified cells were digested using cell dissociation buffer and cultured in fresh medium to determine factor VIII activity. The 3<sup>rd</sup> generation cells were used for further investigation.

## Activated protein C activity change induced by IL-6 or TNF- $\alpha$ in MVECs by chromogenic substrate

Following the method described by Zhang et al.,<sup>17</sup> colonic mucosa MVECs were incubated with IL-6 or TNF- $\alpha$  for 24 h in the presence of SB203580, SP600125 or U0126, and washed 3 times in Tris-buffered saline (TBS) containing 50 mM Tris-HCl, 120 mM NaCl, 2.7 mM KCl, and 3 mg/mL BSA. Then 200 nM of protein C (Enzyme Research Laboratories, Swansea, UK) and 0.6 U/mL thrombomodulin (TM) were incubated for 1 h at 37°C, and a chromogenic substrate (Chromogenix; Diapharma Group, West Chester, USA) was used to test APC activity.

## Effects of IL-6 or TNF- $\alpha$ on the expression of EPCR, TM, $\beta$ -arrestin1, pP38 MAPK, pJNK MAPK, and pERK MAPK of colonic mucosa MVECs measured using western blot

Next, to determine the signal pathway involved in the inhibition of the PCS in UC, MVECs were used to test the expression of endothelial protein C receptor (EPCR), TM,  $\beta$ -arrestin1, pP38 mitogen-activated protein kinase (MAPK), pJNK MAPK, and pERK MAPK with western blot, using their respective antibodies. Primary antibodies goat anti-EPCR, rabbit anti-TM and goat anti-pJNK MAPK (all from Santa Cruz Biotechnology, Santa Cruz, USA) were used here at a concentration of 1:500; rabbit anti- $\beta$ -arrestin1, rabbit anti-pP38 MAPK, and rabbit anti-pERK MAPK (all from Abcam) were used here at a concentration of 1:500; and the  $\beta$ -actin antibody (Abcam) was used at a concentration of 1:1,000.

## Statistical analysis

The data was compiled and expressed as means  $\pm$  standard error of the mean (SEM). To determine statistical significance, all the data was analyzed using the independent-samples t-test or one-way analysis of variance (ANOVA) followed by the post hoc test of least significant difference (LSD) for multiple comparison test using SPSS v. 13.0 software (SPSS Inc., Chicago, USA). P-values <0.05 were regarded as statistically significant.

## Results

### Macroscopic scores elevated in DSS-induced colitis

The mice that consumed 4% DSS as the sole source of drinking water for 7 days ( $n = 8$ ) developed severe colitis, manifested as colon length shortening ( $p < 0.01$ ), increased spleen weight ( $p < 0.05$ ) and bloody stools, which typically appeared after 3–4 days and continued until the end of the experimental period (Table 1). The macroscopic scores ( $p < 0.01$ ) are presented in Table 1.

Table 1. Pathological impairment parameters, macroscopic scores and microscopic scores of DSS-induced ulcerative colitis (UC) in mice ( $n = 8$  per group)

Variable	Control	UC
Body weight (% of 0 day)	103.1 $\pm$ 5.6	88.3 $\pm$ 3.6
Colon length [cm]	7.2 $\pm$ 0.4	2.9 $\pm$ 0.4**
Spleen weight (% of control)	100.2 $\pm$ 5.4	121.3 $\pm$ 6.9*
Macroscopic scores	0	3.5 $\pm$ 0.3**
Microscopic scores	0	8.9 $\pm$ 0.6**

\* $p < 0.05$  and \*\* $p < 0.01$  vs the control group.

## Microscopic score increased in DSS-induced colitis

Histological examination of the control group animals (n = 8) revealed no signs of colitis. By contrast, the group treated with DSS presented obvious colitis, manifested as multiple erosive lesions, loss of complete crypts in the colon (Table 1), with evident infiltration of inflammatory cells into the colonic submucosa, leading to a higher histological score compared to the controls (p < 0.01, Table 1).

## IgG type plasma cells and CD14<sup>+</sup>CD64<sup>+</sup> macrophages infiltrate the inflamed mucosa of DSS-induced colitis

Our previous research confirmed that CD38 and CD54 staining showed positive expression in the submucosa

of DSS-induced colitis, and a significantly increased number of CD38<sup>+</sup>CD54<sup>+</sup> cells.<sup>18</sup> In the present study, our further analysis was consistent with those results: CD38 and IgG expression were upregulated in isolated plasma cells from the DSS mouse colons (Fig. 1A–C, p < 0.01), while the number of CD38<sup>+</sup>IgM<sup>+</sup> and CD38<sup>+</sup>IgA<sup>+</sup> plasma cells from the DSS mouse colons had not changed in comparison with the controls (Fig. 1A–C, p > 0.05).

F4/80 staining showed that the quantity of macrophages was increased in the DSS mouse colons (Fig. 2A). In order to further determine the profile of the macrophages, the macrophages were separated and identified. The results revealed that the heavily infiltrated macrophages in UC have a unique phenotype: CD14<sup>+</sup>CD64<sup>+</sup> (Fig. 2B–E, p < 0.01); the quantity of CD14<sup>+</sup>CD16/32<sup>+</sup> macrophages was not affected (Fig. 2B–E, p > 0.05).

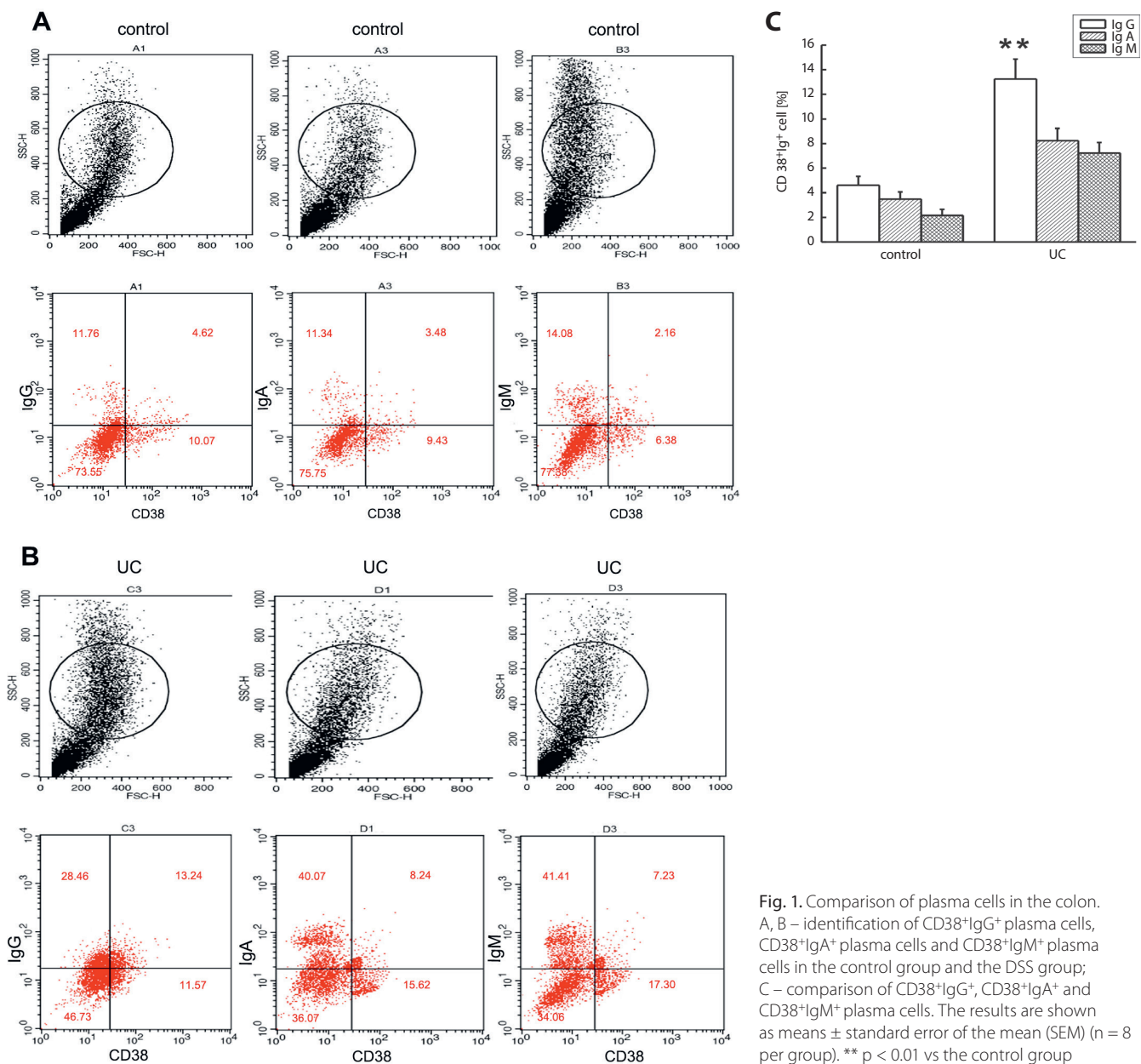


Fig. 1. Comparison of plasma cells in the colon. A, B – identification of CD38<sup>+</sup>IgG<sup>+</sup> plasma cells, CD38<sup>+</sup>IgA<sup>+</sup> plasma cells and CD38<sup>+</sup>IgM<sup>+</sup> plasma cells in the control group and the DSS group; C – comparison of CD38<sup>+</sup>IgG<sup>+</sup>, CD38<sup>+</sup>IgA<sup>+</sup> and CD38<sup>+</sup>IgM<sup>+</sup> plasma cells. The results are shown as means ± standard error of the mean (SEM) (n = 8 per group). \*\* p < 0.01 vs the control group

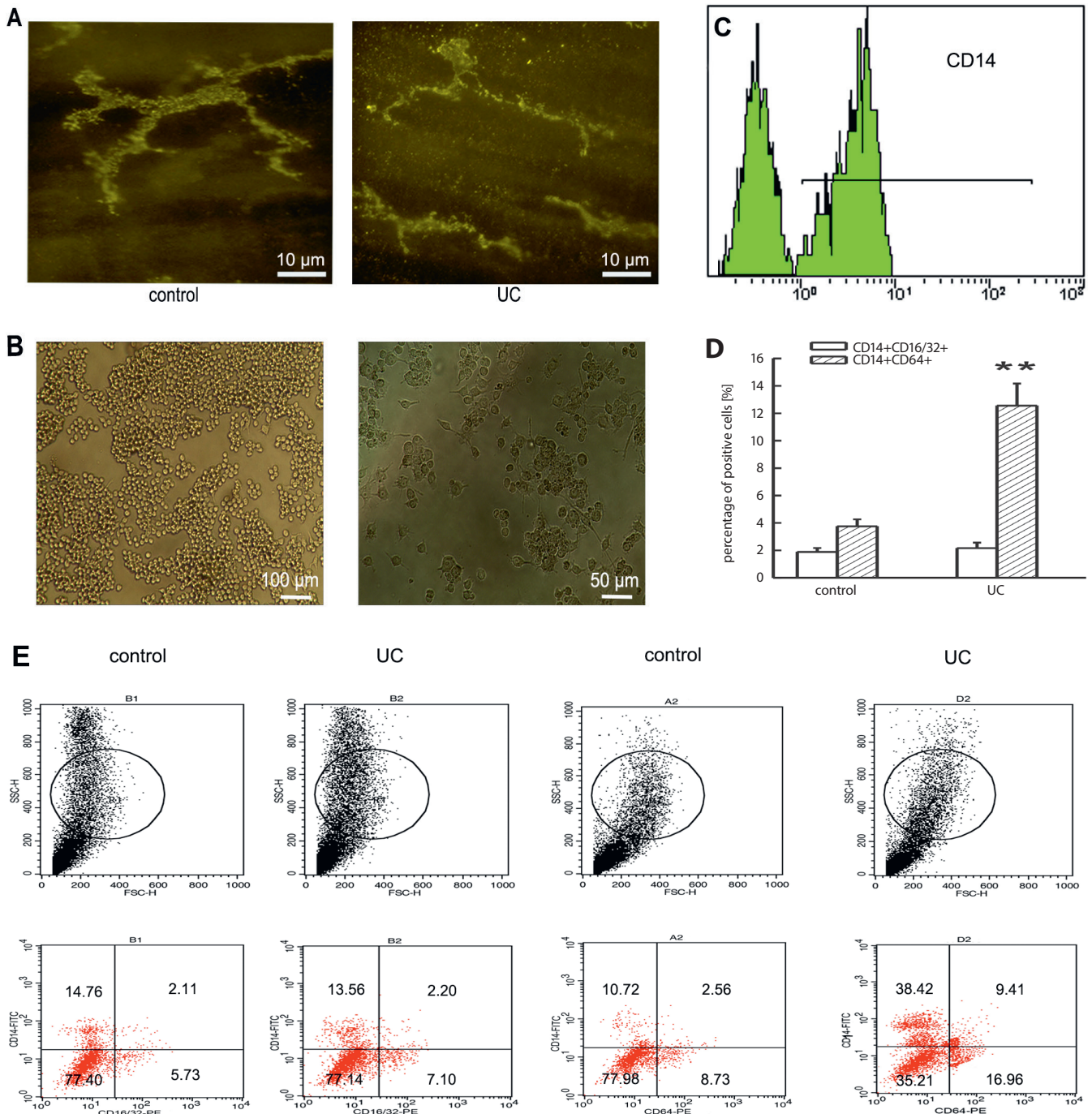


Fig. 2. Comparison of macrophages in the colon. A – F4/80 staining; B, C – isolation and identification of macrophages; D – statistical profiling of CD16/32 or CD64 expression in the control group and UC group; E – CD16/32 and CD64 expression in the control group and UC group. The results are shown as means  $\pm$  standard error of the mean (SEM) (n = 8 per group). \*\*p < 0.01 vs the control group

## IgG type immune complex deposited in colon with DSS-induced colitis

As shown in Fig. 3, IgG-IC was more strongly expressed in the colonic mucosa of the DSS mice when compared to the control group. Vessel walls, especially small vessel walls, and the mesenchymal and glandular epithelia were the main locations of IgG-IC deposition. Low expression of IgA and IgM was found in both the control and the DSS mice.

## Elevated release of pro-inflammatory cytokines from macrophages induced by IgG-IC

The mechanism through which IgG plasma cells contributed to the pathogenesis of UC and the inhibition of PCS remains uncertain. Based on the large deposition of IgG-IC and the increased macrophages in the colonic tissues of DSS colitis, we assessed the potential involvement of IgG-IC-macrophages-pro-inflammatory cytokine

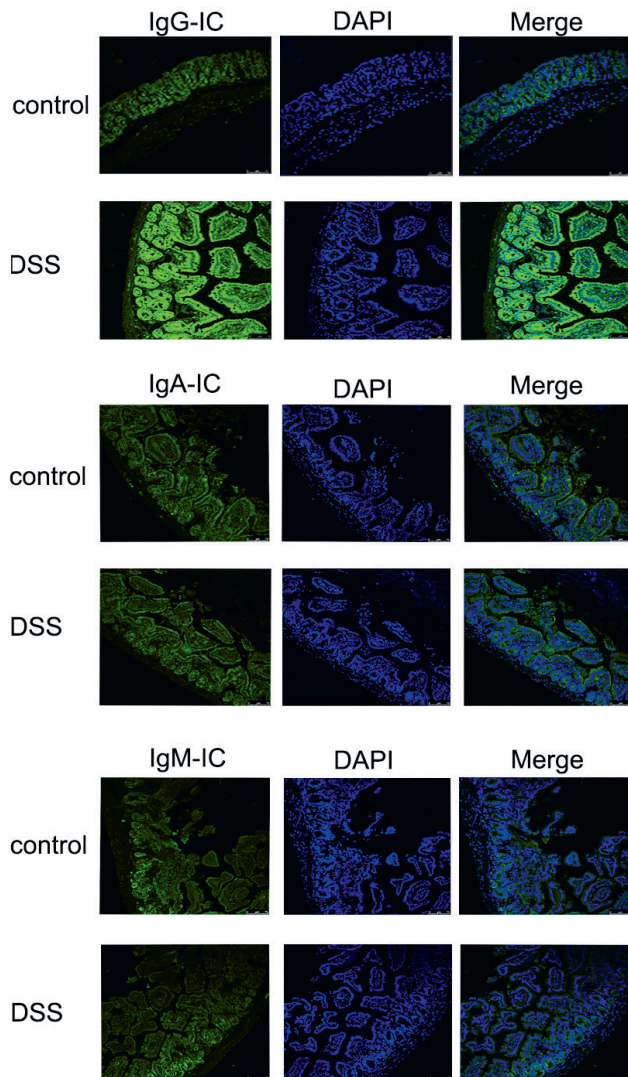


**Fig. 3.** The type of immune complex in colon tissue. The control group and UC group marked by anti-IgA, anti-IgG and anti-IgM antibody (scale bar: 75  $\mu$ m)

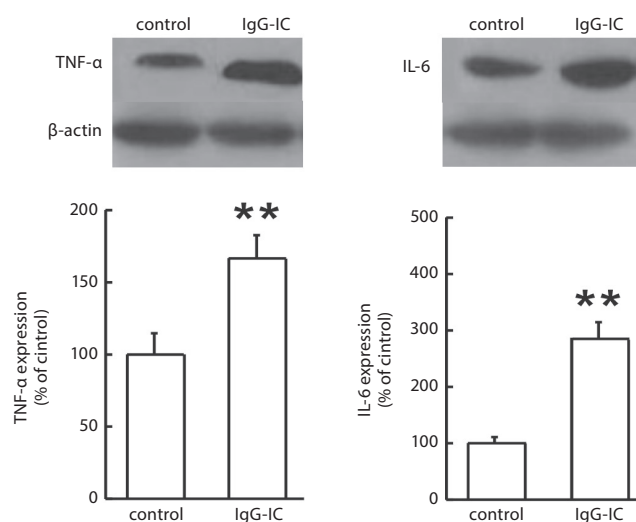


**Fig. 4.** The effect of IgG-IC on TNF- $\alpha$  and IL-6 protein levels in macrophages. The results are shown as means  $\pm$  standard error of the mean (SEM) (n = 8 each group). \*\* p < 0.01 vs the control group

signaling in UC. To confirm the hypothesis, we examined cytokine secretion by macrophages when stimulated with IgG-IC mimicked by the plate-immobilized IgG method. As expected, we found that the TNF- $\alpha$  and IL-6 protein levels were elevated in the macrophages (Fig. 4, p < 0.01).

### Inhibited PCS activity of microvascular cells induced by TNF- $\alpha$ or IL-6

To further explore the detailed mechanism involved in the change in the PCS, we separated and cultured MVECs from colonic mucosa. To identify the cells, we used fluorescence microscopy to detect factor VIII. After incubation with TNF- $\alpha$  or IL-6, APC activity was decreased (p < 0.01, Table 2). The reduction due to TNF- $\alpha$  was reversed by the p38 MAPK inhibitor SB203580 or JNK MAPK inhibitor SP600125; in addition, SB203580 and SP600125 reversed the effect of IL-6 on microvascular cells (p < 0.05 or p < 0.01; Table 2). Meanwhile, after MVECs were incubated with TNF- $\alpha$  or IL-6, the expression of  $\beta$ -arrestin1, pP38 MAPK and pJNK MAPK exhibited an increase (Fig. 5A, p < 0.05 or p < 0.01). The EPCR expression was reduced by TNF- $\alpha$  or IL-6 administration (Fig. 5B, p < 0.05 or p < 0.01). However, TM expression was not affected (Fig. 5B, p > 0.05). Furthermore, the inhibited expression of EPCR was reversed when the TNF- $\alpha$ -stimulated cells were pre-treated with SB203580, SP600125 or U0126 (Fig. 5B, p < 0.05 or p < 0.01), but only SB203580 reversed the effect of IL-6 on microvascular cells (Fig. 5B, p < 0.05); meanwhile, the expression of TM was not influenced by SB203580, SP600125 or U0126 in TNF- $\alpha$ - or IL-6-stimulated MVECs (Fig. 5B, p > 0.05).

**Table 2.** Change in activated protein C (APC) activity induced by tumor necrosis factor  $\alpha$  (TNF- $\alpha$ ) or interleukin (IL-6) in microvascular endothelial cells (MVECs) (n = 8 per group)

Group	APC activity
Control	1.0 $\pm$ 0.1
TNF- $\alpha$	0.6 $\pm$ 0.07**
IL-6	0.4 $\pm$ 0.06**
SB203580+TNF- $\alpha$	0.9 $\pm$ 0.08 <sup>#</sup>
SP600125+TNF- $\alpha$	0.9 $\pm$ 0.07 <sup>#</sup>
U0126+TNF- $\alpha$	0.8 $\pm$ 0.1
SB203580+IL-6	0.7 $\pm$ 0.1 <sup>&amp;</sup>
SP600125+IL-6	0.8 $\pm$ 0.1 <sup>&amp;&amp;</sup>
U0126+IL-6	0.5 $\pm$ 0.07

\*\*p < 0.01 vs the control group; <sup>#</sup>p < 0.05 vs the TNF- $\alpha$  group; <sup>&</sup>p < 0.05 and <sup>&&</sup>p < 0.01 vs the IL-6 group.

## Discussion

Several studies have demonstrated that a large number of IBD patients present with blood hypercoagulability, which includes venous thrombosis and pulmonary

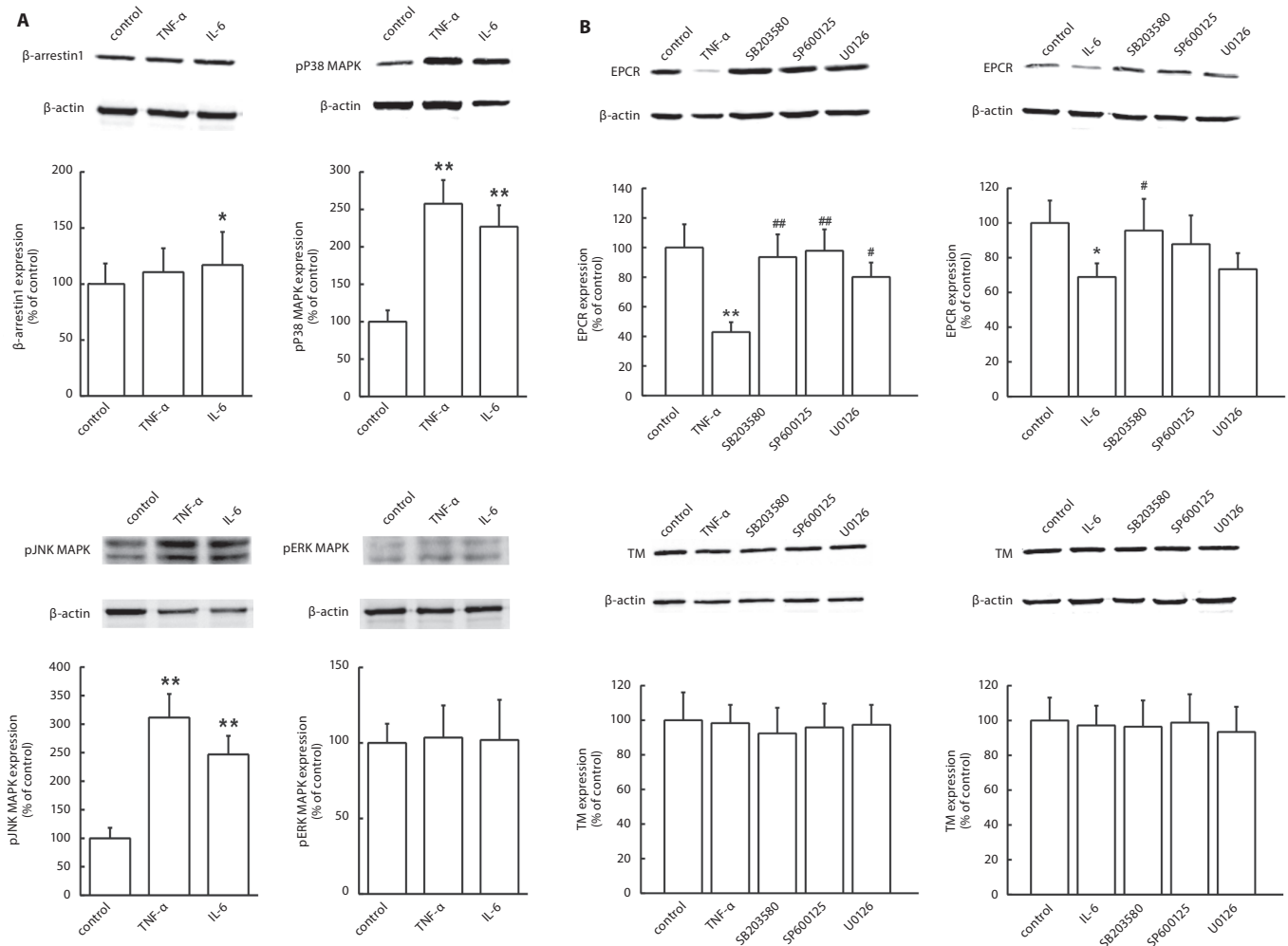


**Fig. 5.** Changes of the PCS in MVECs. A: changes in  $\beta$ -arrestin1, pP38 MAPK, pJNK MAPK, and pERK MAPK protein expression induced by TNF- $\alpha$  or IL-6 in MVECs by western blot; B: changes in EPCR and TM protein expression induced by TNF- $\alpha$  or IL-6 in MVECs by western blot. The results are shown as the means  $\pm$  standard error of the mean (SEM) ( $n = 8$  each group). \* $p < 0.05$ , and \*\* $p < 0.01$  vs the control group; # $p < 0.05$ , and ## $p < 0.01$  vs TNF- $\alpha$  or IL-6 group

embolism.<sup>19–21</sup> Hypercoagulability is accompanied by inflammation and remits when the inflammation disappears. Murthy et al.<sup>22</sup> found that congenital genetic factors do not play a major role in the formation of hypercoagulability in IBD patients. Thrombosis leads to intestinal mucosal ischemia or necrosis and severe ulceration, adding to the intestinal mucosal damage of UC patients. Therefore, thrombosis has been identified as a major contributing factor to the deterioration and death of UC patients.

Until now, no consensus has been reached on the mechanisms involved in coagulation system abnormalities in the pathogenesis of UC,<sup>23,24</sup> while the anticoagulation system is recognized as playing a key role.

The PCS, the most complex and most effective physiological mechanism of anticoagulation, comprises EPCR, protein S (PS), protein C (PC), protein C inhibitor, and TM. It plays an essential role in the regulation of blood coagulation and has a direct effect on maintaining homeostasis of the coagulation and anticoagulation systems.<sup>25</sup> There are few reports about the PCS in UC patients. Ulcerative colitis is closely related to injury of MVECs, and partial

constituents of the PCS are the offspring of endothelial cells. We therefore speculate that the PCS plays a vital role in UC pathogenesis. In our previous research, we observed decreased activity of both PC and PS in the plasma of DSS-induced UC mice, and downregulated expression of EPCR.<sup>6</sup> These findings support the theory that the activity of the PCS is inhibited in DSS-induced mouse colitis, while the detailed mechanism of PCS inhibition remains unclear.

In view of the elevated plasma cells in DSS-induced colitis observed in our previous study,<sup>18</sup> we speculated that plasma cells may play a vital role in UC. It has not been determined whether the infiltrated plasma cells represent the mechanism of PCS inhibition, nor have the definite type and characteristics of the plasma cells involved been identified.<sup>26,27</sup> In order to investigate the changes in the number and type of plasma cells in UC, we observed the number of plasma cells from the inflamed mucosa of UC colons and normal colons using immunofluorescence, and found that the number of plasma cells increased *in vivo*.<sup>18</sup> In addition, flow cytometry was utilized in the present study to test

the number and type of plasma cells from separated lamina propria cells of mouse colonic mucosa. We found that the proportion of CD38<sup>+</sup>IgM<sup>+</sup> plasma cells and CD38<sup>+</sup>IgA<sup>+</sup> plasma cells in the UC mice had not changed when compared to the controls, but CD38<sup>+</sup>IgG<sup>+</sup> plasma cells had increased significantly. These findings provided further confirmation that elevated IgG type plasma cells locally invade the colonic mucosa in UC, and these results were consistent with a recent report on enhanced IgG type plasma cells in UC and other autoimmune diseases.<sup>14</sup> These data suggested that the change in IgG type plasma cells is related to disease activity and plays a vital role in UC.

So far, the detailed mechanism of IgG type plasma cells in UC pathogenesis has not been elucidated. Halstensen et al. reported that IgG and activated immune complexes gather in colonic epithelial cells.<sup>28</sup> Under normal circumstances, tiny amounts of circulatory immune complexes in the body result from the immune response. However, in certain pathophysiological states, decreased phagocytic function of mononuclear macrophages leads to the elevation of immune complexes, furthering the deposition of large amounts of immune complexes on the injured organs. In the present study, DSS-induced colitis showed obvious deposition of immune complexes, mainly of the IgG type. These results were consistent with increased IgG type plasma cells in DSS-induced colitis.

Recent evidence has suggested that macrophages play a key role in homeostasis by inhibiting the dampening of inflammation.<sup>29</sup> In the present study, we found that positive F4/80 staining was higher in the UC mice than in the control group. Considering the increased levels of intestinal mucosa macrophages in UC, we hypothesize that macrophages contribute to inflammation or exacerbate it. Intestinal macrophages were isolated from colonic mucosa of both the UC and control colons, and as expected, the quantity of macrophages in DSS-induced colitis was higher than in the control mice. In addition, no significant differences were observed between DSS-induced colitis mice and normal mice in terms of the number of CD14<sup>+</sup>CD16/32<sup>+</sup> macrophages, and CD14<sup>+</sup>CD64<sup>+</sup> macrophages were significantly increased in DSS-induced colitis. CD64, a member of IgG Fc receptor family, which is mainly expressed on the mononuclear macrophage surface, participates in antibody-dependent cellular cytotoxicity (ADCC) and enhances inflammatory cytokine production by phagocytic cells. When cultured with IgG-IC, macrophages from the control mice produced larger amounts of TNF- $\alpha$  and IL-6 than when they were cultured with hIgG. Therefore, we speculate that IgG-IC induced secretion of inflammatory cytokines such as TNF- $\alpha$  and IL-6 by combining with CD64 on the macrophage surface.

Several studies have found that the immune system and coagulation system are linked in the pathogenesis of IBD.<sup>19–21</sup> Cytokines, including TNF- $\alpha$  and IL-6, have the ability to activate the coagulation pathway<sup>30,31</sup> and induce tissue factor (TF) expression in monocytes and

endothelial cells.<sup>32</sup> However, the role of the inflammatory cytokines produced by macrophages in the changes in the PCS and in the pathogenesis of UC is unclear. In order to elucidate the mechanism of these cytokines in the PC pathway, we isolated and cultured colonic mucosal MVECs. After the MVECs were incubated with TNF- $\alpha$  or IL-6, we found decreased activity of APC and downregulated expression of EPCR. Thus, these results indicated that these inflammatory cytokines resulted in changes in the PC signal by stimulating colonic MVECs.

The MAPK pathway regulates inflammation through several proteins and kinases upstream and downstream, and it further influences gene transcription. Studies have shown that overactivation of MAPK is closely related with UC progression, and may represent a new target for anti-inflammatory therapy.<sup>33–37</sup> Our study found compatible results: pP38 MAPK and pJNK MAPK expression were upregulated at the protein levels, while pERK MAPK expression was not changed, indicating that the change in EPCR was mediated by p38 MAPK and JNK MAPK.

$\beta$ -arrestin serves as a scaffolding protein. It is connected to G protein-coupled receptors and the kinase-mediated signal transduction pathway, and it is involved in the regulation of GPCR-activated ERK, JNK, and p38 MAPK pathways.<sup>38</sup> Recent studies have shown that the regulation of  $\beta$ -arrestin varies on different MAPK signaling pathways.<sup>39–41</sup> Since the MAPK pathway is the key mediator of UC inflammatory signals, and  $\beta$ -arrestin regulates MAPK, we speculate that the  $\beta$ -arrestin-MAPK pathway is involved in the regulation of PCS in UC. Our study showed that the inhibition of EPCR expression induced by TNF- $\alpha$  or IL-6 was reversed by SB203580 and SP600125. In addition, after stimulation with TNF- $\alpha$  or IL-6,  $\beta$ -arrestin1 expression was upregulated, which was accompanied by upregulation of p38 MAPK and pJNK MAPK. These results further confirm that the inhibition of EPCR is mediated by the p38 MAPK and JNK MAPK pathways.

## Conclusions

In summary, we found that IgG plasma cells interacted with colonic CD14<sup>+</sup>CD64<sup>+</sup> macrophages by forming IgG-IC during DSS-induced colitis in mice, and that macrophages produced inflammatory cytokines in response to IgG-IC stimulation, which resulted in inhibition of the PCS via colonic mucosal MVECs. Therefore, enhancement of PCS activity provides a theoretical feasible and clinically significant candidate for identifying new drug targets for the treatment of UC.

## References

1. Baumgart DC, Sandbom WJ. Inflammatory bowel disease: Clinical aspects and established and evolving therapies. *Lancet*. 2007; 369(9573):1641–1657.

2. Lust M, Vulcano M, Danese S. The protein C pathway in inflammatory bowel disease: The missing link between inflammation and coagulation. *Trends Mol Med*. 2008;14(6):237–244.
3. Tolstanova G, Deng X, French SW, et al. Early endothelial damage and increased colonic vascular permeability in the development of experimental ulcerative colitis in rats and mice. *Lab Invest*. 2012; 92(1):9–21.
4. Mosnier LO, Zlokovic BV, Griffin JH. The cytoprotective protein C pathway. *Blood*. 2007;109(8):3161–3172.
5. Griffin JH, Zlokovic BV, Mosnier LO. Protein C anticoagulant and cytoprotective pathways. *Int J Hematol*. 2012;95(4):333–345.
6. Lin XH, Wang HC, Wei DD, et al. Study of the change and role of protein C system in ulcerate colitis [in Chinese]. *Sheng Li Xue Bao*. 2015; 67(2):214–224.
7. Jinno Y, Ohtani H, Nakamura S, et al. Infiltration of CD19<sup>+</sup> plasma cells with frequent labeling of Ki-67 in corticosteroid-resistant active ulcerative colitis. *Virchows Arch*. 2006;448(4):412–421.
8. Schicho R, Bashashati M, Bawa M, et al. The atypical cannabinoid O-1602 protects against experimental colitis and inhibits neutrophil recruitment. *Inflamm Bowel Dis*. 2011;17(8):1651–1664.
9. Hartmann G, Bidlingmaier C, Siegmund B, et al. Specific type IV phosphodiesterase inhibitor rolipram mitigates experimental colitis in mice. *J Pharmacol Exp Ther*. 2000;292(1):22–30.
10. Kihara N, de la Fuente SG, Fujino K, Takahashi T, Pappas TN, Mantyh CR. Vanilloid receptor-1 containing primary sensory neurones mediate dextran sulfate sodium induced colitis in rats. *Gut*. 2003;52(5): 713–719.
11. Medina F, Segundo C, Campos-Caro A, Salcedo I, García-Poley A, Brieva JA. Isolation, maturational level, and functional capacity of human colon lamina propria plasma cells. *Gut*. 2003;52(3):383–389.
12. Li YY, Cao MH, Goetz B, et al. The dual effect of cannabinoid receptor-1 deficiency on the murine postoperative ileus. *PLoS One*. 2013; 8(7):e67427.
13. Chen HL, Wang H, Li WL, et al. TNF- $\alpha$  expression and effects of Dachengqi Decoction compound in gut macrophages [in Chinese]. *World Chin J Digestol*. 2003;11(4):442–445.
14. Uo M, Hisamatsu T, Miyoshi J, et al. Mucosal CXCR4<sup>+</sup> IgG plasma cells contribute to the pathogenesis of human ulcerative colitis through Fc $\gamma$ R-mediated CD14 macrophage activation. *Gut*. 2013;62(12):1734–1744.
15. Li K, Feng JY, Li YY, et al. Anti-inflammatory role of Cannabidiol and O-1602 in Cerulein-induced acute pancreatitis in mice. *Pancreas*. 2013;42(1):123–129.
16. Scaldaferrri F, Sans M, Vetrano S, et al. Crucial role of the protein C pathway in governing microvascular inflammation in inflammatory bowel disease. *J Clin Invest*. 2007;117(7):1951–1960.
17. Zhang X, Huang L, Lu G, Ge L, Hong Y, Hu Z. Amyloid  $\beta$  suppresses protein C activation through inhibition of the endothelial protein C receptor (EPCR). *J Mol Neurosci*. 2014;52(1):117–123.
18. Lin XH, Guo JL, Wen YQ, et al. Role of IgG plasma cells in the change of protein C system in ulcerative colitis [in Chinese]. *Sheng Li Xue Bao*. 2017;69(2):172–182.
19. Bernstein CN, Blanchard JF, Houston DS, Wajda A. The incidence of deep venous thrombosis and pulmonary embolism among patients with inflammatory bowel disease: A population based cohort study. *Thromb Haemost*. 2001;85(3):430–434.
20. Grainge MJ, West J, Card TR. Venous thromboembolism during active disease and remission in inflammatory bowel disease: A cohort study. *Lancet*. 2010;375(9715):657–663.
21. Kappelman MD, Horvath-Puho E, Sandler RS, et al. Thromboembolic risk among Danish children and adults with inflammatory bowel diseases: A population-based nationwide study. *Gut*. 2011;60(7):937–943.
22. Murthy SK, Nguyen GC. Venous thromboembolism in inflammatory bowel disease: An epidemiological review. *Am J Gastroenterol*. 2011; 106(4):713–718.
23. Kume K, Yamasaki M, Tashiro M, et al. Activation of coagulation and fibrinolysis is secondary to bowel inflammation in patients with ulcerative colitis. *Intern Med*. 2007;46(17):1323–1329.
24. Shi YH, Huang PX, Guo CY. Clinical study of platelet function in ulcerate colitis patients [in Chinese]. *J Tongji Univ Med Sci*. 2006;27(2): 48–50.
25. D'Alessio S, Genua M, Vetrano S. The protein C pathway in intestinal barrier function: Challenging the hemostasis paradigm. *Ann NY Acad Sci*. 2012;1258(1):78–85.
26. Gelzayd EA, Kraft SC, Fitch FW, Kirsner JB. Distribution of immunoglobulins in human rectal mucosa. II. Ulcerative colitis and abnormal mucosal control subjects. *Gastroenterology*. 1968;54(3):341–347.
27. Strehl JD, Hartmann A, Agaimy A. Numerous IgG4-positive plasma cells are ubiquitous in diverse localised non-specific chronic inflammatory conditions and need to be distinguished from IgG4-related systemic disorders. *J Clin Pathol*. 2011;64(3):237–243.
28. Halstensen TS, Das KM, Brandtzaeg P. Epithelial deposits of immunoglobulin G1 and activated complement colocalise with the M(r) 40 kD putative autoantigen in ulcerative colitis. *Gut*. 1993;34(5):650–657.
29. Kamada N, Hisamatsu T, Okamoto S, et al. Unique CD14 intestinal macrophages contribute to the pathogenesis of Crohn disease via IL-23/IFN- $\gamma$  axis. *J Clin Invest*. 2008;118(6):2269–2280.
30. Olejár T, Matej R, Zadinová M, Poucková P. Expression of proteinase activated receptor-2 during taurocholate induced acute pancreatitis lesion development. *Int J Gastrointest Cancer*. 2001;30(3):113–122.
31. Levi M, van der Poll T, ten Cate H, van Deventer SJ. The cytokine-mediated imbalance between coagulant and anticoagulant mechanisms in sepsis and endotoxaemia. *Eur J Clin Invest*. 1997;27(1):3–9.
32. Bierhaus A, Zhang Y, Deng Y, et al. Mechanism of the tumor necrosis factor alpha-mediated induction of endothelial tissue factor. *J Biol Chem*. 1995;270(44):26419–26432.
33. Wakeman D, Schneider JE, Liu J, et al. Deletion of p38-alpha mitogen-activated protein kinase within the intestinal epithelium promotes colon tumorigenesis. *Surgery*. 2012;152(2):286–293.
34. Zhao X, Kang B, Lu C, et al. Evaluation of p38 MAPK pathway as a molecular signature in ulcerative colitis. *J Proteome Res*. 2011;10(5): 2216–2225.
35. Reinecke K, Eminel S, Dierck F, et al. The JNK inhibitor XG-102 protects against TNBS-induced colitis. *PLoS One*. 2012;7(3):e30985.
36. Kersting S, Behrendt V, Kersting J, et al. The impact of JNK inhibitor D-JNKI-1 in a murine model of chronic colitis induced by dextran sulfate sodium. *J Inflamm Res*. 2013;6:71–81.
37. Schwanke RC, Marcon R, Meotti FC, et al. Oral administration of the flavonoid myricitrin prevents dextran sulfate sodium-induced experimental colitis in mice through modulation of PI3K/Akt signaling pathway. *Mol Nutr Food Res*. 2013;57(11):1938–1949.
38. Brown MD, Sacks DB. Protein scaffolds in MAP kinase signaling. *Cell Signal*. 2009;21(4):462–469.
39. Lee T, Lee E, Arrollo D, et al. Non-hematopoietic  $\beta$ -arrestin1 confers protection against experimental colitis. *J Cell Physiol*. 2016;231(5): 992–1000.
40. Whalen EJ, Rajagopal S, Lefkowitz RJ. Therapeutic potential of beta-arrestin-and G protein-biased agonists. *Trends Mol Med*. 2011;17(3): 126–139.
41. Lee T, Lee E, Irwin R, Lucas PC, McCabe LR, Parameswaran N.  $\beta$ -Arrestin-1 deficiency protects mice from experimental colitis. *Am J Pathol*. 2013; 182(4):1114–1123.



# Markers of acute kidney injury in children undergoing hematopoietic stem cell transplantation

Monika Augustynowicz<sup>1,A–D</sup>, Agnieszka Bargenda-Lange<sup>1,B–D</sup>,  
Krzysztof Kałwak<sup>2,A,E,F</sup>, Danuta Zwolińska<sup>1,E,F</sup>, Kinga Musiał<sup>1,A–F</sup>

<sup>1</sup> Department of Pediatric Nephrology, Wrocław Medical University, Poland

<sup>2</sup> Department of Bone Marrow Transplantation, Oncology and Pediatric Hematology, Wrocław Medical University, Poland

A – research concept and design; B – collection and/or assembly of data; C – data analysis and interpretation;

D – writing the article; E – critical revision of the article; F – final approval of the article

Advances in Clinical and Experimental Medicine, ISSN 1899–5276 (print), ISSN 2451–2680 (online)

*Adv Clin Exp Med.* 2019;28(8):1111–1118

## Address for correspondence

Kinga Musiał

E-mail: kinga\_musial@hotmail.com

## Funding sources

None declared

## Conflict of interest

None declared

Received on October 29, 2018

Reviewed on November 25, 2018

Accepted on December 13, 2018

Published online on February 11, 2019

## Abstract

Acute kidney injury (AKI), one of the major complications in children undergoing hematopoietic stem cell transplantation (HSCT), is an independent predictor of the patient's survival and a prognostic factor of progression to chronic kidney disease (CKD). Despite the multifaceted role of AKI, its early diagnosis in the course of HSCT remains a challenge. These difficulties may result from the inefficiency of traditional methods used to assess kidney function, like serum creatinine or estimated glomerular filtration rate. Moreover, the list of potential AKI markers tested in HSCT conditions is limited and does not involve indexes evaluated in the pediatric population. This review summarizes current knowledge on the pathophysiology of AKI developing in the course of HSCT; presents well-known markers of AKI that are potentially applicable in children who have undergone HSCT; discusses the role of new markers in diagnosing AKI and predicting the renal outcome in children undergoing HSCT; and analyzes the prospects for the use of new tools for assessing kidney injury in everyday clinical practice.

**Key words:** chronic kidney disease, nephrotoxicity, acute tubular damage, renal outcome, hematopoietic stem cell transplantation

## Cite as

Augustynowicz M, Bargenda-Lange A, Kałwak K, Zwolińska D, Musiał K. Markers of acute kidney injury in children undergoing hematopoietic stem cell transplantation. *Adv Clin Exp Med.* 2019;28(8):1111–1118. doi:10.17219/acem/101573

## DOI

10.17219/acem/101573

## Copyright

© 2019 by Wrocław Medical University

This is an article distributed under the terms of the Creative Commons Attribution Non-Commercial License (<http://creativecommons.org/licenses/by-nc-nd/4.0/>)

Hematopoietic stem cell transplantation (HSCT) is an area of medicine under constant development. In recent years, the number of allogeneic bone marrow transplantations has increased significantly. In addition to hemato-oncological diseases, the indications for HSCT include immunologic, metabolic and genetically determined conditions.

## Current methods of assessing kidney function following hematopoietic stem cell transplantation

As HSCT has become more and more frequently the therapy of choice in children, the number of complications observed has increased. Among them, acute kidney injury (AKI) has become one of the major challenges, as it is an independent predictive factor for patient survival and progression to chronic kidney disease (CKD).<sup>1,2</sup>

Although there are many reviews on HSCT, few of them concern the pediatric population,<sup>3–5</sup> and none of them concentrate on the nephrological aspects of HSCT.

Moreover, the commonly used classifications of AKI comprise various criteria established by the Risk, Injury, Failure, Loss and End-stage (RIFLE) renal failure classification system, the Acute Kidney Injury Network (AKIN) and the Kidney Disease: Improving Global Outcomes (KDIGO) organization.<sup>6–8</sup> However, only pRIFLE criteria apply specifically to children (Table 1).

Due to the diversity of these classifications, world statistics on the incidence of AKI in children are very inconsistent. As shown in a study by Sutherland et al., the incidence of AKI in a single group of hospitalized children

varied significantly depending on the criteria used (51.1%, 37.1% and 40.3% according to pRIFLE, AKIN and KDIGO, respectively).<sup>9</sup> The AKIN and KDIGO classifications rely on changes in serum creatinine concentration, while pRIFLE criteria are additionally based on decreases in the estimated glomerular filtration rate (eGFR) and urine output (Table 1). Moreover, the fact that the pRIFLE criteria take into account the time frame and diversification of the outcome (reversible injury vs progression to CKD) make them the most useful for children.

It is worth noting that in cases of kidney function deterioration, increases in serum creatinine concentration are significantly delayed. Furthermore, many factors, such as nutrition, hydration, gender, age, and muscle mass, influence the serum concentration of creatinine. Hydration status after HSCT varies depending on the time elapsed from the procedure. During the first few days after HSCT, the treatment protocol assumes a high fluid intake (3 L/m<sup>2</sup> of body surface), resulting in transient hyperfiltration. Moreover, the method of eGFR calculation raises certain doubts. The most commonly applied Schwartz formula overestimates eGFR value, especially when it is higher than 75 mL/min/1.73 m<sup>2</sup>. However, attempts to introduce other methods have so far been unsatisfactory.<sup>10–12</sup> As a consequence, evaluation based on serum creatinine concentration remains the most frequent tool to assess kidney function in children undergoing HSCT, despite its many limitations in terms of sensitivity and specificity for AKI. However, recent reports show preliminary attempts to widen the spectrum of AKI indices by testing markers of inflammation or damage specific to selected compounds of the renal parenchyma.

The purpose of this review was to briefly present current knowledge about the pathophysiology of AKI in the course

**Table 1.** Comparison of various criteria defining acute kidney injury

Pediatric (p)RIFLE	eGFR	Urine output
Risk (Stage 1)	decrease <25%	<0.5 mL/kg/h for 8 h
Injury (Stage 2)	decrease <50%	<0.5 mL/kg/h for 16 h
Failure (Stage 3)	decrease <75% or <35 mL/min/1.73 m <sup>2</sup>	<0.3 mL/kg/h for 24 h or anuria for 12 h
Loss	failure >4 weeks	
End-stage kidney disease	persistent failure >3 months	
AKIN criteria	serum creatinine	
Stage 1	increase ≥50% or ≥0.3 mg/dL within 48 h	
Stage 2	increase ≥100%	
Stage 3	increase ≥200%	
KDIGO AKI criteria	serum creatinine	
Stage 1	increase ≥50% or ≥0.3 mg/dL within 7 days	
Stage 2	increase ≥100%	
Stage 3	increase ≥200% or ≥35 mL/min/1.73 m <sup>2</sup>	

of pediatric HSCT and current diagnostic tools for its assessment. We also aimed to discuss new markers that may potentially be useful in the early diagnosis of HSCT-related AKI, although they are not yet used in clinical practice.

## Reasons for acute kidney injury following hematopoietic stem cell transplantation

The first determinant of post-HSCT AKI is the type of HSCT itself. Myeloablative allogeneic HSCT is characterized by the highest incidence of AKI (50–91%), whereas nonmyeloablative allogeneic (29–54%) and autologous HSCT (12–52%) are less frequently involved in AKI.<sup>13</sup>

The pathogenesis of AKI following HSCT is complex and covers pre-renal, renal and post-renal mechanisms.<sup>14</sup> Among them, renal causes are the most common, with ischemia and acute tubular necrosis due to drug nephrotoxicity playing the main role. The causes of renal impairment after HSCT also strongly depend on the amount of time since the transplantation, and can be divided into immediate (tumor lysis syndrome, marrow infusion toxicity), early (hypovolemia due to diarrhea, vomiting and sepsis, drug nephrotoxicity, acute tubular necrosis, interstitial nephritis, reactivation of viral infections resulting in hemorrhagic cystitis, graft vs host disease (GvHD), and hepatic sinusoidal obstruction syndrome (HSOS)) and late (thrombotic microangiopathy, chronic GvHD and radiation).<sup>13</sup>

Describing the whole spectrum of HSCT-related factors predisposing to AKI is beyond the scope of this review; we are therefore going to focus only on selected ones. Among them, GvHD seems to be the best example of the multifactorial nature of HSCT-related AKI.<sup>13</sup>

## Graft vs host disease

In the course of GvHD, the kidneys become targets for T cells. During the first month after HSCT, the process of infiltration of the tubulointerstitial area occurs. Immunocompetent cell migration and cytokine-mediated inflammatory reaction in situ result in damage to the peritubular capillaries, tubules and glomeruli, and in thickening of the vascular intima.<sup>15</sup> Paradoxically, the prophylactic regimen against GvHD, containing cyclosporine, tacrolimus or short-term methotrexate, may become another trigger factor for AKI. Moreover, the indirect propensity towards reactivation of viral infection that arises in the course of GvHD adds to the AKI-promoting background.<sup>15</sup>

## Marrow transfusion toxicity

Cryopreservation of stem cells is a standard component of the clinical protocol in autologous HSCT, whereas it is rare in allogeneic HSCT. The collected cells are washed and resuspended in a solution supplemented with a cryoprotective agent, most typically dimethyl sulfoxide (DMSO). Dimethyl sulfoxide is considered the main causal agent of adverse reactions, such as lysis of erythrocytes, leading to precipitation of heme proteins in the proximal tubules and subsequent acute tubular necrosis.<sup>16</sup>

## Hepatic sinusoidal obstruction syndrome

The pathophysiology of HSOS, present mainly in patients who have undergone myeloablative allogeneic HSCT, remains poorly defined. Total body irradiation and busulfan/cyclophosphamide preconditioning can cause damage to sinusoidal endothelial cells and hepatocytes.<sup>17</sup> The subsequent subendothelial deposition of morphological blood compounds and fibrin results in hepatic venular narrowing and occlusion; portal hypertension then evolves. Consequently, the accumulation of vasodilators in the liver results in systemic hypotension. The compensative activation of the renin-angiotensin-aldosterone system (RAAS) triggers constriction of renal vessels and hypoperfusion.<sup>17</sup>

## Infections

The use of immunosuppressive drugs may lead to reactivation of latent viral infections, affecting approx. 25% of patients who have undergone allogeneic HSCT.<sup>18</sup> The majority of the population is seropositive to the BK virus – a member of the polyomavirus family with tropism to the urinary tract. The reactivation and massive replication of the BK virus lead to the formation of decoy cells (cells with large intranuclear inclusion bodies) programmed to die and release copied viral components, and are implicated in the pathogenesis of hemorrhagic cystitis and urethral stenosis. BK viruria may escalate to viremia and finally to the presence of the BK virus in the tubular epithelial cells of the kidney, and to kidney damage in the course of tubulointerstitial nephritis.

Another potent infectious condition in the course of HSCT is sepsis, triggering both pre-renal (hypovolemia due to inflammatory vasodilation) and renal (direct tubular damage due to cytokine release) circumstances facilitating the development of AKI.

## Transplant-associated thrombotic microangiopathy

Transplant-associated thrombotic microangiopathy (TA-TMA) is in the spectrum of disorders characterized by vascular endothelial injury followed by arteriolar thrombi, intimal swelling and fibrinoid necrosis. Clinically, it is manifested by thrombocytopenia, hemolytic anemia and tissue hypoxia. Although TA-TMA may occur in any organ, the kidneys are affected in 40% of cases, and 20% of them undergo a severe course. The risk factors for TA-TMA include the use of pharmacotherapy with calcineurin inhibitors, acute GvHD, total body irradiation, patient-donor gender mismatch, and infections.<sup>19</sup>

## Nephrotoxicity of chemotherapy

Potentially nephrotoxic drugs are used both during conditioning therapy (busulfan, treosulfan, fludarabine, thiotepa, melphalan, cyclophosphamide) and as GvHD prophylaxis (cyclosporin A, tacrolimus, methotrexate).<sup>20</sup> The pathomechanisms of nephrotoxicity for calcineurin inhibitors are not fully defined. Cyclosporin A and tacrolimus activate the RAAS, leading to vasoconstriction of the renal afferent arterioles and subsequent AKI. They also increase oxidative stress, acting directly on renal endothelial cells. Finally, through increased production of vascular endothelial growth factor (VEGF), they trigger peritubular fibrosis, which is responsible for chronic drug-induced nephropathy. Methotrexate (MTX), especially in high doses, precipitates in acidic pH in the lumen of the renal tubules, leading to tubular toxicity.<sup>20</sup> Male sex, low serum albumin levels, previous kidney pathologies, and interactions with other drugs (including furosemide) may intensify the nephrotoxicity of MTX.

The mechanism of the toxicity of cisplatin is attributed to its accumulation in the kidney, mainly in the epithelial cells of the proximal tubules, leading to their dysfunction.<sup>20</sup> The epithelium of the distal tubules and glomeruli are subsequently affected. Cyclophosphamide has a high affinity to urothelium, so hemorrhagic cystitis is a major clinical manifestation of its usage. However, it also acts detrimentally on the renal tubules by inducing oxidative stress. Isophosphamide is characterized by tropism to the epithelium of the proximal tubules, causing AKI.

Drugs used in the prophylaxis or treatment of infections, such as aminoglycosides, amphotericin B or acyclovir, are well known for their nephrotoxic mechanisms. Amphotericin B acts through renal vasoconstriction and hypoxia of the proximal tubule cells; aminoglycosides accumulate directly in the proximal tubules, changing their permeability; whereas acyclovir precipitates in the tubules, causing their obstruction.<sup>20</sup>

## Markers of acute kidney injury

The high incidence of AKI in the course of HSCT has engendered a search for sensitive and specific markers of kidney damage. Although serum creatinine-based equations remain the major tool for assessing kidney function by eGFR, there is need for more adequate parameters that would allow early diagnosis of AKI, preferably at the stage when it is still reversible. Since the proximal tubule is the first target cell in AKI-triggered renal damage, the research should focus mainly on markers that directly characterize its function.

## Parameters of tubular damage

### Cystatin C

Cystatin C (CysC) is a low molecular weight (13 kDa) non-glycosylated protein generated by all nucleated cells, present in all tissues and physiological fluids. CysC can be assessed by ELISA in both serum and urine. Serum CysC outperforms serum creatinine in assessing eGFR in children.<sup>21</sup> Increases in serum CysC have been shown to correlate with the development of AKI in children from intensive care units and following cardiac surgery, as well as in adults following HSCT.<sup>22</sup> However, it has also been helpful in analyzing glomerular damage due to chemotherapy in children.<sup>23</sup> Moreover, increased serum CysC concentrations have been observed in patients with leukemia, melanoma, as well as colorectal or hepatocellular cancer, but without renal injury. Therefore, high serum CysC is not specific for AKI, because it may well be a marker of malignancy.<sup>24</sup>

On the other hand, CysC is filtered by glomeruli, then reabsorbed and degraded in the proximal tubules. It is not secreted by the tubules, so its urinary concentration is minimal in subjects with normal kidney function, but increases significantly in the course of kidney injury.<sup>25</sup> Therefore, urinary CysC may be a potential early marker of proximal tubule damage in the course of post-HSCT AKI, but no data are available.

### Neutrophil gelatinase-associated lipocalin

Neutrophil gelatinase-associated lipocalin (NGAL) is another low-molecular-weight protein (25 kDa), originally identified in secondary granules of human neutrophils and as such, is released into circulation from organs like the liver, lungs, trachea, colon, uterus, or prostate. It is filtered by the glomeruli and reabsorbed by the proximal tubules.<sup>26</sup>

Serum NGAL acts in a bacteriostatic manner by binding siderophores – bacterial products that scavenge iron. Kidney-derived NGAL accompanies the differentiation and development of the tubular epithelium and is one of the earliest markers of distal nephron damage.<sup>26</sup>

Both serum and urine NGAL are useful predictors of AKI, although its urinary concentration is more sensitive for kidney injury.<sup>27</sup> NGAL is widely used for early diagnosis of AKI, its monitoring and prognosis. It has also become useful in pediatric AKI, mainly in its early diagnosis after cardiac surgery and as a predictor of mortality.

However, NGAL is also overexpressed in other conditions, such as tumors or inflammatory bowel disease.<sup>28</sup> It is used to monitor the nephrotoxicity of drugs like ipsothamide, cisplatin and cyclosporine.<sup>29</sup> Increased plasma NGAL reflects inflammation, including sepsis, whereas urinary NGAL points rather to urinary tract infection.<sup>30</sup> NGAL may also suppress metastatic processes.<sup>28</sup>

The role of urinary NGAL in predicting AKI has been demonstrated in adults who have undergone HSCT for oncological reasons: as markers of AKI, elevated urinary NGAL preceded increased serum creatinine by 2 days.<sup>31</sup> No such investigation has been performed in children who have undergone HSCT.

## Kidney injury molecule 1

Kidney injury molecule 1 (KIM-1) is a glycoprotein, the localization of which is limited to the apical membranes of the proximal tubules. Physiological urinary KIM-1 concentration is negligible, whereas it increases after ischemic or nephrotoxic AKI. Renal biopsies performed after acute tubular necrosis revealed increased expression of KIM-1 in proximal tubule cells.<sup>32</sup> This molecule is also a scavenger receptor of paramount importance for apoptosis and regeneration of damaged epithelial cells in the proximal tubules. Urinary KIM-1 has been shown to be useful in the detection of neoplasms originating in the proximal tubules, ovaries or uterus (clear cell cancer).<sup>28</sup>

Increases in urinary KIM-1 have been found to correlate with AKI due to acute tubular necrosis.<sup>33</sup> In children, KIM-1 has been shown to be a useful marker for AKI following shock-related hypovolemia – more sensitive and specific than serum creatinine, NGAL or interleukin-18 (IL-18). However, the correlation with the severity of AKI in children from an intensive care unit was quite weak, although KIM-1 could strongly predict the need for renal replacement therapy.<sup>34</sup> Kidney injury molecule 1 is also a useful marker of kidney function in children undergoing chemotherapy with MTX or cisplatin derivatives.<sup>35</sup> Although the value of KIM-1 as a marker for AKI has been demonstrated in a recent meta-analysis,<sup>36</sup> none of the data concerned the detection of AKI following HSCT.

## N-acetyl-beta-D-glucosaminidase

N-acetyl-beta-D-glucosaminidase (NAG) is a lysosomal enzyme of high molecular weight, found originally in proximal tubule cells, released after their damage and therefore considered a marker of their dysfunction. The urinary concentration of NAG increases in AKI, as has been shown

in adult patients that have undergone cardiac surgery.<sup>37</sup> Like KIM-1, NAG is a strong predictor of a poor prognosis in adults with AKI.<sup>38</sup>

Preliminary reports from animal studies suggest that NAG may be useful in assessing AKI in the course of acute GvHD following allogeneic HSCT.<sup>39</sup> Urinary NAG could detect tubular damage at the subclinical level and hepatic veno-occlusive disease, although it did not correlate with the level of azotemia in patients who had undergone allogeneic HSCT.<sup>40</sup> Elevated urinary NAG has also been reported in subjects with acute tubular necrosis not related to HSCT. There are 2 recent studies on increased NAG concentration in the urine of adults and children who have undergone HSCT.<sup>41,42</sup> These results are promising, because urinary NAG seems to be an ideal marker of early tubular damage, preceding the development of AKI.

## Inflammatory markers

### Interleukin-18

Interleukin 18 is a pro-inflammatory cytokine, released by monocytes/macrophages, activated by caspase-1 and inducing interferon gamma. Widespread, IL-18 is also present in various kidney structures, like distal tubules, collecting ducts and the ascending limb of the loop of Henle. However, it is not found in proximal tubules or glomeruli. Increased serum IL-18 concentrations are typical of many inflammation-related diseases, including autoimmune disorders like lupus, arthritis, inflammatory bowel disease, psoriasis, hepatitis, diabetes, or sclerosis multiplex.<sup>43</sup> This multiplicity suggests the weak specificity of this marker.

Animal studies have shown elevated urinary concentration of IL-18 in AKI following ureteral obstruction.<sup>44</sup> Due to its pro-inflammatory activity, IL-18 seems to aggravate kidney damage in the course of ischemia/reperfusion injury; patients with acute tubular necrosis presented with higher urinary IL-18 than those with CKD, urinary tract infection, nephrotic syndrome, or pre-renal azotemia.<sup>45</sup> Urinary IL-18 (like NGAL) has been found to be a strong predictor of AKI in children who had undergone cardiac surgery, since the diagnosis was made 12 h earlier than with serum creatinine.<sup>46</sup> The prognostic value of IL-18 in diagnosing AKI, the need for renal replacement therapy and 90-day mortality was demonstrated in a large cohort of adults in an intensive care unit.<sup>47</sup> However, there is still a need for thorough investigation of the applicability of IL-18 to detect AKI following HSCT in children.

### Monocyte chemoattractant protein 1

Monocyte chemoattractant protein (MCP)-1 is one of the key chemokines regulating the migration and infiltration of monocytes/macrophages to the sites of inflammation.

It is also a pathogenic factor in many diseases, including AKI. Rice et al. noted an elevated urinary concentration of MCP-1 in mice at 24 and 72 h after renal ischemia.<sup>48</sup> In another study, increased expression of MCP-1 in the renal cortex of mice with AKI correlated with the level of kidney damage better than NGAL.<sup>49</sup> Urinary MCP-1 has been found to correlate strongly with the level of AKI in patients treated with cisplatin or tacrolimus, as well as with serum creatinine increase in adults 5 weeks after HSCT; it also predicted mortality risk after cardiac surgery.<sup>50</sup> A significant elevation of MCP-1 concentration in children undergoing HSCT has been observed between the 2<sup>nd</sup> and 4<sup>th</sup> week after the procedure, but it was not correlated with AKI.<sup>51</sup>

## New acute kidney injury indexes

### Liver-type fatty acid-binding protein

Liver-type fatty acid-binding protein (L-FABP) is produced mainly in the liver, but its expression is also noticeable in other organs, including the kidneys. It takes part in the transport and metabolism of free fatty acids, acting as an anti-oxidant. In the proximal tubules, it allows intracellular metabolism of fatty acids. It is filtered by the glomeruli and reabsorbed by the proximal tubules.<sup>52</sup> It is not present in the urine of healthy subjects, but has been found to be an early predictor of AKI due to sepsis or drug nephrotoxicity.<sup>53,54</sup> Increased urinary concentrations of L-FABP have also been described in adults with acute decompensated heart failure or surgically treated aortic aneurysm.<sup>55,56</sup> To date, a single promising report has been published on urinary L-FABP as a marker of AKI risk in adult patients following HSCT.<sup>57</sup>

### Insulin-like growth factor-binding protein 7

Insulin-like growth factor-binding protein (IGFBP)-7 is another low-molecular-weight protein (30 kDa) freely filtered by the glomeruli and reabsorbed by the proximal tubules; its increased urinary concentration is most probably the consequence of tubular damage.<sup>58</sup> Indeed, increased urinary IGFBP-7 concentrations have been noticed in patients from intensive care units. They could also predict the renal outcome, distinguishing between patients with and without AKI, or between those with early recovery from AKI and late or non-recovery.<sup>59</sup> Moreover, IGFBP-7 has been found to be a more useful tool than NGAL in the differential diagnosis and prognosis of AKI. Thus, IGFBP-7 seems another ideal candidate as a diagnostic and prognostic marker of AKI. However, no data is available on investigations of urinary IGFBP-7 concentrations in patients who have undergone HSCT, irrespective of their age.

## Netrin-1

Netrin-1 is a 70 kDa axon guidance molecule with an anti-inflammatory activity, expressed in many organs, including the kidneys. In vitro investigations have demonstrated its paramount role in ischemia/reperfusion kidney injury, during which the expression of netrin-1 increased in the apical membranes of proximal tubule cells, acting in a protective manner. Its anti-inflammatory and anti-apoptotic activity has also been found to be highly efficient against cisplatin-induced kidney injury.<sup>60</sup> Moreover, urinary netrin-1 has been reported to be an early predictor of AKI following cardiac surgery.<sup>61</sup> However, no evidence for its role as a biomarker of HSCT-related AKI has been presented to date.

## Markers of acute kidney injury progression to chronic kidney disease

Although potentially reversible, in some cases AKI progresses into CKD. Long-term unfavorable outcomes for children with AKI are defined in the pRIFLE criteria as loss of kidney function (L) and end-stage kidney disease (E). The major nephrological challenge is therefore to identify patients at risk of developing CKD after an episode of AKI. Candidate markers for assessing AKI-to-CKD progression include NGAL, KIM-1 and L-FABP, although convincing data on their utility in long-term observation of children who have undergone HSCT are lacking.<sup>62</sup> Another promising biomarker is clusterin, identified in animal studies as a factor responsible for anti-inflammatory and anti-fibrotic activity after ischemia/reperfusion injury.<sup>63</sup> However, tools for predicting AKI-to-CKD progression following HSCT are yet to be established.

## Targeted, pleiotropic or combined?

Post-HSCT AKI has a multifactorial background, and as such should be assessed in a complex way. Many questions about the quantity and quality of markers used to evaluate AKI in these conditions remain unanswered. Can we rely on single markers specific for (e.g.) tubular damage, inflammation or drug side effects, or should we search for markers with pleiotropic functions, designating (e.g.) both tissue damage and nephrotoxicity? Is urine the only milieu that adequately shows AKI-related anomalies or should we implement serum markers as additional predictors? Is the early diagnosis of AKI our major goal or should we strive for both protectors of kidney function and predictors of renal outcomes? These questions also remain unanswered in the general field of AKI. However,

some attempts have been made to establish new paradigms of AKI diagnosis, tailored to various pathologies responsible for kidney injury. Parikh and Mansour have suggested combinations of new urinary markers helpful in distinguishing between acute tubular necrosis and reversible prerenal azotemia due to hypoxia (IL-18, NGAL, KIM-1), or between the aforementioned conditions and hepatorenal syndrome (NGAL, L-FABP, IL-18).<sup>64</sup> Another interesting option is the concomitant evaluation of markers in pairs, as in the case of association of [TIMP-2] × [IGFBP-7] in the urine of critically ill adults, where it has identified AKI patients at increased risk of mortality.<sup>65</sup> These examples represent a promising direction, but more studies are needed to establish guidelines applicable in everyday practice, including guidelines for patients undergoing HSCT.

## Clinical perspective

No guidelines for the early detection of AKI in children undergoing HSCT exist. Preliminary data suggest the usefulness of urinary NGAL and L-FABP in adults following HSCT, and urinary NAG has been positively tested in children following HSCT. However, the use of a marker in pediatric clinical practice demands easily available material and accessible age-related reference values. Currently, the data on the latter involve established markers of AKI, such as urinary IL-18, KIM-1, L-FABP, and NGAL.<sup>66</sup> Fortunately, this combination additionally covers differential diagnostics, essential in cases of HSCT-related AKI, between pre-renal azotemia, acute tubular necrosis and liver-based causes of AKI. Moreover, KIM-1, L-FABP and NGAL may predict AKI-to-CKD progression. Therefore, this quartet appears to be the most promising and should be recommended first for clinical testing in children who have undergone HSCT.

## Conclusions

Acute kidney injury is becoming a serious clinical challenge in the era of widespread HSCT availability. The panel of candidate AKI markers is wide, although the majority of them have not yet been tested in post-HSCT conditions. It is clear that the analysis of diagnostic and prognostic tools for AKI in children who have undergone HSCT should take into account the multifactorial nature of the process, including hypoxia, drug toxicity and immune-mediated reactions in the course of GvHD. Although none of the AKI biomarkers discussed in this review is used in everyday clinical practice, urinary IL-18, KIM-1, L-FABP, and NGAL seem like promising candidates to be tested in the pediatric population undergoing HSCT. From a clinical point of view, a reliable panel of AKI markers is an emerging necessity, if the therapy introduced today is to be effective tomorrow.

## References

- Kizilbash SJ, Kashtan CE, Chavers BM, Cao Q, Smith AR. Acute kidney injury and the risk of mortality in children undergoing hematopoietic stem cell transplantation. *Biol Blood Marrow Transplant.* 2016;22(7):1264–1270.
- Ileri T, Ertem M, Ozcakar ZB, et al. Prospective evaluation of acute and chronic renal function in children following matched related donor hematopoietic stem cell transplantation. *Pediatr Transplant.* 2010;14(1):138–144.
- Didsbury MS, Mackie FE, Kennedy SE. A systematic review of acute kidney injury in pediatric allogeneic hematopoietic stem cell recipients. *Pediatr Transplant.* 2015;19(5):460–470.
- Raina R, Herrera N, Krishnappa V, et al. Hematopoietic stem cell transplantation and acute kidney injury in children: A comprehensive review. *Pediatr Transplant.* 2017;21(4):e12935.
- Koh K-N, Sunkara A, Kang G, et al. Acute kidney injury in pediatric patients receiving allogeneic hematopoietic cell transplantation: Incidence, risk factors, and outcomes. *Biol Blood Marrow Transplant.* 2018;24(4):758–764.
- Bellomo R, Ronco C, Kellum JA, Mehta RL, Palevsky P. Acute Dialysis Quality Initiative workgroup: Acute renal failure – definition, outcome measures, animal models, fluid therapy and information technology needs: The Second International Consensus Conference of the Acute Dialysis Quality Initiative (ADQI) Group. *Crit Care.* 2004; 8(4):R204–R212.
- Mehta RL, Kellum JA, Shah SV, et al; Acute Kidney Injury Network. Acute Kidney Injury Network: Report of an initiative to improve outcomes in acute kidney injury. *Crit Care.* 2007;11(2):R31.
- Kidney Disease: Improving Global Outcomes (KDIGO) Acute Kidney Injury Work Group. KDIGO Clinical Practice Guideline for Acute Kidney Injury. *Kidney Int Suppl.* 2012;2:1–138.
- Sutherland SM, Byrnes JJ, Kothari M, et al. AKI in hospitalized children: Comparing the pRIFLE, AKIN, and KDIGO definitions. *Clin J Am Soc Nephrol.* 2015;10(4):554–561.
- Holmes J, Roberts G, May K, et al. The incidence of pediatric acute kidney injury is increased when identified by a change in a creatinine-based electronic alert. *Kidney Int.* 2017;92(2):432–439.
- Laskin BL, Nehus E, Goebel J, Furth S, Davies SM, Jodele S. Estimated versus measured glomerular filtration rate in children before hematopoietic cell transplantation. *Biol Blood Marrow Transplant.* 2014; 20(12):2056–2061.
- Schwartz GJ, Munoz A, Schneider MF, et al. New equations to estimate GFR in children with CKD. *J Am Soc Nephrol.* 2009;20(3): 629–637.
- Kemmner S, Verbeek M, Heemann U. Renal dysfunction following bone marrow transplantation. *J Nephrol.* 2017;30(2):201–209.
- Lopes J, Jorge S, Neves M. Acute kidney injury in HCT: An update. *Bone Marrow Transplant.* 2016;51:755–762.
- Motoyoshi Y, Endo A, Takagi M, et al. Graft versus host disease-dependent renal dysfunction after hematopoietic stem cell transplantation. *CEN Case Rep.* 2014;3(2):202–205.
- Shu Z, Heimfeld S, Gao D. Hematopoietic SCT with cryopreserved grafts: Adverse reactions after transplantation and cryoprotectant removal before infusion. *Bone Marrow Transplant.* 2014;49:469–476.
- Fan CQ, Crawford JM. Sinusoidal obstruction syndrome (hepatic veno-occlusive disease). *J Clin Exp Hepatol.* 2014;4(4):332–346.
- Abudayyeh A, Hamdi A, Lin H, et al. Symptomatic BK virus infection is associated with kidney function decline and poor overall survival in allogeneic hematopoietic stem cell recipients HHS Public Access. *Am J Transplant.* 2016;16(5):1492–1502.
- Rosenthal J. Hematopoietic cell transplantation-associated thrombotic microangiopathy: A review of pathophysiology, diagnosis, and treatment. *J Blood Med.* 2016;7:181–186.
- Perazella MA. Onco-nephrology: Renal toxicities of chemotherapeutic agents. *Clin J Am Soc Nephrol.* 2012;7(10):1713–1721.
- Nakhjavan-Shahraki B, Yousefifard M, Ataei N, et al. Accuracy of cystatin C in prediction of acute kidney injury in children; serum or urine levels: Which one works better? A systematic review and meta-analysis. *BMC Nephrol.* 2017;18(1):120.
- Volpon LC, Sugo EK, Carlotti APCP. Diagnostic and prognostic value of serum cystatin C in critically ill children with acute kidney injury. *Pediatr Crit Care Med.* 2015;16(5):e125–131.

23. Kos J, Lah TT. Cysteine proteinases and their endogenous inhibitors: Target proteins for prognosis, diagnosis and therapy in cancer (review). *Oncol Rep.* 1998;5(6):1349–1361.
24. Lah TT, Kos J. Cysteine proteinases in cancer progression and their clinical relevance for prognosis. *Biol Chem.* 1998;379:125–130.
25. Muto H, Ohashi K, Ando M, Akiyama H, Sakamaki H. Cystatin C level as a marker of renal function in allogeneic hematopoietic stem cell transplantation. *Int J Hematol.* 2010;91(3):471–477.
26. Schmidt-Ott KM, Mori K, Li JY, et al. Dual action of neutrophil gelatinase-associated lipocalin. *J Am Soc Nephrol.* 2007;18(2):407–413.
27. Abdulaziz Kari J, Ahmed Shalaby M, Sofyani K, et al. Urinary neutrophil gelatinase-associated lipocalin (NGAL) and serum cystatin C measurements for early diagnosis of acute kidney injury in children admitted to PICU. *World J Pediatr.* 2018;14(2):134–142.
28. Marchewka Z, Tacik A, Piwowar A. KIM-1 and NGAL as potential biomarkers for the diagnosis and cancer progression. *Postepy Hig Med Dosw.* 2016;70:329–336.
29. Wasilewska A, Zoch-Zwierz W, Taranta-Janusz K, Michaluk-Skutnik J. Neutrophil gelatinase-associated lipocalin (NGAL): A new marker of cyclosporine nephrotoxicity? *Pediatr Nephrol.* 2010;25(5):889–897.
30. Soni SS, Cruz D, Bobek I, et al. NGAL: A biomarker of acute kidney injury and other systemic conditions. *Int Urol Nephrol.* 2010;42(1):141–150.
31. Taghizadeh-Ghehi M, Sarayani A, Ashouri A, Ateei S, Moslehi A, Hadjibabaie M. Urine neutrophil gelatinase associated lipocalin as an early marker of acute kidney injury in hematopoietic stem cell transplantation patients. *Ren Fail.* 2015;37(6):994–998.
32. Han WK, Bailly V, Abichandani R, Thadhani R, Bonventre JV. Kidney Injury Molecule-1 (KIM-1): A novel biomarker for human renal proximal tubule injury. *Kidney Int.* 2002;62:237–244.
33. Huang Y, Don-Wauchope AC. The clinical utility of kidney injury molecule-1 in the prediction, diagnosis and prognosis of acute kidney injury: A systematic review. *Inflamm Allergy Drug Targets.* 2011;10(4):260–271.
34. Westhoff JH, Seibert FS, Waldherr S, et al. Urinary calprotectin, kidney injury molecule-1, and neutrophil gelatinase-associated lipocalin for the prediction of adverse outcome in pediatric acute kidney injury. *Eur J Pediatr.* 2017;176(6):745–755.
35. Carvalho Pedrosa D, Macedo De Oliveira Neves F, Meneses GC, et al. Urinary KIM-1 in children undergoing nephrotoxic antineoplastic treatment: A prospective cohort study. *Pediatr Nephrol.* 2015;30(12):2207–2213.
36. Shao X, Tian L, Xu W, et al. Diagnostic value of urinary kidney injury molecule 1 for acute kidney injury: A meta-analysis. *PLoS One.* 2014;9(1):e84131.
37. Lannemyr L, Lundin E, Reinsfelt B, et al. Renal tubular injury during cardiopulmonary bypass as assessed by urinary release of N-acetyl- $\beta$ -D-glucosaminidase. *Acta Anaesthesiol Scand.* 2017;61(9):1075–1083.
38. Liangos O, Perianayagam MC, Vaidya VS, et al. Urinary N-acetyl-beta-(D)-glucosaminidase activity and kidney injury molecule-1 level are associated with adverse outcomes in acute renal failure. *J Am Soc Nephrol.* 2007;18(3):904–912.
39. Koyner JL, Shaw AD, Chawla LS, et al. Tissue inhibitor metalloproteinase-2 (TIMP-2) and IGF-binding protein-7 (IGFBP7) levels are associated with adverse long-term outcomes in patients with AKI. *J Am Soc Nephrol.* 2015;26(7):1747–1754.
40. Fink J, Cooper M, Burkhart K, McDonald G, Zager Fink RJ, McDonald GB, Zager RA. Marked enzymuria after bone marrow transplantation: A correlate of veno-occlusive disease-induced hepatorenal syndrome. *J Am Soc Nephrol.* 1995;6(6):1655–1656.
41. Volkan Hazar MD, Ozgul Gungor MD, Ayfer Gur Guven MD, et al. Renal function after hematopoietic stem cell transplantation in children. *Pediatr Blood Cancer.* 2009;53(2):97–202.
42. Morito T, Ando M, Tsuchiya K, Nitta K. Early identification of acute kidney injury after hematopoietic stem cell transplantation by the measurement of urinary biomarkers [in Japanese]. *Nihon Jinzo Gakkai Shi.* 2011;53(8):1150–1158.
43. Urbschat A, Obermüller N, Haferkamp A. Biomarkers of kidney injury. *Biomarkers.* 2011;16(Suppl 1):22–30.
44. Franke EI, Vanderbrink BA, Hile KL, et al. Renal IL-18 production is macrophage independent during obstructive injury. *PLoS One.* 2012;7(10):e47417.
45. Wu H, Craft ML, Wang P, et al. IL-18 contributes to renal damage after ischemia-reperfusion. *J Am Soc Nephrol.* 2008;19(12):2331–2341.
46. Parikh CR, Mishra J, Thiessen-Philbrook H, et al. Urinary IL-18 is an early predictive biomarker of acute kidney injury after cardiac surgery. *Kidney Int.* 2006;70(1):199–203.
47. Nisula S, Yang R, Poukkanen M, et al. Predictive value of urine interleukin-18 in the evolution and outcome of acute kidney injury in critically ill adult patients. *Br J Anaesth.* 2015;114(3):460–468.
48. Rice JC, Spence JS, Yetman DL, Safirstein RL. Monocyte chemoattractant protein-1 expression correlates with monocyte infiltration in the post-ischemic kidney. *Ren Fail.* 2002;24(6):703–723.
49. Munshi R, Johnson A, Siew ED, et al. MCP-1 gene activation marks acute kidney injury. *J Am Soc Nephrol.* 2011;22(1):165–175.
50. Moledina DG, Isguven S, McArthur E, et al. Plasma monocyte chemoattractant protein-1 is associated with acute kidney injury and death after cardiac operations. *Ann Thorac Surg.* 2017;104(2):613–620.
51. Dicarlo J, Agarwal-Hashmi R, Shah A, et al. Cytokine and chemokine patterns across 100 days after hematopoietic stem cell transplantation in children. *Biol Blood Marrow Transpl.* 2014;20(3):361–369.
52. Chmurzyńska A. The multigene family of fatty acid-binding proteins (FABPs): Function, structure and polymorphism. *J Appl Genet.* 2006;47(1):39–48.
53. Doi K, Noiri E, Maeda-Mamiya R, et al. Urinary L-type fatty acid-binding protein as a new biomarker of sepsis complicated with acute kidney injury. *Crit Care Med.* 2010;38(10):2037–2042.
54. Negishi K, Noiri E, Sugaya T, et al. A role of liver fatty acid-binding protein in cisplatin-induced acute renal failure. *Kidney Int.* 2007;72(3):348–358.
55. Hishikari K, Hikita H, Nakamura S, et al. Urinary liver-type fatty acid-binding protein level as a predictive biomarker of acute kidney injury in patients with acute decompensated heart failure. *Cardiorenal Med.* 2017;7(4):267–275.
56. Obata Y, Kamijo-Ikemori A, Ichikawa D, et al. Clinical usefulness of urinary liver-type fatty-acid-binding protein as a perioperative marker of acute kidney injury in patients undergoing endovascular or open-abdominal aortic aneurysm repair. *J Anesth.* 2016;30(1):89–99.
57. Shingai N, Morito T, Najima Y, et al. Urinary liver-type fatty acid-binding protein linked with increased risk of acute kidney injury after allogeneic stem cell transplantation. *Biol Blood Marrow Transplant.* 2014;20(12):2010–2014.
58. Emler DR, Pastor-Soler N, Marciszyn A, et al. Insulin-like growth factor binding protein 7 and tissue inhibitor of metalloproteinases-2: Differential expression and secretion in human kidney tubule cells. *Am J Physiol Renal Physiol.* 2017;312(2):F284–F296.
59. Aregger F, Uehlinger DE, Witowski J, et al. Identification of IGFBP-7 by urinary proteomics as a novel prognostic marker in early acute kidney injury. *Kidney Int.* 2014;85(4):909–919.
60. Rajasundari A, Pays L, Mehlen P, Ramesh G. Netrin-1 overexpression in kidney proximal tubular epithelium ameliorates cisplatin nephrotoxicity. *Lab Invest.* 2011;91(12):1717–1726.
61. Ramesh G, Krawczeski CD, Woo JG, Wang Y, Devarajan P. Urinary netrin-1 is an early predictive biomarker of acute kidney injury after cardiac surgery. *Clin J Am Soc Nephrol.* 2010;5(3):395–401.
62. Goldstein SL, Devarajan P. Acute kidney injury in childhood: Should we be worried about progression to CKD? *Pediatr Nephrol.* 2011;26(4):509–522.
63. Guo J, Guan Q, Liu X, et al. Relationship of clusterin with renal inflammation and fibrosis after the recovery phase of ischemia-reperfusion injury. *BMC Nephrol.* 2016;17(1):133.
64. Parikh CR, Mansour SG. Perspective on clinical application of biomarkers in AKI. *J Am Soc Nephrol.* 2017;28(6):1677–1685.
65. Koyner JL, Coca SG, Thiessen-Philbrook H, et al. Urine biomarkers and perioperative acute kidney injury: The impact of preoperative estimated GFR. *Am J Kidney Dis.* 2015;66(6):1006–1014.
66. Bennett MR, Nehus E, Haffner Ch, Ma Q, Devarajan P. Pediatric reference ranges for acute kidney injury biomarkers. *Pediatr Nephrol.* 2015;30(4):677–685.



# Gastrointestinal non-Hodgkin lymphomas

Magdalena Olszewska-Szopa<sup>A–F</sup>, Tomasz Wróbel<sup>A–F</sup>

Department of Hematology, Blood Neoplasms and Bone Marrow Transplantation, Wrocław Medical University, Poland

A – research concept and design; B – collection and/or assembly of data; C – data analysis and interpretation;

D – writing the article; E – critical revision of the article; F – final approval of the article

Advances in Clinical and Experimental Medicine, ISSN 1899–5276 (print), ISSN 2451–2680 (online)

*Adv Clin Exp Med.* 2019;28(8):1119–1124

## Address for correspondence

Magdalena Olszewska-Szopa  
E-mail: molszopa@gmail.com

## Funding sources

None declared

## Conflict of interest

None declared

Received on October 28, 2015

Reviewed on November 23, 2016

Accepted on August 8, 2018

Published online on August 13, 2019

## Abstract

Although gastrointestinal (GI) tract is the most common extranodal site involved in non-Hodgkin lymphoma (NHL), primary gastrointestinal NHL (gNHL) is a rare problem which concerns about 10–15% of NHL patients and 30–40% of extranodal NHL patients. Lymphoid neoplasms may consist of mature B, T and (less commonly) extranodal NK/T cells. The most common diagnoses are diffuse large B-cell lymphoma and marginal zone lymphoma (MALT), but many other lymphomas may be found in the GI tract. There are a few well-known risk factors of gNHL and some of them affect treatment. The most frequent sites of occurrence are the stomach followed by small intestine and ileocecal region. In the last 2 decades, there has been a rapid development in the diagnosis, staging and management of GI lymphoma, but still some of such lymphomas, especially T-cell ones, are a therapeutic challenge. In this review, we present clinical and pathological features of GI lymphomas. We also describe the current status in diagnosis and treatment.

**Key words:** DLBCL, gastrointestinal lymphoma, EATL, MALT

## Cite as

Olszewska-Szopa M, Wróbel T. Gastrointestinal non-Hodgkin lymphomas. *Adv Clin Exp Med.* 2019;28(8):1119–1124.  
doi:10.17219/acem/94068

## DOI

10.17219/acem/94068

## Copyright

© 2019 by Wrocław Medical University

This is an article distributed under the terms of the Creative Commons Attribution Non-Commercial License (<http://creativecommons.org/licenses/by-nc-nd/4.0/>)

## Introduction

Gastrointestinal (GI) tract is the most common extranodal site involved in non-Hodgkin lymphoma (NHL). Primary gastrointestinal non-Hodgkin lymphoma (gNHL), however, is a rare problem which concerns about 10–15% of all NHL patients and 30–40% of extranodal NHL patients.<sup>1</sup> At the same time, gNHL cases account for only 1–4% of GI neoplasms.<sup>2</sup> The most frequent site for gNHL is the stomach (60–75% of all cases), followed by the small intestine and the ileocecal region (Fig. 1).<sup>3</sup>

Histopathological findings in GI tract reveal indolent as well as aggressive lymphomas, which may consist of mature B, T or NK cells. Intestinal B-cell lymphomas are more frequent than T-cell lymphomas (ratio 6:1).<sup>4</sup> Two of the most prevalent diagnoses are diffuse large B-cell lymphoma (DLBCL) and marginal zone lymphoma (MALT). Other histologic subtypes – follicular lymphoma (FL), mantle cell lymphoma (MCL), Burkitt lymphoma (BL), enteropathy-associated lymphoma (EATL), post-transplant lymphoproliferative diseases (PTLD), and others – are less commonly observed (Fig. 2).<sup>1,3</sup>

Clinical picture results mainly from localization of the disease, while histopathologic type of the lymphoma is less relevant. The most common symptoms are abdominal pain, nausea, vomiting, diarrhea, and malabsorption. Violent manifestations of the disease in the form of GI bleeding, perforation or intestinal obstruction are not so frequent.<sup>1</sup>

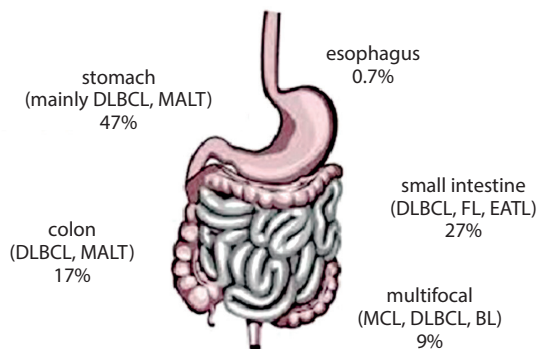


Fig. 1. Gastrointestinal lymphoma topography

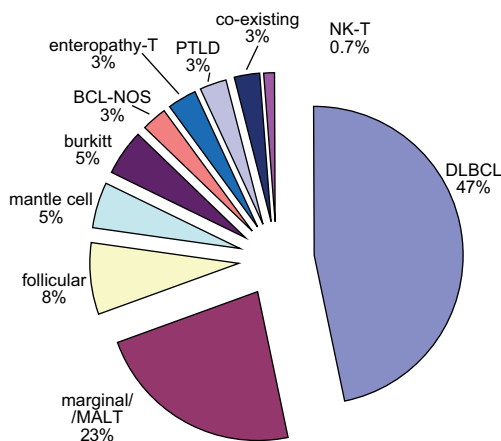


Fig. 2. Gastrointestinal lymphoma distribution

## gNHL from top to bottom

The oropharyngeal region is a location for 2.5% of NHLs. The most frequently involved area is the Waldeyer's ring. The leading symptoms are dysphagia, hearing loss and pain. The median age at the moment of the diagnosis is above 50 years. The most common histopathological finding is DLBCL. Viral factors are known to increase the risk of nasopharyngeal NHL. Contrary to other neoplasms in this location, chemotherapy and radiotherapy are preferred rather than surgery. The esophagus is an extremely rare location for NHL and primary involvement is casuistic. In the majority of cases, DLBCL is diagnosed. The risk factors are immunodeficiency disorders, particularly HIV.<sup>3</sup> The stomach is the most commonly involved site in primary gNHL and comprises 60–70% of gNHL cases. At the same time, it constitutes 3–5% of all gastric neoplasms. Clinical symptoms are typical for this localization: pain, nausea, emesis, and weight loss. Endoscopic ultrasonography (EUS) is an essential tool in this localization and will be discussed in detail later in the text. Primary small intestine lymphomas account for 20% of gNHL and 10–20% of all intestine neoplasms. The most commonly involved region is the ileum.<sup>3</sup> Histopathological findings reveal the following types of disease: MALT, DLBCL, EATL, MCL, and others. Balloon enteroscopy and capsule endoscopy are among the essential imaging techniques in the diagnosis of all small intestine neoplasms. Some small intestine lymphomas including MCL, FL and MALT, occur in the form of polyps, others appear as firm mass (BL) or nodules, scars and erosions (EATL).<sup>3</sup> Colorectal lymphoma accounts for approx. 6–12% of gNHL, but very rarely is the colorectum the primary site for gNHL. In Western countries, lymphomas in this region are of B-cell origin, but in Asia there is an increasing frequency of T-cell-lineage NHL. In some cases of colorectal gNHL, surgery is a treatment as well as a diagnostic tool.<sup>3</sup>

## Imaging techniques

Endoscopy is a fundamental diagnostic technique in gNHLs and it may reveal a wide variety of different forms: from enlarged lymph nodes and lymphoid follicles, which may sometimes appear as reactive, through polyps, to infiltrative and necrotic lesions.<sup>1</sup> Endoscopic ultrasonography is a very valuable method in locoregional staging; for instance, it allows for the visualization of all layers of gastric walls. Moreover, it shows local lymph nodes. Endoscopic ultrasonography is more valuable in indolent lymphomas, in which locoregional staging is important for proper therapeutic decisions. In aggressive lymphomas, chemo- or immunochemotherapy is usually introduced from the beginning and precise local assessment is not so important.<sup>5</sup> The impact of EUS in primary gastric

lymphoma. In the stomach, EUS demonstrates 4 types of patterns: superficially spreading, diffusely infiltrating, mass forming, and mixed. Current stomach MALT classification is based on EUS findings.<sup>1</sup> Computed tomography (CT) and magnetic resonance imaging (MRI) are valuable in disease assessment outside the GI tube. It is important to remember that a CT scan usually does not enable to visualize lymphoma confined to the mucosa.<sup>6</sup> 18F-fluorodeoxyglucose positron emission tomography (FDG-PET) has proven its usefulness in diagnosis and staging of the disease and in response assessment. However, particularly in GI tract neoplasms, FDG-PET may give false positive results. Therefore, new PET tracers, like 18F-fluoro-thymidine, are being tested and the results look promising.<sup>3</sup> In response evaluation, all of abovementioned techniques may play a role, but (at least in gastric lymphoma) histopathological assessment is still recommended.<sup>7</sup>

### Risk factors

The most important risk factor in gNHL is *Helicobacter pylori* (*H. pylori*) infection. It is considered crucial in MALT pathogenesis, but also probably plays a role in DLBCL and BL growth. Another infectious factor is *Campylobacter jejuni* (*C. jejuni*) colonization, which plays a role in immunoproliferative small intestinal disease (IPSID).<sup>8</sup> Until recently, human immunodeficiency virus (HIV) was considered a significant risk factor for gNHL. Nowadays, effective antiretroviral treatment of HIV patients resulted in lymphoma frequency reduction in these patients. Moreover, OS in HIV lymphoma patients does not differ significantly from corresponding immunocompetent patients. The estimated risk of gNHL in HIV carriers is not substantially different from the average population risk. Other immunodeficiency disorders are connected with a higher gNHL risk.<sup>8</sup> It should also be noted that inflammatory diseases, even though not caused by infections, increase the risk of gNHL, and celiac disease (CD) is a quintessential example of this process.<sup>8</sup>

### Staging and prognosis

Ann Arbor staging system does not illustrate the exact clinical stage of the disease and is not valuable in prognosis. The most widely used classification is the Lugano system (Table 1).

Marginal zone lymphoma cases comprise over 50% of primary gNHL cases.<sup>1</sup> It is seen less commonly in the intestines (5% of intestine lymphomas) and colorectal area (25% of colorectal lymphomas).<sup>4</sup> It usually affects patients over 50 years of age, with a slight male prevalence (1.5:1). Strong evidence on the association between *H. pylori* and gastric MALT (gMALT) has been shown.<sup>1</sup> Gastric MALT is usually diagnosed in the early stage: typically, an endoscopy reveals multifocal superficial lesions of the mucosa and most patients present with stage I or II disease (Lugano staging system) while intestinal MALT might infiltrate to the intestinal wall. In the case of intestinal MALT, a differential diagnosis has to include the distinction from reactive lymphoid hyperplasia, which may sometimes mimic neoplastic process.<sup>4</sup> Independently of stage *H. pylori*, eradication therapy should be given to all gMALT patients. Anti-helicobacter regimens contain the following: double antibiotic therapy (clarithromycin + metronidazole or amoxicillin) and proton pump inhibitor. The outcome of the eradication therapy should be evaluated after at least 6 weeks with urea breath test or stool antigen test. It is reasonable to wait for at least 12 months before starting the treatment in patients who achieved endoscopic or clinical response together with *H. pylori* eradication. It is worth remembering that patients with t(11;18)(p21;p21) are unlikely to respond to *H. pylori* eradication. On the other hand, even *H. pylori* negative gMALT patients might respond to *H. pylori* eradication. In patients who do not achieve a lymphoma regression following antibiotic therapy and have localized disease, irradiation should be applied. In generalized disease immunochemotherapy is highly effective.<sup>9</sup>

Primary GI diffuse large B-cell lymphoma, similarly to MALT, is most typically located in the stomach with a prevalence estimated at 30–40% of gastric lymphomas.<sup>10</sup>

Table 1. Gastrointestinal lymphoma staging systems

Lugano	Paris staging system	Tumor extension	Ann Arbor
St I – confined to the GI tract (single primary or multiple, non-contiguous)	T1–2 N0 M0	mucosa, submucosa, muscularis propria, serosa	I <sub>E</sub>
St II – extending into abdomen II <sub>1</sub> – local nodal involvement II <sub>2</sub> – distant nodal involvement	T1–3 N1 M0 T1–3 N2 M0	regional lymph nodes more distant regional nodes	II <sub>E</sub>
St II <sub>E</sub> – penetration of serosa to involve adjacent organs or tissues	T4 N0–2 M0	invasion of adjacent structures with or without abdominal lymph nodes	II <sub>E</sub>
St IV – disseminated extranodal involvement or concomitant supra-diaphragmatic nodal involvement	T1–4 N3 M0 T1–4 N0–3 M1 T1–4 N0–2 M2 T1–4 N0–3 M0–2 Bx T1–4 N0–3 M0–2 B0 T1–4 N0–3 M2 B1	extra-abdominal lymph nodes additional distant (non-continuous) gastrointestinal sites non-gastrointestinal sites bone marrow not assessed bone marrow not involved bone marrow involved	III <sub>E</sub> i IV

At the same time, DLBCL is the most common intestinal lymphoma.<sup>4</sup> Most DLBCLs occur in patients in 6<sup>th</sup> decade of life, with a male predominance. Some evidence suggests the role of atrophic gastritis, especially among immunocompromised patients, in the etiopathology of gastric DLBCL (gDLBCL).<sup>10</sup> As with other DLBCL locations, gDLBCL may arise de novo or from transformation of indolent lymphoma, mainly MALT. De novo DLBCLs are bcl2 and CD10 positive whereas transformed MALT are bcl2 and CD10 negative.<sup>1</sup> Generally speaking, c-myc rearrangements are more common in GI aggressive lymphomas than in nodal lymphomas; in DLBCL they account for 10–45% of cases. But contrary to nodal lymphomas, c-myc rearrangements do not seem to influence negatively the overall survival (OS).<sup>11</sup> Gastrointestinal DLBCL is usually diagnosed in the early stage, with no bone marrow infiltration and low or intermediate the International Prognostic System (IPI). Presumably, outcomes of treatment are better compared to other extranodal and nodal DLBCL. In a retrospective analysis conducted by López-Guillermo et al., 5-year OS in gDLBCL was 62% compared to 52% in the whole DLBCL group.<sup>12</sup> In another analysis, although OS benefits were not proven, prolonged the Progression Free Survival (PFS) was observed in gDLBCL.<sup>13</sup> In the era of chemoimmunotherapy, radiotherapy does not improve OS.<sup>14,15</sup> On the basis of small prospective trials, some authors suggest to start with *H. pylori* eradication only in limited stage *H. pylori*(+) gDLBCL. It concerns both primary and transformed MALT DLBCL if only negative risk factors are not present.<sup>14,16</sup>

Gastrointestinal involvement in MCL is common. The reported frequency is 10–30%. Furthermore, in all probability the data is underestimated. Romaguera et al. conducted an endoscopy in 60 MCL patients. Histopathological involvement of lower GI tract was revealed in 53 patients (88%) and upper GI tract lesions were found in 28 patients (43%).<sup>17</sup> Only 14 (26%) patients presented with clinical GI symptoms. Significant GI tract histopathological involvement usually does not alter treatment schedule.<sup>17</sup> European Society for Medical Oncology (ESMO) guidelines recommend an endoscopy in limited stages I/II to exclude asymptomatic involvement.<sup>18</sup> The most common GI tract involvement manifestation is multiple lymphomatous polyposis.<sup>17</sup> It is worth remembering that PET-CT might give false negative results and fail to reveal lymphomatous polyposis.<sup>19</sup> Primary GI MCL is very rare and accounts for only 2% of primary gNHLs.<sup>20</sup> Primary GI MCL is usually very aggressive, with high MIPI scores. Survival, compared to nodal MCL involving GI, is poor. As the majority of patients are not autologous stem cell transplantation-eligible, rituximab maintenance is suggested to sustain treatment effects.<sup>20</sup>

Immunoproliferative small intestinal disease (IPSID), formerly known as heavy alpha chain disease, is a rare variant of intestinal MALT lymphoma. It constitutes for 30% of all GI lymphomas in the Middle East. In the Western countries, it can be diagnosed among immigrants from

the Middle East. Median age at the moment of the diagnosis is 20–30 years. Recurrent *C. jejuni* infection role in pathogenesis is suspected. In contrast with other infectious agents, *C. jejuni* colonization is not permanent; moreover, there is no evidence that *C. jejuni* plays a role in cancer development.<sup>21</sup> In some cases, successful antibiotic therapy may lead to remission, but in other patients transformation to DLBCL was observed.<sup>1</sup>

Primary extranodal FL is rare. The most common location for gastric FL (gFL) is duodenum.<sup>22</sup> Typically primary intestinal FL is an indolent lymphoma, often limited and with low histological grade (G1–G2). It predominantly affects middle-aged women. Incidental diagnosis in asymptomatic patients undergoing endoscopy for unrelated symptoms is very common.<sup>4</sup> The most common form of the disease is mucosal polyp.<sup>4</sup> The tumor has a favorable prognosis even when the disease is disseminated. The indolent course of the disease is considered similar to nodal FL. In the early stages, there is no need to introduce the treatment.<sup>22,23</sup>

Burkitt lymphoma is usually diagnosed in the form of a mass located predominantly in the ileocecal region. Due to its aggressive nature and chemosensitivity, the standard approach is aggressive chemotherapy. Rituximab addition is more widely recommended in recent years.<sup>24,25</sup> There are casuistic reports on *H. pylori* eradication efficacy in gastric BL (gBL) therapy.<sup>26</sup>

Lymphomatoid granulomatosis (LG) typically involves the lungs and is rarely found in GI tract. It is an angiodesstructive EBV(+) lymphoma with aggressive course and poor prognosis (OS below 2 years).<sup>1</sup>

Plasmablastic lymphoma (PBL) is an aggressive variant of DLBCL usually diagnosed in immunocompromised patients, particularly HIV(+). The most common location is the oral cavity. It may also be found in other GI tract parts, primarily in the anal canal.<sup>4</sup>

Primary effusion lymphoma (PEL) is actually a rare form of highly aggressive “plasmablastic” DLBCL arising mainly in immunocompromised patients. Approximately 30% of extracavitary PEL are diagnosed in the GI tract.<sup>4</sup>

Post-transplant lymphoproliferative disorders (PTLD) are diagnosed in transplant recipients. Gastrointestinal tract involvement may be the primary location or part of the disseminated disease. The most commonly affected part of the GI tract is the distal segment of small intestine.

## Mature T-cell lymphomas

Enteropathy-associated T-cell lymphoma is a rare type of peripheral T-cell lymphoma. Celiac disease is the most common food intolerance in Europe and accounts for 0.5–1% of EATL cases. Refractory CD appears when the patients fail to improve on a gluten-free diet (2–5%). Intraepithelial monoclonal lymphocyte proliferation might arise in refractory CD that leads to EATL. The EATL prevalence

in Western Europe is about 0.14/100,000. It accounts for 1.4% of NHL cases and 10–25% of primary intestinal lymphomas. Usually, the diagnosis is made in the patient's 6<sup>th</sup> decade of life. Men and women are affected with similar frequency.<sup>27</sup> Clinical symptoms are the consequence of malabsorption with abdominal pain, but many patients present with acute symptoms, such as intestinal bleeding, perforation and obstruction. Although EATL usually appears in refractory CD, it may be diagnosed in well-controlled CD and even in previously untreated, healthy people. Enteropathy-associated T-cell lymphoma may be localized in every GI tract part but the most common location is the jejunum. Commonly, it manifests as multiple ulcers, tumors and strictures.<sup>28</sup>

The EATL I type concerns 80–90% of cases. Lymphoma cells derive from CD with villous atrophy and crypt hyperplasia. Tumor cells are medium-sized to large and pleomorphic; reactive inflammatory infiltrate is common and even necrosis might be present. Cells are frequently CD30-positive (which leads to therapeutic implications). The EATL II type is most common in Asia. Very often it does not follow CD. Tumor cells are monomorphic, small to medium-sized. Neither inflammatory infiltrations nor necrosis is observed. Lymphoma cells are DC 30-negative.<sup>4,29</sup>

Conventional chemotherapy based on anthracyclines effects is not satisfactory. Median 5-year OS is 8–20%.<sup>30</sup> The idea of surgical treatment was to debulk the disease and excise tumor masses with high risk of obstruction or perforation during chemotherapy, but so far, surgical treatment did not improve the response.<sup>31</sup> There is no specific prognostic index for EATL. It seems that low IPI correlates with better OS,<sup>30</sup> but according to some authors, more PIT is more accurate in EATL risk stratification.<sup>29</sup> Single risk factors that might be relevant for PFS and OS are: tumor size >5 cm, poor performance status, high CRP, and high LDH.<sup>29</sup>

Sieniawski et al. introduced intensive IVE/MTX (ifosfamide, epirubicin, etoposide/methotrexate) regimen in 26 ASCT-eligible EATL patients. The patients received 1 cyclophosphamide, doxorubicin, oncovin, prednisone (CHOP) course, 3 ifosfamide, epirubicin, etoposide (IVE) courses and 1 intermediate dose methotrexate course. Chemotherapy was followed by ASCT procedure. The outcome of the patients treated in this protocol was better than median OS achieved after standard chemotherapy. Briefly, 65% of patients achieved CR vs 42% in the control group ( $p = 0.06$ ); 39% of the patients died (including 31% lymphoma-related deaths), whereas in the control group, 81% died (61% died of the EATL) ( $p = 0.001$  and  $0.005$ , respectively). High response rate correlated with 5-year OS benefits: 60% IVE/MTX-treated patients achieved 5-year OS vs 22% of patients in the control group ( $p = 0.003$ ). This is symptomatic that in IVE/MTX only 1 partial remission was obtained and there were no partial remission (PR) in the control group. These results seem to be indicative of the aggressive character of the disease and are arguments for aggressive first-line treatment. IVE/MTX-ASCT regimen may lead

to potentially severe toxic complications, such as the following: myelotoxicity, encephalopathy, sepsis, and renal impairment.<sup>28</sup> There is more data for aggressive approach in EATL. A retrospective study was conducted by European Society for Blood and Marrow Transplantation (EBMT): 44 EATL patients that underwent ASCT consolidation in 2000–2010 were analyzed. First line regimens were heterogeneous: schedules based on anthracyclines, methotrexate, and ifosfamide. More than 50% of the patients were treated with more than 1 chemotherapy line before ASCT. Thirty-one patients (70%) were in first complete remission (CR) or PR at the time of the ASCT. Age, gender, disease stage, and B-cell symptoms at diagnosis were not associated with significant PFS or OS differences. The authors concluded that ASCT conducted in first CR/PR is the most effective treatment. Four-year OS in this group was 66% vs 35% in the remaining patients ( $p = 0.62$ ). However, according to the authors, only 50% of the patients, due to their age, performance status are ASCT-eligible.<sup>32</sup> There are attempts to introduce new drugs in EATL treatment. Khalaf et al. described brentuximab vedotin efficacy in a EATL patient who was CD30<sup>+</sup> highly positive. Very good partial remission was observed after 3 cycles. Complete remission was achieved after 8 cycles and sustained during 9-month observation. The most important side effect observed during treatment was exacerbation of neuropathy, which was present at the beginning of the therapy. The authors suggest that brentuximab might be an option for the patients with poor tolerance of more intensive chemotherapy.<sup>33</sup> Sibon et al. added brentuximab to other regimens. The patients, after achieving remission, underwent ASCT procedure. Preliminary data is very encouraging.<sup>34</sup> The data on positive effects of alemtuzumab addition to chemotherapy is anecdotal. Furthermore, no durable effects were achieved with this drug in EATL treatment. Available data on RIC-allogeneic SCT (sibling) efficacy is also sparse.<sup>31</sup>

Considering the poor prognosis and low chemotherapy effectiveness, there have been attempts to introduce preemptive treatment in CD, i.e., cladribine. However, the safety and efficacy data are very sparse.<sup>31</sup>

Extranodal NK/T-cell lymphoma of the nasal type (ENKTL) is usually located in the nasopharyngeal region. However, sometimes it occurs in various parts of the GI tract.<sup>1</sup> Virtually always ENKTL is associated with EBV infection.<sup>1</sup> Differential diagnosis should be made between ENKTL and NK enteropathy (which is a benign GI proliferation) or indolent T-cell lymphoproliferative disease of the GI tract, which are both very rare.

## Summary

Lymphoproliferative disorders of the GI tract are not common and primary GI lymphomas are rare. Gastrointestinal lesions, when found in lymphoma patients, should always be verified and differential diagnosis with other

diseases should be done (Table 2). Though new imaging techniques are developing rapidly, endoscopy is still the most important diagnostic tool in gastrointestinal lymphomas. Histopathological type may vary, with the 2 most common morphologic subtypes being MALT and DLBCL. The most typical location of GI lymphomas is the stomach. The discovery of association of *H. pylori* infection to gastric lymphoma led to serious approach modification in this disease. Nowadays, in the antiretroviral HAART era, HIV seems to lose its importance as a risk factor. T-cell lymphomas are more aggressive than B-lineage NHL and there is still much to do to improve patient outcome.

Table 2. Differential diagnosis of gastrointestinal lymphomas

GI lymphomas – differential diagnosis
Crohn disease
Adenocarcinoma and other solid tumors
Benign lymphoid hyperplasia
Peptic ulcer disease
Celiac disease
Bacterial and fungal infections of GI tract

## References

- Bautista-Quach MA, Ake CD, Chen M, Wang J. Gastrointestinal lymphomas: Morphology, immunophenotype and molecular features. *J Gastrointest Oncol*. 2012;3(3):209–225.
- Sieniawski M, Angamuthu N, Boyd K, et al. Evaluation of enteropathy-associated T-cell lymphoma comparing standard therapies with a novel regimen including autologous stem cell transplantation. *Blood*. 2010;115(18):3664–3670.
- Ghimire P, Wu GY, Zhu L. Primary gastrointestinal lymphoma. *World J Gastroenterol*. 2011;17(6):697–707.
- Foukas PG, de Leval L. Recent advances in intestinal lymphomas. *Histopathology*. 2015;66(1):112–136.
- Janssen J. The impact of EUS in primary gastric lymphoma. *Best Pract Res Clin Gastroenterol*. 2009;23(5):671–678.
- Byun JH, Ha HK, Kim AY, et al. CT findings in peripheral T-cell lymphoma involving the gastrointestinal tract. *Radiology*. 2003;227(1):59–67.
- Boot H. Diagnosis and staging in gastrointestinal lymphoma. *Best Pract Res Clin Gastroenterol*. 2010;24(1):3–12.
- Andrews CN, John Gill M, Urbanski SJ, Stewart D, Perini R, Beck P. Changing epidemiology and risk factors for gastrointestinal non-Hodgkin's lymphoma in a North American population: Population-based study. *Am J Gastroenterol*. 2008;103(7):1762–1769.
- Zucca E, Copie-Bergman C, Ricardi U, Thieblemont C, Raderer M, Ladetto M; on behalf of the ESMO Guidelines Working Group. Gastric marginal zone lymphoma of MALT type: ESMO Clinical Practice Guidelines for diagnosis, treatment and follow-up. *Ann Oncol*. 2013;24(Suppl 6):144–148.
- Martinelli G, Gigli F, Calabrese L, et al. Early stage gastric diffuse large B-cell lymphomas: Results of a randomized trial comparing chemotherapy alone versus chemotherapy + involved field radiotherapy. *Leuk Lymphoma*. 2009;50(6):925–931.
- Choi SY, Kim SJ, Kim WS, Kim K, Ko YH. Aggressive B cell lymphomas of the gastrointestinal tract: Clinicopathologic and genetic analysis. *Virchows Arch*. 2011;459(5):495–502.
- López-Guillermo A, Colomo L, Jiménez M, et al. Diffuse large B-cell lymphoma: Clinical and biological characterization and outcome according to the nodal or extranodal primary origin. *J Clin Oncol*. 2005;23(12):2797–2804.
- Nakajima Y, Tomita N, Itabashi M, et al. Analysis of outcomes in patients with supra-diaphragmatic vs infra-diaphragmatic diffuse large B cell lymphoma treated with R-CHOP therapy. *Leuk Res*. 2015;39(2):198–203.
- Cuccurullo R, Govi S, Ferreri AJM. De-escalating therapy in gastric aggressive lymphoma. *World J Gastroenterol*. 2014;20(27):8993–8997.
- Avilés A, Nambo M.J, Neri N, et al. The role of surgery in primary gastric lymphoma: Results of a controlled clinical trial. *Ann Surg*. 2004;240(1):44–50.
- Kuo SH, Yeh KH, Wu MS, et al. *Helicobacter pylori* eradication therapy is effective in the treatment of early-stage *H. pylori*-positive gastric diffuse large B-cell lymphomas. *Blood*. 2012;119(21):4838–4844.
- Romaguera JE, Medeiros LJ, Hagemester FB, et al. Frequency of gastrointestinal involvement and its clinical significance in mantle cell lymphoma. *Cancer*. 2003;97(3):586–591.
- Dreyling M, Geisler C, Hermine O, et al; ESMO Guidelines Working Group. Newly diagnosed and relapsed mantle cell lymphoma: ESMO Clinical Practice Guidelines for diagnosis, treatment and follow-up. *Ann Oncol*. 2014;25(Suppl 3):iii83–92. doi:10.1093/annonc/mdu264
- Saito M, Miyazaki M, Tanino M. <sup>18</sup>F-FDG PET/CT imaging for a gastrointestinal mantle cell lymphoma with multiple lymphomatous polyposis. *World J Gastroenterol*. 2014;20(17):5141–5146.
- Dasappa L, Suresh Babu MC, et al. Primary gastrointestinal mantle cell lymphoma: A retrospective study. *J Gastrointest Cancer*. 2014;45(4):481–486.
- Zucca E, Bertoni F, Vannata B, Cavalli F. Emerging role of infectious etiologies in the pathogenesis of marginal zone B-cell lymphomas. *Clin Cancer Res*. 2014;20(20):5207–5216.
- Misdraji J, Harris NL, Hasserjian RP, Lauwers GY, Ferry JA. Primary follicular lymphoma of the gastrointestinal tract. *Am J Surg Pathol*. 2011;35(9):1255–1263.
- Damaj G, Verkarre V, Delmer A, et al. Primary follicular lymphoma of the gastrointestinal tract: A study of 25 cases and a literature review. *Ann Oncol*. 2003;14(4):623–629.
- Perkins AS, Friedberg JW. Burkitt lymphoma in adults. *Hematology Am Soc Hematol Educ Program*. 2008:341–348.
- Hoelzer D, Walewski J, Döhner H, et al; German Multicenter Study Group for Adult Acute Lymphoblastic Leukemia. Improved outcome of adult Burkitt lymphoma/leukemia with rituximab and chemotherapy: Report of a large prospective multicenter trial. *Blood*. 2014;124(26):3870–3879.
- Baumgaertner I, Copie-Bergman C, Levy M, et al. Complete remission of gastric Burkitt's lymphoma after eradication of *Helicobacter pylori*. *World J Gastroenterol*. 2009;15(45):5746–5750.
- Zettl A, deLeeuw R, Haralambieva E, Mueller-Hermelink HK. Enteropathy-type T-cell lymphoma. *Am J Clin Pathol*. 2007;127(5):701–706.
- Sieniawski M, Angamuthu N, Boyd K, et al. Evaluation of enteropathy-associated T-cell lymphoma comparing standard therapies with a novel regimen including autologous stem cell transplantation. *Blood*. 2010;115(18):3664–3670.
- Delabie J, Holte H, Vose JM, et al. Enteropathy-associated T-cell lymphoma: Clinical and histological findings from the international peripheral T-cell lymphoma project. *Blood*. 2011;118(1):148–155.
- Nijeboer P, de Baaij LR, Visser O, et al. Treatment response in enteropathy associated T-cell lymphoma: Survival in a large multicenter cohort. *Am J Hematol*. 2015;90(6):493–498.
- Di Sabatino A, Biagi F, Gobbi PG, Corazza GR. How I treat enteropathy-associated T-cell lymphoma. *Blood*. 2012;119(11):2458–2468.
- Jantunen E, Boumendil A, Finel H, et al; Lymphoma Working Party of the EBMT. Autologous stem cell transplantation for enteropathy-associated T-cell lymphoma: A retrospective study by the EBMT. *Blood*. 2013;121(13):2529–2532.
- Khalaf WF, Caldwell ME, Reddy N. Brentuximab in the treatment of CD30-positive enteropathy-associated T-cell lymphoma. *J Natl Compr Canc Netw*. 2013;11(2):137–140.
- Sibon D, Malamut G. Enteropathy-associated T-cell lymphoma type I, but not refractory celiac disease, strongly expresses CD30 and might benefit from brentuximab. *Vedotin Blood*. 2013;122:4252.

# Methods of integrating the human nervous system with electronic circuits

Tymoteusz Skok<sup>1,A–F</sup>, Paweł Tabakow<sup>2,D–F</sup>, Krzysztof Chmielak<sup>2,D–F</sup>

<sup>1</sup> Student Scientific Circle at the Department of Neurosurgery, Wrocław Medical University, Poland

<sup>2</sup> Department of Neurosurgery, Wrocław Medical University, Poland

A – research concept and design; B – collection and/or assembly of data; C – data analysis and interpretation; D – writing the article; E – critical revision of the article; F – final approval of the article

Advances in Clinical and Experimental Medicine, ISSN 1899–5276 (print), ISSN 2451–2680 (online)

*Adv Clin Exp Med.* 2019;28(8):1125–1135

## Address for correspondence

Tymoteusz Skok  
E-mail: tymoteusz.skok@gmail.com

## Funding sources

None declared

## Conflict of interest

None declared

Received on June 4, 2018

Reviewed on October 1, 2018

Accepted on January 28, 2019

Published online on August 12, 2019

## Abstract

In recent years, many attempts have been made to connect electrical circuits with the human nervous system. The objective of type of research was diverse – from the desire to understand the physiology of the nervous system, through attempting to substitute nervous tissue defects with synthetic systems, to creating an interface that allows computers to be controlled directly with one's thought. Regardless of the original purpose, the creation of any form of such a combination would entail a series of subsequent discoveries, allowing for a real revolution in both theoretical and clinical neuroscience. Computers based on neurons, neurochips or mind prostheses are just some examples of technologies that could soon become part of everyday life. Despite numerous attempts, there is still no interface that meets all the expectations of the scholars. However, many scientific groups seem to be on the right track and their achievements raise extraordinary expectations. This paper evaluates historical theories and contemporary ideas about such interfaces to smoothly describe the major medical and scientific utility of the subject. Thus it presents the main issues surrounding the concept of integrating the human nervous system with electronic circuits.

**Key words:** brain–computer interface, biosensors, peripheral nerve interface

## Cite as

Skok T, Tabakow P, Chmielak K. Methods of integrating the human nervous system with electronic circuits. *Adv Clin Exp Med.* 2019;28(8):1125–1135. doi:10.17219/acem/103414

## DOI

10.17219/acem/103414

## Copyright

© 2019 by Wrocław Medical University

This is an article distributed under the terms of the Creative Commons Attribution Non-Commercial License (<http://creativecommons.org/licenses/by-nc-nd/4.0/>)

## Introduction

The first historical attempts to interpret the relationship between mind and body were undertaken by Alexandrian doctors around 250 BC. They concluded that “*pneuma psychikon*” (“mental spirit”) moves along the nerve fibers, which stimulate the muscles of the animals to contract. This theory was taken up by Galen, who included it in his works on the subject of the human body. For the next 1,500 years, European medicine did not try to oppose any of his theses.<sup>1</sup> In 1664, Jan Swammerdam made a breakthrough discovery in the field of neurophysiology. He discovered that the muscle of a dissected frog retains the ability to contract post mortem and that this contraction can be induced by irritating the nerve connected to the muscle. This discovery led to the demise of current views on the induction of motor reactions.<sup>2</sup> Thus, the “*pneuma psychikon*” theory was renounced by the scientific community. However, Swammerdam was not able to answer how the nerve irritation causes the muscles to contract.<sup>3</sup>

In 1713, Isaac Newton suggested that this phenomenon could be related to electrical activities occurring in the living organism. The final scientific evidence for the existence of electrical phenomena in tissues was described at the end of the 18<sup>th</sup> century. In 1791, Luigi Galvani proved that the stimulation of the muscle in Swammerdam’s experiment is associated with the conduction of an electrical impulse.<sup>4</sup> A new field of science, electrophysiology, was established. A systematic description of how electrical impulses control processes occurring in living organisms was performed. In 1825, Leopoldo Nobili invented the first galvanometer, which allowed him to study in detail the electrical phenomena in tissues. Subsequent discoveries by Helmholtz, Bernstein and Overton made it possible to determine the features that characterize neuromuscular agitation.<sup>5</sup> The work of Ramón y Cajal, Berger and Cole later laid the foundations for modern methods of perceiving the electrical activity of the human nervous system.

The real revolution, however, began with the development of the voltage-clamp method by Cole and Marmont.<sup>6</sup> Thanks to this technique, Hodgkin and Huxley investigated the mechanisms of electrical activity in neurons, for which they also received the Nobel Prize in 1963. Their work enabled a whole range of discoveries related to the physiology of propagation of electrical arousal in neurons. Simultaneously with electrophysiology, a completely new trend developed in culture and science. In 1911, Jean de la Hire in his novel “*Le Mystère des XV*” presented the concept of connecting man with a machine. This idea was quickly picked up by other science-fiction writers. It has resulted in numerous stories, novels and films about the use of artificial implants in the human body. At the same time, Pierre Teilhard de Chardin, in his book “*The Future of Mankind*” (1949), used, for the first time, the term “transhumanizing”. It meant raising, with the help of technology, the potential of human capabilities

to the maximum level. Soon, the concepts of improving the human body, including the nervous system, were collectively referred to as transhumanism. With the emergence of this concept, a group of philosophers and ethicists started considering the possible consequences of the development of such a type of technology.<sup>7</sup>

The first idea to use an electrical system to eliminate a human body defect precedes the book of de Chardin. Research conducted in 1940 by Jones, Stevens and Lurie made it possible to hypothesize the possibility of using electrostimulation in the case of damage of the cochlea. Thanks to this, Djourno and Eyriès decided to conduct a revolutionary operation. In 1957, they managed to connect the 8<sup>th</sup> cranial nerve (vestibulo-cochlear) with an electrode, and thus to perform the first cochlear implant insertion surgery. It was not only the first electric auditory implant, but also the first successful electrical implant in general.<sup>8</sup> Since that time, many concepts have been created in the field of electronics implementation in human tissue.

At the beginning the 21<sup>st</sup> century, Grattarola laid the foundations of a new branch of science – neuroengineering. In 2003, the first international conference on neuroengineering was held, and in 2004 the first neuroengineering journal – “*The Journal of Neural Engineering*” – was established. Neuroengineering is a science on the border of neurobiology, physics, mathematics, electronics, and bioengineering. Creating an interface between nerve tissue and an electrical circuit is just one of many issues that this field deals with. Other issues related to neuroengineering are techniques of the stimulation of nervous tissue regeneration, neuroimaging, the creation of mathematical models of neural network behaviors, and many more.<sup>9,10</sup>

The aim of this paper is to present the history and current knowledge and experience in the field of research on the application of methods to connect the human nervous system to artificial electric circuits.

## Material and methods

During the development of this paper, the data described was acquired mainly through the use of the PubMed search engine. Other search engines, such as: ScienceDirect, Nature and Google Scholar, played a supportive role in situations when the authors were interested in finding a very particular article, and it was not included in the PubMed database.

To explore the subject, the authors set a number of issues to be explained in terms of every method described. They formed those issues afterwards in the following list of questions:

- Which ideas had already been proposed to integrate nervous tissue with electrical circuits?
- Was such an idea realized? If so, did it meet all the goals set by the authors of the technique?



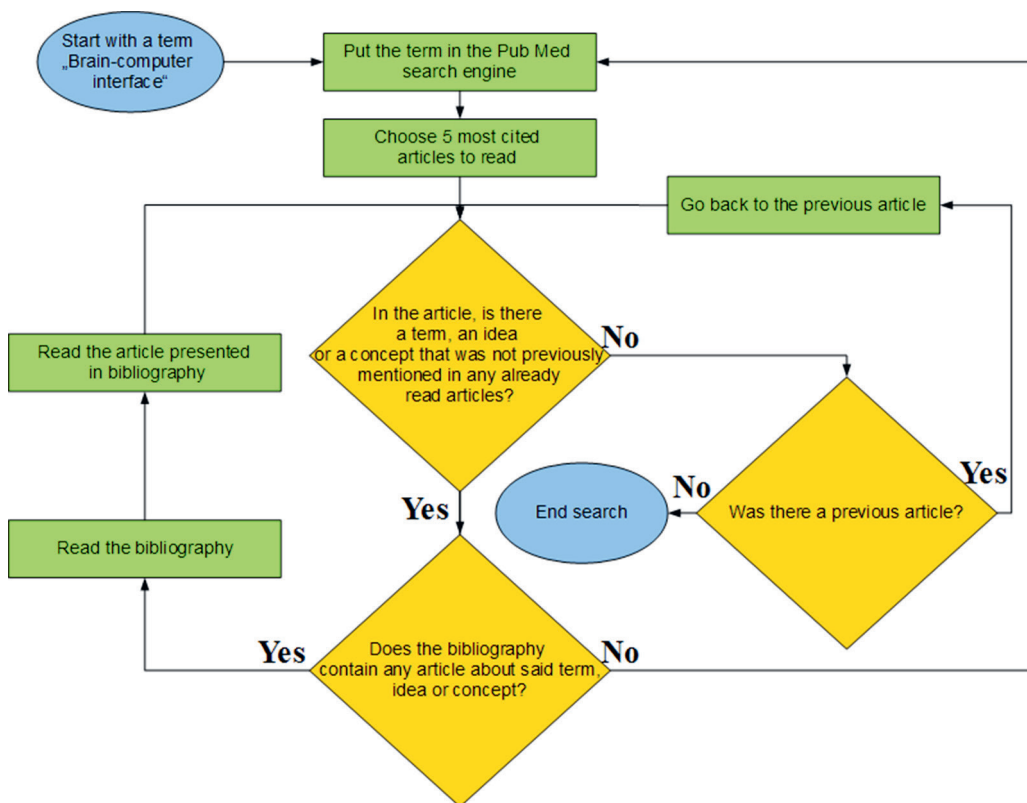


Fig. 1. Flowchart diagram illustrating the authors' search strategy

– If it didn't, what are the restrictions of this technique? Has the idea been further developed? What are the predictions for development of the technique?

The lack of answers in newly reviewed papers created a need for further research. The authors were looking for new articles, based on the bibliographies of the previously evaluated papers and many search terms aimed particularly at this task.

During the construction of the bibliography, the authors have tried to include papers meeting as many of the following criteria as possible: original paper; answers at least 2 of the problems mentioned above; greatest possible applicability of the described techniques; most detailed description of the topic; accurate, methodological results. The algorithm guiding the authors during material collection is presented in Fig. 1.

## Results

### Paper search

The PubMed, ScienceDirect, Nature, and Google Scholar databases were searched. Over 20,000 articles were considered for review during the research. After a selection based on the number of citations, 120 articles were reviewed and 60 have been included in bibliography. The material described was collected both from original papers and other review articles. This allows the reader to examine various insights on the subject of the work.

## Basic principles of electrophysiological data processing

Most of the techniques described in this article are based on electrical readings measured with electrodes. Neurons, depolarizing, elicit an electromagnetic field around them. This field can stimulate electrons in electrodes to move, thus creating an electric current. The individual properties of an electrode, such as proximity to the signal and internal impedance, have an impact on the ability to record those arousals. Therefore, depending on the method, the quantity of impulses noticed by the electrode may vary in number. Its reading capacity can range between a single neuron, a small group of cells and even thousands of neurons. Such data can be further processed peripherally (for example by a differential amplifier), and then they can be directly coded in the form of digital records. One of many popular devices for such translation is, i.e., the open source Open BCI platform. Information is allocated in the primary storage of the computer, where it can be further used as a mathematic variable. Computer software can process this data in any way the user wants. For example, for EEG readings, there are many software packages that enable easy data processing, like EEGLAB (Swartz Center for Computational Neuroscience, University of California at San Diego, USA) or the Neurophysiological Biomarker Toolbox (VU University Amsterdam, the Netherlands). It is also possible to reverse the way of signal conduction. The effect would be generation of an electromagnetic field around the electrodes, thus facilitating the depolarization

in nearby neurons. This is how afferent stimulation of the nervous system could be evoked. Therefore, appropriate programs for electrode firing patterns can elicit an artificial feeling of sensation or stimulate body effectors (muscles) to perform complex movements.

## Technology review

In general, the technology that connects the nervous system with electronic systems can be divided into 3 large categories:

- devices that record and control pulse transmission in the cerebral cortex and the central nervous system (BCI – brain–computer interface);
- devices that record and control the transmission of nerve impulses in the peripheral nerves (PNI – peripheral nerve interface);
- biosensors that record nerve cell activity in vitro.

Table 1. Possible medical use of electronic interfaces for nerve tissue

Interface type	Condition	Mechanism of action
Non-invasive BCI (EEG)	lock-in syndrom spinal cord injury	general control of external devices, like cursor on computer screen
Invasive BCI	lock-in syndrom spinal cord injury	precise control of external devices, like robotic arms
		bypassing injury by direct motoneuron or muscle stimulation
	visual or auditory impairment	restitution of visual or auditory function
	direct brain injury	replacement of the missing brain tissue (so far only hippocampal injuries)
PNI	limb amputation	interfaces for high quality prosthesis control

BCI – brain–computer interface; EEG – electroencephalography; PNI – peripheral nerve interface.

## Brain–computer interface

The term BCI was used for the first time by Jacques Vidal in 1973. In his work “Toward direct brain–computer communication”, he described how, using an EEG apparatus, a machine could hypothetically read a brain’s decision-making process. He later constructed a system in which the respondent, with the help of evoked potentials, could control the appropriate symbol on the screen of a monitor. The subject was also able to guide the cursor through a simple maze puzzle.<sup>11</sup> The concept created by Vidal was developed and expanded in the following years. New trends appeared in the field of BCI technology. Contemporary brain–computer interfaces are not just machines based on EEG. The name BCI is actually defined as any device capable of collecting, analyzing and processing data directly from the brain.<sup>12</sup> Recently, a huge number of different

concepts, projects and plans for BCI have been created. Bringing them all together in one article seems unrealistic. Therefore, only the dominant ideas and trends in the field of BCI technology will be discussed. Brain–computer interfaces are usually divided according to their invasiveness.<sup>13</sup> They can be non-invasive, partially-invasive and invasive.

## Non-invasive brain–computer interface

Since 1970s the use of electroencephalography remains the most popular solution in the field of non-invasive BCI. This is mainly due to purely technical issues. Modern brainwave-reading devices can have the form of only several electrodes, which can be attached to the surface of the head. This makes them much handier and more practical than sophisticated research equipment. Connecting the EEG to the subject can take only a few minutes. Thus, the simplicity and convenience associated with the EEG tempts many researchers to use it in BCI. In recent years, a whole multitude of devices and instruments have been created. They allow, among others: writing on a computer screen,<sup>14</sup> wheelchair control<sup>15</sup> and web browsing.<sup>16</sup> They can even be used purely for entertainment purposes, such as playing computer games.<sup>17</sup>

The EEG-BCI technology still leaves much to be desired. Its biggest problem is the relatively low sensitivity and specificity, resulting in an inability to unambiguously read the signals sent by the subject. The relatively large number of errors made by the interface makes it impossible to use it in everyday life.<sup>18</sup> Nevertheless, work is ongoing on improving the methods of reading and interpretation, which may lead to the elimination of these drawbacks in the near future.

Other ideas in the field of non-invasive BCI are interfaces based on magnetic resonance imaging (MRI) and magnetoencephalography (MEG). The MRI-BCI technique has significant limitations. It has not yet been determined how the specific cognitive states of the brain could be read using an MRI machine. In addition, the tests may only be carried out in facilities with a resonance imager. This is a bigger problem, because the price of this type of equipment significantly limits its availability and universality. Despite this, attempts are still being made to implement fMRI-BCI technology in medicine. So-called “real-time MRI feedback” is sometimes used in post-stroke rehabilitation (learning how to reactivate subsequent levels of the pyramid system) as well as in teaching patients how to cope with pain and emotions.<sup>19</sup>

Magnetoencephalography (MEG) carries disadvantages similar to MRI. Large and cumbersome equipment generates the readings, the understanding of which still causes significant difficulties for modern science. At the same time, like the other interfaces of this group, the MEG apparatus is very imprecise and the subjects need a lot of time to learn how to use it. Most likely, MEG technology will not lead to the creation of a useful BCI in the near future.<sup>20</sup>

### Partially-invasive brain–computer interface

Current semi-invasive methods of BCI interface implantation are basically limited only to electrocorticography (ECoG) methods. Although ECoG is a method very similar to the EEG, the electrodes are located not on the surface of the patient's skull, but directly in the epidural or subdural space. This has many advantages over the EEG.<sup>21</sup> Electrocorticography represents a much higher resolution, higher amplitude of changes, and therefore greater sensitivity, higher bandwidth and smaller susceptibility to electrical interference due to muscle contraction and eye movement. However, semi-invasive interfaces have also significant limitations. Their basic disadvantage in comparison to EEG-BCI is the need to carry out operations with a risk of undesirable adverse events. Nevertheless, ECoG-BCI continues to be considered a promising technology. It does not come into direct contact with the cerebral cortex. This makes the microglial reaction and the formation of glial scars around electrodes delayed in time and less prominent (as in the case of fully invasive interfaces), allowing for a longer viability of the device (Fig. 2).

### Invasive brain–computer interface

Invasive BCI allows the most detailed perception of electrical activity in the human central nervous system. Depending on the spatial resolution of the recorder, 2 types of invasive BCI can be distinguished: multi-unit activity (MUA) recording and single-unit activity (SUA) recording. The concept of SUA recording seems to be the most exciting. This is a technology in which individual electrodes would be able to contact and cooperate with single neurons. Unfortunately, currently, it is not possible to create a BCI consistent with such an idea. It seems, however, that

the possibility of creating a direct connection between a neuron and electronics is heralded by the emergence of so-called neural mesh technology. It involves injecting electrodes into the cerebral cortex, which, slowly developing, over time would be able to come into contact with each neuron individually.<sup>22</sup>

In MUA recordings, electrodes interact with whole groups of neurons in their vicinity. Devices of this type have already succeeded in supporting patients with tetraplegia, lock-in syndrome or other neurological deficits. In 1998, Philip Kennedy constructed the first machine that was directly connected with the human brain. Based on principles of neural regeneration and low impedance recording, he used a glass tube with neurotrophic factors and wires made out of gold to achieve a stable BCI interface (the so-called neurotrophic electrode). During his test with a patient suffering from severe amyotrophic lateral sclerosis, he managed to implant his system in the human motor cortex. Thus, he created an effective way of communication between the patient and his environment.<sup>23</sup> A similar concept has been used in the Brain Gate project – a venture that was created to enable paralyzed people more effective communication with the surrounding world.<sup>24</sup> Brain Gate decided to use a pattern of stable, numerous needle-like electrodes to establish a connection between the motor cortex and a computer (the Utah electrode array). The aim of the Brain Gate project was to give patients with lock-in syndrome the ability to communicate with the environment using the cursor on the computer screen or artificial, robotic arms. Other research groups soon followed the steps of Brain Gate and since 2002, there have been many projects whose aim was to allow neuroprotheses to be controlled by people with tetraparesis<sup>25,26</sup> (Fig. 3).

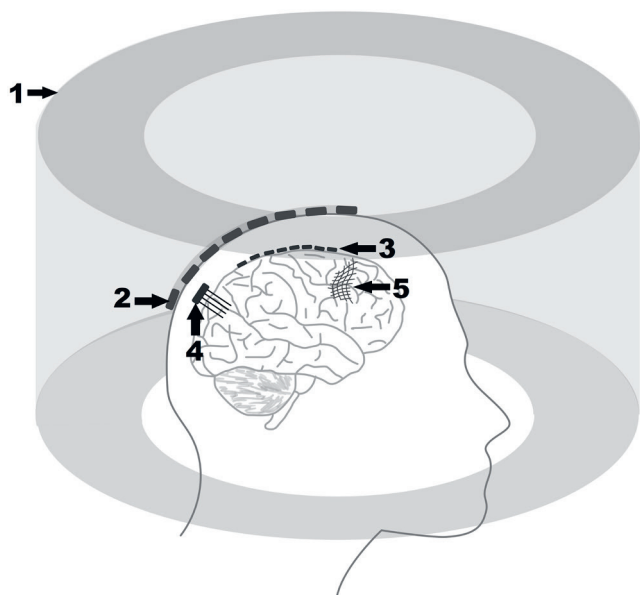


Fig. 2. Different approaches to brain–computer interface:  
1. Magnetoencephalographic BCI/magnetic resonance BCI;  
2. Electroencephalographic BCI; 3. Electrocorticography BCI;  
4. Multi-unit activity recording BCI; 5. Single-unit activity recording BCI



Fig. 3. Matthew Nagle, the first paralyzed person that ever used Brain Gate technology<sup>27</sup>

Although BCI-controlled artificial robotic limbs are a great tool to improve the quality of life of patients with spinal cord injury, an alternative therapeutic concept for these patients has recently been developed. It is based on a method of direct wireless transmission from the brain of signals for voluntary contraction of the paralyzed muscles by bypassing the area of spinal cord injury. Capogrosso et al. have managed to record signals both from motor cortex and spinal motoneurons in primates.<sup>28</sup> By optimizing the data, they recreated a spinal cord motoneuron firing pattern, and ordinated it with signals from the motor cortex. The Wi-Fi microarray receptor in the head and epidural electrical stimulator implanted in the lumbar spinal cord locomotor generator of a monkey made it possible to alleviate gait deficits after spinal cord injury.<sup>28</sup> Another approach was proposed by a research group from Columbus, USA. Their idea was not concentrated on translating brain signals to spinal cord motoneurons, but directly to the patient's muscles. This enabled a 24-year-old C5/C6 quadriplegic patient to restore the ability for voluntary movement of his wrist and hand. He was even able to perform complex tasks, like playing on a computer game controller or pouring dice from one cup to another.<sup>29</sup> Invasive BCI are also capable of replacement of neurons in the lesioned central nervous system (CNS). An example of such an application is the treatment of visual deficits by application of prostheses activating the visual cortex. By implantation of the electrodes on the occipital lobe, William Harvey Dobbelle caused electrical stimulation in the appropriate areas of the cortex, thus evoking visual sensations in the subject. This enabled blind people to experience a complete sense of vision. By combining this type of interface with a camera, Dobbelle helped blind people to function more freely in society.<sup>30</sup> Although there are more contemporary ideas of visual function supplementation, so far only 2 projects have received the CE mark for use in Europe – Argus II and Alpha IMS. Argus II is an artificial implant that, in response to light received by a camera, stimulates optic nerve and remaining retina cells.<sup>31</sup> Subretinal Visual Implant Alpha IMS, on the other hand, detects light stimulus directly inside the eye. Subsequently, it activates the retina's bipolar cells, creating a sensation of seeing.<sup>32</sup>

Another example of the usage of invasive BCI for the replacement of structures of the CNS is the project developed by Theodor Berger. It involves the creation of a prosthesis that would correspond to the function of the lesioned hippocampus. It is supposed to help people with memory deficits due to hippocampal lesion.<sup>33</sup>

Invasive BCI also have disadvantages. As an invasive method, they may require complex surgeries with risk of complications. The main concern about invasive BCI is the fact that glial scarring develops over time, preventing the reception of signals.<sup>34</sup> In conclusion, a comparison of non-invasive and invasive BCI shows that there will be an indication for both technologies. It is highly probable that non-invasive BCI will never be able to match invasive

in its detail and functionality. The EEG-BCI is still likely to be used in the fields of neurorehabilitation. With the development of science and the emergence of ever-better systems, it seems that invasive BCI will overcome non-invasive BCI in most applications, certainly those associated with the restoration of motor functions.<sup>35</sup>

## Peripheral nerve interface

Peripheral nerve interface (PNI) allows a registration of electrical stimuli in peripheral nerves.<sup>36</sup> The technology boom associated with PNI began around the 1990s and is still developing. There are more and more new concepts on the methods of electrode implantation, the types of used materials and the ability to enhance the signal coming from the axons. The ideas around peripheral nerve interfaces are mainly focused on creating an interface for intuitive use of artificial limb prostheses. There are 3 basic approaches attributed to PNI: external nerve PNI, intra-nervous PNI and regenerative PNI.<sup>37</sup>

### External nerve peripheral nerve interface

Nerve cuffs (Fig. 4A) is the most basic approach in the field of PNI. They are electrodes, attached to the surface of the nerve, so as to perceive its internal electrical activity.<sup>38</sup> There are many models of these devices, including cylindrical, helical and annular types. They all have a low specificity in recognizing nerve stimuli. Moreover, poor implementation of such an interface, as a result of nerve compression, manifests itself with a strong reaction from the connective tissue of the epineurium. This leads to quick scar formation and destabilization of the interface.<sup>39</sup>

The epineurium surrounding individual nerve fascicles is a relatively compact tissue, while the perineurium connecting these fibers with each other is relatively loose and plastic. This has made it possible to create a flat-interface nerve electrode (FINE) interface, which, when implemented on the nerve, changes its architecture (Fig. 4B). The nerve takes the form of a flat strip with nerve bunches placed flat next to each other. In this way, individual electrodes are able to study the electrical activity in the corresponding parallel tufts. At the same time, with the right choice of parameters, FINE does not adversely affect the physiological and histological features of the nerve.<sup>40</sup> Tests to use this technology in medical practice are still ongoing.<sup>41</sup>

### Intra-nervous peripheral nerve interface

The classic intra-nervous types of PNI include such projects as TIME (transverse intra-fascicular multichannel electrode) (Fig. 4C), LIFE (longitudinal intra-fascicular electrode) (Fig. 4D) and SPINE (slowly penetrating inter-fascicular nerve electrode) (Fig. 4E). Longitudinal intra-fascicular electrode and TIME are longitudinal electrodes, threaded with needles directly in the nerve structures. Longitudinal intra-fascicular electrodes are arranged in parallel along the nerve fascicle, according to the course

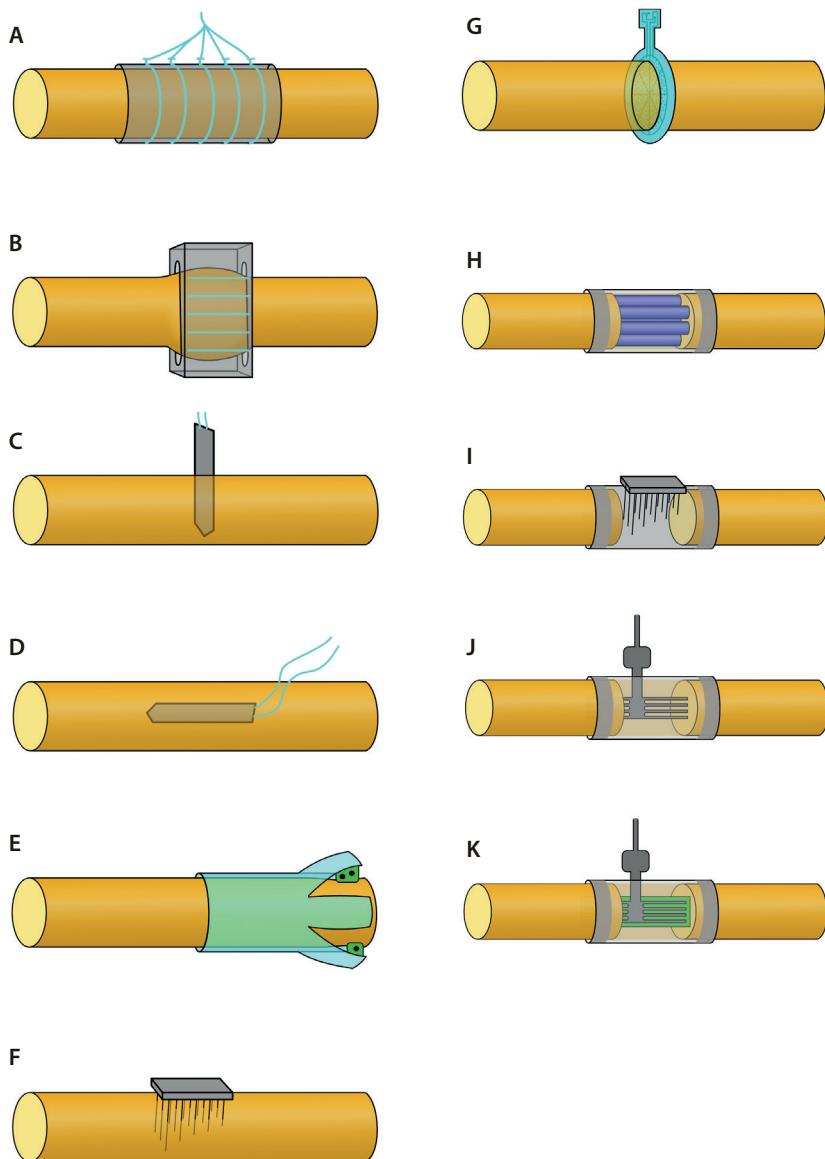


**Fig. 4.** Different approaches to peripheral nerve interfaces: A. Nerve cuffs; B. FINE (flat-interface nerve electrode); C. TIME (transverse intra-fascicular multichannel electrode); D. LIFE (longitudinal intra-fascicular electrode); E. SPINE (slowly penetrating interfascicular nerve electrode); F. USEA (Utah slant electrode array); G. SNI (sieve-nerve interface); H. MNI (microchannel-nerve interface); I. REMI (regenerative multielectrode interface) J. RSE (regenerative scaffold electrode); K. TEENI (tissue-engineered electronic nerve interface)

of the nerve.<sup>42</sup> Transverse intra-fascicular multichannel electrodes are implanted perpendicular to the nerve. They pierce the bundles through, transversely across the entire width of the nerve fascicle.<sup>43</sup> In SPINE, blunt electrodes press slowly on epineurium, squeezing into the nerve. Simultaneously, they rearrange nerve architecture to contact the largest possible number of nerve fibers. The changes in the mutual position of the fibers were to facilitate effective signal reception through the interface.<sup>44</sup> Unfortunately, it is difficult to find a modern publication on this technique. Most likely, it suffered from the same condition that TIME and LIFE suffer to this day. As a result of irritation of nerve structures around the electrodes, a scar made of glial cells arises over time. This makes the interface unresponsive to arousal and therefore unusable. Despite this, attempts are still being made to implant these types of electrodes. The use of more advanced artificial materials and biomaterials raises the hope of eliminating the phenomenon of the response of the body to the electrode.<sup>45</sup>

The USEA (Utah slant electrode array) (Fig. 4F) interface is composed of 100 electrodes, 0.5–1.5 mm long. Each of them is mounted on a 10-electrode array of 10 rows. The USEA is placed on the nerve by puncturing the peri- and epineurium with electrodes. In this way, each electrode offers a channel for the perception of electrical activity in the appropriate nerve compartment. Despite the relative simplicity of the idea, the USEA seems to be very successful in clinical trials. In the tests conducted on patients after amputation, the subjects were able to smoothly move the virtual hand on the monitor screen. It even managed to evoke the sensation of touch with the help of electric stimuli.<sup>46</sup> It is also worth mentioning that this model of electrode system is also used in invasive BCI techniques. It has been used, among others, in the aforementioned Brain Gate project.

Sieve-nerve interface (SNI) (Fig. 4G) and microchannel-nerve interface (MNI) (Fig. 4H) are technologies on the border

of invasive and regenerative PNI. The SNI is a transverse intersection of the nerve, followed by implantation of the SNI, consisting of electrodes, in the place of the nerve cut.<sup>47</sup> Regenerating, single axons pass through the mesh of the sieve, which allows the perception of the potentials generated by them. The MNI is not much different from this approach. According to Musick et al.,<sup>48</sup> regenerative microchannel electrodes are essentially long sieve implants that host millimeter lengths of the nerve. Both concepts are very invasive and often lead to intensive foreign body response reactions. A summary of the peripheral nerve interfaces used is shown in Fig. 4. A comparison of different types of PNI in reference to selectivity and interface invasiveness is shown in Fig. 5.

#### Regenerative multielectrode interface

Regenerative multielectrode interface (REMI) (Fig. 4I), regenerative scaffold electrode (RSE) (Fig. 4J) and tissue-engineered electronic nerve interface (TEENI) (Fig. 4K) are

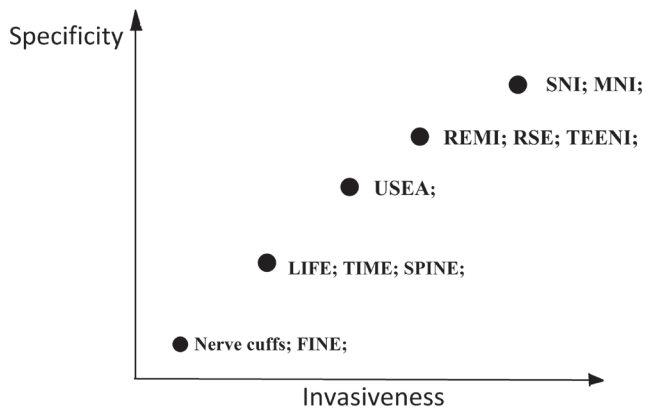


Fig. 5. Comparison of different types of peripheral nerve interfaces based on the level of signal selectivity and interface invasiveness

ideas quite similar to each other. In each of these projects, the 2 ends of the dissected nerve are placed in a special, bio-compatible tunnel-shaped dressing. Inside of such a dressing, different types of electrodes can be placed. Regenerating nerve fibers elongate slowly, interacting with the systems in the tunnel and connecting with them. What distinguishes the different approaches is the type of electrodes used. In the REMI project, they look like those from the USEA. The difference is that the nerve grows into the electrodes, as opposed to the electrodes driven into the nerve.<sup>49</sup> In RSE, a flat plate with electrodes forms a scaffold inside the tube for nerve development.<sup>50</sup> Finally, in TEENI, electrodes are loosely suspended in a special hydrogel. This substance contains various elements of the extracellular matrix to support nerve regeneration. Each of these ideas is still being researched and further developed.

Peripheral nerves possess quite a good ability to regenerate, compared to those of central origin. After cutting the nerve, following a period of Wallerian degeneration, it continuously starts to elongate its fibers, looking for a way to re-innervate its target. If the cut nerve stumps are successfully surgically reconnected, its fibers regenerate along endoneural connective tissue channels coated with proliferating Schwann cells (SC) and are guided by neurotrophic factors released by SC as well as by tropic factors released from the target area. After limb amputation, many muscle groups remain mechanically inactive. For example, the pectoralis major muscle after shoulder disarticulation is no longer able to perform the function of arm adduction. It turns out that it is possible to denervate the muscle (in such case, lateral and medial pectoral nerves can be cleaved) and innervate it again by other nerves (i.e., nerves arising from the lateral, posterior and medial brachial plexus fasciculus, like the musculocutaneous, ulnar, radial, and medial nerve). This procedure is known as targeted muscle re-innervation (TMR) (Fig. 6). As a result, the impulses guided by the motoneurons of the arm are again reflected in motor muscle activity. Briefly, when a patient thinks about arm flexion in his elbow joint, it causes the contraction of muscle fibers of pectoralis major (which are

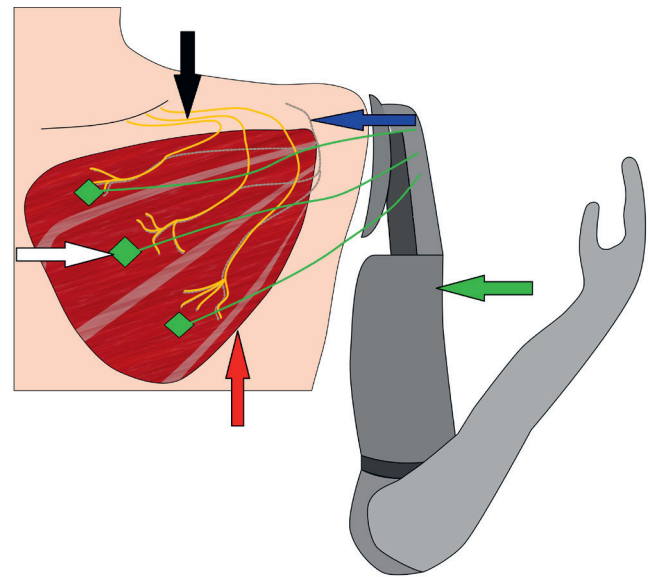


Fig. 6. Scheme of the targeted muscle re-innervation technique. Pectoralis major muscle is denervated, and then re-innervated with a whole set of nerves originating from the brachial plexus – the ulnar, median and radial nerves. The signal from the muscle contraction is taken by the electrodes of the electromyograph and converted to signals controlling the artificial limb

Black arrow – brachial plexus; blue arrow – cleaved pectoral nerves, no longer innervating their target; red arrow – pectoralis major muscle; white arrows – electromyographic electrodes; green arrow – artificial limb prosthesis.

innervated by the musculocutaneous nerve). Such signals can be read using electromyographic electrodes and converted into precise signals for moving the prosthesis.

Interestingly, the fields responsible for sensory impressions corresponding to the ulnar, radial and median nerve appear on the skin above the fragments of muscles that underwent neurotization. A patient after TMR, touched at the right place on the skin of the chest, feels it as a touch on the surface of the hand or forearm. The technique of direct muscle neurotization by nerve stumps causes a significant reduction in the occurrence of adverse sensory phenomena after amputation. The feeling of phantom pain and post-amputation pain from neuroma formation often disappears.<sup>51</sup> This technique, although it has produced quite spectacular effects on prosthesis motor control, provides only a limited number of separate control signals. Therefore, it is still difficult to restore functional degrees of freedom and allow simultaneous independent movements of the fingers, wrists and elbows.

Another approach in this matter, tested so far only in rats, is to place re-growing nerve stumps into synthetic scaffolds along with maturing myoblasts, called regenerative peripheral nerve interface (RPNI). This technique promises more control over the signals from individual nerve fibers, and therefore, more detailed reception of the signals.<sup>52</sup> It is possible that RPNI will be the key to creating limb prostheses with efficiency comparable to their biological counterparts.

## In vitro biosensors

Examination of isolated, living nerve cells is tedious work, but necessary for a complete understanding of the physiology of the nervous system. Research of this type is dictated not only by the need to broaden the horizons of neuroscience. Such cells also play a very important role in pharmacological tests, as they make it possible to assess the direct influence of selected chemical substances on the physiological processes occurring in cells. The first step towards research on the activity of individual neurons was the previously-mentioned patch-clamp technique. Limitations connected to it, however, have contributed to the development of other methods of research, each of which is still used in the laboratory environment.

### Patch-clamping approach

The patch-clamp technique was described by Neher and Sakmann in 1976. It uses a micropipette whose end is placed on the surface of the cell membrane. By changing gradients in the concentration of ions across the cell membrane, the micropipette can record the electrical activity of neurons.<sup>53</sup> The patch-clamping method has made many revolutionary discoveries possible in the field of neuro- and electrophysiology. Such a popular research method has tempted scientists to construct a patch-clamp device for the perception of whole neuron systems. As a result, simple neurochips were created using this technique.<sup>54</sup> This type of technology can be used in laboratories to study neuron physiology and their response to drugs. For this purpose, they are commonly used in laboratories. This concept can also be applied in vivo to analyze patterns of depolarization of single neurons in the brains of laboratory animals.

### Multielectrode array

Multielectrode array (MEA) is a technique usually used for research on neuron physiology. In order to create such a system, nerve cells, most often taken from rats, are cultured on surfaces containing microelectrodes. In this way, researchers can accurately read and stimulate the activity of both individual neurons and entire groups of them. Typically, MEA is a flat chip with a structure reminiscent of a “sandwich”. The first, basal layer is basically a dielectric that does not conduct electricity. The next is created with electric conductors that connect to the electrodes in the 3<sup>rd</sup> layer. The last layer consists again of the dielectric, interrupted by places with flat electrodes coming into contact with the cells. This concept was presented for the first time in 1972.<sup>55</sup> It is, however, only a general concept that can be interpreted in different ways and supported by many additional research methods (fluorescent calcium indicators, genetic markers and optogenetics).<sup>56</sup> Multielectrode array is widely used in pharmacology and toxicology. They are successfully used not only for the study of neurons, but also for cardiomyocytes and skeletal muscle.<sup>57</sup> As part

of this technique, it is possible to study the activity of both single nerve cells and large tissue structures, such as neural networks.

### Neural field effect transistor

The use of FET (field effect transistor) systems in the integration of neurons with electronic circuits is a derivative of the ISFET (ion-sensitive field effect transistor) technology commonly used in modern medicine. In 1925, the first patent of the key device of the modern era, the FET field transceiver, appeared. The concept was proposed by J.E. Lilienfeld. Later, in 1935, Oskar Heil described the possibility of controlling the resistance in a semiconducting material. Ultimately, the patent for the first fully functional field effect transistor was granted to Nishizawa and Watanabe in 1950. The full understanding of the principles of such a device emerged in 1952 with the work of William Shockley. Briefly, FET consists of 3 electrodes – a source, a drain and a gate, all connected to the channel. Through the source the current enters the transistor, and then it flows through the channel and escapes through the drain. However, this happens only if an appropriate voltage was applied on the gate. If there is no voltage to the gate, the transistor acts as a resistor with very high resistance, which prevents the flow of current. Depending on the method of giving voltage to the gate, the flow of current through the channel can be controlled in various ways. In 1970, Piet Bergveld proposed to use an electrode as the gate that would perceive the electrical voltage resulting from ion concentration in a solution (ISFET). The idea turned out to be revolutionary and is nowadays very widely used in pH measurements or devices testing the presence of biological molecules (e.g., glucose or DNA).<sup>58</sup>

At the beginning of the 1990s, Fromherz et al. succeeded in connecting an FET system with a living cell. The basic concept behind this project was the idea that a nerve cell could control the gate using the generated electromagnetic field.<sup>59</sup> Due to the fact that modern computers are based on transistors, it is believed that this technology may prove to be crucial for the effective connection of nervous tissue with an electronic system. Additionally, FET sensor systems that are currently in use can be used in neurophysiological and toxicological studies, and studies of the effects of drugs and the environment on the metabolism of nerve cells. Ultimately, such systems can also be used to study neuronal plasticity and communication between them.<sup>60</sup>

## Summary


In this review paper, we have attempted to briefly present the history and state of the art of the development of methods of connecting the human nervous system with electronic systems for therapeutic purposes. Many of the technological solutions described in this article have


already been proven as extremely useful in contemporary neurorestorative medicine. Brain–computer interfaces, both non-invasive and invasive, play an important role in the rehabilitation of people with severe movement impairment. Patients with severe visual and hearing impairment benefit from retinal and cochlear implants and can lead a relatively normal life. The spectacular success of the targeted muscle re-innervation technique has led to improvement in the life of quality of people after upper limb amputation.

Our analysis of the variety of available technical solutions has enabled us to determine the properties of the ideal interface between the nervous system and the electronic system. This interface should be characterized by high sensitivity and resolution of the received neuronal signals, and minimal invasiveness of the technique in its in vivo implantation as well as high and long-term biocompatibility. We believe that it will be possible to develop interfaces that would fully decode central or peripheral neuronal activity for the treatment of spinal cord injuries and other lesions of the CNS and for ideal control of artificial limb prostheses. In addition, the work of scientists may soon provide a stable interface that allows a person to communicate with a computer with just a simple thought.

#### ORCID iDs

Tymoteusz Skok  <https://orcid.org/0000-0001-9094-9620>

Paweł Tabakow  <https://orcid.org/0000-0001-8638-3871>

Krzysztof Chmielak  <https://orcid.org/0000-0001-9383-7667>

#### References

- Cobb M. Timeline: Exorcizing the animal spirits. Jan Swammerdam on nerve function. *Nat Rev Neurosci.* 2002;3(5):395–400.
- Sleigh C. Jan Swammerdam's frogs. *Notes Rec R Soc Lond.* 2012;66(4):373–392.
- Verkhatsky A, Parpura V. History of electrophysiology and the patch clamp. *Methods Mol Biol.* 2014;1183:1–19.
- Wallace W. The vibrating nerve impulse in Newton, Willis and Gassendi: First steps in a mechanical theory of communication. *Brain Cogn.* 2003;51(1):66–94.
- Verkhatsky A, Krishtal OA, Petersen OH. From Galvani to patch clamp: The development of electrophysiology. *Pflugers Arch.* 2006;453(3):233–247.
- Harrar JE. The potentiostat and the voltage clamp. *Electrochem Soc Interface.* 2013;22(4):42–44.
- McNamee MJ, Edwards SD. Transhumanism, medical technology and slippery slopes. *J Med Ethics.* 2006;32(9):513–518.
- Mudry A, Mills M. The early history of the cochlear implant: A retrospective. *JAMA Otolaryngol Head Neck Surg.* 2013;139(5):446–453.
- Durand DM. What is neural engineering? *J Neural Eng.* 2006;4(4). doi:10.1088/1741-2552/4/4/e01
- Finkel LH. Neuroengineering models of brain disease. *Annu Rev Biomed Eng.* 2000;2(1):577–606.
- Vidal JJ. Real-time detection of brain events in EEG. *Proc IEEE Inst Electr Electron Eng.* 1977;65(5):633–641.
- Shih JJ, Krusienski DJ, Wolpaw JR. Brain-computer interfaces in medicine. *Mayo Clin Proc.* 2012;87(3):268–279.
- Anupama HS, Cauvery NK, Lingaraju GM. Brain computer interface and its types – a study. *IJASEAT.* 2012;3(2):739–745.
- Nezamfar H, Salehi SSM, Moghadamfalahi M, Erdogmus D. A context-aware c-VEP-based BCI typing interface using EEG signals. *IEEE J-STSP.* 2016;10(5):932–941.
- Kaufmann T, Herweg A, Kübler A. Toward brain-computer interface based wheelchair control utilizing tactually-evoked event-related potentials. *J Neuroeng Rehabil.* 2014;11:7.
- Sirvent JL, Azorin JM, Iáñez E, Úbeda A, Fernández E. P300-based brain-computer interface for internet browsing. In: *Trends in Practical Applications of Agents and Multiagent Systems.* Advances in Intelligent and Soft Computing. 8<sup>th</sup> International Conference on Practical Applications of Agents and Multiagent Systems. 2010;615–622.
- Pires G, Torres M, Casaleiro N, Nunes U, Castelo-Branco M. Playing Tetris with non-invasive BCI. Paper presented at: the 2011 IEEE 1<sup>st</sup> International Conference on Serious Games and Applications for Health (SeGAH); November 16–18 2011; Braga, Portugal.
- Spüler M. A high-speed brain-computer interface (BCI) using dry EEG electrodes. *PLoS One.* 2017;12(2):e0172400.
- Sitaram R, Caria A, Veit R, et al. fMRI brain-computer interface: A tool for neuroscientific research and treatment. *Comput Intell Neurosci.* 2007;2007:25487.
- Mellinger J, Schalk G, Braun C, et al. An MEG-based brain-computer interface (BCI). *Neuroimage.* 2007;36(3):581–593.
- Schalk G, Leuthardt EC. Brain-computer interfaces using electrocorticographic signals. *IEEE Rev Biomed Eng.* 2011;4:140–154.
- Liu J, Fu T-M, Cheng Z, et al. Syringe-injectable electronics. *Nat Nanotechnology.* 2015;10(7):629–636.
- Kennedy PR, Bakay RA. Restoration of neural output from a paralyzed patient by a direct brain connection. *Neuroreport.* 1998;9(8):1707–1711.
- Brower V. When mind meets machine. *EMBO Rep.* 2005;6(2):108–110.
- Collinger JL, Wodlinger B, Downey JE, et al. High-performance neuroprosthetic control by an individual with tetraplegia. *Lancet.* 2013;381(9866):557–564.
- Jarosiewicz B, Sarma AA, Bacher D, et al. Virtual typing by people with tetraplegia using a self-calibrating intracortical brain-computer interface. *Sci Transl Med.* 2015;7(313):313ra179.
- Ludwig KA. *Neuroprosthetic Devices: Inputs and Outputs.* Ph.D. Thesis, University of Michigan, Ann Arbor, MI, USA, 2009.
- Capogrosso M, Milekovic T, Borton, D, et al. A brain–spine interface alleviating gait deficits after spinal cord injury in primates. *Nature.* 2016;539(7628):284–288.
- Bouton CE, Shaikhouni A, Annetta NV, et al. Restoring cortical control of functional movement in a human with quadriplegia. *Nature.* 2016;533(7602):247–250.
- Dobelle WH. Artificial vision for the blind by connecting a television camera to the visual cortex. *ASAIO J.* 2000;46(1):3–9.
- Rachitskaya AV, Yuan A, Marino MJ, Reese J, Ehlers JP. Intraoperative OCT imaging of the Argus II Retinal Prosthesis System. *Ophthalmic Surg Lasers Imaging Retina.* 2016;47(11):999–1003.
- Stingl K, Bartz-Schmidt KU, Besch D, et al. Subretinal Visual Implant Alpha IMS: Clinical trial interim report. *Vision Res.* 2015;111(Pt B):149–160.
- Berger TW, Song D, Chan RHM, et al. A hippocampal cognitive prosthesis: Multi-input, multi-output nonlinear modeling and VLSI implementation. *IEEE Trans Neural Syst Rehabil Eng.* 2012;20(2):198–211.
- Griffith RW, Humphrey DR. Long-term gliosis around chronically implanted platinum electrodes in the Rhesus macaque motor cortex. *Neurosci Lett.* 2006;406(1–2):81–86.
- Waldert S. Invasive vs non-invasive neuronal signals for brain-machine interfaces: Will one prevail? *Front Neurosci.* 2016;10:295.
- Tyler DJ, Polasek KH, Schiefer MA. Chapter 63 – Peripheral nerve interfaces. In: Tubbs R, Rizk E, Shoja MM, Loukas M, Barbaro N, Spinner RJ, eds. *Nerves and Nerve Injuries.* San Diego, CA: Academic Press; 2015:1033–1054.
- Spearman BS, Desai VH, Mobini S, et al. Neural interfaces: Tissue-engineered peripheral nerve interfaces. *Adv Funct Mater.* 2018;28(12):1870076. doi:10.1002/adfm.201870076
- Naples GG, Mortimer JT, Scheiner A, Sweeney JD. A spiral nerve cuff electrode for peripheral nerve stimulation. *IEEE Trans Biomed Eng.* 1988;35(11):905–916.
- Foldes EL, Ackermann DM, Bhadra N, Kilgore KL, Bhadra N. Design, fabrication and evaluation of a conforming circumpolar peripheral nerve cuff electrode for acute experimental use. *J Neurosci Methods.* 2011;196(1):31–37.



40. Tyler DJ, Durand DM. Chronic response of the rat sciatic nerve to the flat interface nerve electrode. *Ann Biomed Eng.* 2003;31(6):633–642.
41. Dweiri YM, Stone MA, Tyler DJ, McCallum GA, Durand DM. Fabrication of high contact-density, flat-interface nerve electrodes for recording and stimulation applications. *J Vis Exp.* 2016;4(116).
42. Yoshida K, Hennings K, Kammer S. Acute performance of the thin-film longitudinal intra-fascicular electrode. Paper presented at: the First IEEE/RAS-EMBS International Conference on Biomedical Robotics and Biomechatronics (BioRob 2006); February 20–22, 2006; Pisa, Italy.
43. Boretius T, Badia J, Pascual-Font A, et al. A transverse intrafascicular multichannel electrode (TIME) to interface with the peripheral nerve. *Biosens Bioelectron.* 2010;26(1):62–69.
44. Yoshida K, Stieglitz T, Qiao S. Bioelectric interfaces for the peripheral nervous system. Paper presented at: the 36<sup>th</sup> Annual International Conference of the IEEE Engineering in Medicine and Biology Society; August 26–30 2014; Chicago, IL.
45. Tyler DJ, Durand DM. A slowly penetrating interfascicular nerve electrode for selective activation of peripheral nerves. *IEEE Trans Rehabil Eng.* 1997;5(1):51–61.
46. Clark GA, Ledbetter NM, Warren DJ, Harrison RR. Recording sensory and motor information from peripheral nerves with Utah slanted electrode arrays. *Conf Proc IEEE Eng Med Biol Soc.* 2011;2011:4641–4644.
47. Birenbaum NK, MacEwan MR, Ray WZ. Interfacing peripheral nerve with macro-sieve electrodes following spinal cord injury. *Neural Regen Res.* 2017;12(6):906–909.
48. Musick KM, Rigosa J, Narasimhan S, et al. Chronic multichannel neural recordings from soft regenerative microchannel electrodes during gait. *Sci Rep.* 2015;5:14363.
49. Lotfi P, Garde K, Chouhan A, Bengali E, Romero M. Modality-specific axonal regeneration: Toward selective regenerative neural interfaces. *Front Neuroeng.* 2011;4:11.
50. Clements IP, Mukhatyar VJ, Srinivasan A, Bentley JT, Andreasen DS, Belamkonda RV. Regenerative scaffold electrodes for peripheral nerve interfacing. *IEEE Trans Neural Syst Rehabil Eng.* 2013;21(4):554–566.
51. Cheesborough JE, Smith LH, Kuiken TA, Dumanian GA. Targeted muscle reinnervation and advanced prosthetic arms. *Semin Plast Surg.* 2015;29(1):62–72.
52. Urbanchek MG, Kung TA, Frost CM, et al. Development of a regenerative peripheral nerve interface for control of a neuroprosthetic limb. *Biomed Res Int.* 2016;12:1–8.
53. Kornreich BG. The patch clamp technique: Principles and technical considerations. *J Vet Cardiol.* 2007;9(1):25–37.
54. Py C, Denhoff MW, Sabourin N, Weber J, Shiu M, Zhao P. Priming and testing silicon patch-clamp neurochips. *N Biotechnol.* 2014;31(5):430–435.
55. Pine J. A history of MEA development. In: Taketani M, Baudry M, eds. *Advances in Network Electrophysiology: Using Multi-Electrode Arrays.* Boston, MA: Springer US; 2006:3–23.
56. Rutten W, Mouveroux JM, Buitenweg J, et al. Neuroelectronic interfacing with cultured multielectrode arrays toward a cultured probe. *Proc IEEE Inst Electr Electron Eng.* 2001;89(7):1013–1029.
57. Rabieh N, Ojovan SM, Shmoel N, Erez, H, Maydan E, Spira ME. On-chip, multisite extracellular and intracellular recordings from primary cultured skeletal myotubes. *Scientific Reports.* 2016;6:36498.
58. Walsh KB, DeRoller N, Zhu Y, Koley G. Application of ion-sensitive field effect transistors for ion channel screening. *Biosens Bioelectron.* 2014;54:448–454.
59. Fromherz P, Offenhausser A, Vetter T, Weis J. A neuron-silicon junction: A Retzius cell of the leech on an insulated-gate field-effect transistor. *Science.* 1991;252(5010):1290–1293.
60. Liu Q, Wu C, Cai H, Hu N, Zhou J, Wang P. Cell-based biosensors and their application in biomedicine. *Chem Rev.* 2014;114(12):6423–6461.



# Negative body image in breast cancer patients

Agata Kołodziejczyk<sup>1,A,D–F</sup>, Tomasz Pawłowski<sup>2,A,D–F</sup>

<sup>1</sup> Lower-Silesian Oncology Centre, Wrocław, Poland

<sup>2</sup> Division of Psychotherapy and Psychosomatic Medicine, Department of Psychiatry, Wrocław Medical University, Poland

A – research concept and design; B – collection and/or assembly of data; C – data analysis and interpretation;  
D – writing the article; E – critical revision of the article; F – final approval of the article

Advances in Clinical and Experimental Medicine, ISSN 1899–5276 (print), ISSN 2451–2680 (online)

*Adv Clin Exp Med.* 2019;28(8):1137–1142

## Address for correspondence

Tomasz Pawłowski  
E-mail: tomasz.pawlowski@umed.wroc.pl

## Funding sources

None declared

## Conflict of interest

None declared

Received on January 11, 2019  
Reviewed on January 23, 2019  
Accepted on February 3, 2019

Published online on February 26, 2019

## Abstract

The aim of this overview study is to familiarize readers with the impact of changes to body image (BI) among patients treated for breast cancer. Body image is subjected to many changes during oncological treatment and every method of treatment (surgery, chemotherapy, radiotherapy, and hormone therapy) can have a negative impact on the way the treated patients perceive their bodies. The article differentiates the susceptibility of patients to a worsened self-image due to their pre-disease personality, socioeconomic factors, age, and declared sense of control during the oncological treatment. Herein, the areas of patients' lives which are the most affected by negative BI are discussed: quality of life and functioning in society, with particular emphasis on the return to work and sexuality. The ways of protecting patients' BI throughout treatment which have been proposed in the literature are presented in conclusions.

**Key words:** breast cancer, body image, posttraumatic growth

## Cite as

Kołodziejczyk A, Pawłowski T. Negative body image in breast cancer patients. *Adv Clin Exp Med.* 2019;28(8):1137–1142. doi:10.17219/acem/103626

## DOI

10.17219/acem/103626

## Copyright

© 2019 by Wrocław Medical University  
This is an article distributed under the terms of the Creative Commons Attribution Non-Commercial License (<http://creativecommons.org/licenses/by-nc-nd/3.0/>)

## Introduction

The aim of this paper is to outline the problem of worsening body image (BI) among women treated for breast cancer. Body image in oncological disease is susceptible to many disturbing changes, which are often overlooked since issues of BI are treated as secondary to the fight for life and health. However, it cannot be overlooked that patients treated for breast cancer experience many negative changes in relation to body self already during the treatment and after the end of treatment they struggle with the effects of less positive self-perception.<sup>1,2</sup> Negative BI has a significant impact on the quality of life, sexuality and social functioning of patients. In addition, it may become an obstacle to posttraumatic growth (PTG).

Posttraumatic growth refers to all of the positive outcomes that arise as a result of stressful, life-threatening experiences.<sup>3</sup> Expected signs of PTG can include a change in philosophy or lifestyle, developments in interpersonal relationships, or a sense of increased effectiveness. The following factors are thought to determine the occurrence of PTG: personality factors, the specifics of the stressful situation, support, emotions, behaviors related to dealing with the disease, and strategies of coping with stress.<sup>4,5</sup> It can be considered whether patients' susceptibility to changes in BI could be another variable that may influence the occurrence of PTG. Therefore, this paper and further research could be important in contributing to the support of oncological patients in this aspect.

There are many definitions of BI, but each of them focuses on the role of one's corporeality in shaping one's sense of identity – the body self. Paul Schilder described BI in the most literal way: he defined BI as a conception, an image of one's own body created in the mind.<sup>6</sup> Many psychological theories, with the psychodynamic approach at the forefront, also raised the issue of BI.<sup>7</sup> A representative of this approach in psychology, David Krueger,<sup>8</sup> drew attention to the essence of BI in the "creation" of a person, in building one's identity with reference both to self-perception and to the functions of the body. Another theorist of BI, Alexander Lowen,<sup>9</sup> in referring to the vital role of BI in our lives, created the concept of a "betrayal" of the body. This concept, referring to the feeling of losing control over one's own body, a lack of acceptance of one's body, and negative emotions towards oneself, is applicable to patients treated for breast cancer. Frank Rohrich's concept completes the definition of BI.<sup>7</sup> He divides experiences related to the body into perception – namely, perception of the body – a cognitive approach to the body, emotions, and specific behaviors related to the body. We present this division to draw attention to the multifaceted nature of potential problems that may result from a disturbed BI.

The multidimensionality of BI is also reflected in the instruments developed to measure this construct. The 2 most commonly used instruments are the Body Esteem Scale, referring directly to the psychodynamic tradition,<sup>7</sup> and

the Multidimensional Body-Self Relation Questionnaire, representing the cognitive point of view.<sup>26</sup>

To emphasize more strongly the importance of BI in oncological disease, we would like to highlight the variability of identity during the illness. Changes to the body can contribute to a decline in self-esteem, a deterioration of mood and irrational beliefs about oneself. The changing body is also a symbol of the disease; it becomes equated with the cultural image of the disease.<sup>1</sup> A body consumed by disease, which does not fit the contemporary canonical ideals, becomes a source of negative emotions.

This paper aims to show the changes that occur in the bodies of women treated for breast cancer and the problems that may arise from the resulting changes in BI. It will focus on factors that can differentiate patients in terms of changes in the BI, as well as in the areas most affected by these changes.

## Breast cancer and changes in the body

In light of advancements in medicine today, it can be said that there is a huge variety of treatments for breast cancer. Within the 4 basic oncological procedures – namely, surgery, chemotherapy, radiotherapy, and hormone therapy – there will be a lot of changes in the body, the effects of which the patients will have to deal with.

### Changes in the body after surgery

Nowadays, surgery is one of the most commonly used methods of breast cancer treatment. There are many variants of breast cancer surgery and each of them leaves the woman's body mutilated to some extent. In contrast to procedures standard 10–15 years ago, bilateral mastectomy is a rarity. This is a positive development which is supported by the studies by Rosenberg et al. in which they found that after this very surgery patients reported the most negative BI.<sup>10</sup> Other variants of this procedure are breast-saving surgery, unilateral mastectomy or mastectomy with reconstruction. An important variable of each of these treatments is the extent to which the disease has spread to the lymph nodes.<sup>11</sup> Each of these surgeries can cause many difficulties. Each one more or less requires patients to deal with remnants of the surgery, such as postoperative scars, foreign bodies like surgical drains, swelling, redness, lymphedema, and others. All of them may result in severe pain causing, e.g., worsened cognitive functioning or depressed mood, leading to a deterioration in quality of life.

However, the aesthetic aspect of such treatments is also important. Depending on the severity of the disease, the extent of changes, as well as the skills and experience of surgeons, the effect of the surgery may differ and the patient may have problems accepting the asymmetry of the breasts, the disproportion between them or the need

to wear bra pads to comfortably display cleavage.<sup>12</sup> It can cause problems with self-acceptance, but may also result in problems concerning sexuality and the quality of one's relationships.

With the steady progress of treatment methods and the increasing frequency of breast reconstruction surgeries, problems can be expected with the "new" BI among patients with implants. Such surgery may be associated with unnatural sensations in the reconstructed breast, a sense of artificiality, or even the potential for the implant to be rejected.<sup>13</sup> Psychological problems stem from patients' prolonged stress over beliefs of what is normal and what may be alarming during convalescence. It also can lead to indirect problems accepting one's "new" body and engaging in intimate relations.

Finally, it should be remembered that each of the surgical procedures is associated with pain, redness and swelling in the surgical field, which can also negatively affect the patients' well-being in relation to their perception of own bodies. In our professional practice, we find that patients often do not want to see their breasts after the surgery and they look away while changing clothes in order to avoid doing so. From a psychological point of view, it poses the question of how long a patient can reject their post-surgery body and what will confronting it mean for the patient's mood or cognitive and social functioning.

## Changes in the body after chemotherapy

Chemotherapy is one of the treatments for breast cancer with perhaps the most prominent side effects which greatly impact the patients' appearance and, thus, have a very negative effect on their BI.<sup>1</sup>

The side effect that is most associated with chemotherapy treatment is hair loss.<sup>1</sup> Even the loss of hair on the head alone is often a traumatic experience for the patient.<sup>14</sup> Studies show that patients' assessment of their BI after chemotherapy worsens dramatically, mainly due to the need to wear wigs or headscarves.<sup>2</sup> There are many consequences, ranging from a decrease in self-esteem or a decreased sense of sexuality and attractiveness to social difficulties and relationship problems.<sup>14</sup> However, it should be remembered that hair loss during chemotherapy does not apply only to the hair on one's head. As the treatment progresses, the patients can lose their eyebrows, eyelashes, nasal hair, and pubic hair. The loss of hair in the nose leads to complications such as nosebleeds and discomfort in breathing. Eyes without eyelashes are more difficult to open and more susceptible to infection and dirt. A lack of pubic hair can lead to irritation of one's intimate parts and problems with urination.<sup>1</sup>

It should be noted that physical difficulties are often related to psychological deterioration. In this case, sexual disorders, relationship problems, a lack of self-satisfaction, and negative beliefs about oneself should be considered, among other things.

In addition to the problems resulting from hair loss, chemotherapy can also contribute to weight loss. This may be due to the decreased appetite, nausea, frequent vomiting, loss of energy, and drowsiness associated with this type of treatment. The opposite situation may occur, as well. Cytostatic therapy may contribute to weight gain, especially if steroids are also used.

Other changes in the body occurring during chemotherapy include increased perspiration, changes in facial features, brittle or blackened fingernails resulting from fungal infection, oral fungal infections, and complexion problems, such as an earthy or unhealthy complexion. This often leads to low moods, anxiety and feelings of shame, causing patients to stay at home or to neglect some of their duties.

## Changes in the body after radiotherapy

Radiotherapy has a different effect on the appearance of the body. Possible consequences include burns, skin irritation, edema, radiation scars and reactions, and inflamed and festering wounds. It should also be taken into account that radiotherapy is a long treatment (4–6 weeks), causing fatigue and discomfort, which can also negatively affect the sense of attractiveness and cause psychological distress.

## Changes in the body after hormone therapy

Hormone therapy is more and more frequently used to complement the main treatment. In order to understand the changes that occur in a woman's body while taking hormonal drugs, patients should be divided into 2 groups: pre- and postmenopausal. Before starting treatment, postmenopausal patients are asked to discontinue use of any hormonal drugs that are intended to reduce the symptoms of menopause. As a result, patients see a return of symptoms such as hyperhidrosis, hot flashes, irritability, weight gain, vaginal dryness, and others.<sup>15</sup> Moreover, patients confront many psychological disturbances connected with common beliefs about menopause. It often causes women to feel older, less socially and physically attractive, and more frustrated and depressed. These symptoms may persist throughout the whole duration of the hormone therapy, i.e., up to 10 years after the main treatment ends.

The use of hormone therapy in patients who have not yet reached menopause should be considered differently. In their case, hormone therapy hastens the onset of menopause. In this situation, patients struggle with the same symptoms as postmenopausal patients. Additionally, hastened menopause causes infertility. Therefore, patients in the prime of their lives often stop feeling attractive, suffer lower self-esteem<sup>16</sup> and are sometimes put into a situation where they must accept that they will not have any more children or will not be able to have children at all, which impacts their mental and overall well-being, often causing

symptoms of depression and anxiety resulting from beliefs about not fulfilling women's "social and natural duty".

To conclude, oncological treatment of breast cancer can significantly affect a woman's BI.<sup>11</sup> There are as many problems potentially resulting from different types of treatment as there are treatment options. Which problems will occur depends largely on the individual characteristics of each patient.

## Variability of body image in patients treated for breast cancer

Not every patient will declare the same extent of worsened BI due to changes resulting from oncological treatment. Numerous studies report that there are many variables that determine how patients cope with the changes in their body and how it affects their functioning during treatment and after the disease.<sup>17</sup> We will present 4 areas that may affect how patients see their bodies affected by breast cancer: the patients' pre-disease personality, socioeconomic factors and common knowledge about cancers prior to treatment, patients' age, and the sense of control reported during treatment.

### Pre-disease personality and perception of body changes

The personality of the patient before her disease will have a big impact on how she feels about the changes in her body once treatment ends.<sup>18</sup> The patient's identity is put to the test in expanding it to the image of the diseased self while dealing with all the changes resulting from such a crisis. Studies report that changes in the BI of patients who have completed breast cancer treatment largely depend on their BI before the disease. From the data provided by Rhondali et al.,<sup>18</sup> it appears that patients who had a positive BI prior to their disease deal with the changes that result from treatment better than the patients who initially reported a negative BI. In addition, the same studies claim that patients who initially declare a negative BI show more symptoms of depression during cancer treatment. Patients who find it harder to observe changes in their body have difficulty looking in the mirror. Patients describe the hair loss resulting from chemotherapy as a particularly difficult experience.<sup>14</sup> According to some studies, patients who do not deal well with changes to their BI experience a decrease in self-esteem.<sup>2</sup> The changing BI impacts on their identity and destroys the often unstable balance and self-image. Patients evaluate the changes in the body as a reminder of the disease, something that prevents them from forgetting that they are ill, that an inseparable part of their identity is the sense of a diseased self.<sup>1</sup>

There are also reports which state that the ability to deal with emotions before the disease will affect the extent of changes to the BI.<sup>18</sup> More stable patients who cope

better with their feelings will suffer less from the changing BI than emotionally unstable patients with disordered identities.

## Socioeconomic factors and public views on oncological disease

A very important factor influencing whether or not patients will negatively assess changes within their body is their socioeconomic status and public views on oncological treatment.<sup>19</sup> Studies show that socioeconomic status, education and employment play a role in BI disorders. The study group of Chang et al.<sup>19</sup> proves that employment and higher education will contribute to lower self-esteem once treatment ends. They also state that a higher per capita income in the patient's family heralds a better BI for the patient. The first conclusion can be explained by the greater awareness among patients with higher education of the consequences of cancer treatment and by the fear associated with returning to work, a fear associated with rejection and ostracism and reported by many women who have completed oncological treatment.<sup>19</sup> This fear is worsened by widespread, inaccurate public beliefs about the disease. As a result, patients' readjustment to life after the disease is very difficult and the changes to their BI are a painful reminder that after treatment they will stand out and thus be exposed to many unpleasant social situations. Many patients do not want their appearance to embarrass others,<sup>2</sup> nor do they want to be treated differently than others. For this reason, women often refrain from leaving the house after oncological treatment. Both their social and professional lives suffer because of this trepidation.<sup>14</sup>

On the other hand, a higher socioeconomic status means that patients have a greater ability to mask changes in their body which may contribute to their well-being. Such patients may, i.e., buy a wig made from real hair or may begin treatment in more specialized clinics equipped with cooling caps, or they can make use of better cosmetics, etc. to take more control over their appearance.

## Patients' age and changes in body image

Another key factor that can bring about changes in BI is age. Studies show that younger patients do not deal with oncological treatment and its consequences as well as older patients.<sup>20</sup> Studies by Janz et al. prove that younger patients are less well-adjusted mentally to crises such as cancer.<sup>12</sup> Such conclusions are supported by studies from Miller et al.,<sup>21</sup> which show that younger women experience more preoperative stress than older women. The same studies show that BI in younger patients will be completely different and, therefore, it will change in different ways as a result of the treatment methods used. A patient's young age may indicate more radical treatment methods and thus is more likely to increase the stress associated with serious

changes to the body. For example, chemotherapy, which has the worst associations in society as well as the most negative assessments from oncology patients, is used more frequently in young patients.<sup>1</sup> Moreover, there are studies which prove that young patients who initially had a negative BI will cope with cancer treatment worse than older patients with an equally negative self-image.<sup>13</sup>

One may suspect that a worse BI in young women may result from problems of both physical and psychological nature. Struggling at a young age with physical limitations, a decreased sense of attractiveness, lowered self-esteem, or deliberations on the impact of treatment on one's future is extremely burdensome; the body is exhausted by disease and its transformation reminds patients of the disease, so there is an extremely negative impact on young women and their BI.

### Sense of control during the treatment and body image

The last factor affecting the differences in BI among patients after completing cancer treatment is the subjective sense of control during treatment. Studies by Chang et al. show that patients who reported a sense of influence over the decisions regarding their treatment coped better with their treatment and, thus, with the changes to their body resulting from the treatment they chose.<sup>19</sup>

Other studies show a hierarchy of well-being, depending on the type of surgery, reporting that patients who decided to have breast reconstruction had a less negative BI than patients who underwent mastectomy.<sup>16</sup>

### The influence on social functioning of a negative body image during oncological treatment

Among the many aspects of the lives of patients treated for breast cancer which are affected by their worsened BI, the subject literature seems to focus in particular on 3 basic ones: quality of life, sexuality and social functioning.

As the most general construct covering many aspects of life, quality of life was included in many studies.<sup>12,19,22</sup> The overview study by Lemieux et al. includes the issue of quality of life among patients treated with chemotherapy for breast cancer.<sup>1</sup> They recognized anxiety symptoms, a general feeling of stress, sexuality, self-esteem, social functioning, and the return to work as part of quality of life. Patients reported problems in all of these aspects. It turned out that patients treated with chemotherapy reported particularly low results on the life quality scale. They also reported the largest decrease in sexuality due to the treatment. Other studies<sup>10</sup> focused on physical and psychosocial functioning, partner interactions, sexual functioning, and medical interactions. All of these categories can be said to describe the quality of life. The results of these studies indicated that patients who underwent

breast cancer treatment felt uncomfortable with the changes in their bodies, felt embarrassed to show others a body affected by disease and were particularly uncomfortable showing others their postoperative scars.

Another area significantly affected by negative BI after oncological treatment is social functioning. According to reports,<sup>2</sup> patients are extremely stressed by society's reception of changes in the body and have great difficulty readapting to life in society after their treatment. Another study confirmed this deterioration in the social life of patients after treatment.<sup>19</sup> In these studies, patients reported grave concerns about making others embarrassed because of their appearance. Many studies also emphasize the difficulties patients have leaving the house after treatment.<sup>1</sup> This may be due to symptoms of depression caused by their negative BI, reluctance to admit to having the disease, or fear of social ostracism or other negative reactions from society.<sup>23</sup> Studies also point to another particularly important aspect of social life – returning to work. It turns out that patients report feeling a huge amount of stress associated with returning to their duties.<sup>1</sup> This is expressed, e.g., by the problem of getting dressed for work in such a way as to feel comfortable yet not to draw attention to oneself.

The conclusion that follows from these considerations is that many patients treated for breast cancer experience negative changes to their BI, changes which affect their functioning in society, family life and quality of life. For this reason, this issue should be addressed globally and the research should focus on how to prevent the negative impact to the BI of patients suffering from breast cancer.

### Summary

There are many areas of life that can be negatively affected by changes in BI. Many of the studies and articles quoted above conclude that it is important to take care of the BI of patients suffering from breast cancer. The most general argument is the influence that BI has on the patients' quality of life. This can include social functioning, well-being, sexuality, satisfaction with relationships, etc.

An analysis of the presented articles suggests that work on patients' BI should be applied at 3 stages of treatment: at the beginning of, during and after the main treatment.


Focusing on BI before starting treatment could prepare patients for the treatment outcomes and the changes that await them. Studies<sup>24</sup> have proven that a worse initial BI in patients indicates further deterioration in well-being throughout treatment. Therefore, it is worth working on the patients' BI before treatment. On the other hand, as shown in the presented material, it seems worth trying to increase social awareness of cancer and its consequences. This would aim to change the perceptions of people who are ill, and thus to ensure that they do not develop a sense of rejection and alienation due to their disease. It seems all the more important that we learn from

some studies that there is a group of people who choose not to undergo cancer treatment because of the changes in the body resulting from chemotherapy.<sup>1</sup>

Other studies point out that among cancer patients, the negative BI persisted for 12 weeks or longer after the end of treatment.<sup>24,25</sup> This proves the importance of working on the patients' BI during and after treatment. The effect of such work would be to limit the negative effects of changes to the patients' BI and perhaps to create space for PTG, which is a desirable outcome for patients completing oncological treatment. A negative BI can be a powerful obstacle to PTG.<sup>3,4</sup>

### ORCID iDs

Agata Kołodziejczyk  <https://orcid.org/0000-0002-8498-8049>

Tomasz Pawłowski  <https://orcid.org/0000-0002-3997-609X>

### References

- Lemieux J, Mausell E, Provencher L. Chemotherapy-induced alopecia and effects on quality of life among women with breast cancer: A literature review. *Psychooncology*. 2008;17(4):317–328.
- Garcia SN, de Castro Figueiredo Pereira Coelho R, Dias dos Santos PN, Alves Maftum M, de Fatime Mantovani M, Puchaliski Kalinke L. Changes in social function and body image in women diagnosed with breast cancer undergoing chemotherapy. *Acta Scientiarum. Health Sciences*. 2017;39(1):57–64.
- Danhauer SC, Case LD, Tedeschi R, et al. Predictors of posttraumatic growth in women with breast cancer. *Psychooncology*. 2013;22(12):1–15.
- Inan FS, Ustun B. Breast cancer and posttraumatic growth. *J Breast Health*. 2014;10(2):75–78.
- Chow YK, Masiak J, Mikołajewska E, et al. Limbic brain structures and burnout: A systematic review. *Adv Med Sci*. 2018;63(1):192–198.
- Schilder P. *The image and appearance of the human body: Studies in the constructive energies of the psyche*. London, UK: Paul Kegan; 1935.
- Schier K. *Dorosłe dzieci. Psychologiczna problematyka odwrócenia ról w rodzinie*. Warszawa, Poland: Wydawnictwo Naukowe SCHOLAR; 2014.
- Krueger DW. Psychodynamic perspectives on body image. In: Cash TF, Pruzinsky T, eds. *Body Image: A Handbook of Theory, Research and Clinical Practice*. New York, NY: Guilford Press; 2002:30–37.
- Lowen A. *Zdrada ciała*. Koszalin, Poland: Ośrodek Bioenergetycznej Pracy z Ciałem, Pomocy i Edukacji Psychologicznej; 2011.
- Rosenberg, SM, Tamimi RM, Gelber S, et al. Body image in recently diagnosed young women with early breast cancer. *Psychooncology*. 2013;22(8):1849–1855.
- Morone G, Iosa M, Fusco A, et al. Effects of a multidisciplinary educational rehabilitative intervention in breast cancer survivors: The role of body image on quality of life outcomes. *ScientificWorldJournal*. 2014;1–11.
- Janz NK, Mujahid M, Lantz PM, et al. Population-based study of the relationship of treatment and sociodemographics on quality of life for early stage breast cancer. *Qual Life Res*. 2005;14(6):1467–1479. <https://doi.org/10.1007/s11136-005-0288-6>
- Schover LR, Yetman RJ, Tuason LJ, Meisler E, Esselstyn CB, Hermann RE. Partial mastectomy and breast reconstruction: A comparison of their effects on psychosocial adjustment, body image and sexuality. *Cancer*. 1995;75(1):54–64.
- Kim IR, Cho J, Choi EK, et al. Perception, attitudes, preparedness and experience of chemotherapy-induced alopecia among breast cancer patients: A qualitative study. *Asian Pac J Cancer Prev*. 2012;13(4):1383–1388.
- Pacian A, Kulik TB, Chruściel P, Pacian J, Skórzyńska H, Zakrzewska W. Uwarunkowania psychospołeczne jakości życia kobiet w okresie klimakterium leczonych z powodu raka piersi. *Prz Menopauzalny*. 2012;5:423–427.
- Fobair P, Stewart SL, CHang S, D'Onofrio C, Banks PJ, Bloom JR. Body image and sexual problems in young women with breast cancer. *Psychooncology*. 2006;15(7):579–594.
- Rezaei M, Elyasi F, Janbabai G, Moosazadeh M, Hamzehgardeshi Z. Factors influencing body image in women with breast cancer: A comprehensive literature review. *Iran Red Crescent Med J*. 2016;18(10):1–9.
- Rhondali W, Chisholm GB, Filbet M, et al. Screening for body image dissatisfaction in patients with advanced cancer: A pilot study. *J Palliat Med*. 2015;18(2):153–156.
- Chang O, Choi EK, Kim IR, et al. Association between socioeconomic status and altered appearance distress, body image and quality of life among breast cancer patients. *Asian Pac J Cancer Prev*. 2014;15(20):8607–8612.
- Paterson C, Lengacher CA, Donovan KA, Kip KE, Toftagen CS. Body image in younger breast cancer survivors: A systematic review. *Cancer Nurs*. 2016;39(1):39–58.
- Miller SJ, Schnur JB, Weinberger-Litman SL, Montgomery GH. The relationship between body image, age and distress in women facing breast cancer surgery. *Palliat Support Care*. 2014;12(5):363–367.
- Kim MK, Kim T, Moon HG, et al. Effect of cosmetic outcome on quality of life after breast cancer surgery. *Eur J Surg Oncol*. 2015;41(3):426–432.
- Nowicki A, Rządkowska B. Depresja i lęk u chorych z nowotworami złośliwymi. *Współ Onkol*. 2005;9(9):396–403.
- Rhoten BA, Deng J, Dietrich MS, Murphy B, Ridner SH. Body image and depressive symptoms in patients with head and neck cancer: An important relationship. *Support Care Cancer*. 2014;22(11):3053–3060. doi:10.1007/s00520-014-2312-2
- King MT, Kenny P, Shiell A, Hall J, Boyages J. Quality of life three months and one year after first treatment for early stage breast cancer: Influence of treatment and patient characteristics. *Qual Life Res*. 2000;9(7):789–800.
- Cash TF. Cognitive-behavioral perspectives on body image. In: Cash TF, Smolak L eds. *Body image: A handbook of science, practice, and prevention*. New York, NY: Guilford Press; 2011:39–47.



# Advanced heart failure: A review

Klementyna Kępińska<sup>1,B–D,F</sup>, Daria Maria Adamczak<sup>2,A,C–F</sup>, Marta Kałużna-Oleksy<sup>2,E,F</sup>

<sup>1</sup> Faculty of Medicine, Poznan University of Medical Sciences, Poland

<sup>2</sup> 1<sup>st</sup> Department of Cardiology, Faculty of Medicine, Poznan University of Medical Sciences, Poland

A – research concept and design; B – collection and/or assembly of data; C – data analysis and interpretation;

D – writing the article; E – critical revision of the article; F – final approval of the article

Advances in Clinical and Experimental Medicine, ISSN 1899–5276 (print), ISSN 2451–2680 (online)

*Adv Clin Exp Med.* 2019;28(8):1143–1148

## Address for correspondence

Daria Maria Adamczak

E-mail: [daria.m.adamczak@gmail.com](mailto:daria.m.adamczak@gmail.com)

## Funding sources

None declared

## Conflict of interest

None declared

## Acknowledgements

We would like to thank Professor Ewa Straburzyńska-Migaj for her valuable scientific remarks. We would also like to thank Victoria Krzywicki and Peter Szafaryn from Poznan University of Medical Sciences, Center for Medical Education in English, for their editorial assistance.

Received on July 4, 2018

Reviewed on October 29, 2018

Accepted on February 5, 2019

Published online on March 4, 2019

## Abstract

Heart failure (HF) has been recognized as a pandemic and is a serious clinical and health problem associated with significant mortality, morbidity and expenditure on healthcare, especially among older people. Progress in medicine has made it possible for an increasing number of people with HF to live longer than ever before. Therefore, a new and serious clinical problem has appeared – advanced heart failure (AHF). A better understanding of this issue is very important, because there are many more patients waiting for transplantations than there are available hearts. The role of the medical team is to keep the patient in the best condition until the heart transplant/implantation of left ventricular assist devices or at least to ensure the best possible quality of life. This article reviews the available data on AHF. The authors have succinctly presented different definitions and methods of the AHF diagnosis established by medical societies, as well as epidemiological data, methods of assessment, and possible treatment strategies.

**Key words:** heart failure, advanced heart failure, stage D, decompensation

## Cite as

Kępińska K, Adamczak DM, Kałużna-Oleksy M. Advanced heart failure: A review. *Adv Clin Exp Med.* 2019;28(8):1143–1148. doi:10.17219/acem/103669

## DOI

10.17219/acem/103669

## Copyright

© 2019 by Wrocław Medical University

This is an article distributed under the terms of the Creative Commons Attribution Non-Commercial License (<http://creativecommons.org/licenses/by-nc-nd/4.0/>)

## Definition of advanced heart failure

According to the European Society of Cardiology, the term “advanced heart failure” (AHF) was used to characterize patients with severe symptoms, recurrent decompensation and severe cardiac dysfunction.<sup>1</sup> There is no single condition that defines AHF; however, there is a pattern of clinical characteristics that may suggest that the patient suffers from it.<sup>2</sup> The newest definition describes AHF as a stage of heart failure (HF) where the conventional treatment (the optimal medical, surgical and device therapy) is insufficient to control the symptoms. Moreover, advanced therapies (e.g., cardiac transplantation and mechanical circulatory support) or palliative therapies are needed. Advanced HF patients remain severely symptomatic, despite the optimal guideline-directed management, regardless of left ventricular ejection fraction (LVEF). Ambulatory patients of class IV according to the New York Heart Association (NYHA) may also be included.<sup>3</sup> This type of HF is often described as refractory or stage D according to the American Heart Association (AHA).<sup>4</sup>

## Different diagnostic criteria

It is difficult to clearly define AHF. Different approaches of cardiac societies to this issue are summarized in Table 1

**Table 2.** The differences between stage C and stage D advanced heart failure (AHF) in comparison to the functional capabilities of patients (the New York Heart Association (NYHA) class)

ACCF/AHA stages of HF		NYHA functional classification	
C	Structural heart disease with prior or current symptoms of HF.	I	No limitation of physical activity. Ordinary physical activity does not cause the symptoms of HF.
		II	Slight limitation of physical activity. Comfortable at rest, but ordinary physical activity results in the symptoms of HF.
		III	Marked limitation of physical activity. Comfortable at rest, but less than ordinary activity causes the symptoms of HF.
		IV	Unable to carry on any physical activity without the symptoms of HF, or the symptoms of HF at rest.
D	Refractory HF requiring specialized interventions.	IV	Unable to carry on any physical activity without the symptoms of HF, or the symptoms of HF at rest.

and Table 2. The NYHA classification of patients seems to be insufficient to optimally determine which patients qualify for particular available medical and pacing therapies, cardiac transplantation or mechanical circulatory support. Patients requiring the latter should be classified using the Interagency Registry of Mechanically Assisted Circulatory Support (INTERMACS) profiles.<sup>6</sup>

**Table 1.** Different diagnostic criteria of advanced heart failure (AHF)

European Society of Cardiology (ESC) <sup>3</sup>	American College of Cardiology Foundation/ American Heart Association (ACCF/AHA) <sup>4,5</sup>
<p>All the following criteria must be present, despite the optimal guideline-directed treatment:</p> <ol style="list-style-type: none"> <li>1. Severe and persistent symptoms of HF (NYHA class III (advanced) or IV).</li> <li>2. Severe cardiac dysfunction defined by a reduced LVEF (<math>\leq 30\%</math>), isolated RV failure or non-operable severe valve abnormalities, or congenital abnormalities, or persistently high (or increasing) BNP or NT-proBNP values and data of severe diastolic dysfunction, or LV structural abnormalities according to the ESC definition of HFpEF and HFmrEF.</li> <li>3. Episodes of pulmonary or systemic congestion requiring high-dose intravenous diuretics (or diuretic combinations) or episodes of low output requiring inotropes or vasoactive drugs, or malignant arrhythmias causing &gt;1 unplanned visit or hospitalization in the last 12 months.</li> <li>4. Severe impairment of exercise capacity with inability to exercise or low 6MWT (<math>&lt; 300</math> m) or <math>pVO_2</math> (<math>&lt; 12-14</math> mL/kg/min), estimated to be of cardiac origin.</li> </ol> <p>In addition to the above, extra-cardiac organ dysfunction due to heart failure (e.g., cardiac cachexia, liver or kidney dysfunction) or type 2 pulmonary hypertension may be present, but are not required.</p> <p>Criteria 1 and 4 can be met in patients who have cardiac dysfunction (as described in criterion 2), but who also have substantial limitation due to other conditions (e.g., severe pulmonary disease, non-cardiac cirrhosis, or – most commonly – by renal disease with mixed etiology). These patients still have limited quality of life and survival due to advanced disease and warrant the same intensity of evaluation as someone in whom the only disease is cardiac, but the therapeutic options for these patients are usually more limited.</p>	<ul style="list-style-type: none"> <li>– Repeated (<math>\geq 2</math>) hospitalizations or emergency department visits for HF in the past year.</li> <li>– Progressive deterioration in renal function (e.g., rise in BUN and creatinine).</li> <li>– Weight loss without other cause (e.g., cardiac cachexia).</li> <li>– Intolerance to ACEI due to hypotension and/or worsening renal function.</li> <li>– Intolerance to <math>\beta</math>-blockers due to worsening HF or hypotension.</li> <li>– Frequent systolic blood pressure <math>&lt; 90</math> mm Hg.</li> <li>– Persistent dyspnea with dressing or bathing requiring rest.</li> <li>– Inability to walk 1 block on the level ground due to dyspnea or fatigue.</li> <li>– Recent need to escalate diuretics to maintain the volume status, often reaching daily furosemide equivalent doses over 160 mg/day and/or the use of supplemental metolazone therapy.</li> <li>– Progressive decline in serum sodium, usually to <math>&lt; 133</math> mEq/L.</li> <li>– Frequent implantable cardioverter defibrillator shocks.</li> </ul>

ACEI – angiotensin-converting enzyme inhibitor; BNP – brain natriuretic peptide; BUN – blood urea nitrogen; HF – heart failure; HFmrEF – HF with mid-range ejection fraction; HFpEF – HF with preserved ejection fraction; LV – left ventricle; LVEF – left ventricular ejection fraction; NT-proBNP – N-terminal portion of proBNP; NYHA – the New York Heart Association;  $pVO_2$  – peak oxygen consumption; RV – right ventricle; 6MWT – 6-minute walk test distance.

## Epidemiology and mortality

Heart failure is a global pandemic and continues to increase in prevalence. At least 26 million people worldwide are affected.<sup>7</sup> Patients with AHF comprise an estimated 1–10% of the overall HF population and the prevalence is increasing due to better treatment and survival.<sup>3</sup> Data from Olmstead County, USA, suggests that <1% of patients suffer from stage D HF and are subject to exceptionally high mortality.<sup>5,8</sup> According to the Randomized Evaluation of Mechanical Assistance for the Treatment of Congestive Heart Failure (REMATCH) trial, patients in stage D who were treated medically experienced 75% mortality at 1 year and no survival at 2 years.<sup>5,9</sup> Another trial concerning optimally treated patients – the Investigation of Non-Transplant-Eligible Patients Who Are Inotrope Dependent (IN-TREPID) – had survival rates of 22% at 6 months and 11% at 1 year.<sup>5,10</sup> In a random population-based sample from Olmstead County, stage D HF was associated with only a 20% 5-year survival.<sup>5,8</sup> The poorest survival, 6% at 1 year, concerns patients who are moving on to end-of-life care on continuous inotropes.<sup>5,10</sup> Moreover, the mortality risk increases with each subsequent HF hospitalization and low blood pressure.<sup>2,11–14</sup> While AHF can occur in patients suffering from HF with both preserved and reduced LVEF, a drop in ejection fraction or a very low ejection fraction ( $\leq 25$ –30%) has been associated with a worse prognosis. Right ventricular dysfunction is associated with an adverse prognosis regardless of ejection fraction.<sup>2</sup> Advanced HF is also associated with poor quality of life for patients.<sup>15</sup>

## Clinical manifestations

The signs and symptoms of AHF vary; however, certain clinical manifestations may indicate stage D HF, especially with synchronous presentation. It is important to emphasize that these signs and symptoms listed below occur in the optimal therapy, including the insertion of all appropriate devices (e.g., cardiac resynchronization therapy – CRT) and with all reversible causes of HF addressed. The most common clinical manifestations are<sup>2</sup>:

- dyspnea;
- fatigue;
- exercise intolerance – which also includes the inability to perform activities of daily living, such as bathing or dressing;
- unintentional weight loss – which sometimes leads to cachexia, associated with the loss of muscle and fat, despite proper caloric intake due to catabolic/anabolic imbalances;
- refractory volume overload – despite escalating doses of diuretics (furosemide  $\geq 160$  mg/day) or frequent use of metolazone; clinically it may be visible as pulmonary congestion, peripheral edema and elevated jugular pressure;

- worsening renal function – despite high doses of diuretics, inadequate diuresis may be presented;
- hypotension and the signs of inadequate perfusion; moreover, the need to cut back the doses of angiotensin-converting-enzyme inhibitors (ACEI) and  $\beta$ -blockers due to symptomatic hypotension suggests AHF<sup>2,15,16</sup>;
- congestive hepatopathy – especially due to right-sided HF, which is often accompanied by left-sided HF;
- refractory arrhythmias – with or without device shocks.

Advanced HF usually occurs as an evolution and progression of HF, but it can also be developed acutely, e.g., after acute myocarditis. There are 2 basic pathophysiologic myocardial mechanisms that cause reduced cardiac output and HF: systolic and diastolic dysfunction.<sup>17</sup> The causes of each dysfunction are variable and should be diagnosed.

Useful prognostic indicators are outlined below (Adapted from Metra et al.<sup>18</sup>).

## Prognostic determinants of poor outcome in patients with advanced heart failure

- Demographic:
  - advanced age;
  - male gender.
- Clinical:
  - frequent rehospitalizations;
  - advanced NYHA class;
  - intolerance to neurohormonal antagonists;
  - persistent/relapsing signs of pulmonary or peripheral congestion;
  - hypotension;
  - co-morbidities (diabetes, renal failure, hepatic failure, anemia, chronic obstructive pulmonary disease, hyperthyroidism or hypothyroidism, etc.).
- Electrocardiography:
  - resting tachycardia;
  - wide QRS complex.
- Laboratory:
  - hyponatremia;
  - renal insufficiency (blood urea nitrogen (BUN)/serum creatinine);
  - anemia (hemoglobin  $< 8$  mg/dL);
  - hepatic insufficiency;
  - neurohormones (e.g., norepinephrine, endothelin);
  - natriuretic peptides;
  - cardiac myocyte necrosis markers (troponins);
  - inflammatory markers (e.g., C-reactive protein).
- Doppler-echocardiography and right heart catheterization:
  - low LVEF/increased left ventricular end-systolic volume index;
  - decreased left ventricular long-axis systolic shortening;
  - mitral regurgitation/increased left atrial volume;

- signs of increased LV filling pressure;
  - low right ventricular ejection fraction (RVEF);
  - increased pulmonary vascular resistance.
- Functional capacity:
- inability to perform an exercise test;
  - increased ventilatory response to exercise (the minute ventilation and CO<sub>2</sub> production ratio (VE/CO<sub>2</sub>) slope);
  - low peak oxygen consumption (pVO<sub>2</sub>) [mL/kg/min];
  - low 6-minute walk test distance (6MWTDD).

## Diagnosis

There are no particular tests which can confirm the presence of AHF. As a result, there is a need to perform several diagnostic procedures in order to diagnose AHF and exclude other diseases with similar symptoms. Such procedures include:

- blood tests:
  - complete blood count,
  - electrolytes – AHF is a cause of hyponatremia,
  - renal function test: BUN, creatinine, glomerular filtration rate – abnormalities might be visible due to the worsening of renal function,
  - liver function test: alanine aminotransferase, aspartate aminotransferase, bilirubin – abnormalities due to congestive hepatopathy,
  - elevated levels of brain natriuretic peptide (BNP) or N-terminal portion of proBNP (NT-proBNP) are usually present;
- chest X-ray – used to detect pulmonary edema, pleural effusions, pulmonary vascular congestion, and other episodes of fluid retention;
- electrocardiogram (ECG) – useful in the detection of atrial fibrillation, which is more common in patients with AHF; ventricular arrhythmias may also occur<sup>19</sup>;
- exercise testing, e.g., 6MWTDD (≤300 m) and/or cardiopulmonary exercise testing;
- echocardiography – a complete transthoracic echocardiogram should be performed in all patients suspected of having AHF to assess the changes in biventricular and valvular function that may be contributing to the worsening of the symptoms;
- right heart catheterization – required in patients undergoing evaluation for mechanical circulatory support and cardiac transplantation.<sup>2</sup>

## Differential diagnosis

The exclusion of other, often reversible, pathologies is vital before making a final diagnosis of AHF. Conditions that most commonly imitate the signs and symptoms of AHF include:

- underlying kidney disease, which causes the worsening of renal function;

- cardiorenal syndrome;
- lung disease (especially chronic obstructive pulmonary disease, present in up to 40% of patients) as a cause of dyspnea<sup>2</sup>;
- liver disease, such as cirrhosis, which may evoke the symptoms of retention of fluid (including ascites, edema of lower extremities and fatigue);
- non-optimal therapy.

Furthermore, it is necessary to search for reversible causes of HF, such as tachyarrhythmias, inflammatory diseases, endocrine disorders (e.g., hyperthyroidism), as well as cardiomyopathies: peripartum, Takotsubo or induced by drugs and alcohol. Any reversible reason of cardiomyopathy should be considered as a potential causative and curable factor of AHF. Arrhythmias associated with arrhythmogenic cardiomyopathy include long-standing atrial fibrillation, atrial flutter, atrial tachycardia, reentrant supraventricular tachycardia, accessory pathway tachycardia, frequent ectopic beats, and ventricular tachycardia. The optimal rhythm control or even the restoration of the sinus rhythm is crucial in this case.<sup>20</sup>

Moreover, patients with HF often suffer from malnutrition and that also might be the cause of symptoms similar to those presented in AHF. It is also important to differentiate end-stage HF, which is always irreversible, from AHF, which, by contrast, might be reversible to some extent.

## Treatment

- Medical treatment:
  - Angiotensin-converting-enzyme inhibitors or angiotensin receptor blockers (ARB) in case of intolerance of ACEI.
  - $\beta$ -blockers.
  - Mineralocorticoid antagonists. According to the ESC guidelines concerning AHF, the combination of 3 neurohormonal antagonists should be attempted in all patients with advanced chronic HF. All patients should receive an ACEI and a  $\beta$ -blocker unless there is intolerance. Either an ARB (e.g., candesartan) or mineralocorticoid antagonist (e.g., spironolactone) should then be added.<sup>18</sup>
  - Diuretics – usually high doses are necessary. When used intravenously, continuous infusion of loop diuretics is more efficient than the bolus therapy.<sup>18</sup> The combination of thiazide or spironolactone with loop diuretics has been proposed to overcome the diuretic resistance, commonly present in patients with AHF.<sup>4,18</sup>
  - Nitrates – used to relieve concomitant angina, but the long-term effects are visible only in conjunction with hydralazine in black patients according to African-American Heart Failure Trial.<sup>18,21</sup>
  - Digoxin – used in patients with concomitant atrial fibrillation.
  - Anti-platelet and anti-thrombotic agents – used in patients with atrial fibrillation, unless contraindicated.

- Continuous infusion of inotropes – can be used to improve end-of-life quality, but it is vital to be attentive to the adverse effects of catecholamines (e.g., excessively high heart rate), which can cause the worsening of cardiac function.
- Ivabradine – appears to be a promising approach. It is well tolerated, effectively reduces heart rate, increases stroke volume and preserves cardiac output.<sup>22</sup>
- New drugs: sacubitril/valsartan – a representative of a new group of drugs (angiotensine-receptor-neprilysin inhibitors – ARNI), recommended to be used instead of ACEI/ARB (spectacular results of the PARADIGM-HF trial) and levosimendan – a calcium sensitizer and inodilator, which increases the force of contraction, decreases preload and afterload, and also exerts some cardioprotective effect (in acutely decompensated congestive HF and, according to the LION-HEART study, in advanced HF).<sup>23–25</sup>
- Cardiac resynchronization therapy.
- Implantable cardioverter defibrillator (ICD) – however not in NYHA IV class, unless the patient is under consideration for CRT implantation, left ventricular assist devices therapy or heart transplantation.
- Surgical strategies:
  - Heart transplantation – the treatment of choice for patients without contraindications.<sup>3</sup>
  - Mechanical support – implantable ventricular assist devices might be used as a bridge to recovery or heart transplantation, or as a destination therapy (the last indication is not approved in Poland).
- Palliative medicine/hospice care – at the terminal stadium of the disease.

The treatment of patients with a coexistence of AHF and atrial fibrillation is especially difficult due to limited therapeutic options and a higher risk of bleeding (high prevalence of renal and liver failure). The His-bundle-pacing-based ICD may be an innovative approach in decompensated chronic HF and concomitant permanent atrial fibrillation.<sup>26</sup>

## Summary

Although AHF is a common worldwide problem, there are many questions that remain unanswered. Many prognostic indicators are still unknown and there are no randomized controlled trials of novel pharmacologic and device interventions. Nevertheless, some medical societies pin their hopes on Entresto™, although its use in AHF is not supported by guidelines. Furthermore, in our clinical practice concerning AHF, we very often struggle with significant ethical dilemmas that should be always solved in cooperation with a patient. We need to ask if our patient wants aggressive treatment or resuscitation in case of a sudden cardiac arrest. We must know if the quality of life is for the patient more important than living as long as possible. Answers to these questions are vital in making

proper medical decisions and allow us to provide appropriate and sustainable treatment for the patient, which should be always the main goal for any medical team.

## References

1. Ponikowski P, Voors AA, Anker SD, et al; ESC Scientific Document Group. 2016 ESC Guidelines for the diagnosis and treatment of acute and chronic heart failure: The Task Force for the diagnosis and treatment of acute and chronic heart failure of the European Society of Cardiology (ESC). Developed with the special contribution of the Heart Failure Association (HFA) of the ESC. *Eur J Heart Fail.* 2016;18(8):891–975.
2. Setoguchi S, Stevenson LW, Schneeweiss S. Repeated hospitalizations predict mortality in the community population with heart failure. *Am Heart J.* 2007;154(2):260–266.
3. Crespo-Leiro MG, Metra M, Lund LH, et al. Advanced heart failure: A position statement of the Heart Failure Association of the European Society of Cardiology. *Eur J Heart Fail.* 2018;20(11):1505–1535.
4. Yancy CW, Jessup M, Bozkurt B, et al; American College of Cardiology Foundation/American Heart Association Task Force on Practice Guidelines. 2013 ACCF/AHA guideline for the management of heart failure: Executive summary. A report of the American College of Cardiology Foundation/American Heart Association Task Force on practice guidelines. *Circulation.* 2013;128(16):1810–1852.
5. Fang JC, Ewald GA, Allen LA, et al; Heart Failure Society of America Guidelines Committee. Advanced (stage D) heart failure: A statement from the Heart Failure Society of America Guidelines Committee. *J Card Fail.* 2015;21(6):519–534.
6. Stevenson LW, Pagani FD, Young JB, et al. INTERMACS profiles of advanced heart failure: The current picture. *J Heart Lung Transplant.* 2009;28(6):535–541.
7. Savarese G, Lund LH. Global public health burden of heart failure. *Card Fail Rev.* 2017;3(1):7–11.
8. Ammar KA, Jacobsen SJ, Mahoney DW, et al. Prevalence and prognostic significance of heart failure stages: Application of the American College of Cardiology/American Heart Association heart failure staging criteria in the community. *Circulation.* 2007;115(12):1563–1570.
9. Rose EA, Gelijns AC, Moskowitz AJ, et al; Randomized Evaluation of Mechanical Assistance for the Treatment of Congestive Heart Failure (REMATCH) Study Group. Long-term use of a left ventricular assist device for end-stage heart failure. *N Engl J Med.* 2001;345(20):1435–1443.
10. Hershberger RE, Nauman D, Walker TL, Dutton D, Burgess D. Care processes and clinical outcomes of continuous outpatient support with inotropes (COSI) in patients with refractory end-stage heart failure. *J Card Fail.* 2003;9(3):180–187.
11. Solomon SD, Dobson J, Pocock S, et al; Candesartan in Heart failure: Assessment of Reduction in Mortality and morbidity (CHARM) Investigators. Influence of nonfatal hospitalization for heart failure on subsequent mortality in patients with chronic heart failure. *Circulation.* 2007;116(13):1482–1487.
12. Lee DS, Austin PC, Rouleau JL, Liu PP, Naimark D, Tu JV. Predicting mortality among patients hospitalized for heart failure: Derivation and validation of a clinical model. *JAMA.* 2003;290(19):2581–2587.
13. Fonarow GC, Adams KF, Abraham WT, Yancy CW, Boscardin WJ; ADHERE Scientific Advisory Committee, Study Group, and Investigators. Risk stratification for in-hospital mortality in acutely decompensated heart failure: Classification and regression tree analysis. *JAMA.* 2005;293(5):572–580.
14. Pocock SJ, Ariti CA, McMurray JJV, et al.; Meta-Analysis Global Group in Chronic Heart Failure. Predicting survival in heart failure: A risk score based on 39,372 patients from 30 studies. *Eur Heart J.* 2013;34(19):1404–1413.
15. Allen LA, Gheorghiade M, Reid KJ, et al. Identifying patients hospitalized with heart failure at risk for unfavorable future quality of life. *Circ Cardiovasc Qual Outcomes.* 2011;4(4):389–398.
16. Kittleson M, Hurwitz S, Shah MR, et al. Development of circulatory-renal limitations to angiotensin-converting enzyme inhibitors identifies patients with severe heart failure and early mortality. *J Am Coll Cardiol.* 2003;41(11):2029–2035.

17. Echouffo-Tcheugui JB, Erqou S, Butler J, Yancy CW, Fonarow GC. Assessing the risk of progression from asymptomatic left ventricular dysfunction to overt heart failure: A systematic overview and meta-analysis. *JACC Heart Fail.* 2016;4(4):237–248.
18. Metra M, Ponikowski P, Dickstein K, et al; Heart Failure Association of the European Society of Cardiology. Advanced chronic heart failure: A position statement from the Study Group on Advanced Heart Failure of the Heart Failure Association of the European Society of Cardiology. *Eur J Heart Fail.* 2007;9(6–7):684–694.
19. Middlekauff HR, Stevenson WG, Stevenson LW. Prognostic significance of atrial fibrillation in advanced heart failure: A study of 390 patients. *Circulation.* 1991;84(1):40–48.
20. Patel H, Madanieh R, Kosmas CE, Vatti KS, Vittorio TJ. Reversible cardiomyopathies. *Clin Med Insights Cardiol.* 2015;9(Suppl 2):7–14.
21. Taylor AL, Ziesche S, Yancy C, et al; African-American Heart Failure Trial Investigators. Combination of isosorbide dinitrate and hydralazine in blacks with heart failure. *N Engl J Med.* 2004;351(20):2049–2057.
22. De Ferrari GM, Mazzuero A, Agnesina L, et al. Favourable effects of heart rate reduction with intravenous administration of ivabradine in patients with advanced heart failure. *Eur J Heart Fail.* 2008;10(6):550–555.
23. McMurray JJV, Packer M, Desai AS, et al; PARADIGM-HF Investigators and Committees. Angiotensin-neprilysin inhibition versus enalapril in heart failure. *N Engl J Med.* 2014;371(11):993–1004.
24. De Luca L, Colucci WS, Nieminen MS, Massie BM, Gheorghiade M. Evidence-based use of levosimendan in different clinical settings. *Eur Heart J.* 2006;27(16):1908–1920.
25. Comín-Colet J, Manito N, Segovia-Cubero J, et al; LION-HEART Study Investigators. Efficacy and safety of intermittent intravenous outpatient administration of levosimendan in patients with advanced heart failure: The LION-HEART multicentre randomized trial. *Eur J Heart Fail.* 2018;20(7):1128–1136.
26. Adamowicz J, Slawuta A, Sokolowska M, et al. His-bundle-pacing-based ICD as an innovative approach in decompensated chronic heart failure and concomitant permanent atrial fibrillation. *Eur J Heart Fail.* 2018;20 (Suppl S1):5–638.